Multifunctional Smart Coatings Derived from Biomass Extracts for Mild Steel and Aluminium Alloys

By

Rajimol P. R.

10CC18A39009

A thesis submitted to the
Academy of Scientific and Innovative Research
for the award of degree of
DOCTOR OF PHILOSOPHY

in

SCIENCE

Under the supervision of

Dr. T. P. D. RAJAN

CSIR-National Institute for Interdisciplinary Science and Technology (CSIR-NIIST)
Thiruvananthapuram-695019

Academy of Scientific and Innovative Research
AcSIR Headquarters, CSIR-HRDC Campus
Sector 19, Kamla Nehru Nagar,
Ghaziabad, U.P.-201 002, India

May 2023

Dedicated to my beloved Family

CSIR-National Institute for Interdisciplinary Science and Technology
(Formerly Regional Research Laboratory)

Council of Scientific & Industrial Research (CSIR),
Industrial Estate P.O.,
Trivandrum - 695 019, Kerala, INDIA

Certificate

This is to certify that the work incorporated in this Ph.D. thesis entitled, **"Multifunctional Smart Coatings derived from Biomass Extracts for Mild Steel and Aluminium Alloys"**, submitted by **Ms. Rajimol P. R.**, to the Academy of Scientific and Innovative Research (AcSIR) in fulfilment of the requirements for the award of the Degree of *Doctor of Philosophy in Sciences*, embodies original research work carried out by the student. We further certify that this work has not been submitted to any other University or Institution in part or full for the award of any degree or diploma. Research materials obtained from other sources and used in this research work have been duly acknowledged in the thesis. Images, illustrations, figures, tables etc., used in the thesis from other sources, have also been duly cited and acknowledged.

Rajimol P. R.	**Dr. T. P. D. Rajan**	**Dr. K. V. Radhakrishnan**
	(Supervisor)	**(Co-Supervisor)**
19-05-2023	19-05-2023	19-05-2023

STATEMENTS OF ACADEMIC INTEGRITY

I, Rajimol P. R., a PhD student of the Academy of Scientific and Innovative Research (AcSIR) with Registration No. 10CC18A39009 hereby undertake that, the thesis entitled **"Multifunctional Smart Coatings Derived from Biomass Extracts for Mild Steel and Aluminium Alloys"** has been prepared by me and that the document reports original work carried out by me and is free of any plagiarism in compliance with the UGC regulations on *"Promotion of Academic Integrity and Prevention of Plagiarism in Higher Educational Institutions (2018)"* and the CSIR Guidelines for "*Ethics in Research and in Governance (2020)*".

Rajimol P. R.
19-05-2023
Thiruvananthapuram

It is hereby certified that the work done by the student, under our supervision, is plagiarism free in accordance with the UGC Regulations on *"Promotion of Academic Integrity and Prevention of Plagiarism in Higher Educational Institutions (2018)"* and the CSIR Guidelines for "*Ethics in Research and in Governance (2020)*".

Dr. T. P. D. Rajan
19-05-2023
Thiruvananthapuram

Dr. K. V. Radhakrishnan
19-05-2023
Thiruvananthapuram

DECLARATION

I, **Rajimol P. R.**, bearing AcSIR Registration No. 10CC18A39009 declare that my thesis entitled, **"Multifunctional Smart Coatings Derived from Biomass Extracts for Mild Steel and Aluminium Alloys"** is plagiarism free in accordance with the UGC Regulations on *"Promotion of Academic Integrity and Prevention of Plagiarism in Higher Educational Institutions (2018)"* and the CSIR Guidelines for "*Ethics in Research and in Governance (2020)*".

I would be solely held responsible if any plagiarised content in my thesis is detected, which is violative of the UGC regulations 2018.

Rajimol P. R.

19-05-2023

Thiruvananthapuram

ACKNOWLEDGEMENTS

*It is with immense pleasure and great respect that I place on record my deep sense of gratitude to my research supervisors **Dr. T. P. D. Rajan** and **Dr. K. V. Radhakrishnan**, for suggesting the research topic and for their inspiring guidance, constant support, patience and encouragement that led to the successful completion of this work.*

I wish to thank Dr. C. Anandharamakrishnan and Dr. A. Ajayaghosh, present and former Directors of CSIR-NIIST Thiruvananthapuram, for providing the necessary facilities for carrying out the research work.

I would like to acknowledge Dr. V. Karunakaran Venugopal, Dr. R. Luxmi Varma, and Dr. C. H. Suresh, the present and former AcSIR programme coordinators, CSIR-NIIST for the timely help and advice for the academic procedures of AcSIR.

I am very thankful to Dr. Ravishankar L., Dr. Kausthabh Kumar Maiti., and Dr. Hareesh U. S. (my Doctoral Advisory Committee members) for their help, support, suggestion and encouragement throughout my Ph. D. period.

I would like to express my sincere gratitude to Dr. Jubi John, Dr. Sushanta Kumar Sahoo and Dr. Rajeev K Sukumaran for all the academic support, inspiring presence and support during these days.

I like to thank all the AcSIR faculty members of CSIR-NIIST for their help and support during the coursework period.

My sincere thanks are also due to:

Dr. K. V. Radhakrishnan, Dr. P. Sujatha Devi, and Dr. R. Luxmi Varma present and former Heads, Chemical Sciences and Technology Division for their endless support.

Dr. Ananthakumar, Dr. Savithry S, and Dr. Ravi M, present and former Heads, Material Sciences and Technology Division for their endless support

All the Scientists of the Organic Chemistry Section and Metallic Materials and Minerals Section for their encouragement and help.

Mrs. Saumini Mathew, Mrs. S. Viji, Mr. Kiran Mohan, Mr. Peer Muhammad, Mr. Hareesh Raj are acknowledged for their help in various analyses.

All members of Dr. TPDR group and Dr. KVR group are greatly acknowledged for their love, care and support throughout my research period.

Dr. Biji, Mr. Krishnakumar, Dr. Vishnu, Dr. Neethu, Mr. Kiran J S, Dr. Veena, Dr. Arun, Mr. Anoop, Ms. Akhina and Ms. Haritha are greatly acknowledged for their companionship and love.

Ms. Arsha, Ms, Revathy, Mr. Arun, Ms. Anju, and Mr. Aashamz are greatly acknowledged for their friendship and support.

Ms. Anjali, Mrs. Athira Raj, Mr. Samuel A.S., Mrs. Febeena, Ms. Krishna (MSc project students/summer interns) for helping me to carry out some of my lab work.

All present and former members of CSTD and MSTD, Batchmates for their friendship and creative inspirations.

All my teachers, Dr. Saju M. Sebastian and Dr. K. C. Joseph and friends for their care and support.

My parents (Mr. Ravi and Mrs. Susheela), brothers (Mr. Retheesh and Mr. Rajesh) and family members for their endless caring love and support.

UGC for the financial assistance

Above all, I thank Almighty for bestowing his blessings upon me and giving all these people to help and encourage me, for the successful completion of the work.

Rajimol P. R.

TABLE OF CONTENTS

LIST OF TABLES

LIST OF FIGURES

LIST OF ABBREVIATIONS

°C	:	Degree Celsius
µg	:	Microgram
µL	:	Microlitre
µm	:	Micro metre
1-D	:	One dimensional
2-D	:	Two dimensional
AATCC-100	:	American Association of Textile Chemists and Colorists-100
AATCC-147	:	American Association of Textile Chemists and Colorists-147
AC	:	Alternating current
AcOH	:	Acetic acid
Acm^{-2}	:	Ampere per centimetre square
Al-6061	:	Auminium-6061
APE	:	*Andrographis paniculata* hydroethanolic extract
ATP	:	Adenosine triphosphate
BET	:	Brunauer-Emmett-Teller
BJH	:	Barrett-Joyner-Halenda
BRG	:	Bergenin
CA	:	Citric acid
Calcd	:	Calculated
CC	:	Column chromatography
C_c	:	Capacitance of coating
$CDCl_3$	:	Deuterated chloroform
C_{dl}	:	Double layer capacitance
cm	:	Centimetre

cm^2	:	Centimetre square
cm^3/g	:	Centimetre cube per gram
CNSE	:	*Cocus nucifera* shell extract
CO	:	Castor oil
COMB	:	Combination of
C_{oxi}	:	Capacitance of oxidation product
CTAB	:	Cetyltrimethyl Ammonium Bromide
Cu	:	Copper
d	:	Doublet
DCM	:	Dichloromethane
dd	:	Doublet of doublets
DGEBA	:	Diglycidyl ether of bisphenol A
DI	:	Deionised water
DMSO	:	Dimethyl sulfoxide
DNA	:	Deoxyribonucleic acid
DOE	:	Degree of epoxidation
dt	:	Doublet of triplet
E	:	Potential
E. coli	:	*Escherichia coli*
ECO	:	Epoxidized castor oil
E_{corr}	:	Corrosion potential
EDAX	:	Energy-dispersive X-ray analysis
EDS	:	Energy Dispersive Spectroscopy
EEC	:	Equivalent electrochemical circuit
EIS		Electrochemical impedance spectroscopy
EP	:	Epoxy
Equiv.	:	Equivalent

ESE	:	*Elephantopus scaber* hydroethanolic extract
EtOAc	:	Ethyl acetate
Fe	:	Iron
FE- SEM	:	Field emission scanning electron microscopy
FT-IR	:	Fourier transform infrared
g	:	Gram
G/L	:	Gram per litre
GDP	:	Gross domestic product
h	:	Hour
HCl	:	Hydrochloric acid
HRMS	:	High-resolution mass spectrometry
Hz	:	Hertz
i	:	Corrosion current
i_{corr}	:	Corrosion current density
IE	:	Inhibition efficiency
IR	:	Infrared
J	:	Coupling constant
K	:	Kelvin scale
kHz	:	Kilo hertz
LB	:	Luria-Bertani
m	:	Multiplet (in NMR)
m^2/g	:	Metre square per gram
MeOH	:	Methanol
mg	:	Milligram
MGE	:	Marigold hydroethanolic extract
MGH	:	Marigold hexane extract
MHz	:	Mega hertz

min	:	Minute
mL	:	Milliliter
ML	:	Malabaricone C
mm	:	Milli metre
MS	:	Mild steel
MSNP	:	Mesoporous silica nano particle
mV	:	Milli volt
MW	:	Molecular weight
NaCl	:	Sodium Chloride
NaOH	:	Sodium hydroxide
NLE	:	Neem leaves ethanol hydroethanolic extract
NMR	:	Nuclear magnetic resonance
OCP	:	Open circuit potential
OXY	:	Oxyresveratrol
P. aeruginosa	:	Pseudomonas aeruginosa
PP	:	Potentiodynamic polarisation
ppm	:	Parts per million
QCTGN	:	Quercetagetin
R_c	:	Resistance offered by the coating
R_{ct}	:	Charge transfer resistance
Rf	:	Retention factor
RNA	:	Ribonucleic acid
R_{oxi}	:	Resistance offered by the corrosion product
R_s	:	Solution resistance
RT	:	Room temperature
S. aureus	:	Staphylococcus aureus
SCE	:	Saturated calomel electrode
SEM	:	Scanning electron microscope

t	:	Triplet
T_{10}	:	The temperature at 10% weight loss in TG
TEM	:	Tunnelling electron microscope
THF	:	Tetrahydrofuran
TLC	:	Thin layer chromatography
TMS	:	Tetramethylsilane
UV	:	Ultraviolet
V	:	volt
VIL	:	VIL extract
W_i and W_o	:	Weight loss in the presence and absence of an inhibitor
wt.	:	Weight
Z'	:	Impedance (real)
Z''	:	Impedance (imaginary)
δ ppm	:	Delta (Here NMR chemical shift in parts per million)
η	:	Eta (here, inhibition efficiency)
λ_{max}	:	The wavelength at which absorbance is maximum
μAcm^{-2}	:	Micro Ampere per centimetre square
$\Omega\ cm^2$	:	Ohm centimetre square

PREFACE

Development of eco-friendly, renewable, and sustainable coating materials is one of the major challenges faced by coating and polymer industry. All the petroleum sources are rapidly depleting and will culminate in resource scarcity in the near future. Moreover, the mining and purifying petroleum crude oil and the vast global usage of petroleum-based products will lead to severe environmental pollution, emission of greenhouse gases, and, thus, extreme climate change. Among the resins used for high-performance coating, Diglycidyl ether of bisphenol A (DGEBA) epoxy is the most common, accounting for about 75% of total epoxy consumption owing to its excellent properties. However, Bisphenol A and epichlorohydrin, the major components of DGEBA epoxy, is highly toxic, an endocrine disruptor, carcinogen, mutagen, and reprotoxic (CMR) classified substance results in many serious health issues, and thus the food and drug control department of many countries debarred the use. Many organic and inorganic corrosion inhibitors, like chromates, phosphates, and azoles, etc., are banned in many countries due to their negative impact on human health and the environment. Heavy metals are also excellent corrosion inhibitors but are also very lethal. This problem can be solved by developing green and sustainable bio-based polymers and composites for various applications with comparable properties with their petroleum-based counterparts.

The replacement of petroleum-based epoxy with bio-based epoxy and synthetic organic and inorganic inhibitors with plant extracts and phytochemicals will lead to the developments of an environmentally friendly and side-effect-free bio-sourced corrosion inhibitor coatings. Also, smart coatings with anti-corrosion, self-healing, hydrophobic and antimicrobial properties can achieve reduced maintenance costs, increased life, fewer accidents, and preventing the propagation and proliferation of pathogens etc. For this, a plant extract or compound with excellent corrosion inhibition property along with antimicrobial property should be identified. Also, a method to load the inhibitor with increased shelf-life, controlled release property and trigger response should be ensured.

Plants having active phytochemicals for multifunctional smart coatings were selected based on the literature study, local traditional knowledge, availability and from the advice of experts in phytochemistry. Various extracts were studied, and the most active extract was identified and used for further studies. The active phytochemicals available in gram scale were identified. Solvent extraction followed by column chromatography yielded the compounds. Structures were confirmed using spectroscopic techniques. The vegetable oil with high unsaturation was

selected, the solvent extraction of the seeds yielded the oil. Epoxidation reaction followed by curing with a natural hardener gave completely bio-based polymer matrix with no side effects. The mesoporous silica container was synthesised by template synthesis procedure. Inhibitors were loaded inside the container by simple physisorption method. Uniform distribution of the inhibitors in the epoxy yielded modified epoxy system with enhanced properties.

The corrosion inhibition efficiency was tested using various methods like surface topology evaluation, weight loss measurements, potentiodynamic polarisation studies and electrochemical impedance measurements. The self-healing efficiency was evaluated by studying the healing of an artificial scratch examining by SEM. The qualitative antimicrobial test was done by zone of inhibition assay and quantitatively confirmed by AATCC-100. Contact angle measurements were carried out.

Chapter 1 gives a brief introduction to natural product based multifunctional corrosion inhibitors for smart coatings. The multifunctionality of plant-based anticorrosive smart coatings as an advantage in various fields is described in this chapter. It also explains the idea of different smart coatings, and gives a detailed literature survey of various bio-based smart coatings.

Chapter 2 is on development of a multifunctional smart epoxy coating from extract of marigold flower waste and its marker compound quercetagetin. It was incorporated into mesoporous silica nanocontainers and embedded in the polymer matrix. The higher activity of hydroethanolic extract led to isolation of the potent green corrosion inhibitor Quercetagetin (QCTGN). Among the various coatings studied with extracts and the compound, the matrix containing 3% of the QCTGN-MSNP was found to be most effective for the corrosion prevention of mild steel and Al-6061 alloy in the marine environment. The coating also exhibited antimicrobial and self-healing properties, and complete self-healing was observed within 48 hours.

Chapter 3 describes the smart multifunctional epoxy coating prepared by incorporating bio-nanocomposites of two isolated phytochemicals, bergenin and malabaricone C, showed excellent corrosion inhibition properties and self-sanitizing effect. This smart antimicrobial and corrosion-resistant coating was active in acidic, basic and neutral media containing 3.5 wt. %

NaCl. Polarization studies and EIS data showed that an epoxy composite coating containing 3% bergenin nanocomposite prevents corrosion on mild steel and aluminium alloys than pure epoxy coating.

Chapter 4 deals with the development of a synergistic epoxy formulation by the incorporation of hydro-ethanolic extracts of *Azadirachta indica*, *Elephantopus scaber* and *Andrographis paniculata*. The combination of three plant extracts resulted in an increased corrosion inhibition potential and antimicrobial efficiency due to the synergistic combination of the compounds. The coating with the synergistic formulation exhibited 99.99% of inhibition against gram positive and gram negative bacteria. The coating exhibited excellent corrosion inhibition performance with an efficiency of 99.97% for mild steel in saline medium. The contact angle of the surface is improved by silane incorporation to improve the corrosion inhibition efficiency and stability of the coatings.

Chapter 5 illustrates the use of Oxyresveratrol (OXY) extracted from coconut shell waste and subsequently used as a green corrosion inhibitor, encapsulated in mesoporous silica (MSNP) nanocontainers. Castor oil is a non-edible vegetable oil, it is epoxidized and crosslinked with bio-sourced citric acid and reinforced with oxyresveratrol-silica nanoparticles. The bio-based composite coating showed excellent anti-corrosive properties with improved thermal stability. At 2 wt.% of OXY-MSNP content, the corrosion potential shifted to -0.028 V from -0.666 V, and the corrosion current reduced significantly from 30.53 μAcm^{-2} to 0.0074 μAcm^{-2} with an inhibition efficiency of 99.97%. This bio-based coating showed self-sanitizing, self-healing, and anticorrosion properties by the utilization of waste materials in a sustainable manner. **Chapter 6** summarises various studies carried out on the development of multifunctional smart coatings from different plant phytochemicals as corrosion inhibitor and antimicrobial agent.

Chapter 1

Bio-based Smart Multifunctional Anticorrosive Coatings

Abstract

Various protection methods like corrosion inhibitors, cathodic protection, anodic protection, and protective coatings are used for metal surface protection by considering multiple factors like corrosive media being exposed, the expected corrosion type, and the application of the surface etc. The application of inhibitors to protect metal surfaces against corrosion in aggressive media is an accepted practice. Using minimal corrosion inhibitors gives a good amount of corrosion protection. Severe health issues and detrimental effects on the environment have been caused by many organic and inorganic synthetic inhibitors like phosphate, chromates, and some azole derivatives. An emerging need for inhibitors with fewer or no side effects and which are cheaper has arisen. Plant-based inhibitors have properties like "lower side effects," "green chemistry," "eco-friendly," and are "derived from sustainable sources." The primary candidates in corrosion inhibition coatings are whole extracts, isolated phytochemicals, plant oils, etc.

Smart coatings are innovative coatings, also known as “intelligent" coatings. They can spontaneously respond to changes in the microenvironment, such as heat, light irradiation, mechanical induction, wettability, temperature, pressure, ion exchange, pH variation, aggressive corrosive ions, etc., through stimuli-responsive mechanisms. These coatings are artistically prepared for various applications and expected to perform for several cycles spanning many years. Examples of natural product-based innovative coatings include but are not limited to antimicrobial coatings, anti-corrosion coatings, antifouling coatings, self-healing coatings, hydrophilic/hydrophobic self-cleaning coatings, intumescent coatings, etc. The various properties of plant extracts and phytochemicals, like antimicrobial properties, hydrophobic/ hydrophilic properties, high hetero atom density, hydrogen-bonding capacity, etc., are the reason for these spontaneous, intelligent responses. The multifunctionality of plant-based anticorrosive smart coatings as an advantage in various fields is described in this chapter.

1.1. Introduction

The gradual destruction of the pure metals and their alloys into their more stable forms like oxides, hydroxides, carbonates, or sulfides due to environmental or electrochemical factors leads to corrosion. It is an unwanted but spontaneous process resulting in many disasters and has a substantial economic impact that affects the development of a nation. Many infrastructure failures, imperfections, accidents, and financial losses occur due to this unwanted phenomenon. On average, a developed country loses about 4-5% of its gross domestic product (GDP) yearly due to corrosion. The resultant effect can be experienced in growth retardation in the nation's diverse fields [1].

Surface corrosion prevention methods like corrosion inhibitors, cathodic protection, anodic protection, and insulating coatings have been used for mild steel and aluminium alloys, considering various factors like the type of corrosion expected, application of the surface being considered, and nature of the corrosive media. The use of inhibitors to protect metal surfaces against corrosion in aggressive media is an accepted practice. A minimal amount of corrosion inhibitors can give a very fair rate of corrosion protection, which promotes the use of corrosion inhibitors, among other methods. Many countries banned the use of inhibitors like phosphate, chromates, and some azole derivatives, which though cheap, created severe health issues and detrimental environmental effects. The replacement by rare earth metals was not considered economically viable. This led to an emerging need for an inhibitor with lesser side effects and higher economic impact.

Nano containers have been used as a targeted delivery agent for drug molecules and corrosion inhibitors for the past few decades. Properties like a controlled release of the active molecules and response to stimuli are ideal for these applications [2–5]. Mesoporous silica nanoparticles are suitable for loading green corrosion inhibitors among the various delivery agents. Incorporating plant extracts and individual phytochemicals into prevailing coating techniques is an interdisciplinary contribution to corrosion protection [6]. Loaded nanocontainers embedded in the epoxy matrix are an excellent choice for corrosion prevention by coating methods.

Due to their distinct properties, mild steel and aluminium alloys are essential in various sectors. Mild steel became the first-rate material in many industries like farming, petroleum-based products, and construction because of its properties like appropriate malleability, core mechanical strength, and availability. As these materials are susceptible

to chloride ions in these environments, the failures associated with water treatment plants, cooling systems, and pipelines are enough to rule out all the merits discussed [7]. The higher thermal conductivity of aluminium makes it suitable for heat exchangers. In contrast, the non-toxic properties of aluminium make it the right choice for cooking utensils, serving dishes, and storage containers. While comparing the corrosion properties of mild steel and aluminium, it is evident that mild steel is more prone to corrosion than aluminium. A layer of insoluble aluminium oxide on the aluminium surface only provides corrosion resistance at a neutral pH. As pH changes to acidic or basic or the presence of aggressive chloride ions, leads to the dissolution of the insoluble oxide layer resulting in corrosion [8]. So, inventing an effective inhibitor for both mild steel and aluminium alloys is crucial.

1.2. Natural Product-based Corrosion Inhibitors

Previously used synthetic organic and inorganic inhibitors were of meagre cost and good inhibition efficiency. Chromates, phosphates, heavy metals, and azole derivatives were the widely used and most effective corrosion inhibitors earlier, but now they are banned in many countries worldwide. Chromate is a very effective inhibitor for all types of metallic corrosion because of its higher oxidation property. It acts as a mixed inhibitor and reduces electrochemical activity by inhibiting both anodic and cathodic reactions. Minute concentrations of the ion can inhibit corrosion to a great extent. The loading capacity of the chromates in coatings is deficient; thus, the chromates tend to leach out of the surface, which sometimes lowers the efficiency [9]. Despite the higher rate of metal protection nature, the chromates' leachability and higher oxidation properties make them environmentally unfriendly. Direct interaction with the skin, inhalation, and ingestion through polluted water will lead to chromium pollution in the body. The hexavalent chromium ions are carcinogenic and can cause DNA and RNA damage [10]. This challenge with using hexavalent chromium has encouraged exploring natural products as corrosion inhibitors.

Plant-based compounds and extracts have been researched and found to be effective corrosion inhibitors. Plant biomass is an environmentally friendly, low-cost renewable source. Plant-based compounds' antibacterial, antiviral, and antifungal capabilities reflect their multifunctional properties. These characteristics have made them valuable considerations for various intelligent coatings. Many plant oil derivatives are used as monomers for making eco-friendly corrosion-resistant polymers. Epoxidized castor oil, epoxidized soybean oil, and cardanol derivatives are excellent choices. Adding a strong

inhibitor to this polymer matrix can increase the ability manifold. Phytochemicals are excellent choices for this application.

The extract of the whole plant or any particular part, like the leaf, seed, root, stem, etc., is extracted with a specific solvent. The isolated phytochemicals can act as corrosion inhibitors. The activity of the extract will depend on the nature of the significant phytochemicals present in it. Phytochemicals can be classified into primary and secondary metabolites depending on their biological function. Primary metabolites are responsible for growth, and secondary metabolites are responsible for the defence mechanism of plants against insects, other parasites, and disease-causing microbes. Many chromatographic techniques, such as column chromatography, liquid chromatography, high-performance liquid chromatography (HPLC), and gas chromatography (GC), can be applied to analyse phytochemicals quantitatively. Maceration, percolation, and soxhlet extraction methods are prominently employed in phytochemical screening studies. But there are some advanced methods, such as ultrasound-assisted extraction (UAE), supercritical fluid extraction (SFE), microwave-assisted extraction (MAE), and accelerated solvent extraction [11].

Extraction can be broadly classified as isolation with organic solvents and green extraction. In extraction with organic solvents of varying polarity, dried materials are soaked in and stirred with different organic solvents like hexane, ethyl acetate, chloroform, acetone, DCM, ethanol, or methanol. The active phytochemicals will dissolve in the respective solvents depending on their polarity or functional groups present in them. After repeated extraction with these solvents, the solvents are removed under reduced pressure and optimum temperature. The solid residue obtained is vacuum dried and kept in a refrigerator, and column chromatography is the primary technique used for the isolation of secondary metabolites.

Synthetic organic molecules with heteroatoms are suitable inhibitors, but they are costly and have side effects. The use of traditional inhibitors is diminishing as the demand for inhibitors with properties like "lower side effect," "green chemistry," "eco-friendly," and "derived from sustainable sources" increases. The plant kingdom is a readily available, renewable, and sustainable source of many such molecules. Plant extracts like ethanolic extract of *Azadirachta indica* (neem tree) leave [12], and *Mangifera indica* (mango tree) leaves [13] were proved to be suitable inhibitors for mild steel corrosion. Extracts of *Ricinus communis, Emblica officinalis, Terminalia chebula, Andrographis paniculata,* black cumin, henna, and tea wastes have also been explored [14]. Tannic acid and its

modified bio-nano composite are excellent corrosion inhibitors, particularly in the case of mild steel and aluminium alloys [15–17]. Many plants from the Piperaceae family, like *Piper nigrum*, *Piper longum* [18], *Piper guineense* [19], and *Piper sarmentosum* [20], are found to be suitable corrosion inhibitors, especially for aluminium alloys. Some piper species in coatings have added benefits, such as imparting antibacterial and antifungal properties to the metal surface.

The corrosion prevention potential of a compound strongly depends on the capacity to adsorb on metal, which involves replacing a water molecule on the corrosion centre, charge and electron distribution, electron density at the expected coordination centre, the presence of functional group like R–OH, C=O, –N=N, –CHO, solubility in water, the aromaticity of the molecule, and total molecular weight [21]. Individual molecules isolated from the plant extracts are more effective as there is a lower amount of junk materials and other inactive phytochemicals. Quercetin, a flavanol present in many plants like onion, berries, neem, etc., is an excellent green inhibitor against corrosion of Al-6061 alloy[6]. A bis-indole alkaloid derived from the marine alga *Caulerpa racemosa* can form a film on a mild steel surface, providing corrosion protection even in 1M HCl solution [22]. The corrosion inhibition potential of andrographolide from *Andrographis paniculata* was examined using surface analysis, and computational calculations revealed that it could act as an excellent mixed-type corrosion inhibitor for steel [23].

Generally, phytochemicals containing hetero atoms or pi-electron clouds are more effective in corrosion inhibition. Alkaloids, carboxylic acids and their derivatives like esters and lactones, ketones, terpenes, and polyphenols like flavonoids, flavanols, chalcones, flavones, coumarins, tannins, flavanones, lignans, and stilbenes, organosulfur compounds, etc. are potent candidates for corrosion inhibition studies. Structures of some of the compounds from these categories are listed below. The lone pair of electrons available on the heteroatoms like nitrogen, oxygen, phosphorous, and sulphur can interact with the metal ion and thus stabilize and prevent them from further redox reactions. In many phytochemicals, there is an aromatic system or pi-electron cloud. Electron coordination allows these loosely bounded electrons to interact with the metal atoms and ions. Selected examples of phytochemical compounds with expected corrosion-inhibiting properties are shown in **Figure 1.1.**

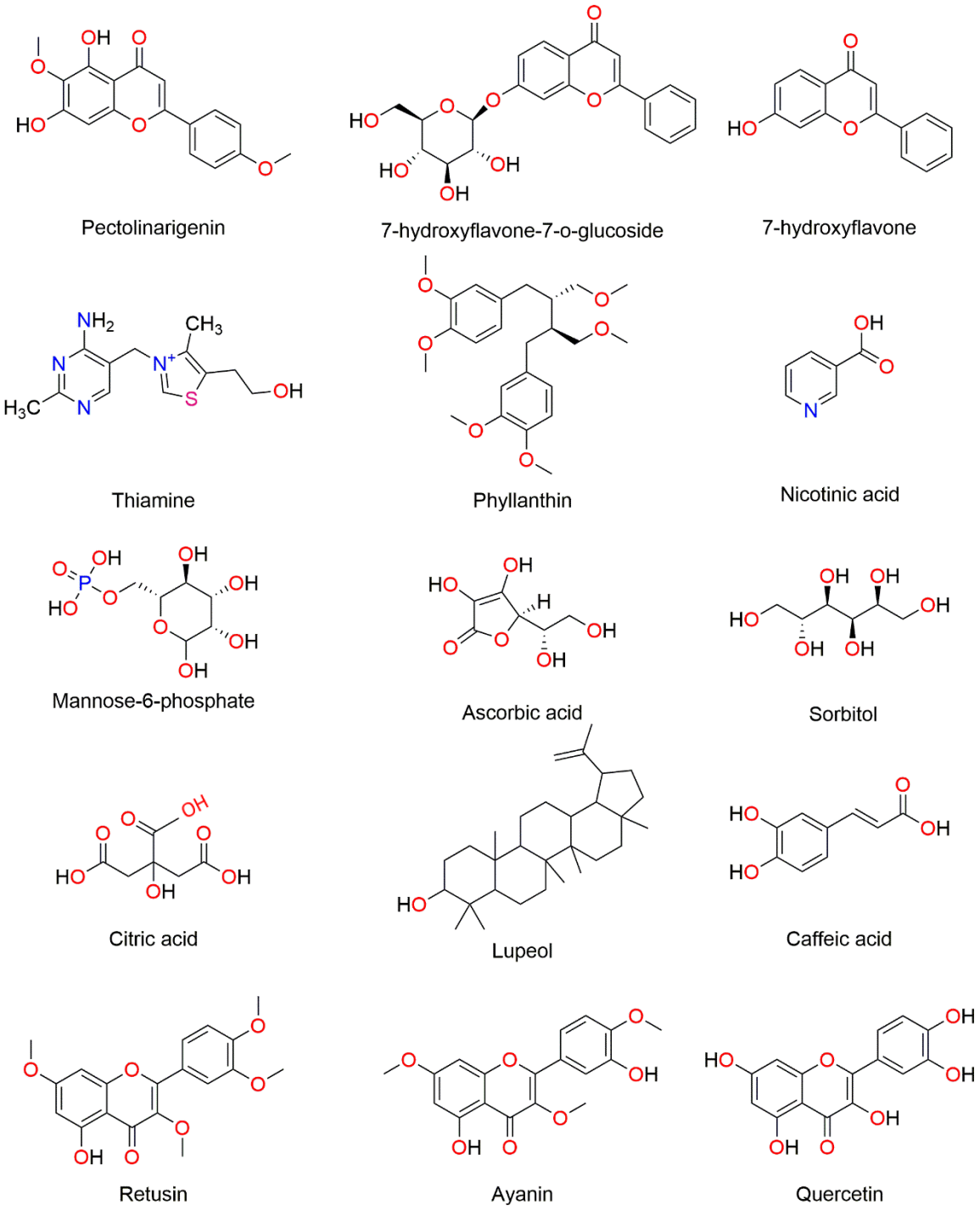

Figure 1.1. Examples of natural-product compounds with expected corrosion inhibition properties.

Many initiatives have been made to replace fossil feedstock chemicals with biomass-derived compounds, mainly vegetable oil derivatives. The driving factors of these massive initiatives are the adverse consequences of petroleum-based products, petroleum

depletion, rising crude oil prices, and, most importantly, the additional benefits of renewable biomasses. The long flexible fatty acid structure behaves as the perfect soft segments for polyurethanes (PUs), and the unsaturation in the chains acts as reaction centers for new structural design. Vegetable oils are a favorite of industrialists and researchers due to their renewable nature, ease of accessibility, capacity to make various structural alterations, low cost, and absence of side effects. The leading plant oil derivatives include epoxy resins, polyurethanes, and polyesters. Because of epoxies' growing health and environmental concerns, the public has embraced vegetable oil-based waterborne polyurethanes the most [24].

1.3. Smart Coatings

Coatings have traditionally been thought of as a passive layer that is insensitive to the environment. Responsive or smart materials can dynamically adapt their properties to an external stimulus. Temperature, light, pressure, wettability, pH variation, harsh corrosive species, or other micro-environmental changes can stimulate smart coatings. "Stimulus-responsive," "intelligent," or "environmentally sensitive" films are different terms for smart coatings. Because of their intrinsic features and chemistry on modification, smart coatings have earned recognition in all areas of science. Examples of smart coatings include corrosion-sensing, antimicrobial, antifouling, self-healing, conductive, and superhydrophobic systems. They are made with both passive and active species so that the uses of their rapid response based on the appropriate stimuli can be realized when employed in an application. Innovative coatings are creatively developed for various applications, and their value lies in their capacity to react to numerous cycles over a long period. By incorporating micro/nanoparticles and combining organic and inorganic groups, intelligent coatings have achieved outstanding qualities over conventional coatings [25,26].

Stimuli-responsive coatings are employed in various sectors and for extensive purposes. These include medical, aviation, textile, transportation, construction, electronics, military, etc., providing multiple services, including corrosion protection. Without physical assistance, they are seen as pragmatic candidates. In many industrial applications, smart coatings aim to improve system efficiency by decreasing inspection times, lowering repair costs, and reducing instrument downtime. It is a class of coating that has the potential to have a significant impact on society [27].

1.3.1. Classification of smart coatings

Smart coatings are a boon to humanity since they reduce human resources waste, maintenance costs, disease prevention, and avert unanticipated mishaps.

1.3.1.1. Smart repair coatings

a) Self-healing coatings

Coatings effectively protect a metal surface from corrosion, but there are chances that this coating can get damaged during shipment, installation, or service, lowering its overall performance [28]. Organic coatings based on epoxy resins were one of the best choices for protecting a metal surface because they prohibit direct contact with oxygen and water. However, standard epoxy coatings fail to prevent the flaw from propagating through the metal matrix when a fracture occurs. As a result, coatings that intelligently respond to damage and avoid degradation material are in high demand [29].

Self-healing coatings belong to the class of intelligent repair coatings inspired by natural wound-healing mechanisms. The concept of self-repair is a prominent feature of the living world that has grabbed the interest of medical and pharmaceutical researchers. Nowadays it is highly relevant in the development of corrosion-resistant materials. Jud and Kausch proposed self-healing in 1979 based on molecular inter-diffusion along with crack interfaces, which White and co-workers further improved in 2001 by incorporating repairing fluids and catalyst grains into the matrix material. These auto-repair coatings have several advantages over conventional coatings, including i) automatic damage repair, ii) auto-preservation of the aesthetics of the coatings and plastic products, and iii) reestablishment of the mechanical integrity of objects that require high strength [30]. Self-healing materials are no longer a pipe dream, and we are not far from a time when artificial materials can reclaim their structural integrity after failure. Building cracks, for example, can close on their own, and scratches on automobile bodies can revert to their previous gleaming appearance [1].

Adding self-healing characteristics to man-made materials might occasionally fail to act without stimulation. As a result, self-healing can be classified into autonomic self-healing and non-autonomic self-healing. Non-autonomic self-healing systems require prompting from the outside to begin their function. While autonomous self-healing doesn't necessitate outside assistance, the damage itself initiates repair mechanisms. There are several methods for obtaining a material’s self-healing capability, like,

- Release of a healing agent or catalyst
- Reversible chemical bonds like a Diels Alder reaction
- Shape memory effect
- Nanoparticle migration
- Co-deposition etc.

The release of healing agents from the matrix is one of the critical steps in a self-healing mechanism. Direct incorporation into the matrix is many times detrimental to the service life of the coating. Thus, inhibitor-holding fillers are used either on the macroscale or the nanoscale. Methods, such as microcapsule embedment, hollow fiber embedment, and microvascular systems, can store the healing agent or monomers. During synthesis, liquid active agents such as monomers, catalysts, dyes, and hardeners are immersed in polymeric systems in micro particles, empty fibers, or channels. These reservoirs are broken in the case of a fracture, and active substances are spilled into the cracks by capillary force, where they solidify with pre-dispersed catalysts and cure the damage. The spread of the crack is the driving factor in this autonomic repair [1]. Major self-healing mechanisms in polymers are described in **Figure 1.2**. The illustration demonstrates how curing species in micro/nanocapsules incorporated in polymer matrices causes auto-repairing [31].

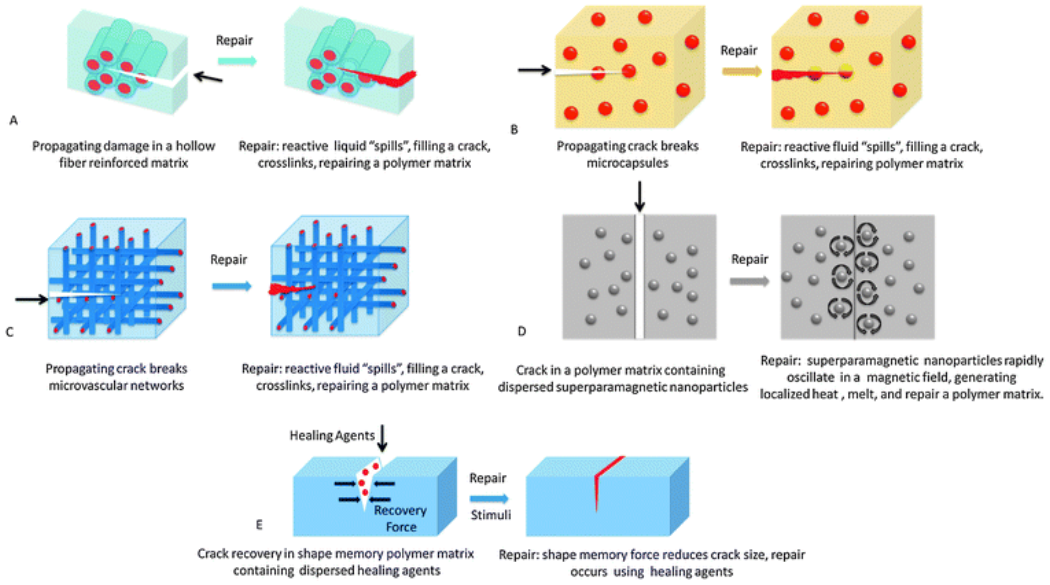

Figure 1.2. (A-E) Self-repairing mechanisms in polymer matrices with healing agents in nanocontainers [31].

1.3.1.2. Active sensing coatings

a) Corrosion sensing coatings

If left unnoticed, the corrosion of metals and alloys will lead to degradation of materials and subsequent loss of structural integrity which may result in accidents and huge economic losses. So, early corrosion detection is the most effective way to prevent all these side effects. The application of corrosion-sensing coatings to the metal surface can avoid structural failure and the high cost associated with maintenance. When a material is first degrading, the corrosion risk is monitored using corrosion sensing coatings. The anodic zone, which experiences corrosion, has an acidic pH, while the cathodic region has an alkaline pH. One of the active study fields is the pH-triggered release of corrosion indicators and healing agents from micro- or nanocapsules. Colourful or fluorescent dyes can be used as corrosion-detecting indicators. By modifying the preparation process and time, the microcapsule or nanocapsules size and pH sensitivity can be managed [32].

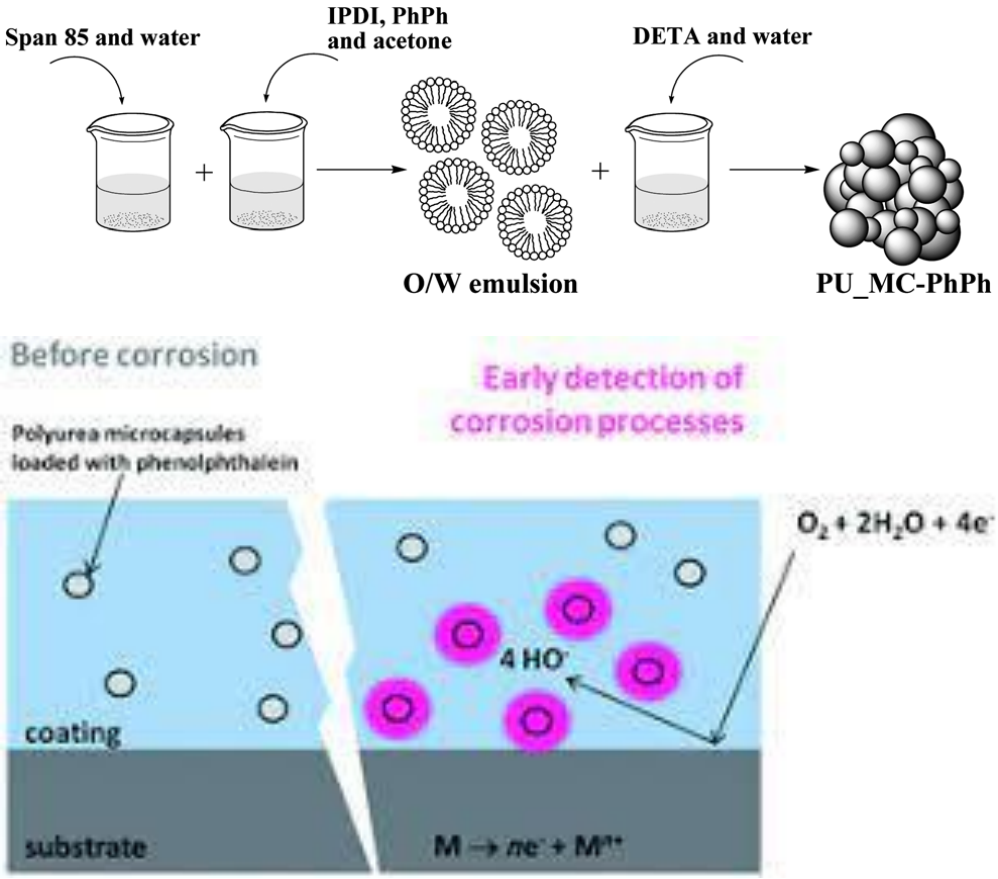

Figure 1.3. Preparation of PU_MC and encapsulation of phenolphthalein, b) mechanism of action of corrosion detection [32].

b) Pressure-sensing coatings

Pressure-sensing coatings have been used on wind tunnel models and flight vehicles to measure the surface pressures for aerodynamic and acoustic investigations. By observing variations in light intensity, it can calculate surface pressure distributions. Most of the time, surfaces are painted with luminous coatings, then stimulated by light of the proper wavelength and photographed using digital cameras [33]. The porous pressure-sensitive paint (PSP), a different type, has a response time of about 1 s and incorporates a binder (a porous substance with a lot of surface area to hold luminophores directly). According to **Figure 1.4**, the ability of oxygen molecules in the test gas to directly extinguish light without entering the binder layer causes the response time. Anodized aluminium, anodized titanium, polymer/ceramic, thin-layer chromatography (TLC) plate etc., have been used as porous materials [34].

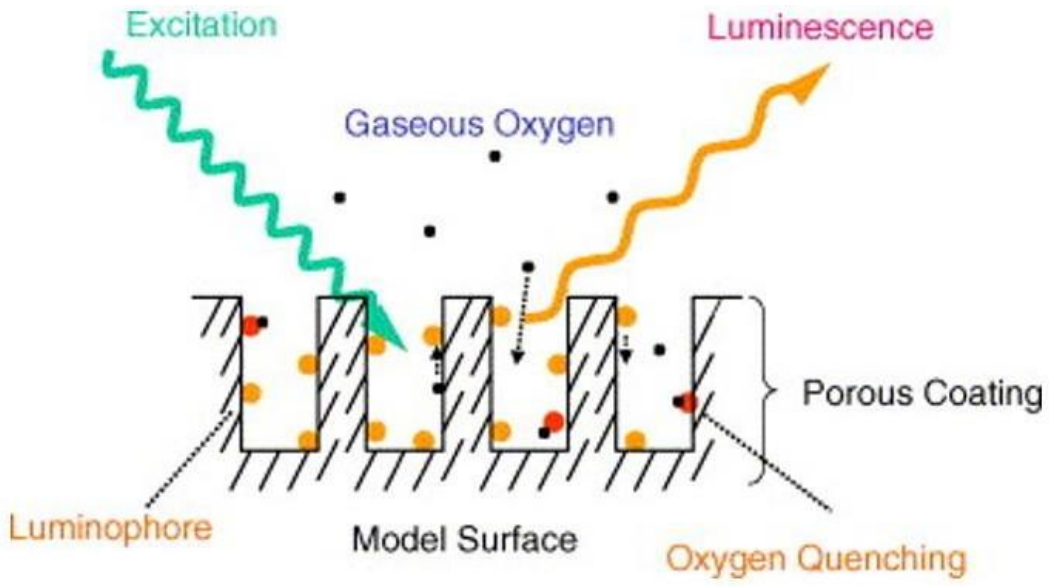

Figure 1.4. Schematic illustration of porous pressure-sensitive paint (PSP) [35]

1.3.1.3.Optically-active coatings

a) Smart window coating

These are thin films with spectrally selective properties on the surface of the glass. Their capacity to control the amount of radiant radiation between large limitations defines them. The term "energy-efficient window coatings" is frequently used to describe these

coatings [36,37]. Smart window coatings are necessary to block the sun's incoming infrared radiation in warm weather while retaining heat within a space in the winter. Since the coatings' active components block both visible and near-infrared light, it is possible to adjust the window settings to optimise the energy efficiency. As a result, procedures that use a lot of energy are considerably reduced. Photochromic coatings, thermochromic coatings, suspended particle devices (SPD), polymer dispersed liquid crystal devices (PDLC), electrochromic coatings, etc., can all be used to create smart window coatings [38,39].

A noteworthy study by Liu et al. was based on the synergistic effect of surface-fluorinated TiO_2 (F-TiO_2) and potassium-doped tungsten bronze (K_xWO_3) powder to produce FT-KWO nanocomposite films for windows. Strong near-infrared, ultraviolet light-shielding, well visible light transmittance, superior photocatalytic activity, and remarkable hydrophilic capacity were all attained with the created films. The multifunctional NIR shielding-photocatalytic nanocomposite window film that has been proposed is intended to address the energy crisis and the environment's deteriorating conditions. In **Figure 1.5**, the working model is described [40].

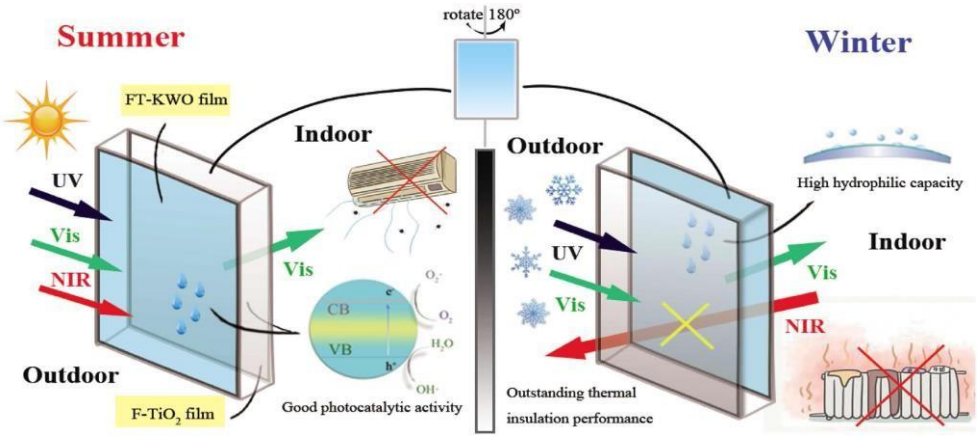

Figure 1.5. Schematic of the FT-KWO and F-TiO_2 coated window applied to different conditions [40].

1.3.1.4. Easy-to-clean coatings

a) Self-cleaning coatings

Using either hydrophilic or hydrophobic strategies, nature-inspired self-cleaning coatings based on surface contact angles provide an autonomous action of dirt removal from a surface. Two different approaches have been used to investigate self-cleaning

surfaces. The first approach includes putting a photocatalytic coating on the substrate surface, which uses ultraviolet light from the sun to break down organic dirt catalytically. At the same time, the surface becomes superhydrophilic, distributing water evenly across the coating and causing dripping to leave fewer drying traces. The idea behind the second self-cleaning method is the Lotus effect phenomenon, where the surface becomes superhydrophobic. The contact angle of water determines the degree of hydrophobicity. Hydrophobic surfaces have contact angles greater than 90^{o}, while superhydrophobic surfaces have contact angles up to 150^{o} or more and repel water droplets altogether [41]. The SEM images of different self-cleaning surfaces and their self-cleaning mechanisms [42] are shown in **Figure 1.6.**

i) ii)

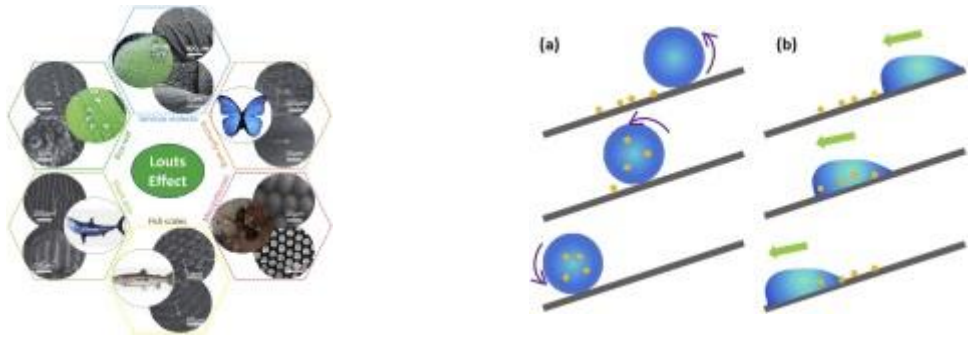

Figure 1.6. (i) Self-cleaning surfaces present in nature and corresponding Scanning Electron Microscope images **(ii)** Lotus effect **(a)** self-cleaning and **(b)** wetting based on contact angle differences.

By roughening the surface of a hydrophobic surface, superhydrophobic coatings can be created. The self-cleaning action of a coating depends on the sliding angle (SA) and water contact angle (WCA); the water drop should slide off from the surface without leaving any trace [43]. Superhydrophobic surfaces with a WCA > 150° and a SA< 10° have potential self-cleaning, anti-fogging, anticorrosion, and oil/water separation applications.

b) Anti-graffiti coatings

Graffiti poses a severe threat to heritage materials and damages a wide range of surfaces resulting in expensive cleaning. In many cases, graffiti penetrate the holes in the substrate, causing permanent damage to the painted area. Anti-graffiti coatings can be prepared by incorporating particle repellent to both water and oil. The resulting surface will be an easy-to-clean surface that can survive repeated graffiti attacks. Fluorinating agents

are an excellent choice for developing anti-graffiti coatings, which will help lower the surface energy by migrating to the surface, preventing the marker paints from adhering [25]. However, the development of a bio-based product is necessary for the prevention of pollution by fluorinated products. Most of the anti-graffiti products available today in the market are siloxane/silicone-based, which are highly hydrophobic and repel water-based pens and markers [44].

c) Anti-smudge coatings

Anti-smudging coatings are used on various substrates, including plastics, glass, metals, and textiles. They have scratch and abrasion resistance and anti-static, easy-to-clean, anti-reflective, and antimicrobial qualities. Anti-smudge technology solutions reduce the likelihood of smudges forming and make cleaning easier, improving customer satisfaction. A coating that repels dirt, oil, and water, reduces fingerprints and makes it easier to clean electronic display surfaces. It is perfect for phones, tablets, watches, displays, and monitors, among other things. Stains on a building's glass curtain wall also impact its aesthetics and lighting, demanding the workforce to clean at high-altitude resulting in high costs and safety risks. Surface morphology, surface chemistry, and interaction with lubricating components are just a few physicochemical properties that can be tweaked to improve anti-smudge capabilities.

1.3.1.5. Bioactive coatings

a) Anti-fouling coatings

The undesirable accumulation and proliferation of plants, microorganisms, animals, and dirt on surfaces immersed in water are known as bio-fouling. Each year, bio-fouling costs billions of dollars to the marine, shipping, and other global industries and cannot be ignored. Micro-fouling and macro-fouling are two types of marine fouling. Corrosion of metallic parts is a detrimental effect of biofouling, destroying structural components and disrupting the system's overall functioning. Two types of antifouling coatings were used to reduce bio-fouling and its impacts. The first is biocide-containing coatings, while the second is biocide-free coatings. Chemically active self-polishing coatings (SPC) contain booster biocides, and fouling release coatings (FRC) with silicone and fluorine coatings eliminate bio-fouling by reducing the surface energy and elastic modulus; this allowed the foulant to be easily removed through simple mechanical cleaning or water movement. However, FRC flops to inhibit biofilm proliferation but does inhibit

attachment of most macro fouling in dynamic conditions [25,45]. Major antifouling coating approaches in the marine environment are given in **Figure 1.7.**

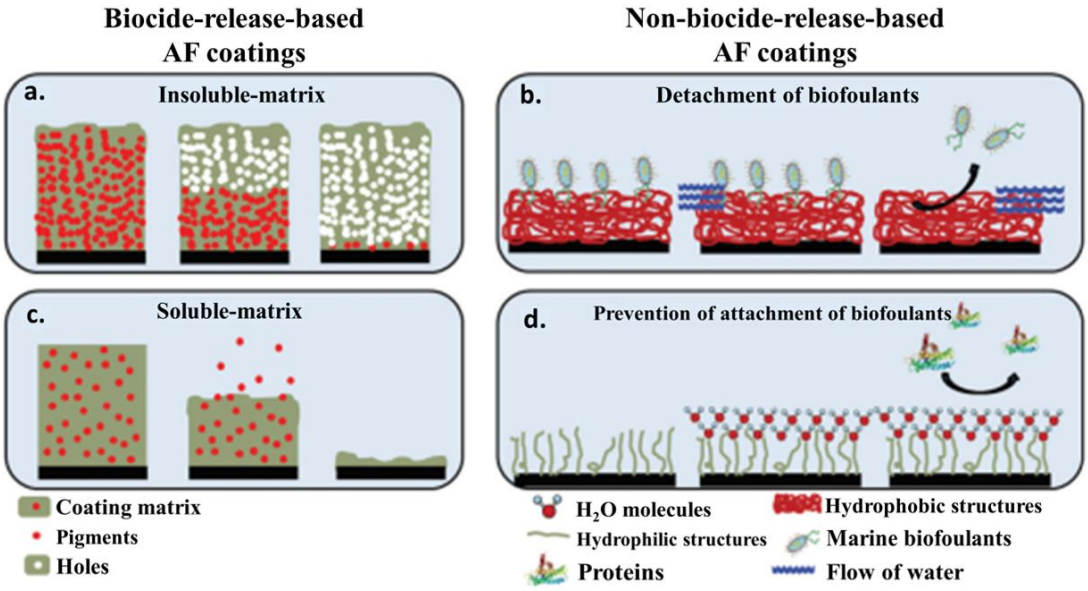

Figure 1.7. (a-d). Antifouling coating approaches in the marine environment [45].

Marine bio-fouling is of great concern because of the substantial economic losses associated with micro and macro colonizing on the shipping hulls, which reduces fuel efficiency and dry-docking operations. Fouling formation has many detrimental effects, but the most important are; increase in fuel consumption by 30-40%, air pollution by emission of greenhouse gases, transport of invasive species, destruction on the hull surface, the damage to underwater structures and bio-corrosion. The coating should be economical and readily available with corrosion inhibition properties, smoothness, and fast drying on application [46,47].

b) Anti-bacterial coatings

Many viruses and bacteria can survive for extended periods in the air or on surfaces. This will transmit the disease through public transportation, hospitals, and other high-touch surfaces in public places, such as floors, walls, and doorknobs. As a result, it is critical to focus on developing coatings that may kill microorganisms by a contact mechanism. The method of action of antimicrobial surface coatings is shown in **Figure 1.8.**

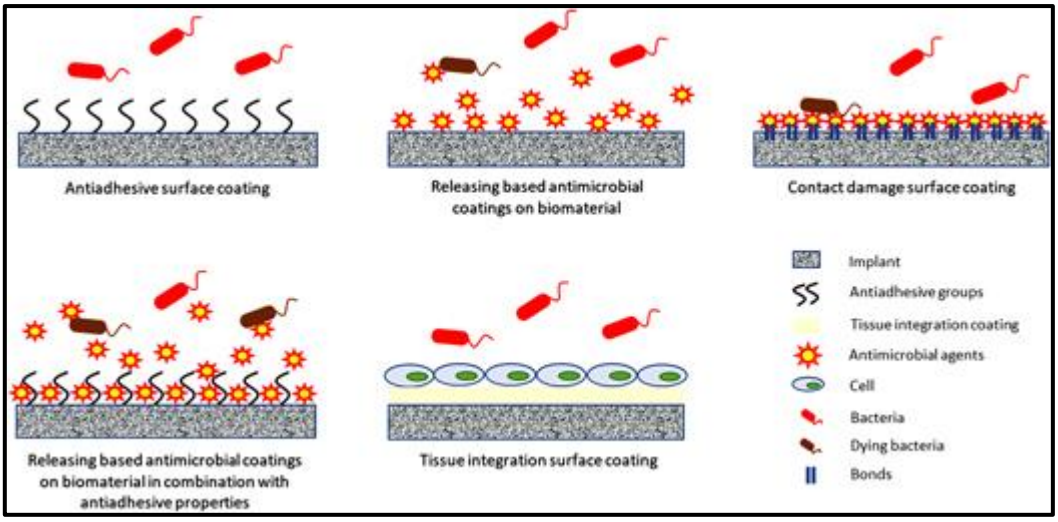

Figure 1.8. Different methods of action of the antimicrobial surface [48].

1.3.1.6. Fire-retardants coatings

Intumescent coatings and non-intumescent coatings are two classes of fire-retardant coatings. Intumescent paints or coatings are used to passively fireproof a structure by slowing the passage of heat from the fire to the internal structure through the surface. This ensures the structural integrity of the buildings and gives us more time to evacuate. Intumescent is utilized in applications such as fire stopping, fireproofing, gasketing, and window casings to provide passive fire protection. Heat exposure causes an intumescent coating to swell, resulting in increased volume and decreased density. They can be used as fireproofing paint on structural parts. Many chemicals are used in intumescent paint, including an acid source, a charring agent, a blowing agent, and a binder. A vital component of an intumescent coating is the binder. Its primary function is to bind all molecules together, but it also serves as a carbon source and impacts the foaming process. The role of various binders, as well as their chemical reactivity, has been studied. When a blend of a linear copolymer with solid reactivity with the acid source and a crosslinked copolymer as the binder in the intumescent paint was used, the thermal insulation significantly increased [49]. From the formulations of water-soluble salts containing phosphate, borax, sulfamate, nitrate, sulphate, boric acid, and halides, the active non-intumescent films discharge fire retarding agents, including gas-phase radicals [50]. These coatings protect the wood, textile, and polymer surfaces more than metal surfaces. In the case of the combination of such matrices, the corrosion-resistant coating can operate as an intelligent coating when exposed to an external heat stimulus.

1.3.1.7. Other smart coatings

a) Anti-reflective coatings

Since the fabled Newtonian age, light transmission and creation have been a field of immense complexity that has perplexed scientists and curious minds. In different optoelectronic devices, anti-reflective coatings have potential usage in photovoltaic solar cells, sensors, display devices, and automobile industries to reduce reflectance, and glare and enhance light transmittance [51]. Anti-reflective coatings (ARCs) are an effective solution for reflectance minimization. The solar panel's top glass cover's anti-reflective coatings, which improved transmission and reduced glare, have been very helpful in this regard.

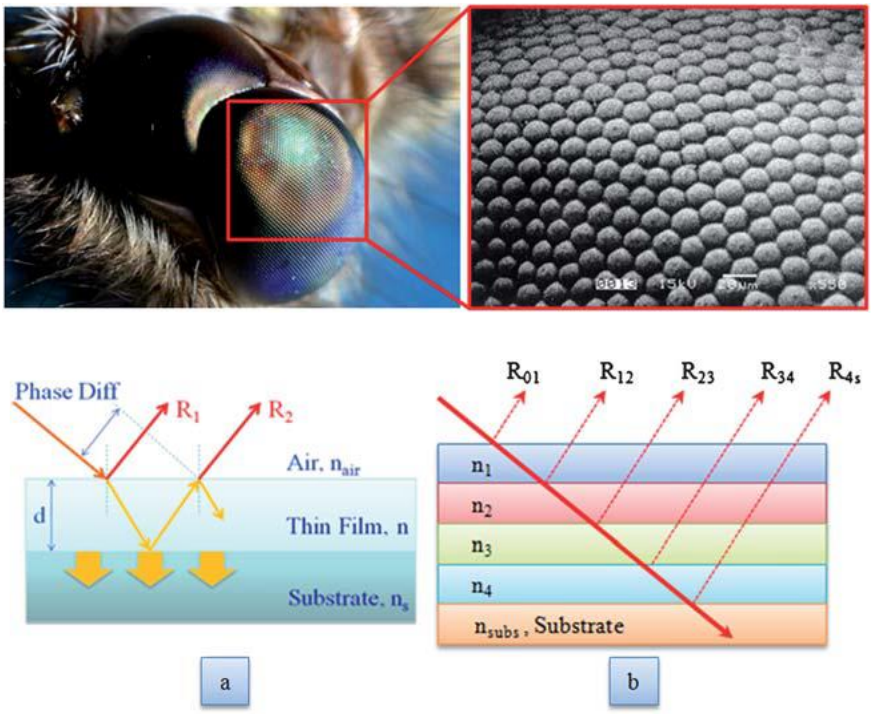

Figure 1.9. a) The eye of the moth **b)** the SEM image (right) showing the nano bumps or protuberances on the outer surface of the corneal lens **c)** Propagation of light rays through (a) a single layer film on a substrate ($n_s > n$) (b) multilayer film on a substrate [52].

The idea of anti-reflectivity originated from nature's optical design for granting conspicuousness or camouflaging to the incredibly wide range of living species. Many anti-reflectance is found in nature itself, and biomimicking of these surfaces led to more excellent inventions. Examples of surfaces that are highly anti-reflective include the bluish colour of Octopus bimaculatus' skin and the metallic to dull green hue of a beetle's cuticle

(interference), zero-order gratings in the cornea of *Zalea Minor* (Diptera), which make it highly anti-reflective (diffraction), and the wings of the butterfly *Arhopala micale* (scattering) [51,52]. The first anti-reflective coatings, were developed by Fraunhofer in 1817 after he discovered that etching a surface in a sulphur and nitric acid atmosphere reduced reflection [52]. Various strategies to produce anti-reflectance surfaces/coatings include porous or patterned surfaces (**Figure 1.9**), gradient surfaces, and multiple layers of coatings.

b) Anti-icing coatings

A large number of problems and economic losses are caused by the icing when supercooled water strikes a solid surface. The formation of this icing from supercooled water is also known as "freezing rain," "atmospheric icing," or "impact ice." This will eventually lead to the glazing of roads, breaking power lines, and stalling of aircraft air foils, etc., causing significant economic losses. The superhydrophobic property can be used to prevent the icing effect. Superhydrophobic surfaces with particle sizes in particular ranges (**Figure 1.10**) have shown anti-icing properties [53]. The ability of superhydrophobic surfaces to trap air effectively limits their ability to interact with liquid water, allowing for the prompt evacuation of condensed and impacting water droplets before they freeze. If the liquid is retained in surface textures as a lubricating layer, it can considerably diminish the adherence of ice that has already formed. As a result, the wind or the ice's gravity could shed the ice [54].

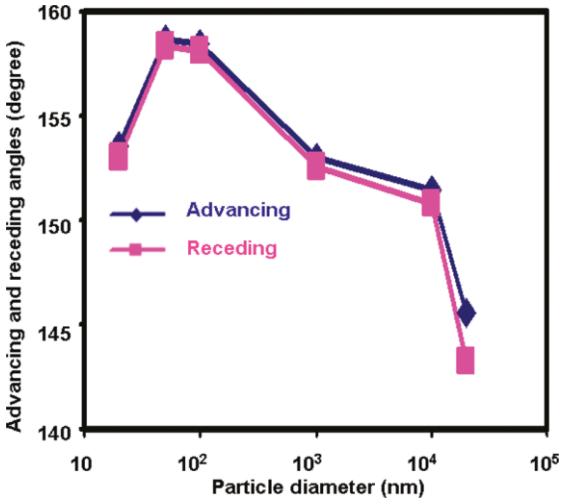

Figure 1.10. Advancing and receding water contact angles of particle-polymer composites as a function of the particle size [53].

c) Anti-fogging coatings

The production of water droplets on transparent solid surfaces is referred to as fogging, and it lowers optical transmission by scattering light. The routine usage of spectacles, goggles, and windshields is significantly hampered by fog. Additionally, fogging decreases the effectiveness of devices like solar energy systems and analytical and medical equipment. Superhydrophilic surfaces with shallow SA values (5°), widely known to prevent water droplets by encouraging the creation of a continuous thin film of water condensed from the air, have attracted much attention in anti-fogging research [55].

The enhancement of anti-fogging properties can also be achieved by improving water repellence by building a micro- or nanostructure onto a low surface-energy material surface with a water contact angle (CA) larger than 150° and a low sliding-off angle of less than 10° (**Figure 1.11**).

Figure 1.11. Illustration of the importance of anti-fogging coatings (https://www.weetect.com/anti-fog-coating/).

1.3.2. Developments in natural product-based smart coatings

Even though many intelligent coatings are developed with synthetic organic and inorganic materials, bio-based equivalents are effective competitors. With the substitution of synthetic components with bio-based components, self-cleaning/healing and anticorrosion coatings have become well-established. Identifying and isolating natural substances and their synthetic derivatives with this multifunctional feature should prioritize future research. The electron cloud is found in unsaturated and aromatic systems, which is

one of the extra benefits of phytochemicals as corrosion inhibitors. Furthermore, bio-based products are undeniably high in carbon. In fire retardant coatings, an enormous amount of carbon in the coating is required [56]. Many plant extracts and phytochemicals have antimicrobial properties, contributing immensely to developing antimicrobial, antifouling, and self-cleaning coatings.

1.3.2.1. Bio-based anticorrosion coatings

Organic coatings create a barrier against the diffusion of oxygen, water, and other harsh ions to the metal surface, thus reducing the rate of corrosion. Organic solvent-based polyurethanes were the prime candidates for corrosion inhibition during the past few decades. Nevertheless, the increasing environmental hazards due to volatile organic compound (VOC) emission, depleting petroleum sources, and health issues associated with petroleum-based epoxy led to the invention of renewable waterborne polyurethanes (WPU). The most promising renewable sources were vegetable oils, which have relatively low prices, low toxicity, and inherent biodegradability. Reactive functional groups are naturally present in some oils, such as hydroxyl in castor oil and epoxy in vernonia oil. Free radical or cationic polymerisation is enough for these vegetable oils to produce polymers without additional chemical modification. However, oils bearing functional groups like esters and double bonds in triglycerides require further chemical modification before converting functional monomers into excellent polymers [57]. However, in the last decades, many hybrid coatings were prepared by effectively incorporating various nanoparticle fillers like ZnO, TiO_2, Cr_2O_3, and Fe_2O_3 to improve the corrosion inhibition efficiency of organic coatings [58].

Hegde et al. created a variety of linseed oil epoxy coatings. Two different hardeners obtained from linseed oil were used to cure epoxidized linseed oil (ELO). The hardeners were produced by reacting linseed oil with maleic anhydride to produce melanized linseed oil (H1), and the second hardener, H2, was produced by reacting H1 with diethylenetriamine in ethyl acetate. Graphene-based fillers in the nanoscale were utilized in various percentages. The percentages of graphene oxide rGO-ELO-H2 coating exhibited superior inhibition efficiency of 99.98% and excellent stability in 3.5 wt.% NaCl. The Nyquist plot in **Figure 1.12** reveals large diameters of the capacitive loops from the graphene filler-loaded biobased coatings strongly indicative of corrosion inhibition. This research demonstrates a simple and environmentally friendly method for integrating

nanofillers into vegetable oil-based coatings, which could be extremely valuable in the coatings and polymer industries [59].

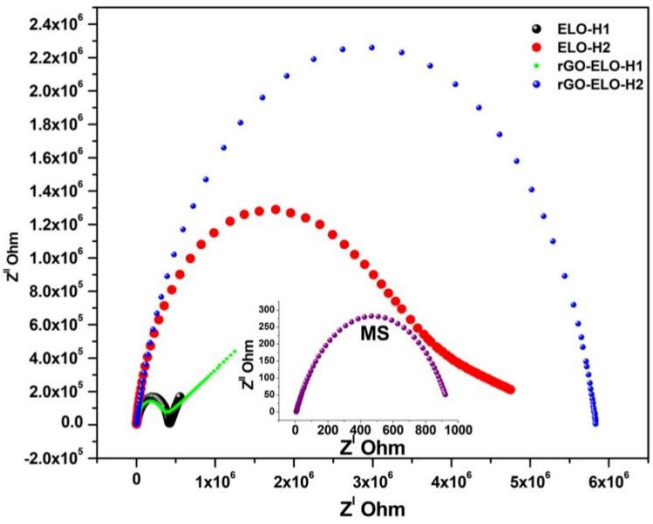

Figure 1.12. Nyquist plot for bare mild steel and coated mild steel coupons after 2 h of immersion in the saline medium [59].

In another study, *Gossypium arboreum* (cottonseed) plant oil was turned into fatty amide and then esterified with various dicarboxylic acids and anhydride of renewable nature to produce a range of polyester amide polyols to substitute petroleum counterparts. Sebacic acid, succinic acid, tartaric acid, maleic acid, and azelaic acid (all isolated from bio-based sources) were among the bio-based renewable dicarboxylic acids and anhydride used in this experiment to replace petroleum counterparts. Compared to petro-based commercial coatings, vegetable oil-based solutions exhibited comparable or greater corrosion inhibition action [60]. **Figure 1.13** represents the corrosion resistance of the bio-based PU coatings on mild steel surfaces in 3.5 wt.% NaCl solution before and after immersion.

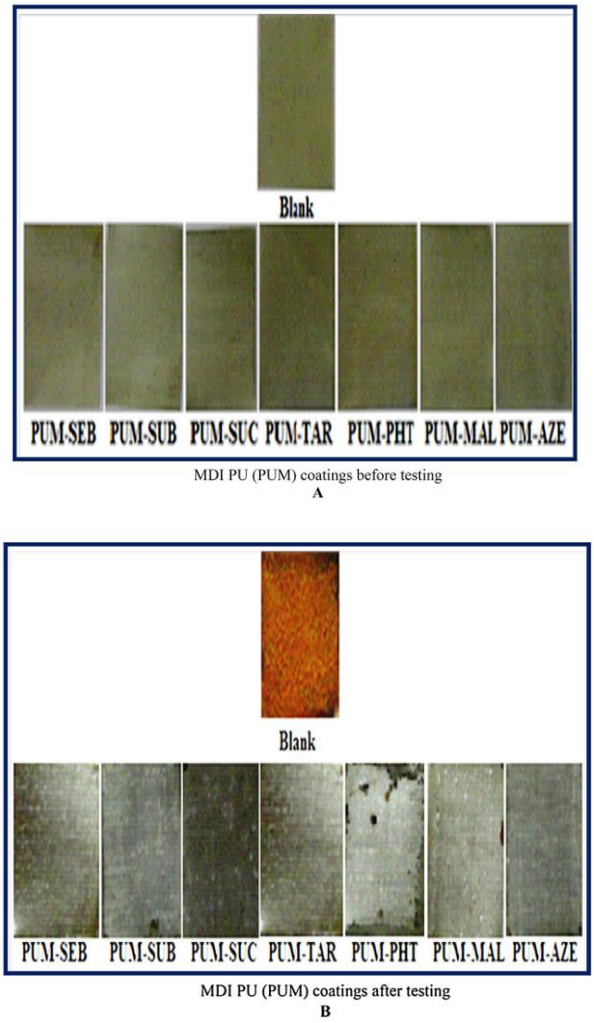

Figure 1.13. The corrosion resistance of different PU coatings on MS surface in saline medium (A-before testing, B-after testing) [59].

Bin Liang et al. developed two types of renewable UV-curable active monomers derived from tung oil: tung-acid-maleic triacrylate (TOAH) and tung-maleic tetraacrylate (TMPG). The two polymers had differing chemical, physical, and mechanical properties. Combining these two bio-based monomers could obtain comparable balanced properties and the best performance in all properties. Pure TMPG addition-cured films were rigid materials with good modulus and thermal stability, whereas pure TOAH addition-cured films had the lowest strength and modulus. To improve the toughness of TMPG and increase the strength of the TOAH, copolymerization of the two active monomers with varied weight ratios was carried out. The UV curing efficacy was evaluated using photo-DSC investigations, and thermogravimetric measurement revealed that the maximum decomposition temperature of the copolymer coatings was all above 420°C. As a result, it

had a faster curing rate, increased hardness, superior thermal stability, and corrosion inhibition [61].

Silva et al. developed a bio-based corrosion-resistant epoxy coating for steel using agricultural waste material. An outstanding waste-to-wealth management demonstration involving direct valorization of the liquid from cashew nutshells (CNSL). For the epoxidation of cardanol and cardol, a solvent-free in situ technique was adopted to get epoxidized cashew nut shell liquid (e-CNSL). The results of different curing agents diethylenetriamine (DETA), isophorone diamine (IPDA), and perfluorodecanoic acid (PFDA) were compared to a standard DGEBA/IPDA coating as a reference. Electrochemical impedance spectroscopy was applied to assess the coatings' anticorrosive capabilities. The findings revealed that e-CNSL-based coatings had much potential as bio-based corrosion prevention coatings and that they could be an excellent alternative to BPA-based products. Due to the chemical composition of CNSL, which combines a phenolic core with a lipidic side chain, the bio-based coatings demonstrated a good balance of flexibility and wettability properties. Excellent chemical resistance, thermal stability, and anticorrosion performance were also achieved, indicating that bio-based coatings could be considered promising sustainable anticorrosive solutions for metal surfaces [62].

1.3.2.2. Bio-based self-healing coatings

The latest advances in bio-based self-repairing films are addressed, with a focus on corrosion resistance. Yixi Chen et al. created a self-healing polymer coating by adding 10% microencapsulated tung oil as a healing agent to conventional epoxy resin. The microcapsules broke when the coating was damaged, releasing tung oil that cured throughout the damaged area. Comparison of mild steel samples with conventional and self-healing coatings in accelerated corrosion tests, samples with self-healing performance at least three times better. Eighty-three percent of the samples showed no corrosion after 150 days of accelerated corrosion examination. Pull-out testing exhibited similar bond stresses as that of normal epoxy coatings [63].

In another significant study, multifunctional waterborne polyurethanes from castor oil with high strength were successfully synthesized by Chaoqun Zhang et al. using dithiodiphenylamine (DTDA). The polymer matrix exhibited high tensile strength up to 38 MPa and self-repairing properties. The films' diverse shape-memory effects, including dual-to quadruple shape memory, were enhanced by the samples' wide glass transition

temperature. Castor oil-based WPU has self-healing properties because of the numerous H-bonds and urethane bonds [24].

Microcapsules with biopolymers derived from cashew nuts and gum arabic were filled via interfacial polymerization. The Q235 steel substrate was protected with an epoxy polymer embedded with these microcapsules. The effectiveness of this composite coating was determined by immersing coated scratched and coated samples without a scratch in seawater and analyzing them with a scanning electron microscope (SEM). The polymer composite's corrosion inhibition efficiency and self-healing property were assessed using surface analytical (SEM) and electrochemical impedance spectroscopy (EIS) techniques. Both polymers suppressed corrosion without a catalyst and showed excellent self-healing properties. The effect was more pronounced with the combined effect of both polymer matrices in a composite [64].

Zheludkevich et al. developed a superior self-healing coating by including a potent inhibitor like cerium ions in a pre-coating of chitosan as a reservoir. The combined result exhibited good corrosion inhibition and self-healing in a localized electrochemical assay [65]. Neem oil, linseed oil, and cardanol are some bio-based materials with self-healing properties currently being researched. Another study discovered that neem oil has exceptional self-healing properties. Another potential mechanism is oxidation in atmospheric oxygen. However, it is barely understood and is thought to be a radical initiated mechanism [66]. The efficiency of linseed oil-filled microcapsules for repairing paint/coating scratches was examined. When linseed oil was discharged under simulated mechanical action, cracks in a paint coating were successfully repaired. Linseed oil healed the region and prevented the substrate from corroding [67]. Samadzadeh et al. investigated the efficacy of encapsulated tung oil. EIS and immersion tests were used to assess corrosion resistance in the healed portion. Tung oil released from shattered microcapsules successfully repaired the artificial crack in the coating [68]. FE-SE images of a ruptured microcapsule containing linseed oil are shown in **Figure 1.14.**

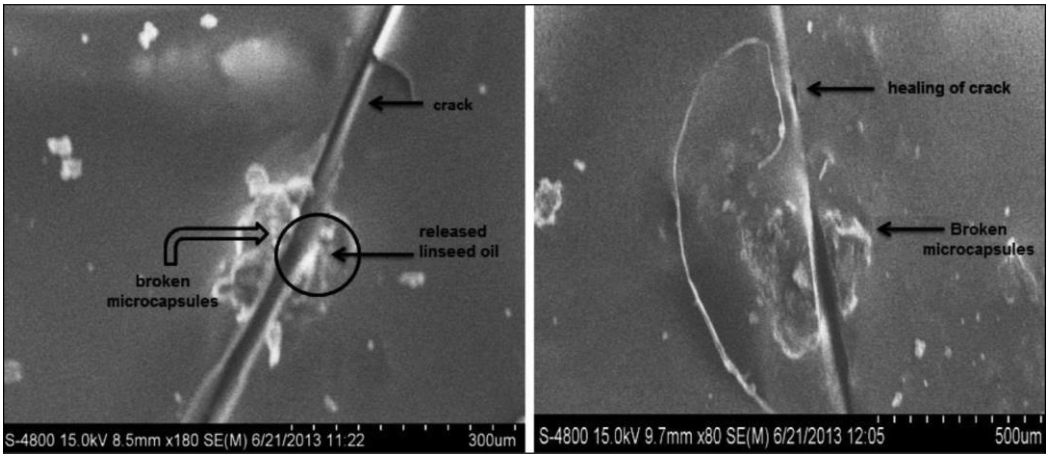

Figure 1.14. FE-SEM images of the Self-healing effect of linseed oil from ruptured microcapsules [66].

Khorasani et al. studied the bio-based self-healing technologies that have been published so far and discovered that coatings with vegetable oils could be made by in-situ polymerization in an oil-in-water emulsion. This process is costly, time-consuming, produces many by-products, and has a low encapsulation yield and reaction efficiency, making it unsuitable for large-scale applications. Electrospray encapsulation can fix the significant synthesis problem, and incorporating a glycidyl group can speed up the healing process [69].

1.3.2.3. Bio-based self-cleaning coatings

Self-cleaning anticorrosive materials with superhydrophobic coatings are incredibly inspiring candidates for improving corrosion performance. In another investigation led by Cheng et al., superhydrophobic polyurethane coatings were prepared from waste cooking oil. The polyurethane prepolymer was developed from waste cooking oil and modified with amino-terminated polydimethylsiloxane (ATP) to obtain a superhydrophobic emulsion. Among various composites of ATP and silicon carbide, the coating with 20 wt.% of particles in polyurethane showed good pull-off strength and thermal conductivity. In addition to the self-cleaning property, the waste oil-based polyurethane coating has good wear resistance, and corrosion inhibition performance can meet the requirements of air coolers in special environments. **Figure 1.15** shows the self-cleaning action of superhydrophobic polyurethane [70]. The WCA and SA are 161^{o} and $3^{o,}$ respectively.

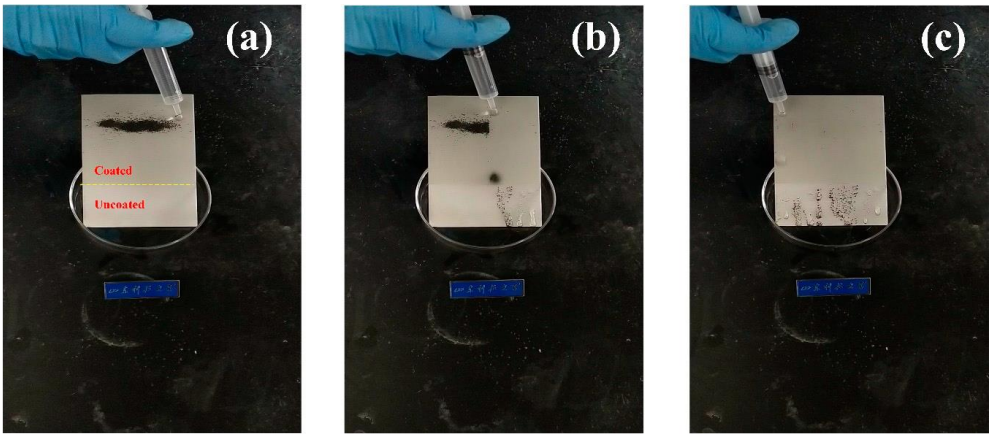

Figure 1.15. Self-cleaning process of the superhydrophobic PU coating. **a**) Before the analysis, **b**) during and **c**) after the investigation.

Atta et al. prepared a self-cleaning superhydrophobic coating with self-healing and anticorrosion properties from a cardanol derivative. Firstly, a Schiff base polymer was made. Cardanol was extracted from cashew nut oil and modified using a bishydrazino-s-triazine derivative, followed by condensation polymerization or reaction with terephthaldehyde. The multifunctional cardanol monomer and polymer were introduced to an epoxy/polyamine hardener solution in various weight percentages. After more than 1500 hours of exposure, all coatings demonstrated better thermal, mechanical, adhesion, and anticorrosion properties than standard epoxy coatings. The 3 wt.% coating has the best self-cleaning and self-healing properties. Coatings increased the contact angle of seawater by more than 150° [71].

The modification of cardanol glycidyl ether with pentaethylenehexamine resulted in hydrophobic polyamine hardeners (PEHA). To make hydrophobic and superhydrophobic epoxy coatings, bisphenol A diglycidyl ether (DGEBA) was cured by dicardanoxy (DCHI) and capped nanoparticles coated on a rough steel surface. Magnetite nanoparticles (Fe_3O_4 NPs) were capped with this to produce superhydrophobic magnetic nanoparticles. According to seawater contact angle measurements, the coating contained DCHI-Fe_3O_4 nanoparticles with a WCA>150°. Excellent adhesion, mechanical, and anticorrosion performances were achieved in salt spray fog analysis of 2000 hours [72].

A superhydrophobic and self-cleaning photoluminescent protein coating was prepared by Xie et al. by incorporating hydrophobic silica nanoparticles in soy protein with some simple chemical reaction steps. The film exhibited fluorescence emission on UV irradiation also resisted wetting by most fluids showing superhydrophobic and self-

cleaning properties. It can resist acid/alkaline corrosion, solvent immersion, and slight mechanical abrasion without losing its basic functional properties [73].

Zheng et al. prepared water-based isosorbide bio-epoxy resin with outstanding hydrophobicity and corrosion protection to eliminate the water absorption and brittleness of standard epoxy coatings without the use of organic solvents. Spin coating was used to coat this epoxy and incorporated superhydrophobic SiO_2 NPs, with a hydrophobic hardener and hexadecyltrimethoxysilane. The coating demonstrated a positive change in corrosion potential from -1.008 V to -0.747 V and a considerable decrease in the i_{corr} value with 92% inhibition efficiency in electrochemical experiments [74]. Zhong et al. used 2-mercaptoethanol-modified castor oil to prepare a self-cleaning coating with anti-graffiti and anti-fingerprint properties [75]. Liang et al. also used epoxidized castor oil to synthesize a corrosion-resistant self-cleaning coating with an organic-inorganic hybrid system with UV curing [76].

1.3.2.4. Bio-based antifouling coatings

Tributyltin and copper compounds have been employed as effective antifouling agents in coatings for decades; however, copper compounds, TBT, and their derivatives have an adverse environmental impact and are not biodegradable. To avoid this, extensive research and development have been done in renewable, eco-friendly, and bio-based antifouling paints and compounds. Many seaweeds and marine vertebrates are found to be devoid of biofilms. This is due to the release of chemicals created by the bacteria that live on them into the environment, which prevents other species from settling. As a result, it proposes that similar bacteria and compounds could be employed instead of TBT and other heavy metal compounds [47].

Bio-fiber-based coatings can perform antifouling functions similar to conventional coatings while minimizing the hazardous base polymer proportion. Antifouling paints have been successfully developed using various natural ingredients as starting materials. Natural antifouling compounds can be found in seaweed, bacteria, algae, corals, sponges, and terrestrial plants, among other things. They use various antifouling methods of physical and chemical control systems, including low drag, wettability, low adhesion, microtexture, chemical secretion, grooming, and sloughing. Tannins are large polyphenolic compounds that have antimicrobial and anticorrosion potential. *Andrographis paniculata* extract and isolated compounds exhibited excellent antibacterial action and anti-biofouling in marine conditions [46].

Jiansen et al. used a thiol-ene reaction and polyaddition to create a bio-based poly(lactic acid)-based PU with hydrolyzable triisopropylsilyl acrylate (TSA) functionality. The coating had high adhesive strength (2.0 MPa) and a slow degradation rate. The polymer coating contains an environmentally benign antifoulant butenolide obtained from marine bacteria, which will give a controlled release when the polymer degrades. Digital holographic microscopy tracking analysis showed the effective antifouling action of the coatings in seawater against Pseudomonas sp. and other marine foulants for more than three months. Within one month, the entire surface of the control was covered with diverse species, primarily tubeworms, bryozoans, and algae, showing significant fouling in the area. On the other hand, the bio-based surface's surface coverage was low even after three months [77].

In another significant study, Somisetti et al. synthesized a natural product-based antifouling polyurethane coating from undecylenic acid, a by-product of castor oil and phosphated cardanol-based polyol. The anti-corrosion and antibacterial properties of the coating were improved by combining the effects of phosphorus and biobased polyol with the components sulfur and nitrogen. For the prepared polyurethane coatings, the corrosion rate was reduced dramatically from 3.010^{-4} to 1.810^{-7} mm per year [78]. The Tafel plots of hydroxylated cardanol (CDPOH) and phosphate cardanol (CDPOH) based polyurethanes are given in **Figure 1.16**.

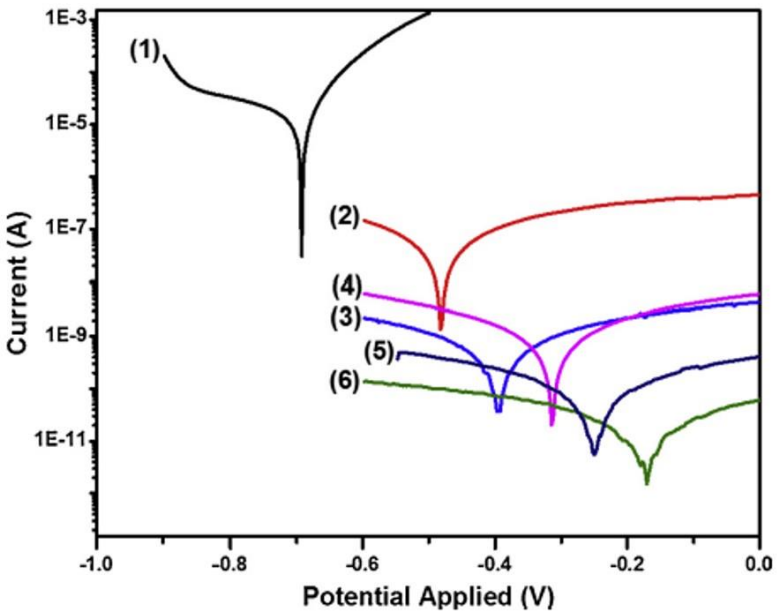

Figure 1.16. Tafel plot of **1)** Bare MS panel, **2)** CDOH-PU, **3)** CDPOH-PU, **4)** CDPOH-5% PU, **5)** CDPOH-15% PU, and **6)** CDPOH-25% PU in 3.5% NaCl.

Natural lacquers have long been utilized as renewable and environmentally beneficial coatings. Chen et al. created a novel fast-curing hybrid lacquer with high adhesion, high barrier performance, corrosion inhibition, excellent mechanical properties, flexibility, and good hardness. Because of the self-enrichment of the amphiphilic telomer, the coating had outstanding fouling-resistant performance against diverse microorganisms and as shown in **Figure 1.17** with the help of fluorescence microscopy [79].

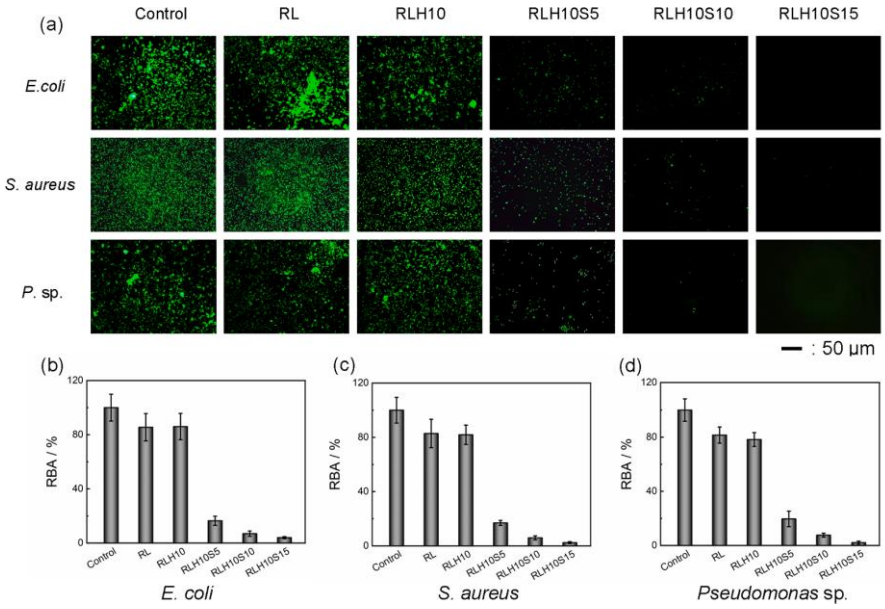

Figure 1.17. a) Fluorescence microscopy images of microorganisms attached to the hybrid lacquer layer when cultured for four hours. Relative bacterial adhesion of **b)** *E. coli*, **c)** *S. aureus*, and **d)** marine bacterium *Pseudomonas* sp.

1.3.2.5. Bio-based antimicrobial coatings

Deacetylation of chitin generates chitosan from crustacean shell waste. Chitosan is used to make a variety of nanocomposites and protective coatings. It has antibacterial and antifungal properties. The interaction between the positively charged amino groups from the chitosan coating and the negative charge on the bacteria's cell membrane, which finally leads to the leaking of cellular components, is the primary explanation for the antibacterial effects. Enzyme deactivation- as a chelating agent, chitosan selectively interacts with metals to inhibit microbial development. Chitosan forms an impenetrable polymeric layer that prevents nutrients from reaching the cell, inhibits protein synthesis, etc. are, the primary mechanism of action of antimicrobial behaviour. Chitosan-based coatings also have excellent corrosion inhibition and self-healing properties [80].

In another significant study, Zhang et al. synthesized vegetable oil-based cationic waterborne polyurethane with long-term antimicrobial coatings with an anticorrosion performance from castor oil and aminoacids [81]. Ulaeto et al. loaded antimicrobial phytochemical Quercetin in mesoporous silica nanoparticles and dispersed it in epoxy. The coatings on Al-6061 alloy showed high corrosion inhibition efficiency and antimicrobial action against *Pseudomonas nitroreducens* [82] (**Figure 1.18**).

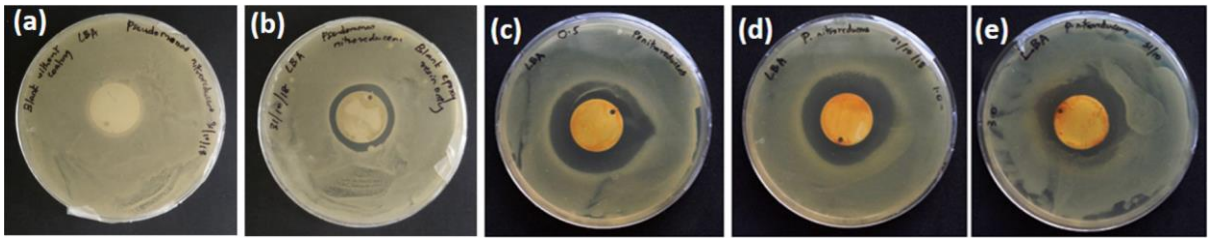

Figure 1.18. Antimicrobial activity of the epoxy layer against *Pseudomonas nitroreducens*; **a)** Control - bare Al **b)** unloaded epoxy on Al, **c–e)** 0.5, 1.0, 3.0 wt. % quercetin composite-epoxy coatings are showing the zones of inhibition [82].

1.3.2.6. Bio-based fire-retardant coatings

The intumescent coatings with different percentages of coconut fibre (CCN), wood waste (MDP), and peach stones (PEA) biomasses were investigated. CCN and MDP had an ideal dry mass percentage of 9%, while PEA had an ideal dry mass percentage of 6%. After fire resistance testing, the coatings expanded by an additional 600% in the case of CCN9, 1300% in the case of MDP9, 1500% in the case of blank, and 1600% in the case of PEA6. The highest temperatures on the back of the material for biomass-based intumescent coatings were 120℃, compared to 474 °C for uncoated steel [56]. Cardanol is classified as an inedible oil, making it an excellent renewable source of feedstock for producing chemicals and materials for various purposes. Although brominated cardanol derivatives have strong fire resistance, brominated derivatives harm the environment. Adding phosphorus atoms to bio-based polymers improves their fire resistance, metal adhesion, and anticorrosion properties significantly [83].

Polypropylene (PP) is a widely used material with superior mechanical strength, electrical insulating properties, and corrosion inhibition, but it is highly flammable. To overcome this defect for application in some fields, Wang et al. synthesized three bio-based salts from three different amino acids, viz. lysine, arginine, and histamine, with phytic acid. The flame retardancy efficiency was analyzed using various methods; in Underwriters

Laboratories test standard UL 94 (UL-94) and Limiting oxygen index study (LOI), it was found that PaArg > PaLys > PaHis; but in cone calorimeter test, the performance was as follows: PaLys > PaArg > PaHis. The efficiency depends on the char forming rate and strength of the formed char. In this aspect, PaArg and PaLys are superior to the other. The second factor affecting the efficiency is the diluting action of the released water, carbon dioxide, and the quenching effect of phosphorous-containing radicals. In this aspect, PaLys has a specific advantage under combustion with a continuous radiation source. This study hopes that using entirely bio-based phytic acid-basic amino acid salt as flame retardants will enable the use of polypropylene with a fire-safety function and outstanding mechanical qualities in many likely fire-causing scenarios [84]. To improve the flame retardance efficiency of PP, Wang et al. employed different phytic acid/piperazine salts (PHYPI). PHYPI displayed good intumescent behaviour with a molar ratio of 1/3 (phytic acid/piperazine) [85].

Zhang et al. created a bio-based epoxy formulation with exceptional flame-retardant properties from itaconic anhydride. Low phosphorus levels considerably increased both the toughness and flame retardancy of epoxy resins in gas and condensed phase flame retardant mechanisms [86]. A novel ricinoleic acid (RA) based phosphorus and nitrogen-bearing flame retardant polyols were successfully formulated by Chu et al. Polyurethane coatings are well-known for their corrosion resistance, but they are also flammable. Fan et al. used melamine starch phytate (PSTM) to turn polyurethane coatings into flame retardant coatings. PSTM promotes thorough charring of PU, which could prevent the foam from combustion [87].

1.3.2.7. Bio-based anti-graffiti coatings

Naturacoat is a sacrificial coating technology developed by Beardow Adam's that offers complete protection against graffiti and pollution, making it ideal for historical and high-profile monuments and locations. It is a paint formulation made from natural polysaccharides and water. It is a sacrificial coating that may be applied with a simple spraying approach. This coating can be easily cleaned if it becomes contaminated or graffiti is spotted by high-pressure warm water around 70°C. This can be applied to Natural stone, brickwork, metals, plastics, ceramics, and marbles [88].

1.3.2.8. Bio-based anti-smudge coatings

Reacting acetylated starch as the polyol and hexamethylene diisocyanate trimer (HDIT) as the hardener, Lei et al. created a bio-based anti-smudge polyurethane coating. Coatings with excellent transparency (>97%) and outstanding anti-smudge qualities can be made by changing the polydimethylsiloxane (PDMS) and Starch content. Liquid pollutants such as inks, water- and oil-based substances can be easily cleaned from the coated surface by "sliding-off," "beading," and "wiping-off" without leaving any traces and marks. The coating's corrosion inhibition performance on a metal substrate was also tested, and it was discovered to be an excellent corrosion inhibitor. As a result, bio-based "green" coatings with omni phobic qualities have the potential to protect surfaces against contamination and corrosion, which is crucial for the long-term development of functional coating materials [89].

1.3.2.9. Bio-based anti-icing coating

Salts, both solid and liquid, are employed in winter for road and surface maintenance because they are good at breaking and preventing the bonding of snow and ice to road surfaces and roofs. Due to the negative impact of salt on buildings and the environment, many alternative materials are being researched for snow and ice control during the winter.

Hydrolysis of starch and other polysaccharides into glucose, followed by hydrogenation and other chemical transformations, can be used to make isosorbide. Zheng et al. created an environmentally benign waterborne hydrophobic bio-epoxy coating by combining dual-scale SiO_2 nanoparticles with (3-glycidyloxypropyl) trimethoxysilane in an aqueous combination containing an isosorbide-based epoxy and a hydrophobic hardener. On an iron foil, a spin-coated sample had a WCA of 153.0 ± 1.1° and a SA of 14.3 ± 1.9°. After sandblasting, it demonstrated outstanding self-cleaning properties and very low dirt accumulation. It exhibited a much lower icing temperature, a significantly longer icing delay time, and a low ice adhesion strength at 0.101 ± 0.019 MPa. The new coating is biobased and environmentally friendly, with potential uses in marine, aircraft, energy harvesting, and sports [90].

Zhong Chen et al. prepared cardanol-derived resins with furfurylamine (FA) or 1,8-diamino-p-menthane (DAPM) as the hardener in solvent-free conditions. The resulting surface exhibited a very low ice adhesion strength at 55.0 ± 5.2 kPa. It also has good

anticorrosive capabilities, as seen by its low i_{corr} and high E_{corr} values. The ice adhesion strength was significantly reduced after PDMS hydrophobization [91].

Ice-phobic surfaces are more practical in real life than anti-icing surfaces. Traditional epoxy coatings were changed by Feng et al. by adding maleic anhydride as a curing agent, as well as a small amount of epoxy resin grafted with fluorine-containing chains. The wettability, adhesion strength of ice on the coated surface and stability of the coating's ice-phobic qualities were all investigated in depth. The modified coating surface became more hydrophobic, requiring less force to remove ice than the unmodified coating surface [92]. The coating surface keeps its hydrophobic and ice-phobic qualities after sanding with abrasive paper. The absence of polar groups is most likely to be responsible for the coating's exceptional and sustainable ice-phobic activity.

1.4. Corrosion Inhibition Mechanism of Natural Product Based Smart Coatings

There are different mechanisms behind the corrosion inhibition action of natural product-based inhibitors. Some may act as cathodic inhibitors, anodic inhibitors, or mixed-type inhibitors. Lowering the rate of diffusion for reactants to the metal surface or lowering the electrical resistance of the surface is another technique [93]. Some other compounds work by their property to make the surface superhydrophobic to minimize the interaction between the surface and water molecule. Some coatings have a self-healing ability that cures the scratches on the surface and prevents further corrosion into the metal lattice. The self-cleaning coatings aid in the anticorrosion mechanism by removing dirt and other impurities from the surfaces, which may otherwise trigger corrosion. The presence of antimicrobial compounds in the coatings can inhibit the corrosion induced by the metabolites of microbes.

The corrosion inhibition potential of the molecules can be attributed to the coordination of lone pairs of electrons to metal. It may be due to a single compound in the extract or it is also possible to be the synergic effect of many molecules present in the system [93]. The action of many inhibitors is by forming a physisorbed or chemisorbed protective film on the metal surface via polar functional groups containing -N, -S, -O and/or conjugated multiple bonds and inhibiting the corrosion-prone surface site [94]. There are a large number of heterocyclic phytochemicals identified in the plant and animal kingdom.

Xin Lai et al. depicted the mechanism of corrosion resistance of green inhibitors by taking chitosan derivatives as an example (**Figure 1.19)**. The major interactions between the inhibitor and the metal involve chemical and physical adsorption, hydrogen bonding and retro donation [95].

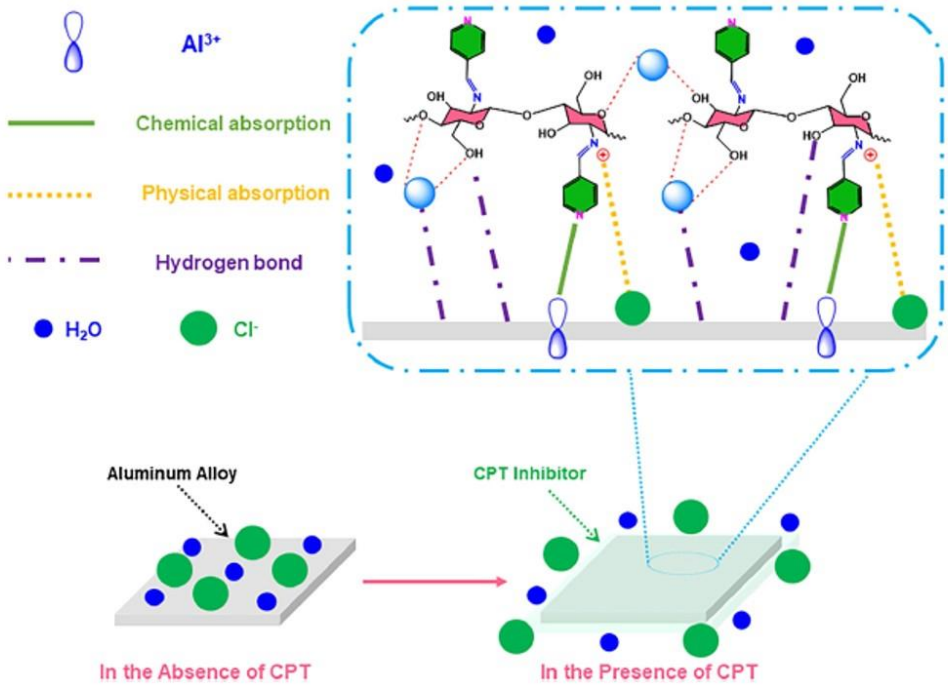

Figure 1.19. The mechanism of action of chitosan derivative (CPT) in corrosion inhibition.

Dahmani et al. studied the anticorrosion property of cinnamon essential oil for copper in 3.0 wt.% of saline medium and identified the constituent responsible and the mechanism of action with the help of Density Functional Theory calculations and Molecular Dynamic studies. The GC-MS analysis reveals that cinnamon oil contains many molecules like α-phellandrene, D-3-Carene, α-terpinene, p-cymene, Limonene, 1,8-cineole, Phenylacetaldehyde, γ-terpinene, acetophenone, Terpinolene, trans β-ocimene, α –Thujone, β –Thujone etc. The amount of electronic transition (ΔN) from the substituent to the metal atom is a key indicator of anticorrosion activity. In recent corrosion inhibition investigations, two novel parameters developed by Gazquez and colleagues, namely electron-donating power and electron-accepting power, have received a lot of attention. These values can be correlated to the HOMO-LUMO concept of the Koopman's Theorem which gives an idea about electron affinity and ionization energy. The MD method can easily anticipate the strength of the interaction between inhibitor compounds and metal surfaces. DFT calculations and MD simulations for trans-cinnamaldehyde, δ-cadinene, and

β-cubebene molecules were done among these identified compounds. All three molecules have the planar structure in the optimized geometry which enhances maximum interaction with the surface. The energy of HOMO also makes some comments regarding the ability of molecules to donate electrons to a low-energy accepting species. The existence of –O atom and π-electrons determines the extent of electron donation in cinnamaldehyde and its interaction with metals. The presence of π-electrons determines the inhibition efficiency of the other two molecules [94].

The important quantum chemical parameters derived from DFT calculations such as EHOMO, ELUMO, energy gap ΔE, polarizability α, electrophilicity ω, nucleophilicity ε, ΔN and electronegativity are the factors controlling the anticorrosion property of all the molecule and the higher rate for cadinene is its correct order of these parameters. Cadinene has lower electronegativity which implies that it tends to discharge its loosely held electrons more easily than the other two compounds. The trend of polarizability indicates that cadinene is easy to polarize than the other two. The order of electrophilicity ω values indicates that cadinene has less tendency to accept the electrons and it is effective against corrosion. The MD simulation showed that the energy of adsorption shows a lower value for cadinene on Cu (**Figure 1.20)**. Both studies reveal the major factors and depending on that the major inhibitor is cadinene followed by cinnamaldehyde along with all other phytochemicals [94].

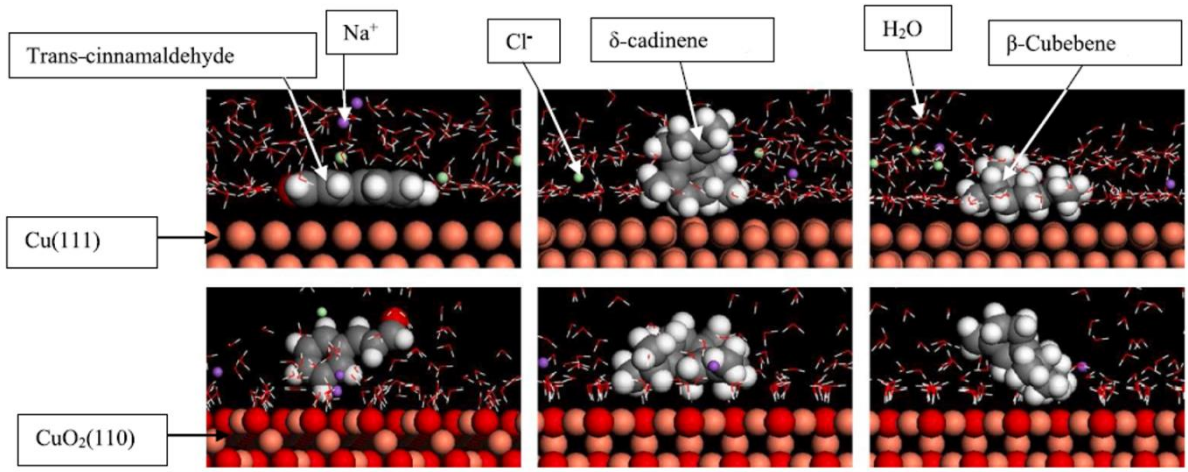

Figure 1.20. Configurations of trans-cinnamaldehyde, δ-cadinene and β-cubebene molecules adsorbed on Cu (111) and CuO_2 (110) in acidified 3.0 wt% saline medium [94].

In another important study, Emeka E. Oguzie et al. shows that a strong chemisorption force was responsible for the interaction between the inhibitor and the metal

surface. They used the chemisorptive interactions between the piperine molecule, the active and primary component of the *piper guineense* extract, and the Fe surface was theoretically modelled using DFT-based quantum chemical computation. The magnitude of the measured adsorption energy shows the piperine molecule's significant chemisorption, confirming the experimental results [96].

1.5. Applications and Commercial Viability of Bio-based Smart Coatings

Medical and healthcare, oil and gas, aerospace, packaging, automotive, consumer electronics, construction, marine, military, energy, textiles, and apparel industries, etc., are among the end-user applications of intelligent coatings. Stimuli-responsive coatings can be designed to suit the needs of individual customers [25]. Easily contaminated surfaces such as motor cars, building walls, fabrics, paper, metals, glass, solar panels, and wooden surfaces can benefit from superhydrophobic self-cleaning coatings to protect them from dirt collection and corrosion attack [97]. These self-cleaning and anti-smudge coatings will save the usage of cleansers and the time paid cleaning everything from personal computers to kitchen surfaces to shower screens.

Anti-fingerprint coatings are in high demand in the automobile industry, thanks to the increasing use of touch panel screens in vehicles. In automotive displays, scratch-proof coatings, anti-fingerprint mirrors, interior surface coatings, wear and corrosion-resistant coatings for engines, lubricant additives, self-cleaning coatings on glass, anticorrosion engine coatings, antimicrobial interior trim, and upholstery coatings, hydrophobic and oleophobic anti-fingerprint coatings are required. A list of some commercialized materials is given below in **Table 1.1.**

Table 1.1. Selected commercially available bio-based smart coatings and coating components.

Products	Characteristics	Applications	Producers
Naturacoat	Bio-based anti-graffiti paint	Bio-based sacrificial protective coating	Beardow Adams www.beardowadams.com
Sigma Air Pure	Renewable natural oil-based protective coating	Protection and indoor air purification	PPG www.ppg.com
UCECOAT®7999	Clear coatings aimed for industrial wood applications	High mechanical and chemical resistance	allnex allnex.com/en
VINNECO®	Bio-based acetic acid derivative	Superhydrophobic coatings	Wacker www.wacker.com
Furalkamine Green epoxy curing agent	Mannich-based hardener derived from pentosane-rich biomass	Specially made for marine coatings	Chemical Process Services Ltd. (Bitrez) www.bitrez.com

1.6. Summary

Bio-based innovative coatings are a hot topic with a lot of unexplored possibilities. Smart or intelligent coatings need critical consideration with a wide range of applications due to the multifunctionality that can be achieved. The list of coatings with smart properties is steadily growing, primarily because dual to multiple functionalities are now possible in most areas owing to natural products that enhance their potential. This chapter emphasizes some of the tasks that these coatings can accomplish in addition to corrosion inhibition with industrial relevance. Recent developments in smart functionalities with inherent corrosion inhibition and the active constituents are discussed. Plant oils and their derivatives, carbohydrate-based polymers, structural polymers, heterocyclic and open-chain

compounds with heteroatom functionalities, etc., showed excellent performance. Isolated phytochemicals, as well as their synthetic modifications, hold a ton of potential. Derivatization can improve the potential to a great extent. Nature still has a library of undiscovered and unexplored molecules with a wide range of properties.

One of the most important techniques in recent developments on smart coatings, primarily for anticorrosive applications, is self-healing coatings using self-healing polymers, UV curing, or reservoirs with healing agents. The triggers can release the healing agent, resulting in a long-term/durable healing effect. Polymers' self-healing properties are based on chemical interactions such as H-bonding, reversible bonds like the Diels Alder reaction etc. Excellent superhydrophobicity with exceptional repellence to various corrosive particles, which is maintained regardless of the metal substrate, is the leading technique for self-cleaning coatings. Aside from the self-cleaning and water resistance features, superhydrophobic surfaces have anti-fouling, anti-icing, anti-scratching, and anti-bacterial properties, all of which help to prevent corrosion.

Within the industry, product development is ongoing, with an emphasis on improved performance, not just to meet client expectations but also to meet regulatory standards. The development of smart coatings from basic academic research concepts to a profitable industrial product remains a major concern. To remove the gap between scientific and technological advancements and future market needs, academics and industry scientists will need to put in a lot more work, time, and collaboration. If we succeed in that, effective multifunctional smart coatings in real-time service will significantly outstrip market expectations without a great increase in market cost. There is a significant opportunity to conduct substantial research in this area. Smart coatings will help in reducing manpower consumption and will improve energy efficiency.

1.7. Scope of Investigation

Anticorrosion coatings made from natural ingredients and their derivatives with a variety of smart properties like self-healing, self-cleaning, anti-smudge, anti-icing, fire retardant, antimicrobial, and so on are the potential and popular topic for current research. Among these coatings, only self-healing and self-cleaning coatings have been thoroughly researched. Other innovative properties of phytochemicals or extracts have yet to be discovered or explored in smart coatings. Nature is an extensive repository of molecules with enormous untapped potential. Studies should focus on finding and isolating natural

compounds and their synthetic derivatives with multifunctional property. Corrosion maintenance costs a lot of money, hence this discovery will have a big impact on a country's GDP and development. One of the most demanding future inventions is a smart coating with several smart properties present altogether in a single system, in addition to corrosion protection. Also, we are living in an era of several pandemics, and the use of sanitizers and disinfectants is not a permanent solution to this problem. The invention of an intelligent antimicrobial coating is a necessity of the time to be used in public places and high-touch surfaces.

Based on the detailed literature study and market survey it was realised that there is an increasing demand for bio-based corrosion inhibitors with no side effects, which are renewable, sustainable, and environmentally friendly. Also, among the smart coatings, studies on bio-based smart coatings are relatively less and very few are available in the market. The stimuli-responsive actions of a smart coating can be achieved by the incorporation of bio-based inhibitor loaded nanocontainer in the polymer matrix. This will further improve the shelf life of the green corrosion inhibitor and its controlled release. A suitable selection of corrosion inhibitors can lead to smart properties like self-healing, antimicrobial and hydrophobicity etc. Among all the polymers available in the market epoxy coatings are most in demand in many industries for different coating applications. Bio-based epoxy derived from vegetable oils is finding potential industrial applications due to its eco-friendliness.

Many organic and inorganic inhibitors with excellent corrosion inhibition potential are being banned nowadays due to their toxicity and non-degradability. Fortunately, there are many bio-based compounds and total extracts which have no side effects towards humans and on nature. In nature, there are different classes of compounds like flavanols, flavonoids, alkaloids, polyphenols, carbonyl compounds, acids, and glycosides of different compounds with high heteroatom density with lone pair of electrons and delocalised π electron cloud. These are excellent candidates to be considered for the development of multifunctional smart anticorrosive coatings.

1.8. Objectives of the Investigation

In the light of the scope of the investigation, the objectives of the present thesis work are:

- Identification & utilization of ecofriendly and easily available bio-mass derived phytochemicals as multifunctional corrosion inhibitors for smart coatings
- Evaluation of crude biomass extract and compounds as corrosion inhibitors for multifunctional smart coatings derived from different plant parts:
    - Marigold floral waste and the marker compound Quercetagetin
    - Bergenin and Malabaricone C from *Vateria indica* leaves and nutmeg
    - Evaluation of synergistic effect on combination of extracts of *Azadirachta indica*, *Andrographis paniculata,* and *Elephantopus scaber*
    - Oxyresveratrol derived from coconut shell (*Cocos nucifera*)
    - Utilisation of vegetable oil (castor oil) for the development of bio-based epoxy
- Synthesis and utilization of porous silica nanocontainer for loading the green corrosion inhibitors
- Development of smart anticorrosive coatings based on biomass-derived additives and their evaluation.
- Incorporation of smart multifunctional properties in barrier epoxy coatings:
    - Self-healing
    - Self-sanitizing
    - Hydrophobicity

References

[1] S.K. Ghosh, Self-Healing Materials: Fundamentals, Design Strategies, and Applications, in: Self-Healing Materials, Wiley-VCH Verlag GmbH & Co. KGaA, Weinheim, Germany, 2008: pp. 1–28. https://doi.org/10.1002/9783527625376.ch1.

[2] Z. Zheng, M. Schenderlein, X. Huang, N.J. Brownbill, F. Blanc, D. Shchukin, Influence of Functionalization of Nanocontainers on Self-Healing Anticorrosive Coatings, ACS Appl Mater Interfaces. 7 (2015) 22756–22766. https://doi.org/10.1021/acsami.5b08028.

[3] Z. Zheng, X. Huang, D. Shchukin, A cost-effective pH-sensitive release system for water source pH detection, Chem. Commun. 50 (2014) 13936–13939. https://doi.org/10.1039/C4CC05597G.

[4] W. Cheng, J. Nie, L. Xu, C. Liang, Y. Peng, G. Liu, T. Wang, L. Mei, L. Huang, X. Zeng, PH-Sensitive Delivery Vehicle Based on Folic Acid-Conjugated Polydopamine-Modified Mesoporous Silica Nanoparticles for Targeted Cancer Therapy, ACS Appl Mater Interfaces. 9 (2017) 18462–18473. https://doi.org/10.1021/acsami.7b02457.

[5] D. Borisova, D. Akçakayiran, M. Schenderlein, H. Möhwald, D.G. Shchukin, Nanocontainer-based anticorrosive coatings: Effect of the container size on the self-healing performance, Adv Funct Mater. 23 (2013) 3799–3812. https://doi.org/10.1002/adfm.201203715.

[6] S.B. Ulaeto, A. V. Nair, J.K. Pancrecious, A.S. Karun, G.M. Mathew, T.P.D. Rajan, B.C. Pai, Smart nanocontainer-based anticorrosive bio-coatings: Evaluation of quercetin for corrosion protection of aluminium alloys, Prog Org Coat. 136 (2019) 105276. https://doi.org/10.1016/j.porgcoat.2019.105276.

[7] S. Akbarzadeh, M. Ramezanzadeh, B. Ramezanzadeh, G. Bahlakeh, Detailed atomic/molecular-level/electronic-scale computer modeling and electrochemical explorations of the adsorption and anti-corrosion effectiveness of the green nitrogen-based phytochemicals on the mild steel surface in the saline solution, J Mol Liq. 319 (2020) 114312. https://doi.org/10.1016/j.molliq.2020.114312.

[8] M. Metikoš-Huković, R. Babić, Z. Grubač, Corrosion protection of aluminium in acidic chloride solutions with nontoxic inhibitors, J Appl Electrochem. 28 (1998) 433–439. https://doi.org/10.1023/A:1003200808093.

[9] M. Zheludkevich, Self-Healing Anticorrosion Coatings, in: Self-Healing Materials, Wiley-VCH Verlag GmbH & Co. KGaA, Weinheim, Germany, 2008: pp. 101–139. https://doi.org/10.1002/9783527625376.ch4.

[10] R.L. Twite, G.P. Bierwagen, Review of alternatives to chromate for corrosion protection of aluminum aerospace alloys, Prog Org Coat. 33 (1998) 91–100. https://doi.org/10.1016/S0300-9440(98)00015-0.

[11] B. Kaufmann, P. Christen, Recent extraction techniques for natural products: microwave-assisted extraction and pressurised solvent extraction, Phytochemical Analysis. 13 (2002) 105–113. https://doi.org/10.1002/pca.631.

[12] S.K. Sharma, A. Peter, I.B. Obot, Potential of Azadirachta indica as a green corrosion inhibitor against mild steel, aluminum, and tin: a review, J Anal Sci Technol. (2015). https://doi.org/10.1186/s40543-015-0067-0.

[13] K.K. Veedu, T.P. Kalarikkal, N. Jayakumar, N.K. Gopalan, Anticorrosive Performance of Mangifera indica L. Leaf Extract-Based Hybrid Coating on Steel, ACSOmega (2019). https://doi.org/10.1021/acsomega.9b00632.

[14] P.B. Raja, M.G. Sethuraman, Natural products as corrosion inhibitor for metals in corrosive media — A review, Materials letters 62 (2008) 113–116. https://doi.org/10.1016/j.matlet.2007.04.079.

[15] B. Qian, M. Michailidis, M. Bilton, T. Hobson, Z. Zheng, D. Shchukin, Tannic complexes coated nanocontainers for controlled release of corrosion inhibitors in self-healing coatings, Electrochim Acta. 297 (2019) 1035–1041. https://doi.org/10.1016/j.electacta.2018.12.062.

[16] J. V Nardeli, C.S. Fugivara, M. Taryba, E.R.P. Pinto, M.F. Montemor, Progress in Organic Coatings Tannin : A natural corrosion inhibitor for aluminum alloys, Prog Org Coat. 135 (2019) 368–381. https://doi.org/10.1016/j.porgcoat.2019.05.035.

[17] B. Zhao, W. Han, W. Zhang, B. Shi, Corrosion inhibition performance of tannins for mild steel in hydrochloric acid solution, Research on Chemical Intermediates. 44 (2018) 407–423. https://doi.org/10.1007/s11164-017-3111-4.

[18] A. Singh, I. Ahamad, M.A. Quraishi, Piper longum extract as green corrosion inhibitor for aluminium in NaOH solution, Arabian Journal of Chemistry. 9 (2016) S1584–S1589. https://doi.org/10.1016/j.arabjc.2012.04.029.

[19] E.E. Oguzie, C.E. Ogukwe, J.N. Ogbulie, F.C. Nwanebu, C.B. Adindu, I.O. Udeze, K.L. Oguzie, F.C. Eze, Broad spectrum corrosion inhibition: corrosion and microbial (SRB) growth inhibiting effects of Piper guineense extract, Journal of Materials science (2012) 3592–3601. https://doi.org/10.1007/s10853-011-6205-1.

[20] Nurul Adilla Rozuli, Tuan Sherwyn Hamidon and M Hazwan Hussin, Evaluation of Piper sarmentosum extract's corrosion inhibitive effects and adsorption characteristics for the corrosion protection of mild steel in 0.5 M HCl, Mater. Res. Express 6 106524 (2019) 0–14.

[21] A.S. Fouda, M.N. El-Haddad, Y.M. Abdallah, Septazole: Antibacterial Drug as a Green Corrosion Inhibitor for Copper in Hydrochloric Acid Solutions, International Journal of Innovative Research in Science, Engineering and Technology (An ISO. 2 (2013) 7073–7085. www.ijirset.com.

[22] C. Kamal, M.G. Sethuraman, Caulerpin □ A bis-Indole Alkaloid As a Green Inhibitor for the Corrosion of Mild Steel in 1 M HCl Solution from the Marine Alga Caulerpa racemosa, (2012).

[23] Prabha AS, Kavitha K, Rajendran S. Inhibition of corrosion of mild steel in simulated oil well water by an aqueous extract of Andrographis paniculata, Indian Journal of Chemical Technology (IJCT). 27(2021) 452-60. https://doi.org/10.56042/ijct.v27i6.33654

[24] C. Zhang, H. Liang, D. Liang, Z. Lin, Q. Chen, P. Feng, Q. Wang, Renewable Castor-Oil-based Waterborne Polyurethane Networks: Simultaneously Showing High Strength, Self-Healing, Processability and Tunable Multishape Memory, Angewandte Chemie International Edition. 60 (2021) 4289–4299. https://doi.org/10.1002/anie.202014299.

[25] S.B. Ulaeto, J.K. Pancrecious, T.P.D. Rajan, B.C. Pai, Smart Coatings, in: S. Mohapatra, T.A. Nguyen, P.B.T.-N.M.-M.O.H.N. Nguyen-Tri (Eds.), Noble Metal-Metal Oxide Hybrid Nanoparticles, Elsevier, 2019: pp. 341–372. https://doi.org/10.1016/B978-0-12-814134-2.00017-6.

[26] J. Baghdachi, Smart Coatings, in: Smart Coatings II, American Chemical Society, 2009: pp. 3–24. https://doi.org/10.1021/bk-2009-1002.ch001.

[27] S. Nagappan, M.S. Moorthy, K.M. Rao, C.-S. Ha, Stimuli-Responsive Smart Polymeric Coatings: An Overview, in: M. Hosseini, A.S.H. Makhlouf (Eds.), Industrial Applications for Intelligent Polymers and Coatings, Springer International Publishing, Cham, 2016: pp. 27–49. https://doi.org/10.1007/978-3-319-26893-4_2.

[28] B. Qian, Z. Song, L. Hao, W. Wang, D. Kong, Self-Healing Epoxy Coatings Based on Nanocontainers for Corrosion Protection of Mild Steel, J Electrochem Soc. 164 (2017) C54–C60. https://doi.org/10.1149/2.1251702jes.

[29] S. Ataei, A. Hassan, P. Azari, B. Pingguan-Murphy, R. Yahya, W.J. Basirun, N. Shahabudin, Electrosprayed PMMA microcapsules containing green soybean oil-based acrylated epoxy and a thiol: a novel resin for smart self-healing coatings, Smart Mater Struct. 29 (2020) 085037. https://doi.org/10.1088/1361-665X/ab9754.

[30] A.K. Guin, S. Nayak, M.K. Bhadu, V. Singh, T.K. Rout, Development and Performance Evaluation of Corrosion Resistance Self-Healing Coating, ISRN Corrosion. 2014 (2014) 979323. https://doi.org/10.1155/2014/979323.

[31] Y. Yang, M.W. Urban, Self-healing polymeric materials, Chem Soc Rev. 42 (2013) 7446. https://doi.org/10.1039/c3cs60109a.

[32] F. Maia, J. Tedim, A.C. Bastos, M.G.S. Ferreira, M.L. Zheludkevich, Active sensing coating for early detection of corrosion processes, RSC Adv. 4 (2014) 17780. https://doi.org/10.1039/c4ra00826j.

[33] James H Bell, Edward T Schairer, Lawrence A Hand, Rabindra D Mehta, Surface pressure measurements using luminescent coatings, Annu Rev Fluid Mech.33: (2001) 155-206, https://doi.org/10.1146/annurev.fluid.33.1.155

[34] J.W. Gregory, H. Sakaue, T. Liu, J.P. Sullivan, Fast Pressure-Sensitive Paint for Flow and Acoustic Diagnostics, Annu Rev Fluid Mech. 46 (2014) 303–330. https://doi.org/10.1146/annurev-fluid-010313-141304.

[35] H. Sakaue, T. Tabei, M. Kameda, Hydrophobic monolayer coating on anodized aluminum pressure-sensitive paint, Sens Actuators B Chem. 119 (2006) 504–511. https://doi.org/https://doi.org/10.1016/j.snb.2006.01.010.

[36] S.M. Babulanam, W. Estrada, M.O. Hakim, S. Yatsuya, A.M. Andersson, J.R. Stevens, J.S.E. Svensson, C.G. Granqvist, Smart Window Coatings: Some Recent Advances, in: C.M. Lampert (Ed.), Proc.SPIE, 1987: p. 64. https://doi.org/10.1117/12.941869.

[37] Y. Li, S. Ji, Y. Gao, H. Luo, M. Kanehira, Core-shell VO_2@TiO_2 nanorods that combine thermochromic and photocatalytic properties for application as energy-saving smart coatings, Sci Rep. 3 (2013) 1370. https://doi.org/10.1038/srep01370.

[38] J.S.E.M. Svensson, C.G. Granqvist, Electrochromic coatings for "smart windows," Solar Energy Materials. 12 (1985) 391–402. https://doi.org/10.1016/0165-1633(85)90033-4.

[39] R. Baetens, B.P. Jelle, A. Gustavsen, Properties, requirements and possibilities of smart windows for dynamic daylight and solar energy control in buildings: A state-of-the-art review, Solar Energy Materials and Solar Cells. 94 (2010) 87–105. https://doi.org/10.1016/j.solmat.2009.08.021.

[40] T. Liu, B. Liu, J. Wang, L. Yang, X. Ma, H. Li, Y. Zhang, S. Yin, T. Sato, T. Sekino, Y. Wang, Smart window coating based on F-TiO_2-K_xWO_3 nanocomposites with heat shielding, ultraviolet isolating, hydrophilic and photocatalytic performance, Sci Rep. 6 (2016) 27373. https://doi.org/10.1038/srep27373.

[41] S.B. Ulaeto, J.K. Pancrecious, T.P.D. Rajan, B.C. Pai, Smart Coatings, in: Noble Metal-Metal Oxide Hybrid Nanoparticles, Elsevier, 2019: pp. 341–372. https://doi.org/10.1016/B978-0-12-814134-2.00017-6.

[42] M. Zhang, S. Feng, L. Wang, Y. Zheng, Lotus effect in wetting and self-cleaning, Biotribology. 5 (2016) 31–43. https://doi.org/10.1016/j.biotri.2015.08.002.

[43] H. Dodiuk, P.F. Rios, A. Dotan, S. Kenig, Hydrophobic and self-cleaning coatings, Polym Adv Technol. 18 (2007) 746–750. https://doi.org/10.1002/pat.957.

[44] I. Bayer, On the Durability and Wear Resistance of Transparent Superhydrophobic Coatings, Coatings. 7 (2017) 12. https://doi.org/10.3390/coatings7010012.

[45] Ayda G. Nurioglu, A. Catarina C. Esteves and Gijsbertus de With, Non-toxic, non-biocide-release antifouling coatings based on molecular structure design for marine applications, J. Mater. Chem. B 3, 6547-6570 (2015), https://doi.org/10.1039/C5TB00232J.

[46] S.K. Kyei, G. Darko, O. Akaranta, Chemistry and application of emerging ecofriendly antifouling paints: a review, J Coat Technol Res. 17 (2020) 315–332. https://doi.org/10.1007/s11998-019-00294-3.

[47] E. Armstrong, K.G. Boyd, J.G. Burgess, Prevention of marine biofouling using natural compounds from marine organisms, in: Elsevier, Biotechnol Annu Rev (2000) 221–241. https://doi.org/10.1016/S1387-2656(00)06024-5.

[48] X. Li, T. Huang, D.E. Heath, N.M. O'Brien-Simpson, A.J. O'Connor, Antimicrobial nanoparticle coatings for medical implants: Design challenges and prospects, Biointerphases. 15 (2020) 060801. https://doi.org/10.1116/6.0000625.

[49] S. Bourbigot, M. Le Bras, S. Duquesne, M. Rochery, Recent Advances for Intumescent Polymers, Macromol Mater Eng. 289 (2004) 499–511. https://doi.org/10.1002/mame.200400007.

[50] S. Liang, N.M. Neisius, S. Gaan, Recent developments in flame retardant polymeric coatings, Prog Org Coat. 76 (2013) 1642–1665. https://doi.org/10.1016/j.porgcoat.2013.07.014.

[51] S. Bashir Khan, H. Wu, C. Pan, Z. Zhang, A Mini Review: Antireflective Coatings Processing Techniques, Applications and Future Perspective, Research & Reviews: Journal of Material Sciences. 05 (2017). https://doi.org/10.4172/2321-6212.1000192.

[52] H.K. Raut, V.A. Ganesh, A.S. Nair, S. Ramakrishna, Anti-reflective coatings: A critical, in-depth review, Energy Environ Sci. 4 (2011) 3779. https://doi.org/10.1039/c1ee01297e.

[53] L. Cao, A.K. Jones, V.K. Sikka, J. Wu, D. Gao, Anti-Icing Superhydrophobic Coatings, Langmuir. 25 (2009) 12444–12448. https://doi.org/10.1021/la902882b.

[54] J. Lv, Y. Song, L. Jiang, J. Wang, Bio-Inspired Strategies for Anti-Icing, ACS Nano. 8 (2014) 3152–3169. https://doi.org/10.1021/nn406522n.

[55] M.W. England, C. Urata, G.J. Dunderdale, A. Hozumi, Anti-Fogging/Self-Healing Properties of Clay-Containing Transparent Nanocomposite Thin Films, ACS Appl Mater Interfaces. 8 (2016) 4318–4322. https://doi.org/10.1021/acsami.5b11961.

[56] M.M. de Souza, S.C. de Sá, A. V Zmozinski, R.S. Peres, C.A. Ferreira, Biomass as the Carbon Source in Intumescent Coatings for Steel Protection against Fire, Ind Eng Chem Res. 55 (2016) 11961–11969. https://doi.org/10.1021/acs.iecr.6b03537.

[57] H. Liang, Y. Feng, J. Lu, L. Liu, Z. Yang, Y. Luo, Y. Zhang, C. Zhang, Bio-based cationic waterborne polyurethanes dispersions prepared from different vegetable oils, Ind Crops Prod. 122 (2018) 448–455. https://doi.org/10.1016/j.indcrop.2018.06.006.

[58] M.M. Aung, W.J. Li, H.N. Lim, Improvement of Anticorrosion Coating Properties in Bio-Based Polymer Epoxy Acrylate Incorporated with Nano Zinc Oxide Particles, Ind Eng Chem Res. 59 (2020) 1753–1763. https://doi.org/10.1021/acs.iecr.9b05639.

[59] M.B. Hegde, K.N.S. Mohana, K. Rajitha, A.M. Madhusudhana, Reduced graphene oxide-epoxidized linseed oil nanocomposite: A highly efficient bio-based anti-

corrosion coating material for mild steel, Prog Org Coat. 159 (2021) 106399. https://doi.org/10.1016/j.porgcoat.2021.106399.

[60] C.K. Patil, S.D. Rajput, R.J. Marathe, R.D. Kulkarni, H. Phadnis, D. Sohn, P.P. Mahulikar, V. V Gite, Synthesis of bio-based polyurethane coatings from vegetable oil and dicarboxylic acids, Prog Org Coat. 106 (2017) 87–95. https://doi.org/10.1016/j.porgcoat.2016.11.024.

[61] B. Liang, S. Kuang, J. Huang, L. Man, Z. Yang, T. Yuan, Synthesis and characterization of novel renewable tung oil-based UV-curable active monomers and bio-based copolymers, Prog Org Coat. 129 (2019) 116–124. https://doi.org/10.1016/j.porgcoat.2019.01.007.

[62] L.R.R. da Silva, F. Avelino, O.B.F. Diogenes, V. de O.F. Sales, K.T. da Silva, W.S. Araujo, S.E. Mazzetto, D. Lomonaco, Development of BPA-free anticorrosive epoxy coatings from agroindustrial waste, Prog Org Coat. 139 (2020) 105449. https://doi.org/10.1016/j.porgcoat.2019.105449.

[63] Y. Chen, C. Xia, Z. Shepard, N. Smith, N. Rice, A.M. Peterson, A. Sakulich, Self-Healing Coatings for Steel-Reinforced Concrete, ACS Sustain Chem Eng. 5 (2017) 3955–3962. https://doi.org/10.1021/acssuschemeng.6b03142.

[64] I.O. Arukalam, E.Y. Ishidi, H.C. Obasi, I.O. Madu, O.E. Ezeani, M.M. Owen, Exploitation of natural gum exudates as green fillers in self-healing corrosion-resistant epoxy coatings, Journal of Polymer Research. 27 (2020) 80. https://doi.org/10.1007/s10965-020-02055-y.

[65] M.L. Zheludkevich, J. Tedim, C.S.R. Freire, S.C.M. Fernandes, S. Kallip, A. Lisenkov, A. Gandini, M.G.S. Ferreira, Self-healing protective coatings with "green" chitosan based pre-layer reservoir of corrosion inhibitor, J Mater Chem. 21 (2011) 4805. https://doi.org/10.1039/c1jm10304k.

[66] A.B. Chaudhari, P.D. Tatiya, R.K. Hedaoo, R.D. Kulkarni, V. V Gite, Polyurethane Prepared from Neem Oil Polyesteramides for Self-Healing Anticorrosive Coatings, Ind Eng Chem Res. 52 (2013) 10189–10197. https://doi.org/10.1021/ie401237s.

[67] C. Suryanarayana, K.C. Rao, D. Kumar, Preparation and characterization of microcapsules containing linseed oil and its use in self-healing coatings, Prog Org Coat. 63 (2008) 72–78. https://doi.org/10.1016/j.porgcoat.2008.04.008.

[68] M. Samadzadeh, S.H. Boura, M. Peikari, A. Ashrafi, M. Kasiriha, Tung oil: An autonomous repairing agent for self-healing epoxy coatings, Prog Org Coat. 70 (2011) 383–387. https://doi.org/10.1016/j.porgcoat.2010.08.017.

[69] S. Ataei, S.N. Khorasani, R.E. Neisiany, Biofriendly vegetable oil healing agents used for developing self-healing coatings: A review, Prog Org Coat. 129 (2019) 77–95. https://doi.org/10.1016/j.porgcoat.2019.01.012.

[70] Y. Cheng, D. Miao, L. Kong, J. Jiang, Z. Guo, Preparation and Performance Test of the Super-Hydrophobic Polyurethane Coating Based on Waste Cooking Oil, Coatings. 9 (2019) 861. https://doi.org/10.3390/coatings9120861.

[71] A.M. Atta, M. A. Ahmed, H. A. Al-Lohedan, A. El-Faham, Multi-Functional Cardanol Triazine Schiff Base Polyimine Additives for Self-Healing and Super-Hydrophobic Epoxy of Steel Coating, Coatings. 10 (2020) 327. https://doi.org/10.3390/coatings10040327.

[72] M.H. Wahby, A.M. Atta, Y.M. Moustafa, A.O. Ezzat, A.I. Hashem, Hydrophobic and Superhydrophobic Bio-Based Nano-Magnetic Epoxy Composites as Organic Coating of Steel, Coatings. 10 (2020) 1201. https://doi.org/10.3390/coatings10121201.

[73] W.-Y. Xie, F. Wang, C. Xu, F. Song, X.-L. Wang, Y.-Z. Wang, A superhydrophobic and self-cleaning photoluminescent protein film with high weatherability, Chemical Engineering Journal. 326 (2017) 436–442. https://doi.org/10.1016/j.cej.2017.05.170.

[74] S. Zheng, D.A. Bellido-Aguilar, Y. Huang, X. Zeng, Q. Zhang, Z. Chen, Mechanically robust hydrophobic bio-based epoxy coatings for anti-corrosion application, Surf Coat Technol. 363 (2019) 43–50. https://doi.org/10.1016/j.surfcoat.2019.02.020.

[75] X. Zhong, L. Lv, H. Hu, X. Jiang, H. Fu, Bio-based coatings with liquid repellency for various applications, Chemical Engineering Journal. 382 (2020) 123042. https://doi.org/10.1016/j.cej.2019.123042.

[76] B. Liang, J. Chen, X. Guo, Z. Yang, T. Yuan, Bio-based organic-inorganic hybrid UV-curable hydrophobic coating prepared from epoxidized vegetable oils, Ind Crops Prod. 163 (2021) 113331. https://doi.org/10.1016/j.indcrop.2021.113331.

[77] J. Pan, Q. Xie, H. Chiang, Q. Peng, P.-Y. Qian, C. Ma, G. Zhang, "From the Nature for the Nature": An Eco-Friendly Antifouling Coating Consisting of Poly(lactic acid)-Based Polyurethane and Natural Antifoulant, ACS Sustain Chem Eng. 8 (2020) 1671–1678. https://doi.org/10.1021/acssuschemeng.9b06917.

[78] V. Somisetti, R. Narayan, R.V.S.N. Kothapalli, Multifunctional polyurethane coatings derived from phosphated cardanol and undecylenic acid based polyols, Prog Org Coat. 134 (2019) 91–102. https://doi.org/https://doi.org/10.1016/j.porgcoat.2019.04.077.

[79] Y. Chen, G. Zhang, G. Zhang, C. Ma, Rapid curing and self-stratifying lacquer coating with antifouling and anticorrosive properties, Chemical Engineering Journal. 421 (2021) 129755. https://doi.org/10.1016/j.cej.2021.129755.

[80] S. Kumar, F. Ye, S. Dobretsov, J. Dutta, Chitosan Nanocomposite Coatings for Food, Paints, and Water Treatment Applications, Applied Sciences. 9 (2019) 2409. https://doi.org/10.3390/app9122409.

[81] H. Liang, Q. Lu, M. Liu, R. Ou, Q. Wang, R.L. Quirino, Y. Luo, C. Zhang, UV absorption, anticorrosion, and long-term antibacterial performance of vegetable oil based cationic waterborne polyurethanes enabled by amino acids, Chemical Engineering Journal. 421 (2021) 127774. https://doi.org/10.1016/j.cej.2020.127774.

[82] S.B. Ulaeto, A. V Nair, J.K. Pancrecious, A.S. Karun, G.M. Mathew, T.P.D. Rajan, B.C. Pai, Smart nanocontainer-based anticorrosive bio-coatings: Evaluation of quercetin for corrosion protection of aluminium alloys, Prog Org Coat. 136 (2019) 105276. https://doi.org/10.1016/j.porgcoat.2019.105276.

[83] H.-X. Ma, J.-J. Li, J.-J. Qiu, Y. Liu, C.-M. Liu, Renewable Cardanol-Based Star-Shaped Prepolymer Containing a Phosphazene Core as a Potential Biobased Green Fire-Retardant Coating, ACS Sustain Chem Eng. 5 (2017) 350–359. https://doi.org/10.1021/acssuschemeng.6b01714.

[84] S. He, Y.-Y. Gao, Z.-Y. Zhao, S.-C. Huang, Z.-X. Chen, C. Deng, Y.-Z. Wang, Fully Bio-Based Phytic Acid–Basic Amino Acid Salt for Flame-Retardant Polypropylene, ACS Appl Polym Mater. 3 (2021) 1488–1498. https://doi.org/10.1021/acsapm.0c01356.

[85] Y.-Y. Gao, C. Deng, Y.-Y. Du, S.-C. Huang, Y.-Z. Wang, A novel bio-based flame retardant for polypropylene from phytic acid, Polym Degrad Stab. 161 (2019) 298–308. https://doi.org/10.1016/j.polymdegradstab.2019.02.005.

[86] J. Zhang, X. Mi, S. Chen, Z. Xu, D. Zhang, M. Miao, J. Wang, A bio-based hyperbranched flame retardant for epoxy resins, Chemical Engineering Journal. 381 (2020) 122719. https://doi.org/10.1016/j.cej.2019.122719.

[87] Y. Xing, Y. Li, Z. Lin, X. Ma, H. Qu, R. Fan, Synthesis and characterization of bio-based intumescent flame retardant and its application in polyurethane, Fire Mater. 44 (2020) 814–824. https://doi.org/10.1002/fam.2877.

[88] M. Adfa, R. Rahmad, M. Ninomiya, S.S. Yudha, K. Tanaka, M. Koketsu, Antileukemic activity of lignans and phenylpropanoids of Cinnamomum parthenoxylon, Bioorg Med Chem Lett. (2015). https://doi.org/10.1016/j.bmcl.2015.12.096.

[89] Y. Liang, D. Zhang, M. Zhou, Y. Xia, X. Chen, S. Oliver, S. Shi, L. Lei, Bio-based omniphobic polyurethane coating providing anti-smudge and anti-corrosion protection, Prog Org Coat. 148 (2020) 105844. https://doi.org/10.1016/j.porgcoat.2020.105844.

[90] S. Zheng, D.A. Bellido-Aguilar, X. Wu, X. Zhan, Y. Huang, X. Zeng, Q. Zhang, Z. Chen, Durable Waterborne Hydrophobic Bio-Epoxy Coating with Improved Anti-Icing and Self-Cleaning Performance, ACS Sustain Chem Eng. 7 (2019) 641–649. https://doi.org/10.1021/acssuschemeng.8b04203.

[91] D.A. Bellido-Aguilar, S. Zheng, Y. Huang, X. Zeng, Q. Zhang, Z. Chen, Solvent-Free Synthesis and Hydrophobization of Biobased Epoxy Coatings for Anti-Icing and Anticorrosion Applications, ACS Sustain Chem Eng. 7 (2019) 19131–19141. https://doi.org/10.1021/acssuschemeng.9b05091.

[92] J. Lv, C. Zhu, H. Qiu, J. Zhang, C. Gu, J. Feng, Robust icephobic epoxy coating using maleic anhydride as a crosslinking agent, Prog Org Coat. 142 (2020) 105561. https://doi.org/10.1016/j.porgcoat.2020.105561.

[93] P.B. Raja, M.G. Sethuraman, Natural products as corrosion inhibitor for metals in corrosive media — A review, Mater Lett. 62 (2008) 113–116. https://doi.org/https://doi.org/10.1016/j.matlet.2007.04.079.

[94] K. Dahmani, M. Galai, M. Ouakki, M. Cherkaoui, R. Touir, S. Erkan, S. Kaya, B. El Ibrahimi, Quantum chemical and molecular dynamic simulation studies for the identification of the extracted cinnamon essential oil constituent responsible for copper corrosion inhibition in acidified 3.0 wt% NaCl medium, Inorg Chem Commun. 124 (2021) 108409. https://doi.org/10.1016/j.inoche.2020.108409.

[95] X. Lai, J. Hu, T. Ruan, J. Zhou, J. Qu, Chitosan derivative corrosion inhibitor for aluminum alloy in sodium chloride solution: A green organic/inorganic hybrid, Carbohydr Polym. 265 (2021) 118074. https://doi.org/10.1016/j.carbpol.2021.118074.

[96] E.E. Oguzie, C.B. Adindu, C.K. Enenebeaku, C.E. Ogukwe, M.A. Chidiebere, K.L. Oguzie, Natural Products for Materials Protection: Mechanism of Corrosion Inhibition of Mild Steel by Acid Extracts of Piper guineense, The Journal of Physical Chemistry C. 116 (2012) 13603–13615. https://doi.org/10.1021/jp300791s.

[97] S.S. Latthe, R.S. Sutar, V.S. Kodag, A.K. Bhosale, A.M. Kumar, K. Kumar Sadasivuni, R. Xing, S. Liu, Self – cleaning superhydrophobic coatings: Potential industrial applications, Prog Org Coat. 128 (2019) 52–58. https://doi.org/10.1016/j.porgcoat.2018.12.008.

Chapter 2

Anticorrosive, Self-sanitizing and Self-healing Smart Coating Using Quercetagetin Derived from Marigold Floral Waste

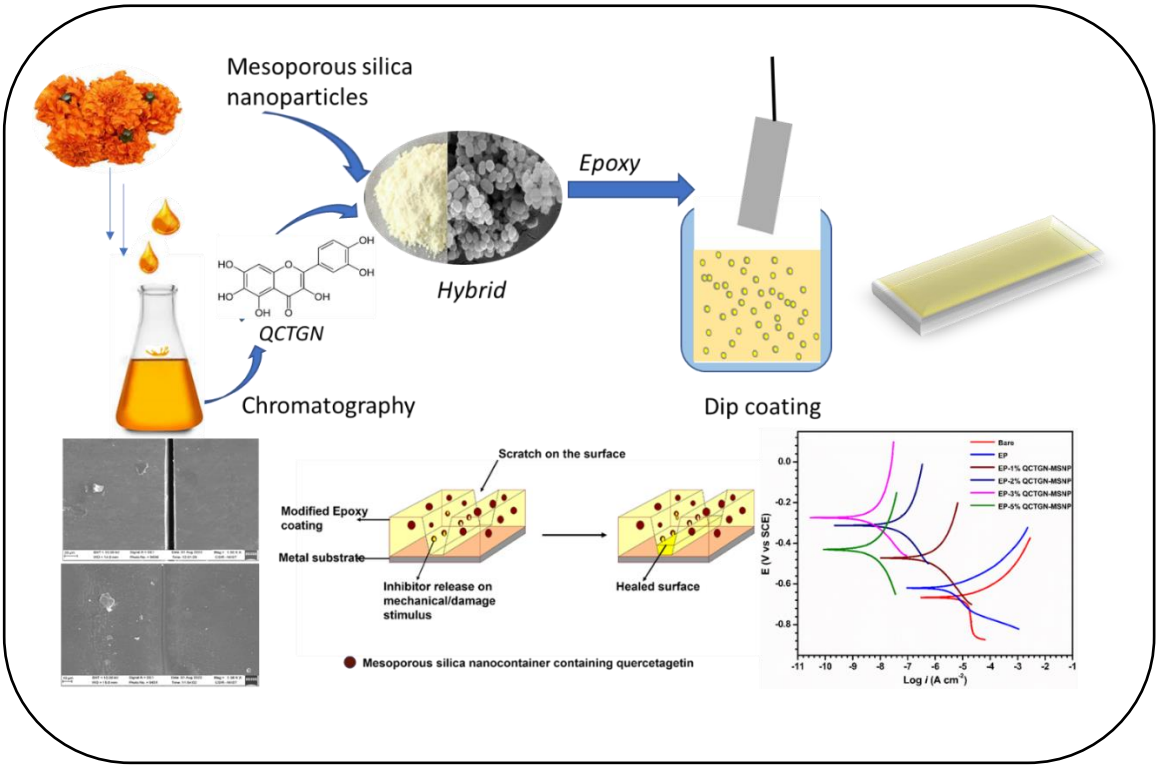

Abstract

A multifunctional smart epoxy coating was developed from marigold flower extract by incorporating mesoporous silica (MSNP) loaded with the marker compound quercetagetin in the polymer matrix. The latter was more active in corrosion inhibition among the hexane and hydroethanolic extracts evaluated. This activity led to isolating the potent green corrosion inhibitor Quercetagetin (QCTGN) from the hydroethanolic extract. Among the various coatings studied with extract and the compound, the matrix containing 3% of the QCTGN-MSNP was found to be most effective for the corrosion prevention of mild steel and Al-6061 alloy in 3.5 wt.% NaCl solution. For mild steel, the Nyquist plot revealed that the charge transfer resistance value increased from 1128 Ω cm^2 to 31240 Ω cm^2. From the potentiodynamic polarisation studies, the E_{corr} value was found to be changed from -0.698 V to -0.274 V, and the i_{corr} value decreased from 12.53 μ Acm^{-2} to 0.006 μ Acm^{-2} with an inhibition efficiency of 99.95% compared to bare alloy. The Al-6061 alloys showed a corrosion inhibition potential of 99.67% compared to bare Al-6061 samples. The coating exhibited antimicrobial properties against gram positive and gram negative bacteria, and complete self-healing was observed within 48 hours.

Keywords: Green corrosion inhibitor Quercetagetin, Smart anticorrosive coatings, Epoxy coating; Antimicrobial coating; Self-healing coating; Marigold extract.

2.1. Introduction

As discussed in the first chapter, corrosion is an unavoidable, spontaneous, and ever-challenging problem in all the industry and engineering fields, leading to financial and safety concerns. The average expenditure of any developing country on corrosion replacements and repair will range between about 3-4% of GDP [1]. For any developing nation, this will drag it down in terms of development, financial stability, and safety of the people. It is impossible to prevent corrosion completely, but we can reduce the corrosion rate using methods like cathodic protection, anodic protection, barrier coatings, etc. Among all these methods, protective coatings are the most widely used, more convenient, and most accepted form of corrosion prevention [2].

Many inorganic and organic inhibitors/ pigments have been reported and used for years but some of them are banned due to toxicity. For instance, chromates and phosphates are banned in many countries due to their carcinogenic and toxic nature. Many organic azoles and amine derivatives are being avoided due to their high cost and non-degradable nature [3]. So, there is a need for a non-toxic, renewable, naturally available corrosion inhibitor all the time. Many plant extracts and individual phytochemicals are reported with excellent corrosion inhibition properties [4]. They have some added benefits; they can impart multifunctional characteristics to the coating, like self-healing, anti-microbial, hydrophobicity, etc.

Nano containers have been used as a targeted delivery agent for drug molecules and corrosion inhibitors for the past few decades. Incorporating this extract or isolated compounds in nanocontainers will help prolong the formulation's shelf life and enable the controlled release of the inhibitor compound [5–7]. Among the various delivery agents, mesoporous silica nanoparticles are ideal for loading green corrosion inhibitors. Depending on the corrosion medium's pH, the inhibitor's release profile from the container varies [8,9].

Incorporating plant extracts and individual phytochemicals into prevailing coating techniques is an interdisciplinary contribution to corrosion protection [10]

In this work, we are focussing on floral waste, a major pollution-causing source. We selected marigold floral waste as our precursor and tried to impart various smart properties to the coating using marigold derivatives. We studied two extracts of marigold floral waste as a waste-to-wealth and green chemistry procedure. We incorporated the most active extract of marigold flower waste and one isolated phytochemical from the most active extract in mesoporous silica nanocontainers, dispersed in epoxy coatings to evaluate its potential as a green corrosion inhibitor composite. In addition to the corrosion prevention ability of MS and Al-6061 alloy, the self-healing potential was also assessed. The quercetagetin-mesoporous silica-epoxy polymer composite exhibited outstanding corrosion resistance and self-healing effects, which have yet to be explored.

2.2. Materials and Methods

2.2.1. Materials

Chromatographic methods were used to isolate the compound quercetagetin from the marigold flower waste extract. cetyltrimethylammonium bromide, tetraethyl orthosilicate, ethanol, hexane, ethyl acetate, and anhydrous n-butanol were purchased from Sigma-Aldrich. Bisphenol A diglycidyl ether (DGEBA), HCl, NaOH, and NaCl were purchased from Merck Specialties Private Limited, India. HY951 hardener was procured from Vantico, India.

2.2.2. Methods

2.2.2.1. Activity-guided isolation of the active compound

Marigold flowers were washed and dried in a hot air oven at 40 ºC for two days. Approximately 750 g of the material was extracted using two different solvents (hexane and a mixture of ethanol and water (80/20 v/v)) at room temperature. The completion of

extraction was ensured by thin-layer chromatography. The collected pool of extracts was concentrated in a rotary evaporator at low pressure and, subsequently, freeze-dried to remove water content. This yielded about 26 g of crude extract in hexane extraction and about 33 g in hydroethanolic extraction. Column chromatography was used further to isolate the marker compound from the active extract.

The phytochemicals in the extracts obtained from various solvents differ in their structure, polarity, and activity. The corrosion inhibition property also depends on the inhibitor compound's structure, polarity, electronegativity, etc. The extract level study was conducted as the preliminary test to identify the most potent compound from the marigold flower, which can be used as the green inhibitor. A low-polarity solvent was used to isolate the low-polar compounds like carotenoids and steroids. A high polarity solvent was used to separate the extract containing polar compounds like flavonoids, alkaloids, acids, and glucosides. Hexane was the low-polarity solvent used, and a 60:40 ethanol-water mixture was the high-polarity solvent chosen for the extraction.

2.2.2.2. Immersion test using selected extract and isolated compound

The mild steel coupons used for the immersion test were 15mm × 15 mm×1mm with a hole to hang the samples to ensure uniform exposure. The marigold-hexane extract and marigold-hydroethanolic extract were investigated for their corrosion inhibition properties in the marine environment. Each dried and weighed specimen was immersed in 200 mL of 3.5 wt.% NaCl solution containing the various concentration of extract at room temperature for 14 days; duplicate samples were also done. There was a sample immersed in a blank NaCl solution for comparison. After 14 days, the substrates were cleaned with double distilled water and acetone and removed all the corrosion products with standard procedure. The weight loss of each sample was calculated from the difference in weight before and after the test. The same method was used for the evaluation of the corrosion

inhibition potential of the isolated compound. The surface morphology was also evaluated in this case for confirmation.

The percentage Inhibition Efficiency (%IE) was calculated from **equation 2.1**

$$\textbf{IE \%} = [(W_0 - W_1)/W_0] \times 100 \quad \text{..... (2.1)}$$

Where W_0 and W_1 are the substrate's weight in the inhibitors' absence and presence [11].

2.2.2.3. Electrochemical impedance spectroscopy and potentiodynamic polarization studies

The hexane extract (MGH) and hydroethanolic extract (MGE) are dispersed in the saline medium at concentrations like 0 ppm, 100 ppm, 200 ppm, and 300 ppm. Polished samples were used as the working electrode, and the electrochemical parameters, inhibition efficiency, etc., were determined. The extract giving better results in terms of E_{corr}, i_{corr}, and R_{ct} will be used for further study in the coating system and the isolation of the active marker corrosion inhibitor compound.

The inhibition efficiency of the inhibitor can be calculated using the following **equations 2.2** and **2.3** [12],

$$\textbf{IE}_{\textbf{EIS}}\ \textbf{\%} = \left[\frac{Rct - R*ct}{Rct}\right] \textbf{x } 100 \quad \text{..... (2.2)}$$

Here,

R^*_{ct} is the resistance offered by the bare sample

R_{ct} is the resistance offered by the coated sample

$$\eta\ \% = \frac{icorr* - icorr}{icorr*} \quad \text{..... (2.3)}$$

i_{corr} and i_{corr}* are the corrosion current densities with and without the inhibitor [12].

2.2.2.4. Synthesis of nanoparticle and bio-nanocomposites

To enhance the shelf-life and controlled release property of the green corrosion inhibitor in the polymer matrix, the active extract, and the isolated compound are loaded in the mesoporous nanoparticles as the same method reported by the authors previously [10,13]. The mesoporous silica nanocontainers were prepared from TEOS by template synthesis method. To 480 mL of DI water, 1G of CTAB was added, and 3.5 mL of 2 M NaOH was added. The solution was kept at 80 °C with a continuous stirring rate of 750 rpm. The precursor TEOS was added to the system in a dropwise manner. After stirring for 2 h, the solution was centrifuged, lyophilized, and the free-flowing white powder calcined at 1000 °C to obtain MSNP. To an ethanolic solution of the inhibitor, container nanoparticles were introduced and kept stirring for 24 h. The ratio between the inhibitor and the container is 2:1 by weight. After 24 h, the solvent was removed in a water bath to obtain the hybrid nanocomposite.

2.2.2.5. Substrate preparation and coating procedure

Mild steel and aluminium-6061 samples of 4×3 cm size was used for electrochemical studies, and 1×1 cm samples were used for immersion tests. All the samples were polished with emery papers ranging from 80-1000 grit size. Degreased with acetone, washed with distilled water, and oven-dried. For aluminium samples, etching was also performed in the acidic and alkaline medium. The polished pieces were kept in a desiccator before the dip-coating procedure to avoid oxidation.

The inhibitor was added to the epoxy in various weight percentages of the total weight of the epoxy and hardener. The inhibitor was dispersed in a minimal amount of butanol, epoxy was added to this and mixed thoroughly. To the homogenous solution, hardener was added (2:1 epoxy: hardener by weight), homogenised, and dip-coated without delay. Allowed to cure at RT for 24 h and later cured at 80 °C for 6 hours.

2.2.2.6. Self-healing and anti-microbial evaluation

The average coating thickness was 34 µm as measured by an optical profilometer. A sharp insertion made an artificial scratch of 0.1 mm thickness razor blade, and the samples were immersed in saline media for a different duration. The SEM images were taken and examined after 0, 12, 24, and 48 h to observe healing potential. A metal disc of 1.7 cm diameter was coated with the modified epoxy formulation. The optimum concentration of inhibitor calculated by the electrochemical method was used for coating and allowed to dry before the activity analysis by the zone of inhibition method. The disc was inoculated with a standardised suspension of the test organism and then incubated for 24 hours at 37 °C. After incubation, the zone of inhibition on the coated disc was measured and compared to the control disc. The size of the zone of inhibition was an indication of the antibacterial nature of the coating. The larger the zone of inhibition, the more effective the coating was in preventing microbial growth.

2.3. Characterization Techniques

Bruker, Ascend 500 MHz NMR Spectrometer (Bruker India Scientific Pvt Ltd.) was used for the structural confirmation of the isolated molecule. PerkinElmer FTIR (PerkinElmer Singapore Pte Ltd.) was used for the functional group identification of the extracts, compound, and prepared nanoparticles. FEI Tecnai G2, T30 was used to capture the TEM micrographs of the nanoparticles. FE- SEM, FEI NOVA NANOSEM 450 was used for the SEM micrographs of the nanoparticles, and Zeiss EVO 18 cryo-SEM Special Edition was used for the SEM micrographs of the metal surfaces and EDS analysis. The N_2 adsorption-desorption procedure was monitored with the help of Micromeritics, Tristar II (USA). The release profile of the inhibitor from the container was evaluated with a Shimadzu UV-27000i UV-Visible spectrophotometer. CH Instruments electrochemical workstation (CHI608E) was used for the EIS and PP studies with a three-electrode system

for coating evaluation. The impedance measurements were performed using an AC signal with a perturbation of 5 mV at OCP in the frequency range of 100 kHz-0.01 Hz. ZsimpWin software fits the generated EIS plots to determine the electrochemical parameters. Numerous circuits were examined until the Chi-square value decreased to less than 9×10^{-4} or no further fitting improvement was observed. We compared all potentials to SCE. At a scan rate of 1 mV/s, cathodic and anodic polarisation curves were observed from -250 mV to +250 mV of the OCP values. Tafel extrapolation method was used to find the i_{corr} and E_{corr}.

2.4. Results and Discussion

2.4.1. Immersion test for the two selected extracts to compare the potential by weight loss measurements

The weight loss of each immersed sample in the presence of the two extracts in various concentrations was determined, and corrosion inhibition efficiency was calculated. The hydroethanolic extract was found to be a more active corrosion inhibitor than the hexane extract, which is depicted in the weight loss diagram (**Figure 2.1**), and the inhibition efficiency is provided in **Table 2.1**. From the average weight loss and calculated corrosion inhibition efficiency, the hydroethanolic extract is found to be more active for metal surface protection in the marine atmosphere. The slight decrease in inhibition efficiency at higher concentrations may be due to the possible peel of the physically adsorbed extract at the more increased thickness.

Table 2.1. Comparison of corrosion inhibition efficiency of the two extracts at various concentrations

Test solution	**Average weight loss (g)**	**Inhibition efficiency** $IE_{\%} = [(W_0-W_1)/ W_0] \times 100$ **(%)**	**Surface coverage**
3.5 wt.% NaCl	0.0228	-	-
MGH 0.1 G/L	0.0145	61.31	0.613
MGH 0.5 G/L	0.0081	64.47	0.645
MGH 1.0 G/L	0.0099	56.57	0.566
MGE 0.1 G/L	0.0101	55.70	0.557
MGE 0.5 G/L	0.0046	79.82	0.798
MGE 1.0 G/L	0.0075	67.10	0.671

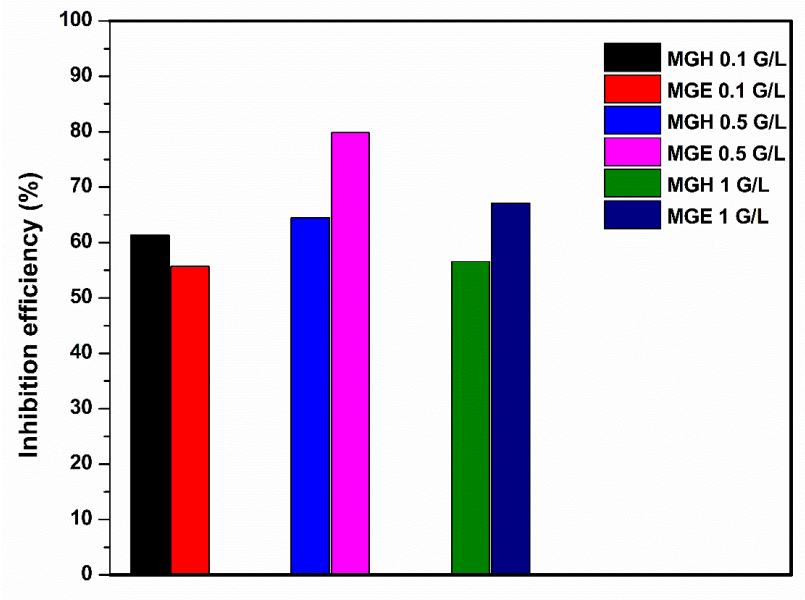

Figure 2.1. Comparison of inhibition efficiency of two extracts at various concentrations

2.4.2. Comparison of corrosion inhibition potential of the extract EIS and polarisation studies

In agreement with the weight loss/ immersion test results, potentiodynamic polarisation and EIS studies also revealed the superior corrosion inhibition efficiency of the MGE extract over the MGH extract. Both extracts at lower concentrations showed a minimal change compared to bare mild steel. At a higher concentration of 200 ppm, both extracts showed a considerable difference in the E_{corr}, i_{corr}, and R_{ct} values **(Table 2.2**). The effect was more prominent in the case of hydroethanolic extract. Even though the i_{corr} values decreased considerably for the hexane extract, the E_{corr} values shifted to a more negative side. Also, both the extracts at higher concentrations showed a slightly negative shift in terms of i_{corr}, E_{corr} and R_{ct} values resulting in a marginally lower inhibition efficiency than 200 ppm. The desorption of the physically adsorbed layer at the higher concentration is the reason for this shift.

In the electrochemical impedance measurements, the presence of the extracts was found to have a positive effect on the resistance arc of the samples. The bare MS samples can be fitted using the equivalent electrochemical circuit (EEC) $R_s(C_{dl}R_{ct})$, where R_s is the resistance offered by the solution, C_{dl} is the double-layer capacitance, and R_{ct} is the charge transfer resistance. In the presence of the extracts, the Nyquist plot fitted well for the EEC of $R_s(C_fR_f(C_{dl}R_{ct}))$. Here the new elements C_f and R_f stand for the capacitance and the resistance offered by the film formed on the surface of the metal substrate [14]. This film formation suggests the physisorption of the active molecules on the metal surface by coordinating bonding with the metal and the lone pair of electrons and pi electrons in the active molecule. Both extracts show the maximum protection by the coating formation at 200 ppm concentration, in agreement with the observations from the Tafel plot (**Figure 2.2**).

Based on these two studies, the hydroethanolic extract was chosen for further studies for the incorporation in the polymer coating and the isolation and evaluation of the marker compound, which might be the reason for the activity of the total extract. The hexane extract behaved as a cathodic-type inhibitor, and the hydroethanolic extract acted as an anodic-type inhibitor.

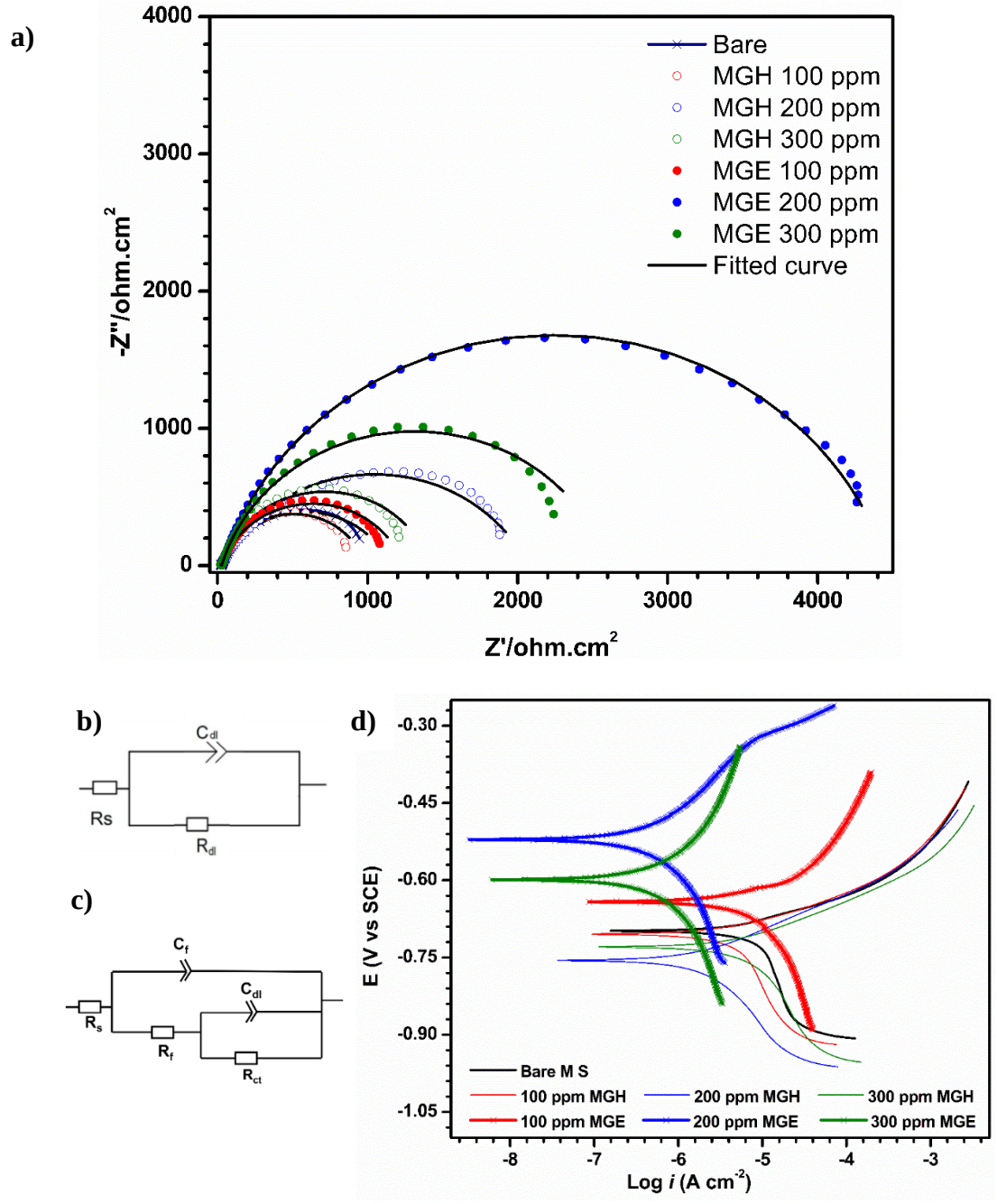

Figure 2.2. Comparison of hexane and ethanol extracts' corrosion inhibition potential by potentiodynamic polarisation studies and electrochemical impedance spectroscopy

Table 2.2. Electrochemical parameters obtained and corrosion inhibition efficiency of hexane and hydroethanolic extract

S/N	Substrate	Potentiodynamic polarisation			EIS	
		E_{corr} (V)	i_{corr} (μ Acm^{-2})	η (%)	R_{ct} (Ω cm^2)	IE_{EIS} (%)
1.	Bare mild steel	-0.698	12.53	-	1128	-
2.	100 ppm MGH	-0.705	5.609	55.23	969.9	-
3.	200 ppm MGH	-0.756	1.902	84.82	2062	45.3
4.	300 ppm MGH	-0.729	6.495	48.16	1410	20
5.	100 ppm MGE	-0.642	11.550	7.82	1239	8.9
6.	200 ppm MGE	-0.521	0.6002	95.20	4465	74.73
7.	300 ppm MGE	-0.599	0.8505	93.21	2598	56.58

2.4.3. Identification and efficiency evaluation of the marker compound present in the extract

2.4.3.1. Isolation and characterisation of the marker compound quercetagetin from MGE

The extract was adsorbed in silica gels and loaded into a silica gel column eluted with varying ethyl acetate and hexane mixture polarities. At 90% ethyl acetate-hexane elution, the compound was obtained as a pale yellow amorphous solid. Its molecular formula was determined as $C_{15}H_{10}O_8$ [calculated as 319.0454 $[M+H]^+$ and observed as 319.0463 from HR ESI-MS. The ^{1}H-NMR spectrum of the compound exhibited signals at δH 6.50 and 7.73 ppm, which were indicative of the presence of H-8 and H-2' protons, respectively. H-5' and H-6' protons of ring B appeared at δ 7.62 (d, J = 8.5 Hz) and 6.88 (d, J = 8.4 Hz),

respectively. The ^{13}C NMR displayed eleven quaternary and four methine carbons. The resonance at δ 92.90 was assigned to the C-8 position, while the 13C-NMR signal at δ 114.6 was assigned to C-2'. The structure was confirmed by comparison with the literature[15], and the structure of the compound is shown below in **Figure 2.3**.

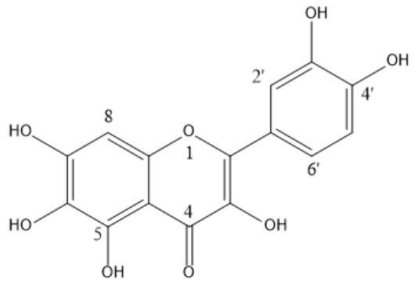

Figure 2.3. Structure of quercetagetin

^{1}H NMR (500 MHz, MeOD): δ_H 7.73 (s, 1H), 7.62 (d, J = 8.5 Hz, 1H), 6.88 (d, J = 8.4 Hz, 1H), 6.50 (s, 1H). ^{13}C NMR (125 MHz, MeOD): δ_C 175.96 (C-4), 153.22 (C-7), 149.71 (C-9), 147.28 (C-4'), 146.70 (C-5), 145.44 (C-2), 144.79 (C-3'), 135.47 (C-3), 128.34 (C-6), 122.94 (C-1'), 120.24(C-6'), 114.79(C-5'), 114.59 (C-2'), 103.39 (C-10), 92.90 (C-8). The ^{1}H-NMR and ^{13}C NMR spectra are shown in **Figure 2.4**.

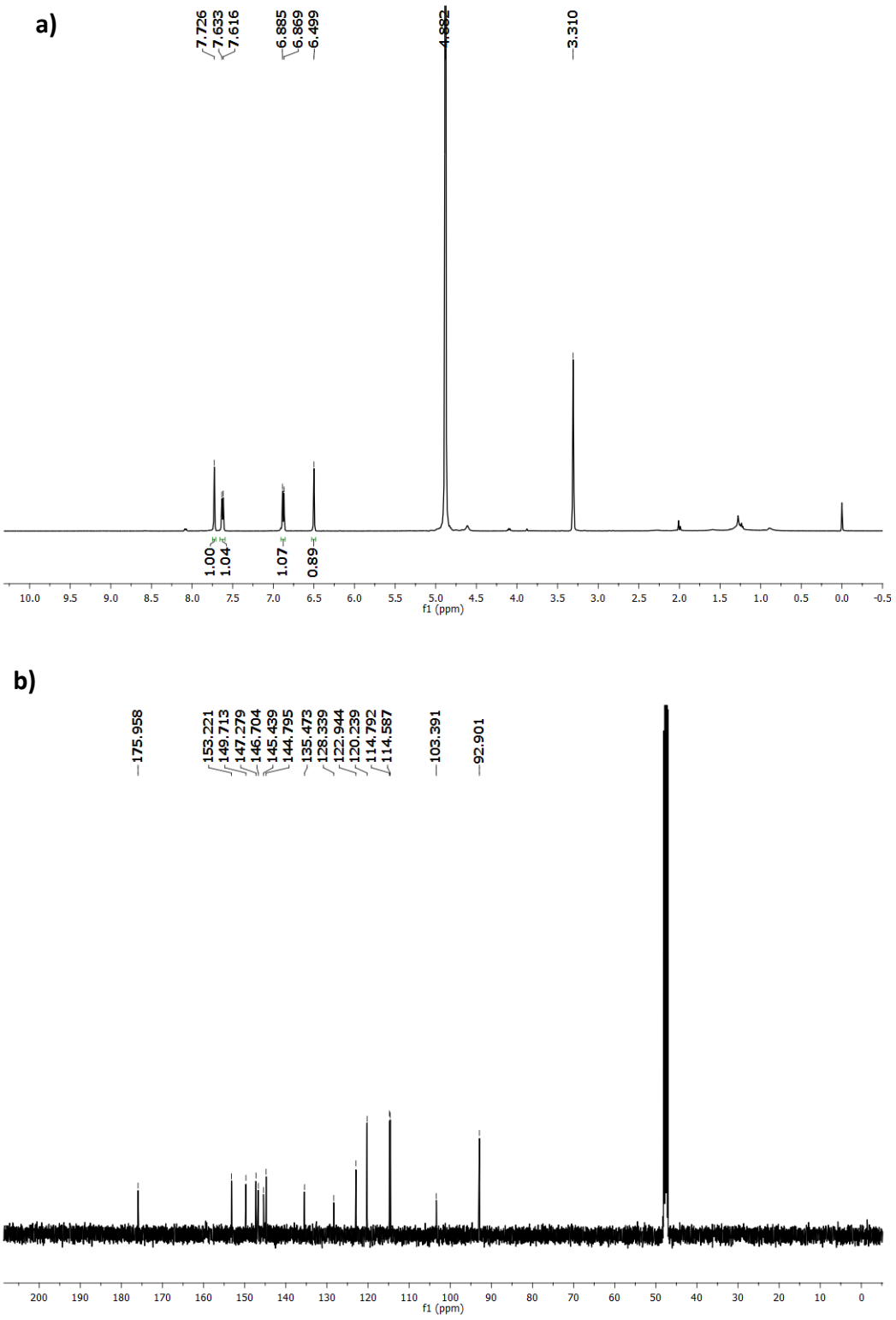

Figure 2.4. a) ^{1}H and **b)** ^{13}C NMR spectrum of quercetagetin in MeOD

2.4.3.2. Immersion and surface topology analysis of quercetagetin as a green corrosion inhibitor

To ensure the efficiency of the quercetagetin molecule as a corrosion inhibitor before the preparation of the nanoparticles and its incorporation in the polymer matrix, the quercetagetin molecule is added to the corrosion saline medium, and the polished mild steel plates are immersed and tested for 15 days. The weight loss and surface topology evaluation was made for the mild steel samples immersed in the saline medium in the presence and absence of the compound. The amount of corrosion products formed can be understood from the elemental analysis; as expected, the presence of quercetagetin reduced the amount of oxide formed (**Figure 2.5**).

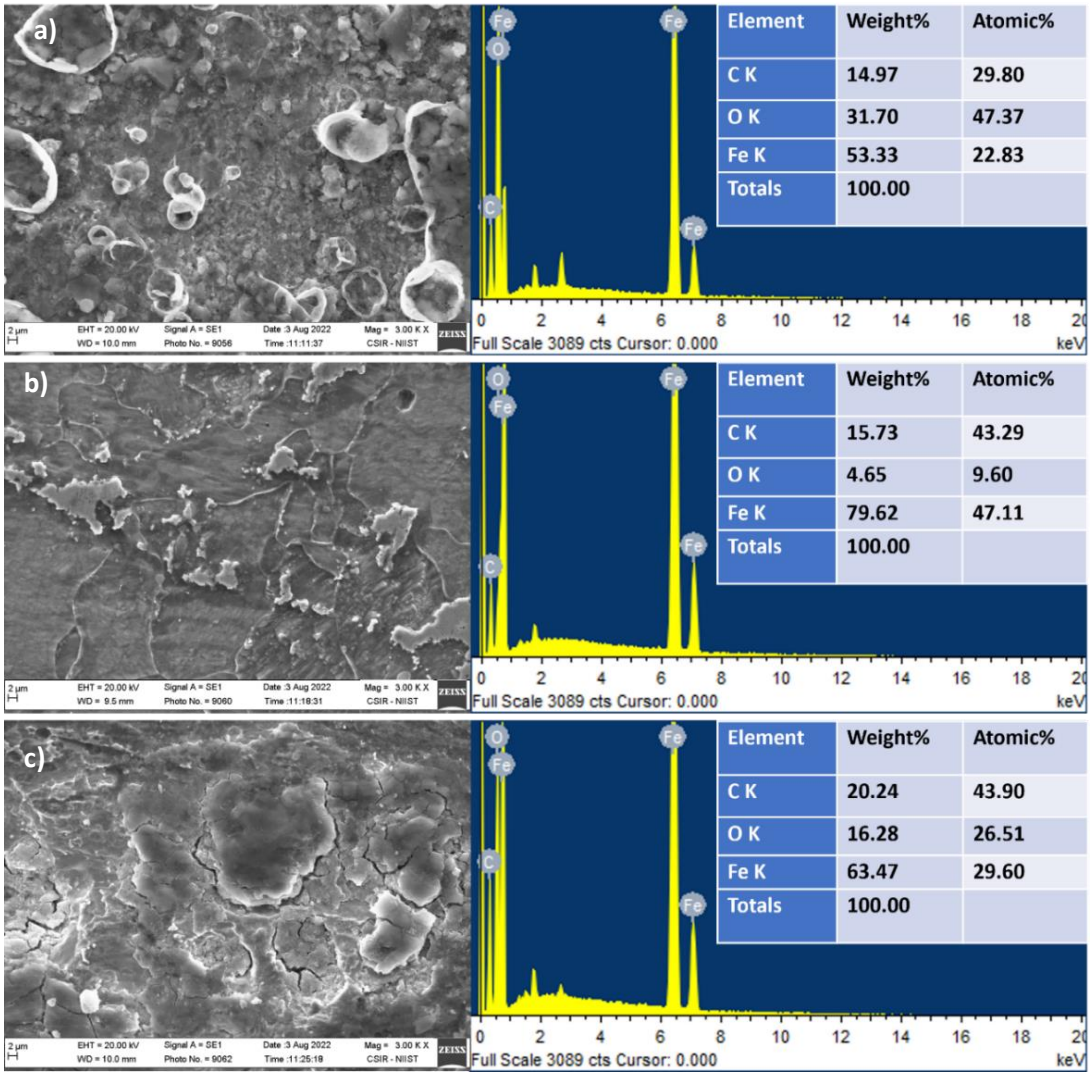

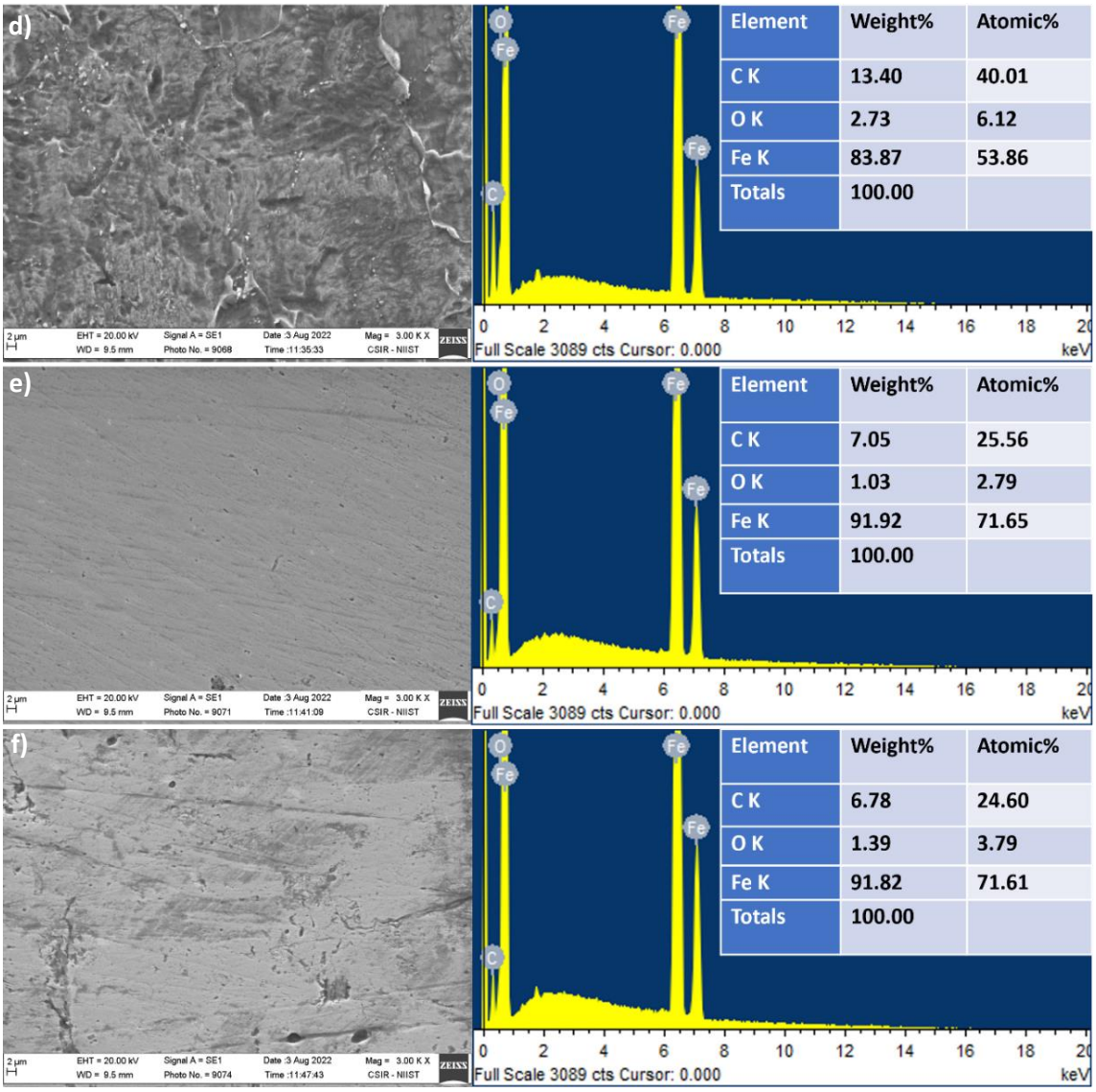

Figure 2.5. SEM micrographs and EDS of MS surface immersed in the saline medium; **a-c)** without the inhibitor in pH 4, pH 7, and pH 10 solutions; **d-f)** in the presence of inhibitor in pH 4, pH 7, and pH 10 solutions.

In the presence of the compound, the surface is smoother and damage-free. Many pits and bruises were observed on the sample's surface immersed in saline solution without the compound. The corrosion products formed in bare saline solution were very high in all the mediums, particularly acidic and alkaline solutions. Many cracks, pits, and solid particles of corrosion products were observed. However, in the presence of quercetagetin, a smooth surface without solid corrosion product formation is observed. The interaction between the

metal surface and the corrosive ions is reduced due to the adsorption of the active molecules. This layer of protection is the reason behind this observation. The functional groups -OH and C=O are capable of coordinate bond formation and thus protecting metal from oxidation.

2.4.4. Preparation and characterisation of bio-nanocomposites from MGE and quercetagetin

Using various techniques, the vacuum-dried nanocomposites are evaluated for stability, loading effectiveness, surface morphology, and elemental analysis. The images of various nanoparticles, viz., the nanocontainer (MSNP), hydroethanolic extract loaded particle (MGE-MSNP), and the quercetagetin loaded composite (QCTGN-MSNP), are shown in **Figure 2.6**.

2.4.4.1. TEM analysis

The surface morphology of the synthesised nanocontainers and the bio-nanocomposites were understood from the TEM images. The particles were spherical and slightly polydisperse in nature. The mesoporous nature of the container was visible from the surface pattern, and the loading of the inhibitor was also evident from the smooth surface of the inhibitor composite. The structural stability was intact even after the loading, and particles were denser because of the reasonable loading of the inhibitor.

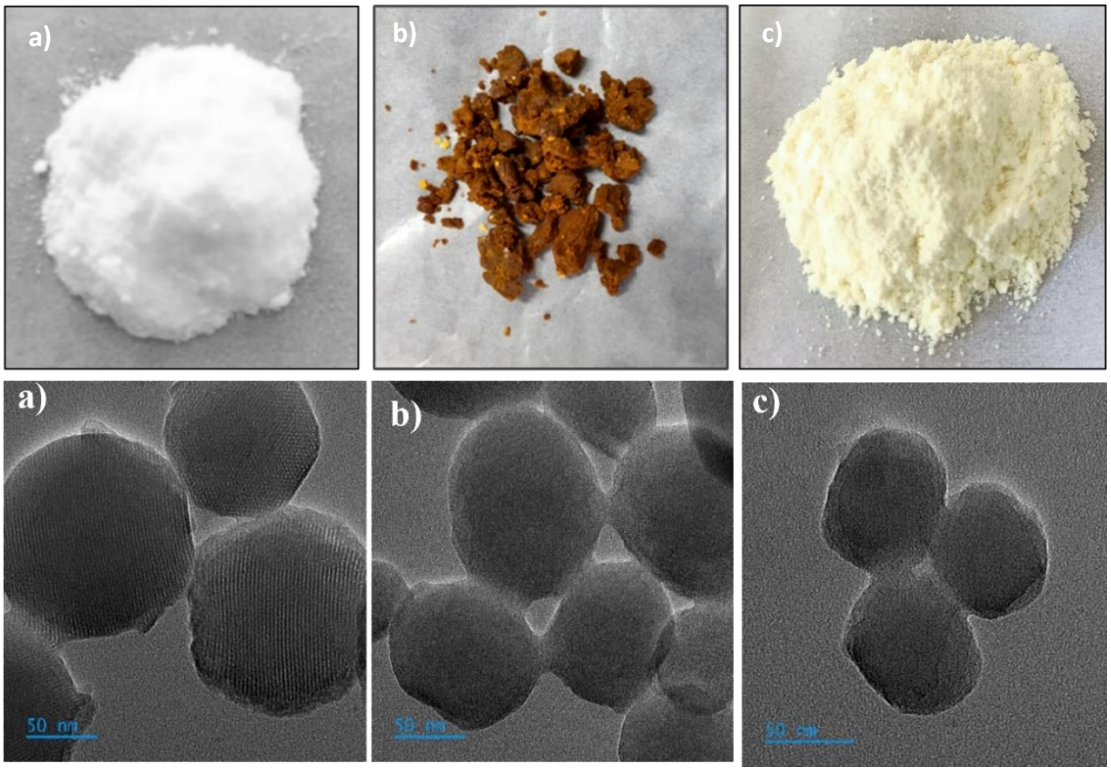

Figure 2.6. Images and TEM micrographs of **a)** MSNP, **b)** MGE-MSNP **c)** QCTGN-MSNP

2.4.4.2. SEM analysis

The structural morphology of the synthesised carrier nanoparticle and the loaded bio-nanocomposite were understood from the SEM micrographs (**Figure 2.7**), and the loading was confirmed with the elemental analysis of the particles. As observed in the TEM micrographs, the particles were of spherical morphology and polydisperse. The nanocontainer showed the presence of only silicon and oxygen, indicating pure silica. The prepared bio-nanocomposites showed a higher percentage of carbon and oxygen in addition to silica, confirming the presence of loaded organic matter.

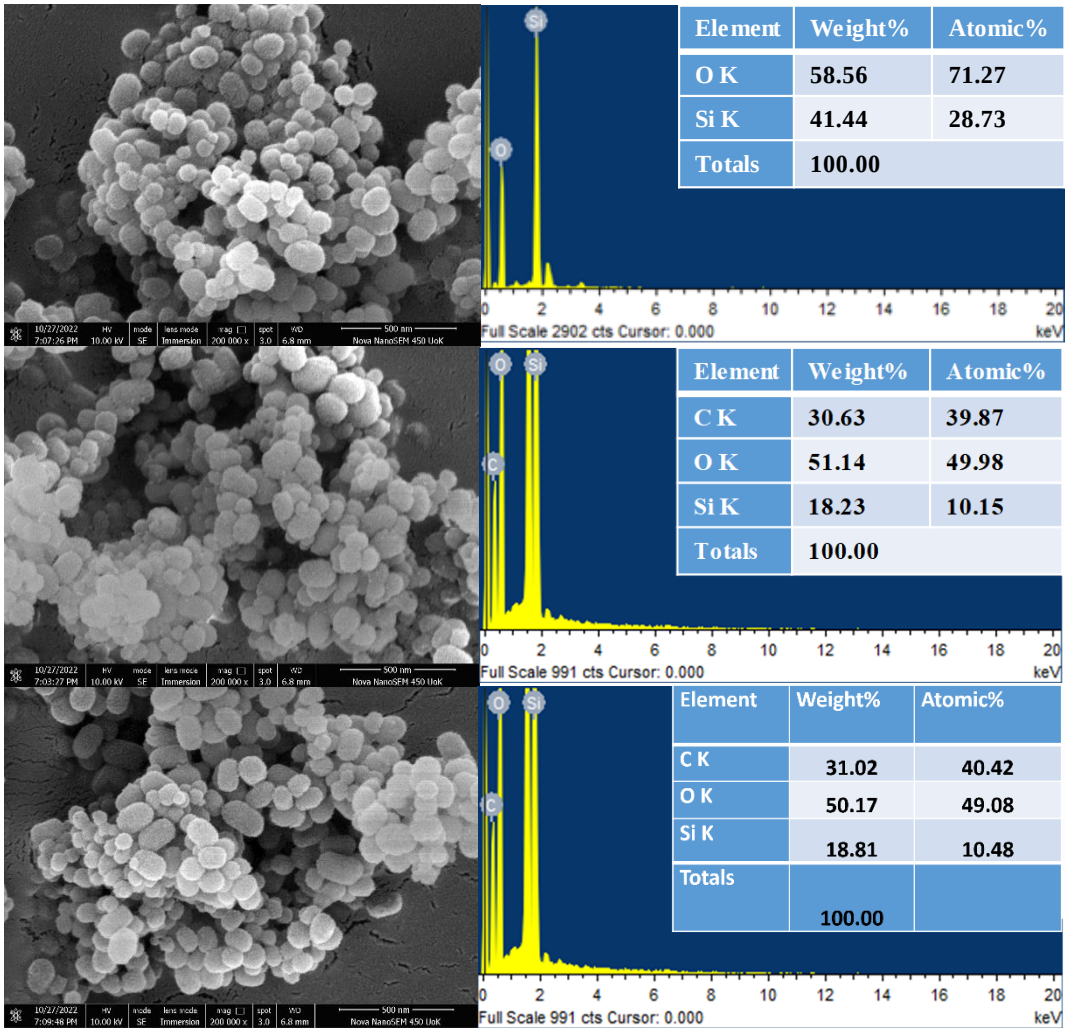

Figure 2.7. SEM micrographs and elemental analysis of **a)** MSNP and **b)** MGE-MSNP, and **c)** QCTGN-MSNP

2.4.4.3. FTIR

FTIR spectroscopy was used to confirm the successful loading of the inhibitors MGE and QCTGN into the nanocontainers. The loading mechanism and the bonding nature are also understood from the FTIR analysis by closely observing any shifts in the peak positions (**Figure 2.8**).

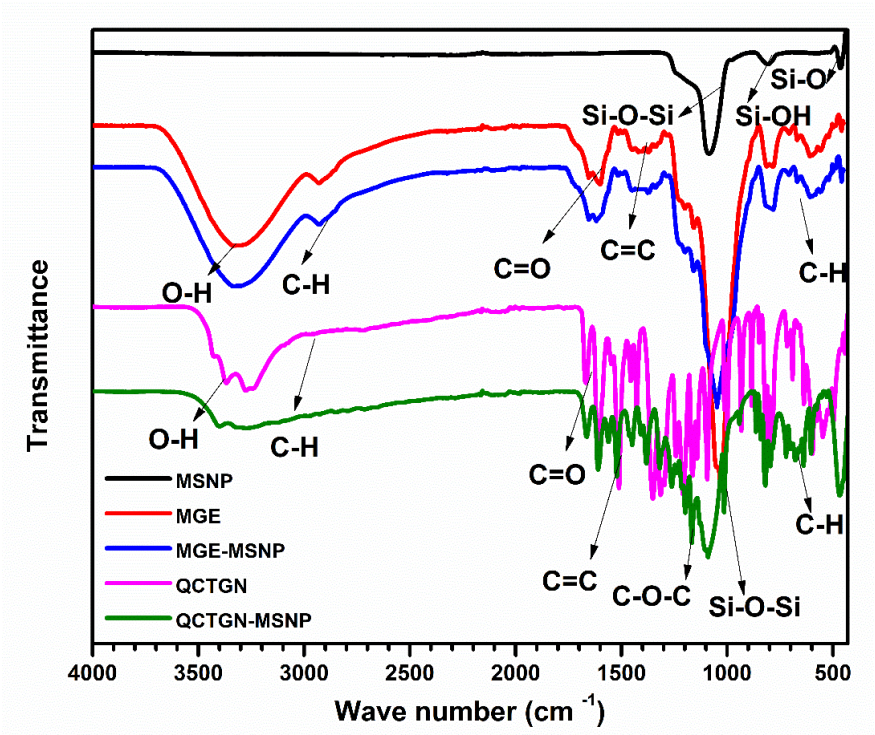

Figure 2.8. Functional group evaluation and confirmation of loading in the mesoporous container by FTIR analysis

The broad peak at 3287 cm^{-1} in MGE and MGE-MSNP corresponds to hydroxyl groups. The peak at 2933 corresponds to aromatic C-H vibrations present in MGE and MGE-MSNP. The hydroxyl peaks for the quercetagetin and QCTGN-MSNP occurred around 3367 cm^{-1} and 3257 cm^{-1}. The peaks corresponding to the carbonyl group were around 1600 cm^{-1} in all the samples except silica. The peak position was slightly shifted to a higher wavenumber region in the case of bio-nanocomposites MGE-MSNP and QCTGN-MSNP due to the coordination between inhibitor and container. In all the inhibitors and composites, the C=C bond absorption peaks were observed around 1094 cm^{-1}. Si-O-Si peaks were found around 1081 cm^{-1} in the silica container and the composites. Si-OH and Si-O vibrations give absorption around 810 cm^{-1} and 463 cm^{-1}, respectively. All the peaks in the inhibitor and the container were present in the bio-nanocomposite, ensuring the successful loading of the inhibitor inside the container. There was no noticeable change in

peak position, or no expenditure of any bond observed. This indicates that only physisorption occurs, and no chemical bond formation occurs during the loading.

2.4.4.4. BET analysis of the nanoparticles for the evaluation of loading

The surface area analysis showed the exceptional loading capacity of the nanocontainers with an enhanced surface area of 729.67 m^2/g and the efficient loading of the inhibitor QCTGN. N_2 adsorption-desorption isotherm is shown in **Figure 2.9**.

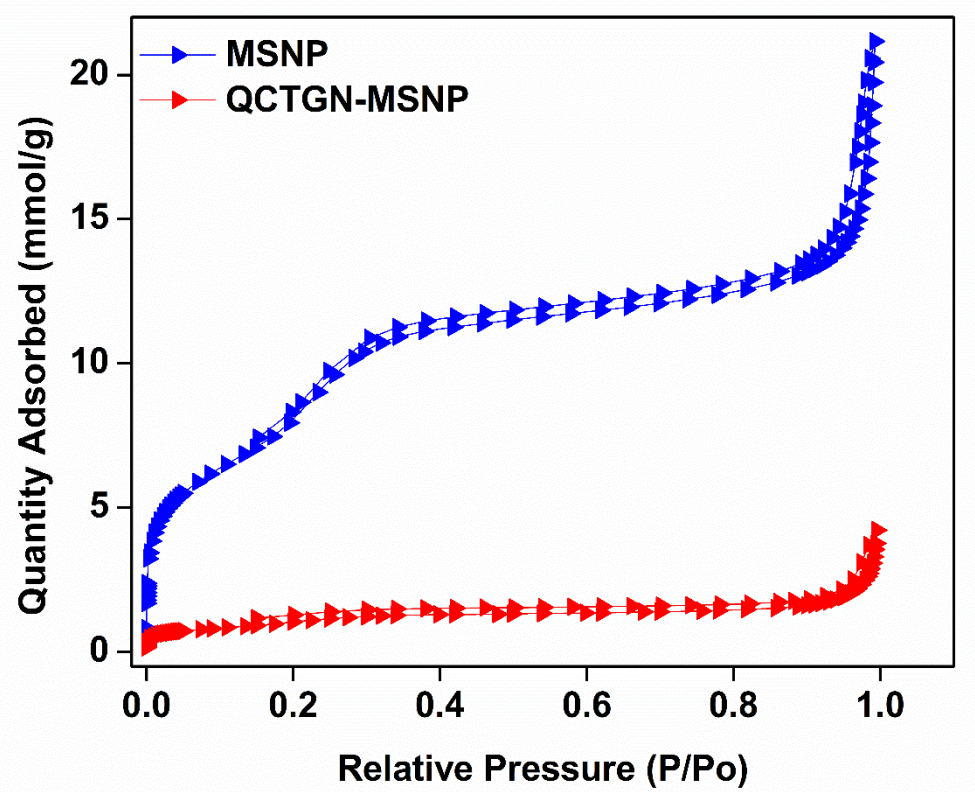

Figure 2.9. N_2 adsorption-desorption isotherm for the evaluation of the surface area and pore size.

The lower adsorption of N_2 in the hysteresis loop of the bio-nanocomposite QCTGN-MSNP shows the loading of inhibitor inside the pores of the container. Surface area, pore diameter, and pore volume are listed in **Table 2.3**. The total surface area of the container MSNP is reduced from 729.67 m^2/g to 88.80 m^2/g, and the pore volume is reduced from 0.68 cm^3/g to 0.12 cm^3/g after loading.

Table 2.3. Parameters obtained from the adsorption/desorption isotherm

Samples	**Surface area (m^2/g)**	**Pore volume (cm^3/g)**	**Pore diameter (nm)**
MSNP	729.67	0.68	3.75
QCTGN-MSNP	88.80	0.12	5.15

2.4.4.5. Thermogravimetric analysis

The thermogram depicted in **Figure 2.10** gives an idea about the thermal stability of the various components of the system under study. Each inhibitor is more stable when loaded in a nanocontainer than its pure form. The crude extract MGE and its nanocomposite MGE-MSNP showed lower stability than the isolated molecule QCTGN and its nanocomposite QCTGN-MSNP. This is because, in the crude extract, the number of components present and the size, structure, and, thus, the thermal stability of each component varies. The polymer matrix with QCTGN-MSNP showed enhanced thermal stability to the pure epoxy polymer matrix. The T_5 and T_{10} values of the pristine epoxy polymer increased by 77 °C and 68 °C, respectively, after adding hybrid nanocomposite to the system.

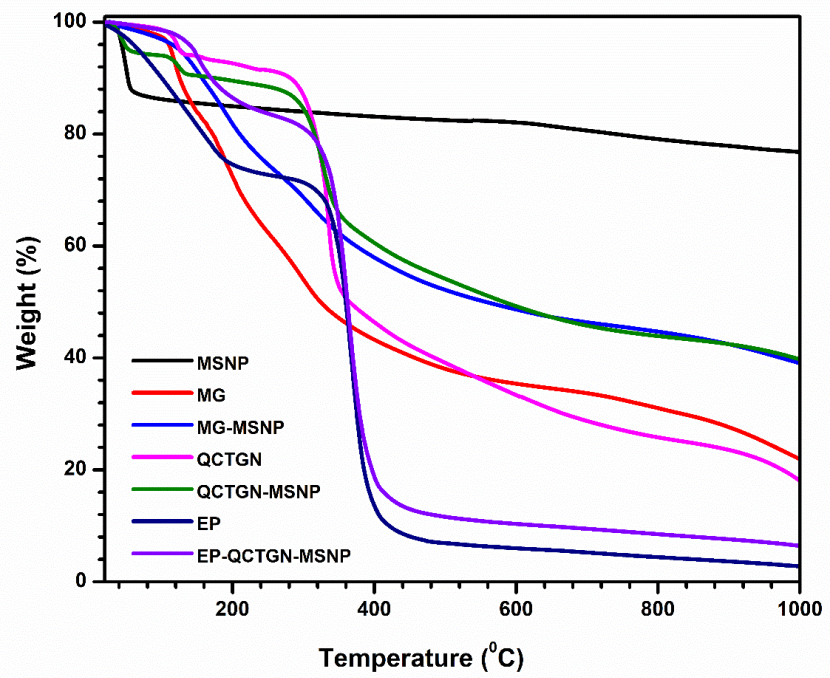

Figure 2.10. Thermal stability comparison of various components in the polymer matrix

2.4.5. Corrosion inhibition potential evaluation of the modified epoxy coatings

2.4.5.1. MGE nanocomposites in epoxy coatings on mild steel

The prepared bio-nanocomposites MGE-MSNP and QCTGN-MSNP were incorporated in the epoxy matrix at various weight percentages of the total weight of the epoxy and the hardener. The effect of the increase in the concentration of the extract in the polymer showed an increasing trend up to 2 wt.%. For the coating containing 3 wt.% of the extract appeared to be more hygroscopic at room temperature, and the electrochemical studies' results also showed a negative shift in values in agreement (**Figure 2.11**). But the 2 wt.% coating showed an excellent corrosion inhibition with an increase in the R_{ct} values from 1128 Ω cm^2 to 21300 Ω cm^2, the i_{corr} values reduced to 0.066 μ Acm^{-2} from 12.53 μ Acm^{-2}, and the E_{corr} values increased to -0.292 V from -0.698 V with an inhibition efficiency of 99.47% (**Table 2.4**). The inhibitor acted as an anodic-type inhibitor by shifting the corrosion potential toward the anodic region.

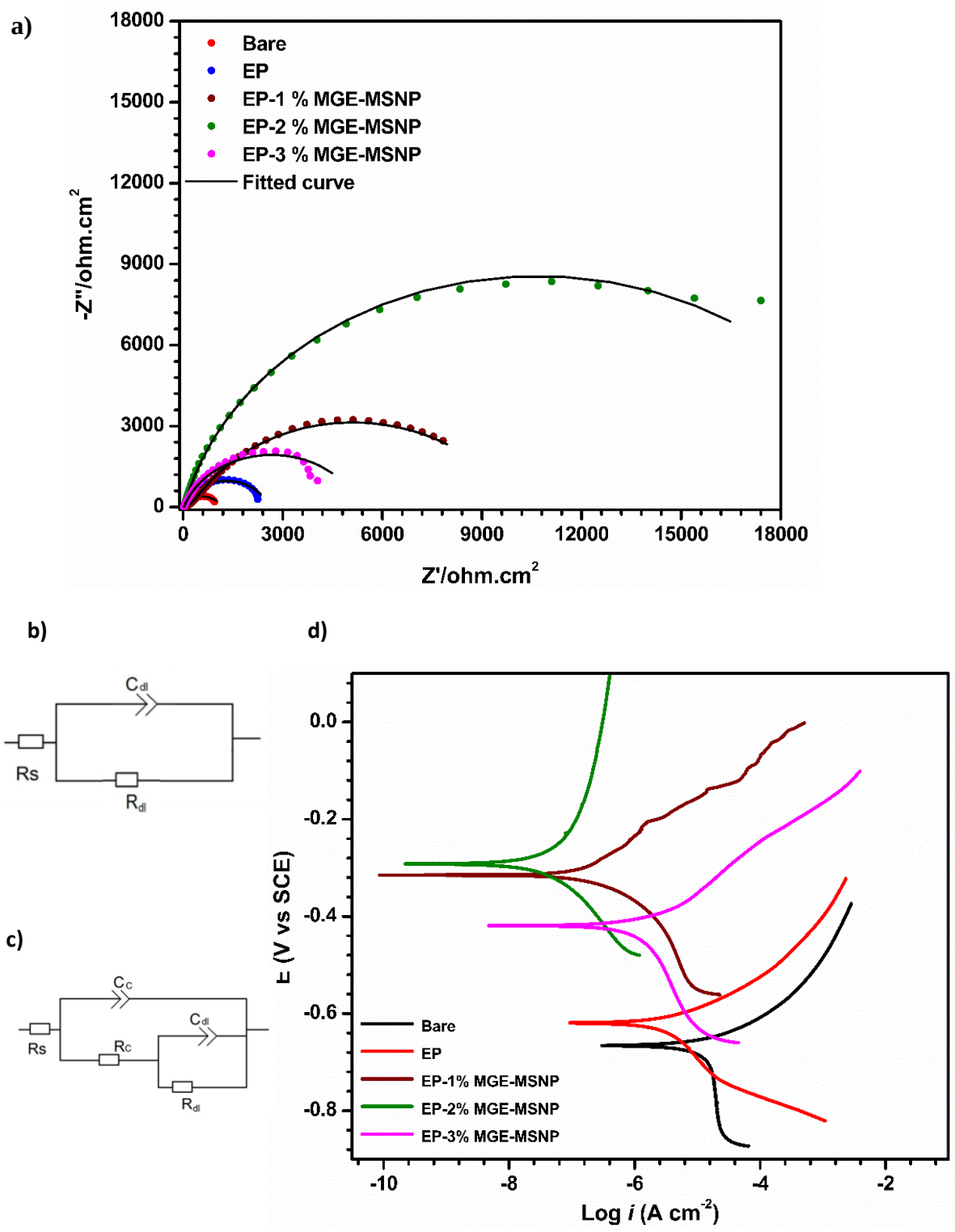

Figure 2.11. Electrochemical study for the coatings containing extract MGE **a)** Nyquist plot **b)** EEC for the bare sample **c)** EEC for the coated samples and **d)** Tafel plot

Table 2.4. Potentiodynamic polarisation parameters obtained for samples under study

S/N	Sample	Potentiodynamic polarisation			EIS	
		E_{corr} (V)	i_{corr} (μ Acm^{-2})	η (%)	R_{ct} (Ω cm^2)	IE $_{EIS}$ (%)
1.	Bare MS	-0.698	12.53	_	1128	_
2.	EP	-0.618	4.817	61.54	2574	56.17
3.	EP-1% MGE-MSNP	-0.315	0.318	97.46	8872	87.28
4.	EP-2% MGE-MSNP	-0.292	0.066	99.47	21300	94.70
5.	EP-3% MGE-MSNP	-0.419	2.037	83.74	5292	78.68

The bare MS samples can be fitted with the circuit the equivalent electrochemical circuit (EEC) $R_s(C_{dl}R_{ct})$, and all the coated samples are well fitted for the equivalent circuit of $R_s(C_cR_c(C_{dl}R_{ct}))$. *Rs* is the solution resistance, and R_{ct} and C_{dl} are the charge transfer resistance and double-layer capacitance, respectively. Instead of using pure capacitance due to the possibility of a dispersion effect between the metal/coating system, *C* represents a constant phase angle element (CPE). The coating offered protection by the resistance element R_c [14,16]. The resistance provided by the coating showed an increasing trend with the rising concentration of MGE-MSNP up to a limit. The maximum corrosion protection was demonstrated by the coating containing 2% of the bio-nanocomposite MGE-MSNP. Beyond that, the coating seems slightly hygroscopic, which affects the efficiency. However, the resistance of the mild steel sample 1128 Ω cm^2 shifted to 21300 Ω cm^2 in the case of the coated sample with an inhibition efficiency of 94.70% in terms of resistance factor R_c.

2.4.5.2. Evaluation of Quercetagetin as the corrosion inhibitor in the epoxy coating for mild steel

As expected from the structure and electron density, the isolated compound from the extract showed higher inhibition efficiency than the total extract. The increase in the concentration in the polymer matrix increased corrosion prevention efficiency. The maximum protection was offered by the coating containing 3 wt.% of QCTGN-MSNP; beyond that, the coating showed a slight decrease in efficiency. This can be attributed to the agglomeration of the nanoparticles at the higher concentration and the resultant porous nature, which allows the penetration of the electrolyte and the corrosive ions up to the metal surface through the polymer matrix [17,18]. The 3 wt.% coatings showed excellent corrosion inhibition with an increase in the resistance values from 1128 Ω cm^2 to 31240 Ω cm^2, the i_{corr} values reduced to 0.0060 μ Acm^{-2} from 12.53 μ Acm^{-2}, and the E_{corr} values increased to -0.274 V from -0.698 V with an inhibition efficiency of 99.95%. The coating behaved as an anodic-type inhibitor, and the slope of both anodic and cathodic reaction branches decreased in the Tafel plot, also, the E_{corr} values shifted to a more anodic potential region.

As in the case of the coatings containing the hydroethanolic extract, the coatings with the isolated compound also fitted for the same EEC (**Figure 2.12**). The bare samples can be fitted with the circuit the equivalent electrochemical circuit $R_s(C_{dl}R_{ct})$, and all the coated samples are well fitted for the equivalent circuit of $R_s(C_cR_c(C_{dl}R_{ct}))$. R_s is the solution resistance, and the constant phase angle element CPE replaced the pure capacitance term. The capacitance and resistance due to the epoxy coatings are represented by C_c, R_c, which occurs at high-frequency regions. The capacitance offered by the electrical double layer between the metal surface and the electrolyte is represented as double-layer capacitance

C_{dl}, and the resulting resistance derived from the capacitance is $R_{ct,}$ respectively, the medium-low frequency elements [14,16].

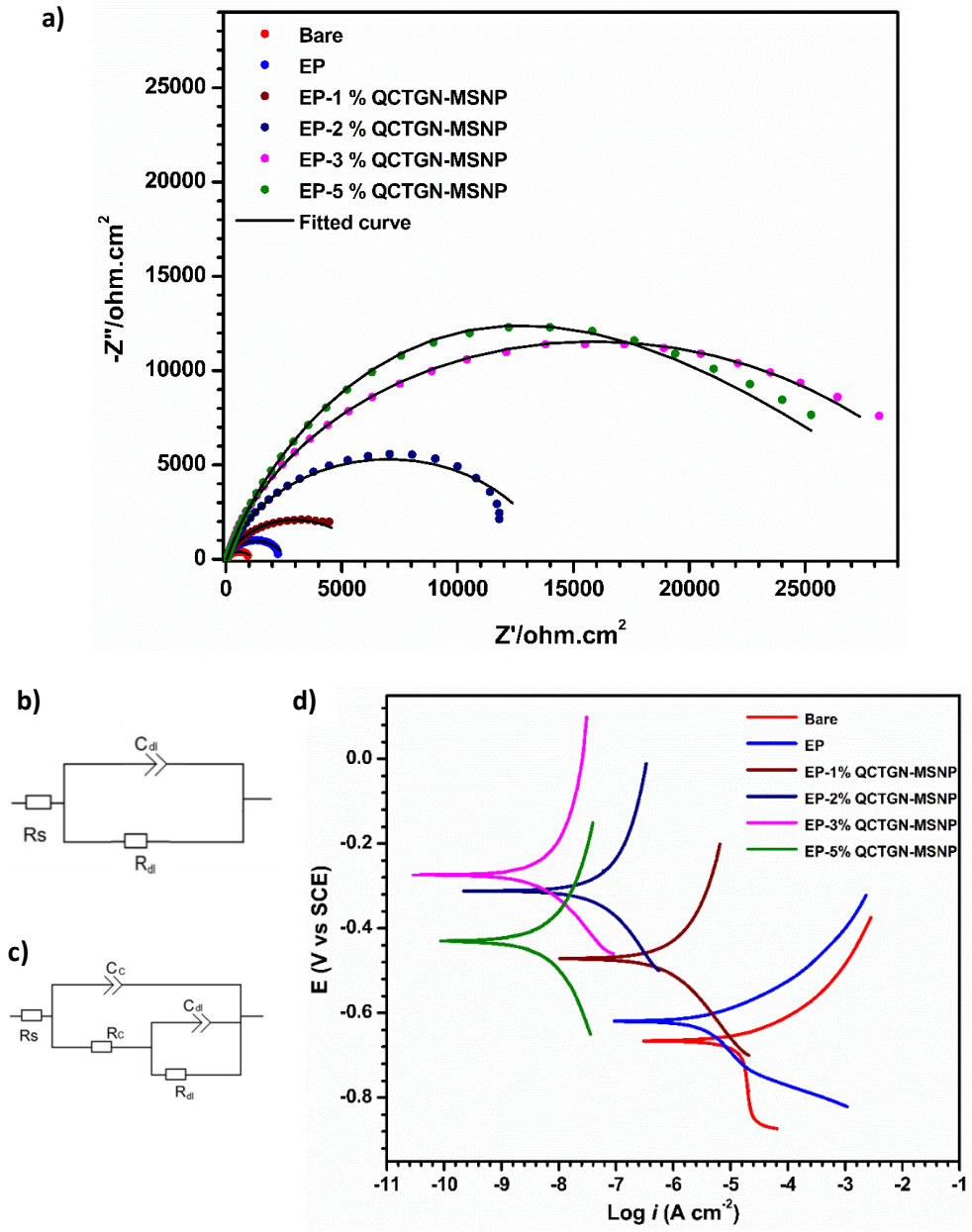

Figure 2.12. a) Nyquist plots, **b)** EEC of the bare sample, **c)** EEC of coated samples, and **d)** Tafel plots of samples containing QCTGN-MSNP at different concentrations.

The maximum performance was offered by the coating comprising 3% of the bio-nanocomposite QCTGN-MSNP, beyond that, the efficiency decreased slightly due to the porous nature resulting from the possible agglomeration of the nanoparticles in the polymer

matrix. Unlike the coating containing the extract, the coating with QCTGN-MSNP was highly stable and not hygroscopic. The resistance R_c increased from 1128 Ω cm^2 to 31240 Ω cm^2 with an inhibition efficiency of 96.38% (**Table 2.5**).

Table 2.5. Electrochemical parameters and corrosion inhibition efficiency of various samples

S/N	Substrate	Potentiodynamic polarisation			EIS	
		E_{corr} (V)	i_{corr} (μ Acm^{-2})	η (%)	R_{ct} (Ω cm^2)	IE_{EIS} (%)
1.	Bare MS	-0.698	12.53	_	1128	
2.	EP	-0.618	4.817	61.54	2574	56.17
3.	EP-1% QCTGN-MSNP	-0.472	0.882	92.96	5934	80.99
4.	EP-2% QCTGN-MSNP	-0.312	0.060	99.51	14030	91.96
5.	EP-3% QCTGN-MSNP	-0.274	0.006	99.95	31240	96.38
6.	EP-5% QCTGN-MSNP	-0.430	0.006	99.95	29910	96.22

2.4.5.3. Release profile of quercetagetin and efficiency of the coatings on MS at different pH

To evaluate the efficiency of the coating in acidic and alkaline environments, the experiments were repeated in saline solutions of pH 4 and 10. The coating was effective for metal protection in both conditions compared to the bare and pure epoxy-coated samples. Tafel plots showing the positive shift in the E_{corr} value and reduced i_{corr} value are shown in **Figure 2.13.** In the case of pure epoxy coatings in both situations, the E_{corr} value shifted to a more negative potential, and the i_{corr} value was reduced. In the case of quercetagetin-modified epoxy coatings, both the E_{corr} and i_{corr} values improved drastically.

The polarisation parameters and corrosion inhibition efficiency percentage are tabulated in **Table 2.6**.

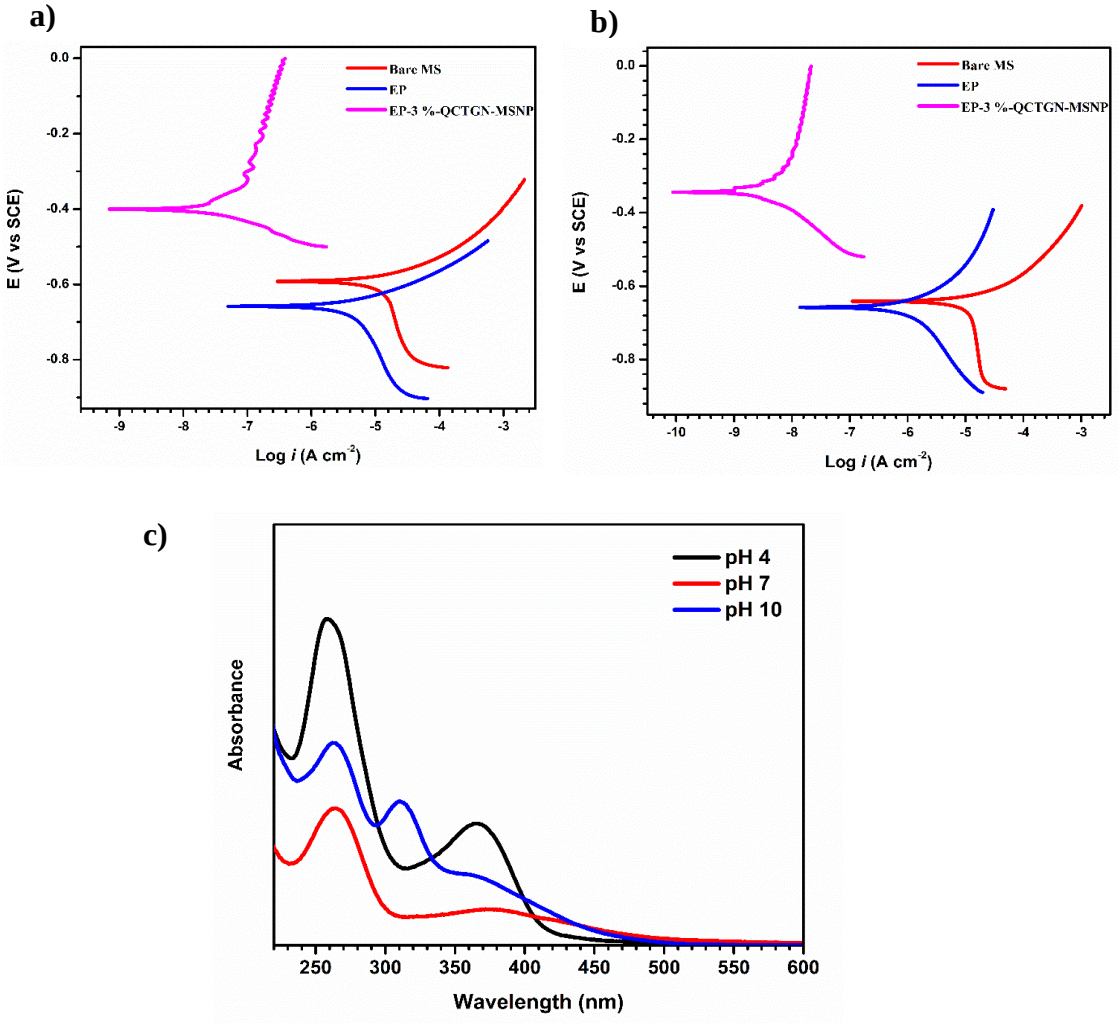

Figure 2.13. Tafel plots for the mild steel and coated MS samples at **a)** pH 4 **b)** pH 10, and **c)** release profile of quercetagetin from the nanocontainers at different pH saline solutions.

The performance of the pure epoxy was reduced to a great extent in the acidic and alkali medium compared to the coating in near neutral solutions. But this drastic change was not observed in the efficiencies of the quercetagetin-modified epoxy coatings in different pH saline solutions. The variations in the release profile of quercetagetin (**Figure 2.13c**) in different mediums are responsible for this action. From the UV analysis, it was found that the release of the inhibitor was found to be more in the acidic and basic mediums.

The smart releasing property of the mesoporous silica nanocontainers in the acidic media enhances the efficiency of the coatings in harsh acidic conditions [19,20]. The hydroxyl groups of the inhibitor in the presence of the base medium will result in an anion structure which in turn increases the solubility of the inhibitor and, thus amount of release from the container. The electron rearrangement and possible resonance structures will result in the formation of an aromatic-dione structure. Which slightly changes the colour of the solution in UV analysis, this change in chromophore unit is responsible for the observed shift in the peak positions at pH 10.

Table 2.6. Potentiodynamic polarisation parameters and corrosion inhibition efficiency of the epoxy and modified epoxy coatings in pH 4 and 10 saline solutions.

S/N	**Substrate**	**Potentiodynamic polarisation pH 4**			**Potentiodynamic polarisation pH 10**		
		E_{corr} (V)	i_{corr} (μ Acm^{-2})	η (%)	E_{corr} (V)	i_{corr} (μ Acm^{-2})	η (%)
1.	Bare mild steel	-0.592	24.51	_	-0.641	29.77	_
2.	EP	-0.658	5.970	75.6	-0.613	5.10	82.9
3.	EP-3%-QCTGN-MSNP	-0.401	0.046	99.81	-0.344	0.007	99.97

2.4.5.4. Evaluation of corrosion inhibition efficiency of quercetagetin incorporated coating for Al-6061 alloy

As observed in the case of MS, the 3% coating system is studied for aluminium alloy protection in 3.5 wt.% NaCl solution at neutral pH. The bare sample's curve can be fitted using $R_s((C_{dl}R_{ct})(C_{oxi}R_{oxi}))$. The modified coating showed exceptional protection

efficiency compared to the bare and pure epoxy-coated samples. The impedance measurements for the coated samples fitted for the circuit $R_s(C_cR_c\ (C_{dl}R_{ct})(C_{oxi}R_{oxi}))$.

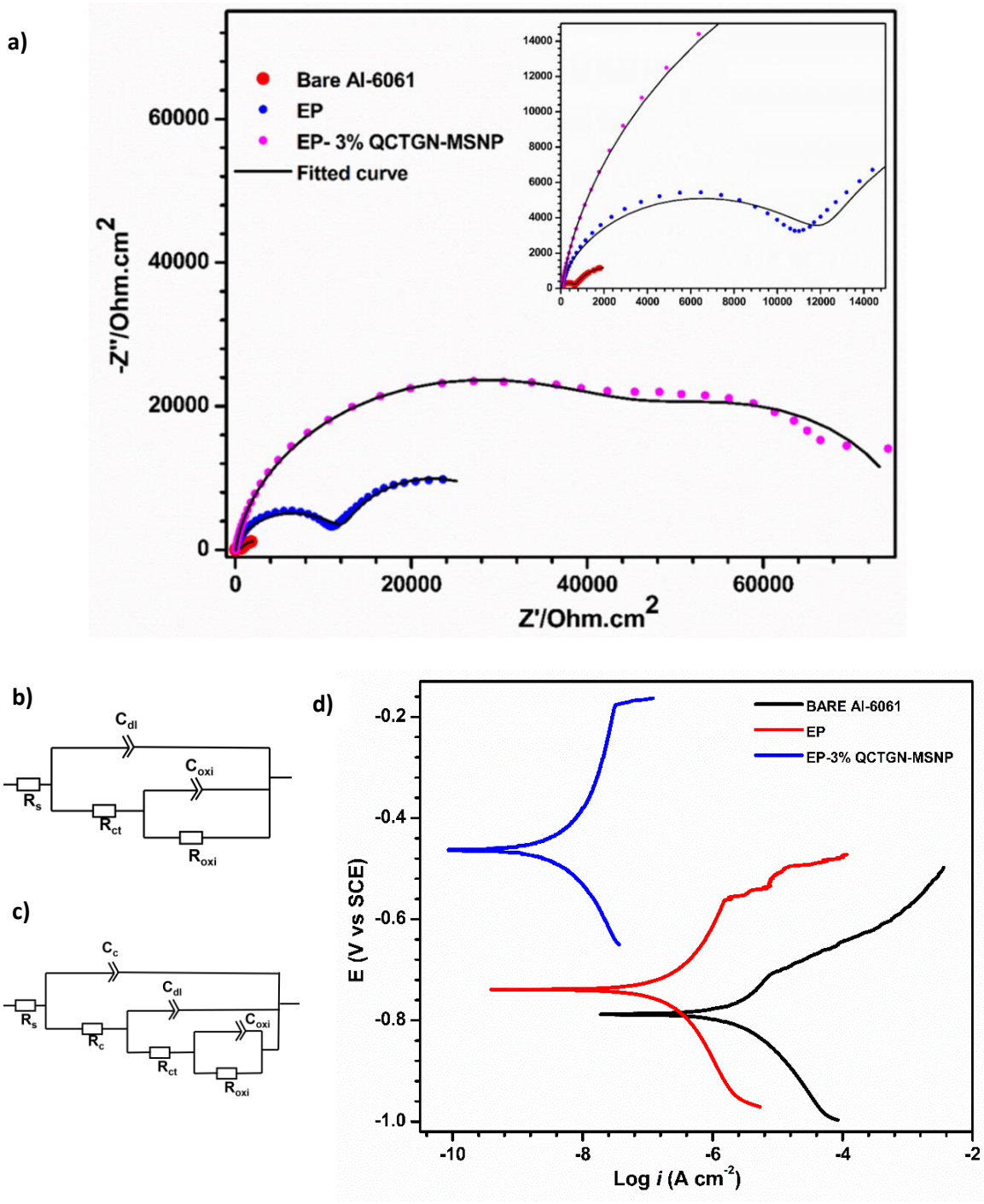

Figure 2.14. Electrochemical study results for various Al-6061 samples in saline medium **a)** Nyquist plot, **b)** EEC for the bare Al-6061 sample, **c)** EEC for the coated sample, and **d)** Tafel plots from the potentiodynamic polarisation measurements.

The resistance value increased from 3634 Ω cm^2 to 77050 Ω cm^2 in the case of 3% coating with an inhibition efficiency of 95.28% in comparison to bare aluminium samples. R_s is the solution resistance, and C_{dl} and R_{ct} are the double-layer capacitance and charge transfer resistance, respectively. The resistance offered by the small amount of corrosion products formed and its diffusion in the polymer matrix is denoted by R_{oxi} and the corresponding capacitance C_{oxi}. The exceptional resistance provided by the polymer matrix and the resultant capacitance are represented as R_c and C_c [14,16]. In the Tafel plot (**Figure 2.14**), the corrosion current density decreased extensively, and the corrosion potential shifted to a more positive potential region. The E_{corr} values changed from -0.788 V to -0.464 V, and the i_{corr} value decreased from 1.941 μ Acm^{-2} to 0.0064 μ Acm^{-2} with an inhibition efficiency of 99.67% (**Table 2.7**).

Table 2.7. Electrochemical parameters and corrosion inhibition efficiency of the Al-6061 samples in saline medium

S/N	Substrate	Potentiodynamic polarisation			EIS	
		E_{corr} (V)	i_{corr} (μ Acm^{-2})	η (%)	R_{ct} (Ω cm^2)	η (%)
1.	Bare Al-6061	-0.788	1.941		3634	
2.	EP	-0.739	0.294	84.85	33210	89.05
3.	EP-3% QCTGN-MSNP	-0.464	0.0064	99.67	77050	95.28

2.4.6. Mechanism of corrosion inhibition

The combination of active and passive corrosion inhibition resulted in this outstanding protection of the metal surface in the marine environment. The polymer epoxy coating showed barrier protection against corrosive ions, and the self-healing efficiency

protected active corrosion inhibition. The presence of the green corrosion inhibitor slowly releasing from the container ensured enhanced corrosion inhibition by various mechanisms. The compound quercetagetin is rich in its structure with heteroatom density of the hydroxyl groups and carbonyl group and pi-electron delocalisation in two aromatic rings, a double bond, and one carbonyl group. The lone pairs in the hetero atoms are located in an sp^3 hybrid orbital in the hydroxyl groups and an sp^2 hybrid orbital in the carbonyl group. All the pi electrons are delocalised in sp^2 hybridised orbitals and are loosely bound. All these electrons can be donated to the metal ions by coordinate bonds, and the electrons from the metal ions can be donated to the molecular orbital of the inhibitor by retro donation [21–23] (**Figure 2.15)**. This electron flow prevents metal oxidation and its complex formation with other corrosive ions. The metal ion and the inhibitor interact like a Lewis acid-base pair *via* a coordination bond [24]. Also, any of the molecules entering the polymer matrix will be hydrogen bonded with the hydroxyl groups of the inhibitor and the polymer in the upper area of the coating. This will prevent the further movement of the water molecules towards the metal ions.

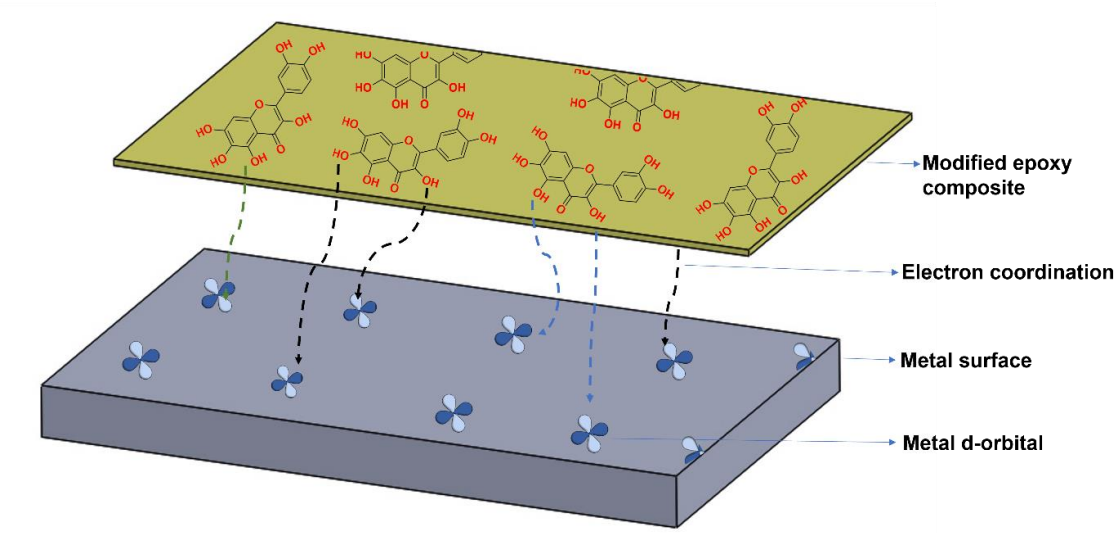

Figure 2.15. Corrosion inhibition mechanism of quercetagetin-modified epoxy polymer composite coating

2.4.7. Self-healing evaluation and mechanism

The possibility of self-healing in a corrosive medium is studied by immersing the 3 wt.% quercetagetin incorporated coating on the aluminium surface with an artificial scratch in 3.5% NaCl solution for 48 hours and examining the SEM micrographs at time intervals of 0 h, 3 h, 6 h, 12 h, 24 h and 48 h (**Figure 2.16**).

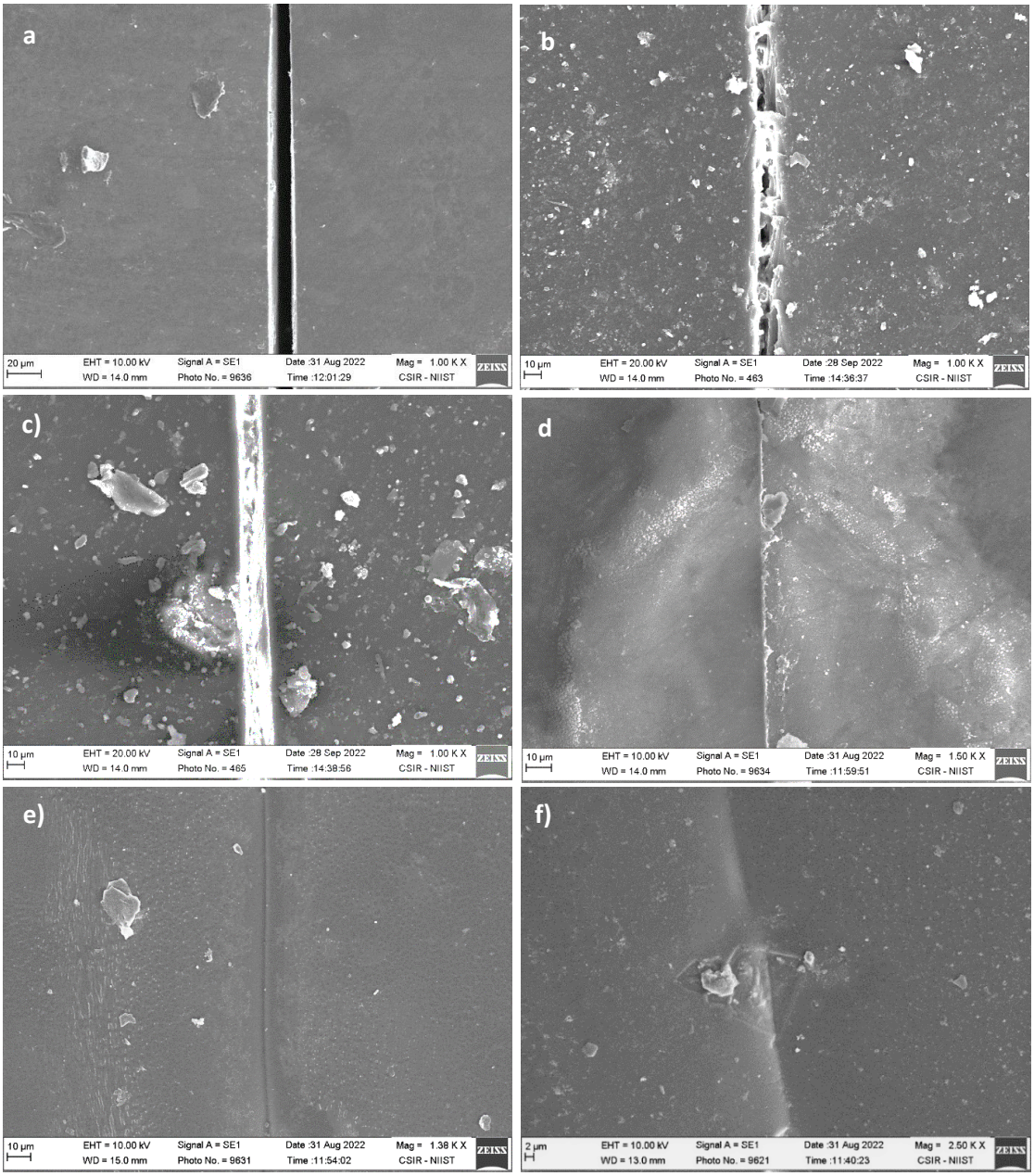

Figure 2.16. SEM micrographs of the surface with artificial scratch immersed in the saline medium at various time intervals **a)** at 0 h, **b)** after 3 h, **c)** after 6 h, **d)** after 12 h, **e)** after 24 h, and **f)** 48 h.

It was observed that the healing started within 3 h and was completed by 48 h; no sign of corrosion product formation or leakage from scratch in the final images observed, suggesting a complete self-healing. The possible mechanism of corrosion inhibition is the release of the inhibitor compound quercetagetin from the nanoparticles and filling the void, thus preventing the metal surface from further damage. The possible reactions with the metal and polymer matrix include coordination and hydrogen bonding. The release of the components from the nanocontainer and possible healing is depicted in **Figure 2.17**.

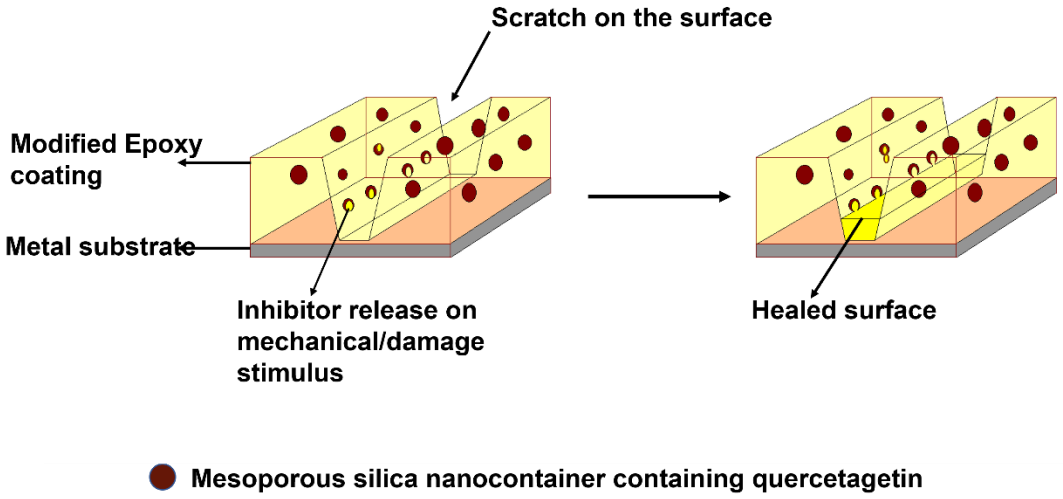

Figure 2.17. Release of the inhibitor from the broken nanocontainers and effective self-healing

2.4.8. Self-sanitising efficiency

The zone of inhibition method was used to qualitatively evaluate the antibacterial nature of the coatings on the metal surface. An aluminium disc of radius 1.7 cm was coated and used in this method. The coated samples were compared with a bare aluminium disc, and the changes in microbial growth were observed. The results indicate that the coatings have good antibacterial properties and can effectively suppress the growth of both gram-positive and gram-negative bacteria. The difference in the zones of inhibition shows that

the coating is more effective against gram-positive bacteria compared to gram-negative bacteria. This could be attributed to the difference in the cell wall structure of the two types of bacteria. The results suggest that the coatings have the potential to be used in medical and industrial applications. **(Figure 2.18**). *E. coli* was the gram-negative bacteria used in the test, and the experiment showed a zone of inhibition of 3.1 cm diameter. *S. aureus* was the gram-positive bacteria used for the analysis, and the test exhibited an average of 3.9 cm diameter for the zone of inhibition. The coating containing an empty mesoporous silica container was not active against the organisms, so the activity was solely due to the inhibitor.

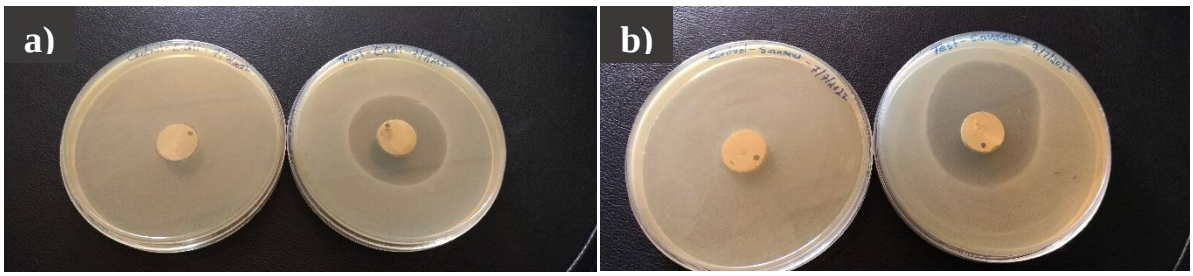

Figure 2.18. Self-sanitising effect of the modified epoxy coating against gram positive and gram negative bacteria

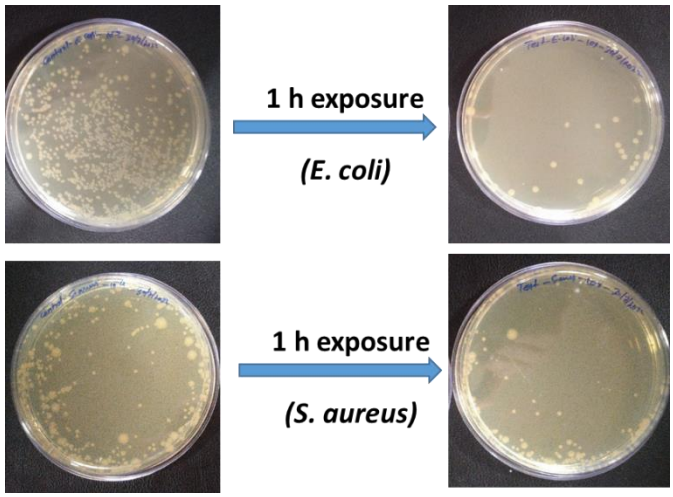

Figure 2.19. The self-sanitizing property confirmed by the quantitative test AATCC-100 showing an inhibition of 81% and 92% killing of *E. coli* and *S. aureus* respectively in 1 h exposure.

In the quantitative test by AATCC-100 method, the results were further confirmed by an inhibition of 81% and 92% killing of *E. coli* and *S. aureus* respectively in 1 h exposure (**Figure 2.19**).

2.5. Conclusions

Marigold extracts and the marker compound quercetagetin from the most active extract were investigated as a corrosion inhibitor for mild steel and Al-6061 alloys in 3.5% NaCl solution by various studies, including weight loss test, surface morphology evaluation, and electrochemical evaluations of the coated polymer surface. The hydroethanolic extract was found to be more active than the hexane extract of the marigold flower. Both the extracts and the isolated compound showed excellent corrosion inhibition properties. The EIS and potentiodynamic polarisation data collectively confirmed that the coating with 3 wt.% QCTGN-MSNP showed superior corrosion inhibition in the studied corrosive environment. In the presence of the inhibitors, R_{ct} values increased from 1128 Ω cm^2 to 31240 Ω cm^2, the i_{corr} values reduced to 0.0060 μ Acm^{-2} from 12.53 μ Acm^{-2}, and the E_{corr} values increased to-0.274 V from -0.698 V with an inhibition efficiency of 99.95% in comparison to bare mild steel. In the case of Al-6061 alloys, the 3 wt.% coatings showed an inhibition efficiency of 99.67%, with the i_{corr} values reduced to 0.0064 μ Acm^{-2} from 1.941 μ Acm^{-2} and the E_{corr} values increased to-0.464 V from -0.788 V. The coating also exhibited excellent self-healing efficiency and antimicrobial potential. Self-healing started within 3 hours and was completed within 48 hours. The coating was effective against both gram positive and gram negative bacteria.

References

[1] W. Nash, L. Zheng, N. Birbilis, Deep learning corrosion detection with confidence, Npj Mater Degrad. 6 (2022) 26. https://doi.org/10.1038/s41529-022-00232-6.

[2] M. Ates, A review on conducting polymer coatings for corrosion protection, J Adhes Sci Technol. 30 (2016) 1510–1536. https://doi.org/10.1080/01694243.2016.1150662.

[3] K.K. Veedu, S. Mohan, S.B. Somappa, N.K. Gopalan, Eco-friendly anticorrosive epoxy coating from Ixora leaf extract: A promising solution for steel protection in marine environment, J Clean Prod. 340 (2022) 130750. https://doi.org/10.1016/j.jclepro.2022.130750.

[4] N. Hossain, M. Asaduzzaman Chowdhury, M. Kchaou, An overview of green corrosion inhibitors for sustainable and environment friendly industrial development, J Adhes Sci Technol. 35 (2021) 673–690. https://doi.org/10.1080/01694243.2020.1816793.

[5] Z. Zheng, M. Schenderlein, X. Huang, N.J. Brownbill, F. Blanc, D. Shchukin, Influence of Functionalization of Nanocontainers on Self-Healing Anticorrosive Coatings, ACS Appl Mater Interfaces. 7 (2015) 22756–22766. https://doi.org/10.1021/acsami.5b08028.

[6] Z. Zheng, X. Huang, D. Shchukin, A cost-effective pH-sensitive release system for water source pH detection, Chem. Commun. 50 (2014) 13936–13939. https://doi.org/10.1039/C4CC05597G.

[7] W. Cheng, J. Nie, L. Xu, C. Liang, Y. Peng, G. Liu, T. Wang, L. Mei, L. Huang, X. Zeng, pH-Sensitive Delivery Vehicle Based on Folic Acid-Conjugated Polydopamine-Modified Mesoporous Silica Nanoparticles for Targeted Cancer Therapy, ACS Appl Mater Interfaces. 9 (2017) 18462–18473. https://doi.org/10.1021/acsami.7b02457.

[8] M. Yeganeh, M. Omidi, T. Rabizadeh, Anti-corrosion behavior of epoxy composite coatings containing molybdate-loaded mesoporous silica, Prog Org Coat. 126 (2019) 18–27. https://doi.org/10.1016/j.porgcoat.2018.10.016.

[9] A. Keyvani, M. Yeganeh, H. Rezaeyan, Application of mesoporous silica nanocontainers as an intelligent host of molybdate corrosion inhibitor embedded in the epoxy coated steel, Progress in Natural Science: Materials International. 27 (2017) 261–267. https://doi.org/10.1016/j.pnsc.2017.02.005.

[10] S.B. Ulaeto, A. V. Nair, J.K. Pancrecious, A.S. Karun, G.M. Mathew, T.P.D. Rajan, B.C. Pai, Smart nanocontainer-based anticorrosive bio-coatings: Evaluation of quercetin for corrosion protection of aluminium alloys, Prog Org Coat. 136 (2019) 105276. https://doi.org/10.1016/j.porgcoat.2019.105276.

[11] G. Ji, S. Anjum, S. Sundaram, R. Prakash, Musa paradisica peel extract as green corrosion inhibitor for mild steel in HCl solution, Corros Sci. 90 (2015) 107–117. https://doi.org/10.1016/j.corsci.2014.10.002.

[12] M. Yeganeh, I. Khosravi-Bigdeli, M. Eskandari, S.R. Alavi Zaree, Corrosion Inhibition of l-Methionine Amino Acid as a Green Corrosion Inhibitor for Stainless Steel in the H_2SO_4 Solution, J Mater Eng Perform. 29 (2020) 3983–3994. https://doi.org/10.1007/s11665-020-04890-y.

[13] S.B. Ulaeto, G.M. Mathew, J.K. Pancrecious, R. P.R., A.S. Karun, R. T.P.D., Azadirachta indica (Neem) self-healing efficacy assessment in epoxy primer coatings: A bio-

responsive strategy for counteracting corrosion, Colloids Surf A Physicochem Eng Asp. 658 (2023) 130684. https://doi.org/10.1016/j.colsurfa.2022.130684.

[14] L. Wen, Y. Wang, Y. Zhou, J.-H. Ouyang, L. Guo, D. Jia, Corrosion evaluation of microarc oxidation coatings formed on 2024 aluminium alloy, Corros Sci. 52 (2010) 2687–2696. https://doi.org/10.1016/j.corsci.2010.04.022.

[15] Senatore, Felice, Mario D'Agostino, and Irene Dini, Two new quercetagetin O-glucosides from Tagetes mandonii, Biochemical systematics and ecology. 27, no. 3 (1999): 309-311. https://doi.org/10.1016/S0305-1978(98)00081-7

[16] D. Zeng, Z. Liu, L. Zou, H. Wu, Corrosion Resistance of Epoxy Coatings Modified by Bis-Silane Prepolymer on Aluminum Alloy, Coatings. 11 (2021) 842. https://doi.org/10.3390/coatings11070842.

[17] B. Ren, Y. Chen, Y. Li, W. Li, S. Gao, H. Li, R. Cao, Rational design of metallic anti-corrosion coatings based on zinc gluconate@ZIF-8, Chemical Engineering Journal. 384 (2020) 123389. https://doi.org/10.1016/j.cej.2019.123389.

[18] N. Wang, Y. Zhang, J. Chen, J. Zhang, Q. Fang, Dopamine modified metal-organic frameworks on anti-corrosion properties of waterborne epoxy coatings, Prog Org Coat. 109 (2017) 126–134. https://doi.org/https://doi.org/10.1016/j.porgcoat.2017.04.024.

[19] J. Jiao, X. Li, S. Zhang, J. Liu, D. Di, Y. Zhang, Q. Zhao, S. Wang, Redox and pH dual-responsive PEG and chitosan-conjugated hollow mesoporous silica for controlled drug release, Materials Science and Engineering: C. 67 (2016) 26–33. https://doi.org/10.1016/j.msec.2016.04.091.

[20] C.-Y. Wang, X.-Y. Lou, Z. Cai, M.-Z. Zhang, C. Jia, J.-C. Qin, Y.-W. Yang, Supramolecular Nanoplatform Based on Mesoporous Silica Nanocarriers and Pillararene Nanogates for Fungus Control, ACS Appl Mater Interfaces. 13 (2021) 32295–32306. https://doi.org/10.1021/acsami.1c08582.

[21] K. Dahmani, M. Galai, M. Ouakki, M. Cherkaoui, R. Touir, S. Erkan, S. Kaya, B. El Ibrahimi, Quantum chemical and molecular dynamic simulation studies for the identification of the extracted cinnamon essential oil constituent responsible for copper corrosion inhibition in acidified 3.0 wt% NaCl medium, Inorg Chem Commun. 124 (2021) 108409. https://doi.org/10.1016/j.inoche.2020.108409.

[22] X. Lai, J. Hu, T. Ruan, J. Zhou, J. Qu, Chitosan derivative corrosion inhibitor for aluminum alloy in sodium chloride solution: A green organic/inorganic hybrid, Carbohydr Polym. 265 (2021) 118074. https://doi.org/10.1016/j.carbpol.2021.118074.

[23] N. Bhardwaj, P. Sharma, V. Kumar, Phytochemicals as steel corrosion inhibitor: an insight into mechanism, Corrosion Reviews. 39 (2021) 27–41. https://doi.org/10.1515/corrrev-2020-0046.

[24] M.M. Fares, A.K. Maayta, M.M. Al-Qudah, Pectin as promising green corrosion inhibitor of aluminum in hydrochloric acid solution, Corros Sci. 60 (2012) 112–117. https://doi.org/10.1016/j.corsci.2012.04.002.

Chapter 3

Smart Anticorrosive and Antimicrobial Epoxy Coating Using Bergenin and Malabaricone C Bio-nanocomposites

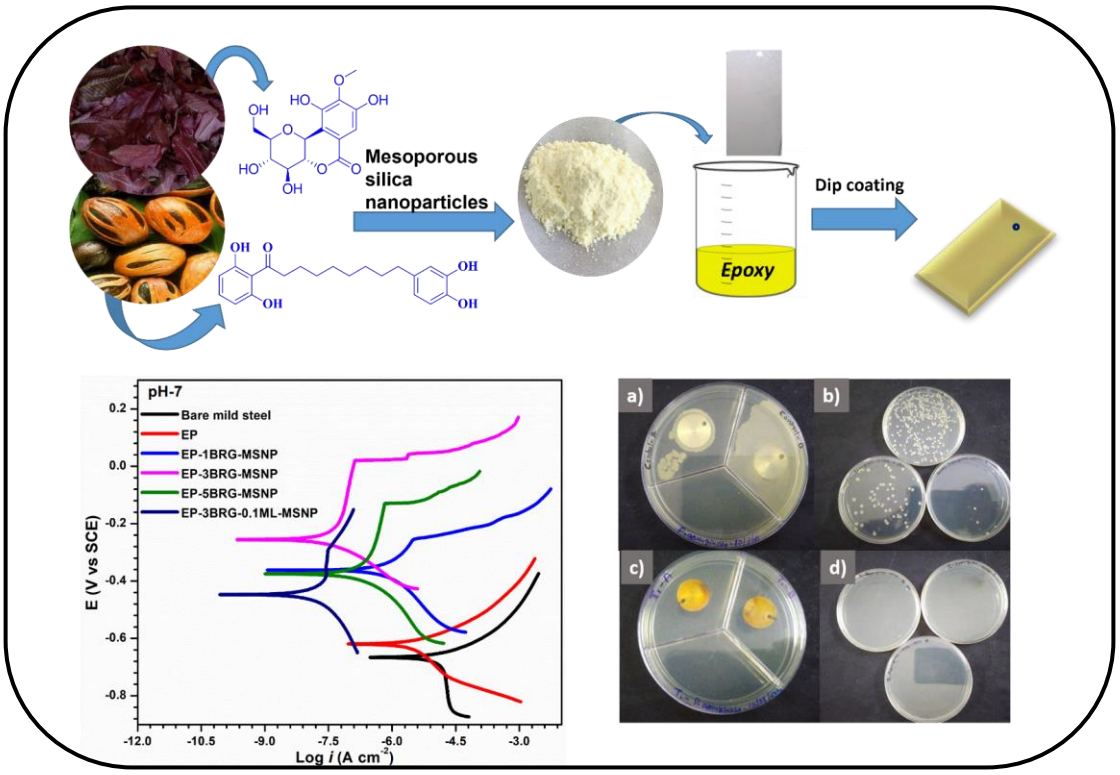

Abstract

Smart multifunctional epoxy coating prepared by incorporating bio-nanocomposites of two isolated phytochemicals bergenin and malabaricone C in mesoporous silica nanoparticles showed excellent corrosion inhibition properties. This smart antimicrobial and corrosion-resistant coating was active in acidic, basic and neutral media containing 3.5 wt.% NaCl. The coatings exhibit their best performance in near-neutral media. Polarisation studies and EIS data showed that an epoxy composite coating containing 3% bergenin nanocomposite prevents corrosion on mild steel and aluminium alloys far better than a pure epoxy coating. Quantitative and qualitative analysis of the antimicrobial action of the coatings revealed that malabaricone C is an excellent antimicrobial agent in smart coating showing 99% efficiency, and the coating exhibited activity against both gram-positive and negative bacteria like *S. aureus* and *P. aeruginosa*.

Keywords: Bergenin, Malabaricone C, Anticorrosion, Antimicrobial, smart coating

3.1. Introduction

The use of inhibitors to protect metal surfaces against corrosion in aggressive media is an accepted practice. A minimal amount of corrosion inhibitors can give a very fair rate of corrosion protection, and this reason promoted the use of corrosion inhibitors, among other methods. Many countries banned the use of inhibitors like phosphate, chromates, and some azole derivatives, which though cheap, created severe health issues and detrimental effects on the environment. The replacement by rare earth metals was not considered economically viable.

The corrosion prevention potential of a compound strongly depends on the capacity to adsorb on metal, which involves replacing a water molecule on the corrosion centre, charge and electron distribution, electron density at the expected coordination centre, the presence of functional group like R–OH, C=O, –N=N, –CHO, solubility in water, the aromaticity of the molecule, and total molecular weight [1]. Individual molecules isolated from the plant extracts are more effective as there is a lower amount of junk materials and other inactive phytochemicals. Quercetin, a flavanol present in many plants like onion, berries, neem, etc., is an excellent green inhibitor against corrosion of Al-6061 alloy [2]. A bis-indole alkaloid derived from the marine alga *Caulerpa racemosa* can form a film on a mild steel surface which provides corrosion protection even in 1M HCl solution [3]. The corrosion inhibition potential of andrographolide from *Andrographis paniculata* was examined using surface analysis, and computational calculations revealed that it could act as an excellent mixed-type corrosion inhibitor for steel [4].

This research aims to form an innovative multifunctional coating with anticorrosive and antimicrobial characteristics using the phytochemicals bergenin and malabaricone C loaded in mesoporous silica nanoparticles. Bergenin is a hydrolyzable tannin and coumarin derivative. It contains two phenolic –OH and three aliphatic hydroxyl groups, which are considered to be potentially active. Primary isolation sources are *Berginial crassifolia*, *Mallotus japonicas*, *Sacoglottis gabonensis* [5], *Bergenia purpurascens* [6], *Endeoplura uchi* [7], and many other trees in Moraceae and Dipterocarpaceae family in common. The compound is well known for its antimicrobial activity (specifically antifungal and antiviral), antioxidant activity, anti-inflammatory activity, hepatoprotective effects, antidiabetic and anticancer properties [5,8]. *Vateria indica*, generally known as White Dammar, is a large evergreen tree growing up to 40-60 meters tall and contains bergenin

as a marker compound in huge amounts. The leaves of *Vateria indica* were collected from the CSIR-NIIST campus, Trivandrum, Kerala, India. The authors identified the plant sample, and the voucher specimen was deposited in the *M. S. Swaminathan Research Foundation* (MSSRF), Wyanad, Kerala, (Voucher Number: M.S.S.H.0763).

Malabaricone C is a diarylnonanoid, and it is one of the significant phytoconstituent present in the Myristicaceae family; the plants are native to Africa, Asia, the Pacific islands, and America. Myristicaceae family is well known for its antimicrobial properties. *Myristica malabarica* seeds were collected from JNTBGRI, Palode, Kerala, and the voucher specimen was deposited (Voucher number: TBGT 83442) in the herbarium of the same institute.

In this chapter, the screening of indigenously developed plant-based antimicrobial coating materials is discussed in addition to anti-corrosion. The recent pandemic situation made people vigilant and thought to an extent about how much they are prone to microbial attack. As a result, antimicrobial materials have been rapidly developed. The common pathogenic microbial strains *Pseudomonas aeruginosa* (gram-negative) and *Staphylococcus aureus* (gram-positive) are being used for the screening process. The compounds or coatings are qualitatively analysed and screened based on modified ASTM protocol (AATCC-147). Quantitatively, such active materials are tested based on the modified ASTM- AATCC-100 protocol.

Solutions of different concentrations of hydro-ethanolic extract of *Vateria indica* leaves in 3.5 wt.% NaCl is prepared, and its anti-corrosion potential was examined as preliminary studies. The promising activity of the whole extract led us to the isolation and characterization of the marker compound bergenin, its further modification into a bio-nano composite, the characterization of the isolated compounds and prepared hybrid composites, its anti-corrosion potential evaluation by various methods like immersion test analysis, electrochemical impedance measurements and potentiodynamic polarisation studies in environments of various pH. The antimicrobial efficiency of the intelligent coating was also evaluated.

3.2. Materials and Methods

3.2.1. Materials

The compounds bergenin and malabaricone C were isolated from the leaves of *Vateria indica* and the seeds of *Myristica malabarica*, respectively, by column chromatographic techniques. Cetyltrimethylammonium bromide was obtained from Sisco

research laboratories Pvt. Ltd., India. Tetraethyl orthosilicate 98%, ethanol 99.90% and anhydrous n-butanol 99.80% from Sigma-Aldrich. HCl and NaOH used for pH adjustments and NaCl were procured from Merck specialties private Limited, India. Bisphenol A diglycidyl ether (DGEBA) was bought from Alfa Aesar, United States and HY951 hardener obtained from Vantico, India. All the chemicals and solvents were of the best grade commercially available and were used without further purification. The strain of *S. aureus* and *P. aerugenosa* were obtained from the NIIST culture collection, Trivandrum, Kerala.

3.2.2. Methods

3.2.2.1. Extraction and isolation procedures

Fresh tender leaves of *Vateria indica* L. were collected, washed, and kept in a hot air oven at 50 °C for three days. About 750 g of dried leaves were crushed in a mechanical blender and extracted with a hydro-ethanolic solution in 6:4 ratios. The extraction was carried out with a mechanical stirrer for six days with 3L solvent which was replaced every two days. The collected solvent was decanted and vaporized at low pressure at 50 °C in a rotary evaporator. Finally, removing the residual solvent by freeze drying afforded 30 g of the crude extract.

The extract was loaded into a column packed with silica gel to isolate the component. The separation was carried out using silica (100-200 mesh) as the stationary phase and varying polarities of Hexane- Ethyl acetate solution as the mobile phase by eluting the column from lower polarity to higher polarity. The spots were detected, and the purity of the compound was analyzed by thin layer chromatography (TLC). While eluting the column with 80% EA-Hex solution, evaporating the solvent in the rotary evaporator, a compound was obtained as a solid in the RB flask in gram scale. Each fraction was analyzed with TLC, and pure fractions were coupled. Bergenin was purified by repeated column chromatography, and structure was confirmed with the help of ^{1}H, ^{13}C, and other 2D NMR techniques in comparison with literature [9,10]. About 8 g of Bergenin was obtained from the extract. The structure of the bergenin is given in **Figure 3.1a**.

About 1kg of dried seeds of *Myristica malabarica* was collected, crushed, and defatted with DCM. The residue is then subjected to acetone extraction. About 50 g of acetone extract is obtained. The various fraction pools containing different compounds are separated using column chromatographic techniques. The fraction pool obtained by eluting the column with 30% EtOAc-Hexane solution showed an intense UV active spot in TLC. On charring in Enholm yellow solution, the TLC turned into intense pink color. It was then

subjected to precipitation using DCM-hexane solution, afforded the compound as a pale yellow crystalline solid. ^{1}H NMR, ^{13}C NMR, other 2D NMR techniques, and mass spectral studies of this compound, and compared to the literature values, the compound was confirmed as Malabaricone C [11] **(Figure 3.1b)**. About 16 g of malabaricone C is obtained from 50 g acetone extract. Purity of the isolated compounds were evaluated by HPLC analysis. Bergenin was found to be 99.673% of purity and malabaricone C was 99.873% pure.

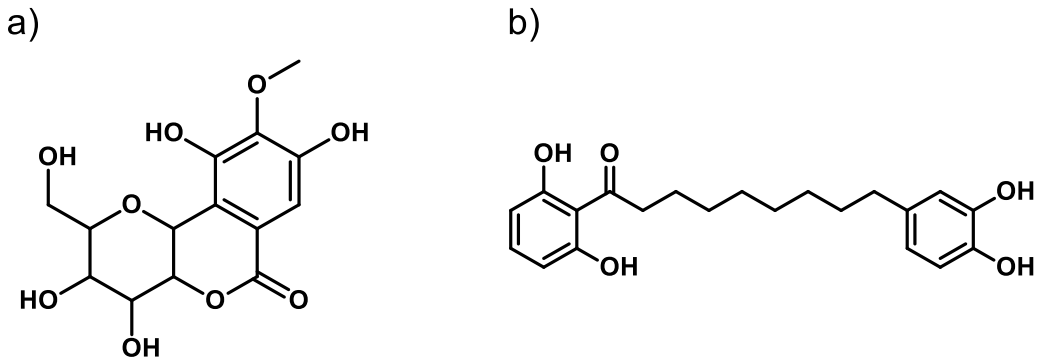

Figure 3.1. Structure of **a)** Bergenin, and **b)** Malabaricone C

3.2.2.2. Development of nanoparticle-green inhibitor composite

The nanocontainer mesoporous silica was synthesized by the following method reported earlier by the authors [2] with slight modifications. Surfactant solution is made by adding 2 g of cetyltrimethylammonium bromide to 960 mL of DI water and stirred well with a magnetic stirrer. The solution is made alkaline by adding 7 mL of 2.0 M NaOH solution with continuous stirring at 30 °C. The solution is slowly heated to 80 °C, and 5 mL of precursor compound TEOS is added drop-wise with a stirring rate sharply maintained at 750 rpm. The solution is stirred for 2 hours under the same conditions and a white powder of silica forms during the process. The solution was centrifuged at a speed of 10000 rpm for 5 minutes, and the precipitate was washed twice with ethanol and deionized water, respectively. To obtain the mesoporous silica nanocontainer, the precipitate was freeze dried.

Bergenin (BRG) was dissolved at a 50 mg/mL concentration in ethanol. Mesoporous silica nanoparticles (MSNP) were added to the solution of bergenin in a 1:2 ratio (MSNP: BRG). 1 g nanoparticles were added to a solution of 2 g compound and kept in a magnetic stirrer at 250 rpm for 24 hours. After 24 hours, the mixture was transferred to a petri dish and solvent was evaporated in a water bath at 60 °C for 12 hours to ensure

maximum loading inside and on the surface of the container. The prepared composite BRG-MSNP is vacuum dried at 60 °C. Similar procedures were repeated to prepare malabaricone C-mesoporous silica nanoparticle bio-nanocomposite (ML-MSNP).

3.2.2.3. Substrate and coating preparation

Mild steel and aluminium 6061 samples were used as the substrate material for the coating and as the working electrodes in the present study. Samples of 30×40×2 mm dimension were used in the study, and they were polished with sandpapers of 80 to 1000 grit size. Polishing procedures were similar for both samples while the surface cleaning procedures adopted were different. The polishing procedure is critical for the inhibitor's adherence to the surface of the metal. Also, the presence of any tiny amount of dirt or foreign material may trigger corrosion. In the case of MS, the samples were polished without scratches. After polishing, the sample surface is cleaned by ultrasonic degreasing with acetone for 10 minutes twice, then cleansed with distilled water, rinsed with acetone, and dried. In the case of aluminium 6061 alloy samples, in addition to the above procedures, etching in alkaline and acid solutions for 60 seconds each was also carried out after polishing, then cleaned, dried, and kept in a vacuum desiccator before use.

The saline medium utilized throughout the investigation was 3.5 wt.% NaCl solution. In the first step, the nanocontainer impregnated with bergenin (BRG-MSNP) was added to the epoxy in different concentrations at 1, 3, and 5 wt.% of the total weight of the epoxy and curing agent. The composite was well dispersed in butanol with the help of an ultrasound sonicator before the addition. This mixture was then poured into the resin and mixed continuously to achieve a homogeneous mixture. After adding the hardener, the mixture is thoroughly mixed again and applied to the metal substrate without any delay. The resin and curing agent ratio were 2:1, and a dip-coating instrument was used to coat the samples at 500 mm/min speed. After room temperature curing of 24 hours, the samples were dried at 50 °C for 24 hours in an oven. Thus, prepared samples were kept in a vacuum desiccator.

3.2.2.4. Immersion test analysis for corrosion protection efficiency

The non-electrochemical test used for the evaluation of corrosion inhibition efficiency was the immersion-weight loss method. This method is handy as it is reliable and straightforward. Immersion testing was done by immersing mild steel and Al-6061 sample coupons of size 1cm x 1 cm in a beaker containing 250 mL of the solution

containing 3.5 wt.% NaCl with and without the presence of green inhibitor at various pH. The samples were immersed in the solution for 30 days. After 30 days the samples were cleaned with distilled water and dried. The difference in the weight of samples prior to and after the immersion were recorded. Surface morphology was analyzed with SEM. The corrosion inhibition efficiency (IE %) and the total surface coverage (θ) by the inhibitor molecule were determined by the **equation (3.1)** [12].

$$IE(\%) = \frac{Wo-Wi}{Wo} \times 100 \quad \text{..... (3.1)}$$

$$\theta = \frac{IE\ (\%)}{100} \quad \text{..... (3.2)}$$

W_0 and W_i represent weight loss for MS and aluminium-6061 specimens in 3.5 wt.% saline medium with and without the presence of green inhibitor.

3.2.2.5. Electrochemical impedance and potentiodynamic polarisation

A conventional three-electrode system with a platinum electrode as the counter electrode, saturated calomel electrode (SCE) with fine Luggin capillary as the reference electrode and dip coated sample with coating removed from one side as the working electrode was used for EIS and Potentiodynamic polarization (PP) studies. The AC signal with a 5 mV amplitude perturbation at OCP in the frequency range 100 kHz–0.01 Hz was employed in the EIS analysis. The working electrode utilised in the investigation was exposed to a 1 cm^2 area. Anticorrosion performance of *Vateria indica* leaf extract was analysed by potentiodynamic and EIS methods. Different concentrations of the extract like 0 ppm, 100 ppm, 300 ppm and 500 ppm solutions in saline solution were prepared, and polished MS and Al-6061 coupons were used to evaluate the performance. E_{corr} and i_{corr} were determined from the Tafel plot, and corrosion inhibition efficiency (η %) were obtained from the **equation (3.3)**,

$$\eta\ \% = \frac{icorr-icorr(VIL)}{icorr} \quad \text{..... (3.3)}$$

Where i_{corr} and $i_{corr\ (VIL)}$ are the current densities without and with the extract of *Vateria indica* leaf.

To find the resistance values, the spectra were fitted using ZSimpWin software. R_{ct} and the Inhibition efficiency various amount of inhibitor in saline media, I.E. $_{EIS}$ % were determined with the following equations.

$$\text{I.E.}_{\text{EIS}}\ \% = \frac{Rct(VIL) - Rct(MS)}{Rct(VIL)} \times 100 \qquad \textbf{..... (3.4)}$$

R_{ct} (VIL) is the charge transfer resistance value of the sample in the presence of *Vateria indica* leaf extract in saline medium and R_{ct} (MS) is the charge transfer resistance value of the bare mild steel samples. The same measurements were also done for epoxy-coated samples with different concentrations of BRG-MSNP bio-nanocomposite. The working electrode was kept in contact with the electrolyte until a steady state was reached (30 min). For the epoxy-coated working electrode the time kept for stabilisation was 24 hours before starting the measurements.

3.2.2.6. Evaluation of antimicrobial action of the coating loaded with bio-nanocomposite

Malabaricone C and similar compounds were reported to have very high antimicrobial activity [13], a minimum quantity of malabaricone C was added to the optimised concentration of bergenin having maximum corrosion protection property. With 3 wt.% of BRG-MSNP, 0.1% of ML-MSNP was added and coated on an aluminium disc of diameter 1.7 cm by dip-coating method and dried as same in the above mentioned procedure. Later the antimicrobial action was determined both qualitatively by the zone of inhibition method and quantitatively by AATCC-147 and AATCC-100 protocols.

a) Qualitative analysis of antimicrobial activity

The antimicrobial activity was screened qualitatively by modified AATCC-147 (ASTM) protocol. In which actively growing 18 hours LB broth grown microbial cultures of *Pseudomonas aeruginosa* and *Staphylococcus aureus*, cultures were used. 100 µl of 10 times normal saline diluted culture broth was used as inoculum for spread plating. The aluminium metal plate coated with anti-microbial agents was taken in 1.7 cm diameter discs were used for testing. The uncoated discs were used as control and for each organism we kept duplicates, to ensure the accuracy and the plates were exposed to UV light for 20 minute to avoid contamination with other organisms. The Luria Bertani (LB) agar plates were used for spread plating, after inoculation the metal plates were kept in the centre region of the petri-plate and incubated for 24 hours at 37 ºC to get the clear zone around the metal plates. Such samples were screened out to test quantitatively to know the percentage reduction of microbial growth.

a) Quantitative analysis of antimicrobial activity

The samples which passed qualitative screening were tested using ASTM- AATCC-100 protocol quantitatively. In this test the culture inoculum was prepared as mentioned in the qualitative test and the microbial load in the inoculum was adjusted as 10^8 on dilution with normal saline. The culture inoculum then added to sterile 9 mL of normal saline taken in 100 mL screw cap conical flasks and the UV sterilized coated metal discs and the control discs, followed by 1 hour, 180 rpm shaking incubation. Duplicate plates were prepared for each sample. After incubation the inoculated saline with sample discs were serially diluted to 0x, 10x, 100x, 1000x and 10000x and done spread plating. The colonies formed after 24 hour incubation was counted and the percentage reduction was estimated to quantify the antimicrobial activity of test samples in comparison with control. The metal plates after incubation were also subjected to LB agar plating in order to find out the residual microbes absorbed on the metal surface.

3.3. Characterization techniques

The structure of the isolated compounds was confirmed with Bruker, Ascend 500 MHz NMR Spectrometer (Bruker India Scientific Pvt Ltd.). Functional groups present in the isolated compounds, nanocontainers, prepared bio-nano composites were analyzed by FTIR spectroscopy. PerkinElmer FTIR, from PerkinElmer Singapore Pte Ltd. was the instrument used for IR studies. TEM images were captured using FEI Tecnai G2, T30 with EDAX working at 300 kV. Thermogravimetric analysis was performed using STA7300 Thermal Analysis System, Hitachi. SEM images were captured using FE- SEM, FEI NOVA NANOSEM 450 and the elemental analysis was carried out using Zeiss EVO 18 cryo-SEM Special Edition attached with EDS operating at 10–30 kV after sputtering with gold. DLS and zeta potential measurements were done using Malvern Zetasizer Nano ZS90, Germany. N_2 adsorption-desorption procedure was done to confirm the mesoporous nature of the container, pore size, pore volume, and specific surface area of MSNP, ML-MSNP, and BRG-MSNP using Micromeritics, Tristar II, USA. BET and BJH methods were used to calculate the surface area, pore size, and pore volume. CH Instruments electrochemical workstation (CHI608E, CH Instruments Inc.) with a conventional three-electrode cell used for electrochemical impedance spectroscopy and potentiodynamic polarization studies. Dip coating was performed with Spectrodip Instruments dip coater (Chennai, India). EIS spectra obtained were fitted with ZSimpWin software. The coating thickness was measured using a Bruker DektakXT stylus optical profilometer. The Vickers

hardness measurements were performed using a Banbros hardness equipment, Model No. VHD-1000A (Banbros engineering Pvt. Ltd., India).

3.4. Results and Discussion

3.4.1. Characterization of the isolated molecule by Nuclear Magnetic Resonance

The compound bergenin was isolated as a colourless amorphous solid. The ^{1}H NMR spectrum **(Figure 3.2a)** exhibited a singlet peak for one aromatic proton at δ_H 6.98 (s) ppm and a sharp singlet for methoxy protons at δ_H 3.90 (s) ppm. In addition, signals observed between δH 3.35 and 4.09 ppm and a doublet at δH 4.94 (J = 10 Hz, 1H) ppm indicating the existence of a sugar moiety of the compound. The ^{13}C NMR spectrum **(Figure 3.2b)** exhibited fourteen carbon signals, including the ester carbonyl carbon at δ_C 163.4 ppm, one methoxy carbon at δ_C 59.8 ppm, and aromatic carbon at δ_C 109.4, 118.1, 150.4, 140.6, 148.1, and 115.9 ppm. The glycosidic units are observed in the range δ_C 83.0 - 62.6 ppm. The compound was confirmed as bergenin based on the literature survey [14] and complete analysis of 1D and 2D NMR spectra. The compound malabaricone C was isolated as a yellow solid. The structure of the compound was confirmed by comparing the ^{1}H NMR (**Figure 3.3a**) and ^{13}C NMR (**Figure 3.3b**) data with the literature [15].

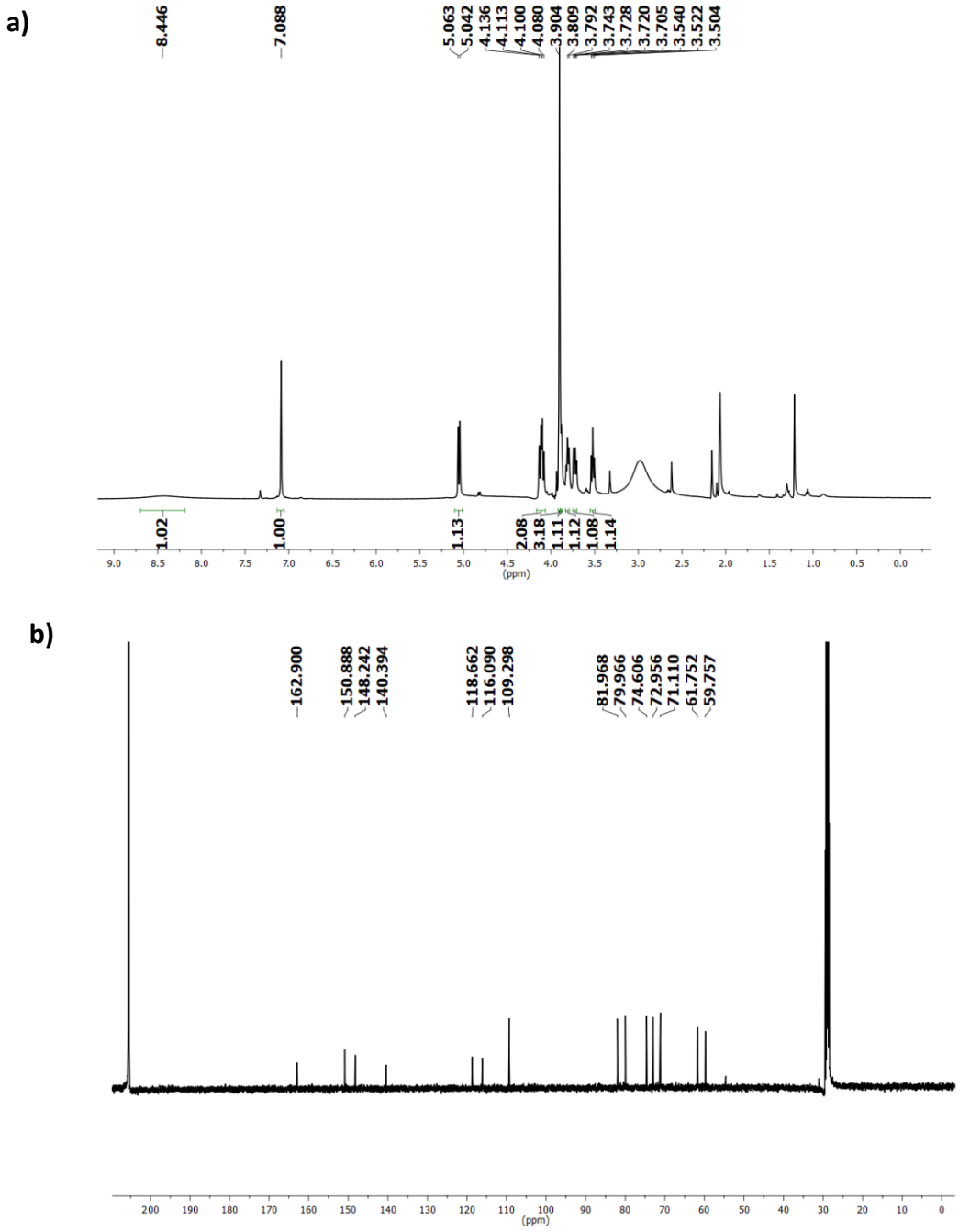

Figure 3.2. a) ^{1}H NMR spectrum (500 MHz, acetone-d_6) of bergenin **b)** ^{13}C NMR spectrum (125 MHz, acetone-d_6) of bergenin.

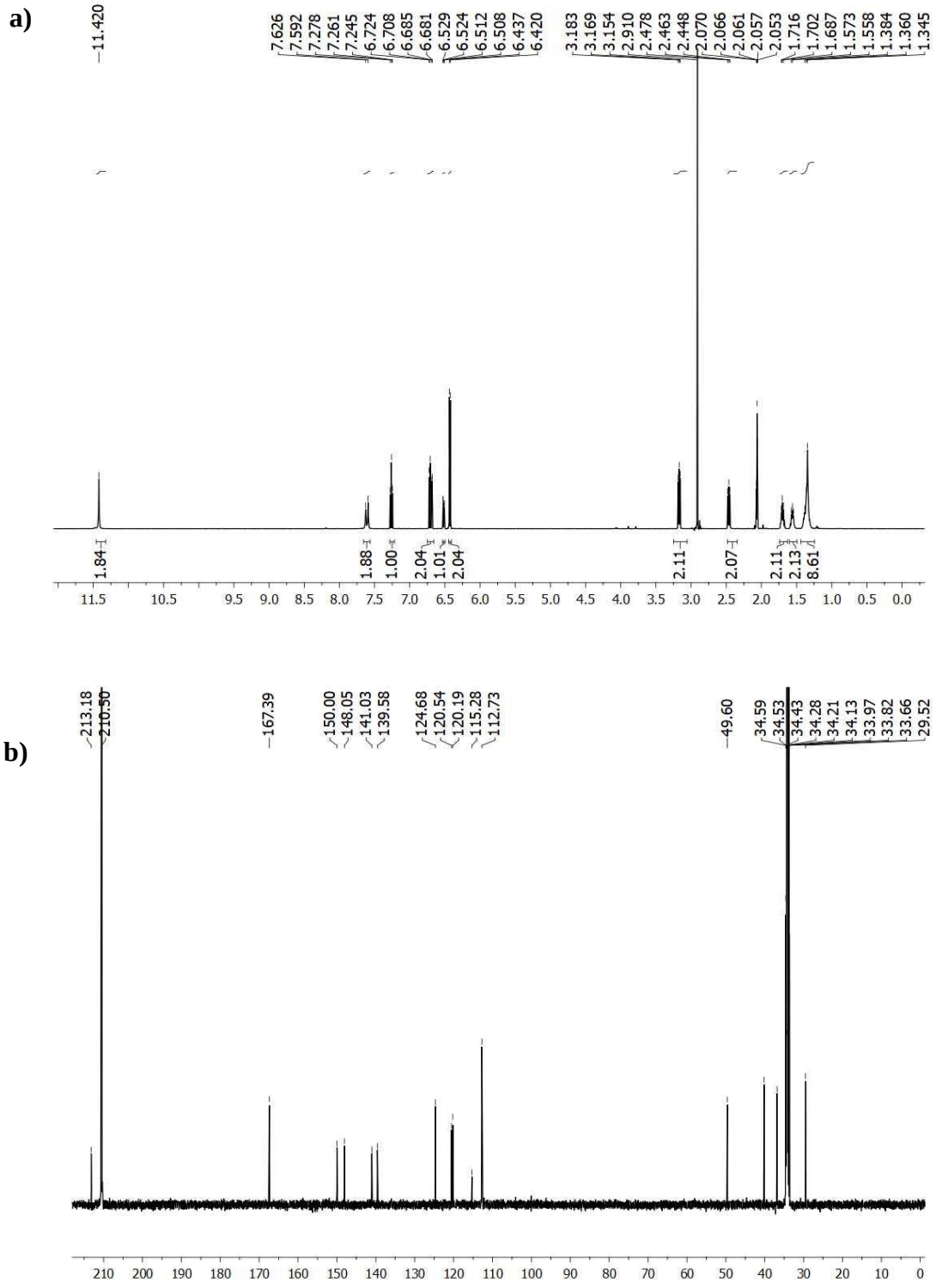

Figure 3.3. a) ^{1}H NMR spectrum (500 MHz, acetone-d_6) of Malabaricone C **b)** ^{13}C NMR spectrum (125 MHz, acetone-d_6) of Malabaricone C

3.4.2. Characterization of the nano-container, nanocomposite and inhibitor coatings

3.4.2.1. ATR-FTIR analysis

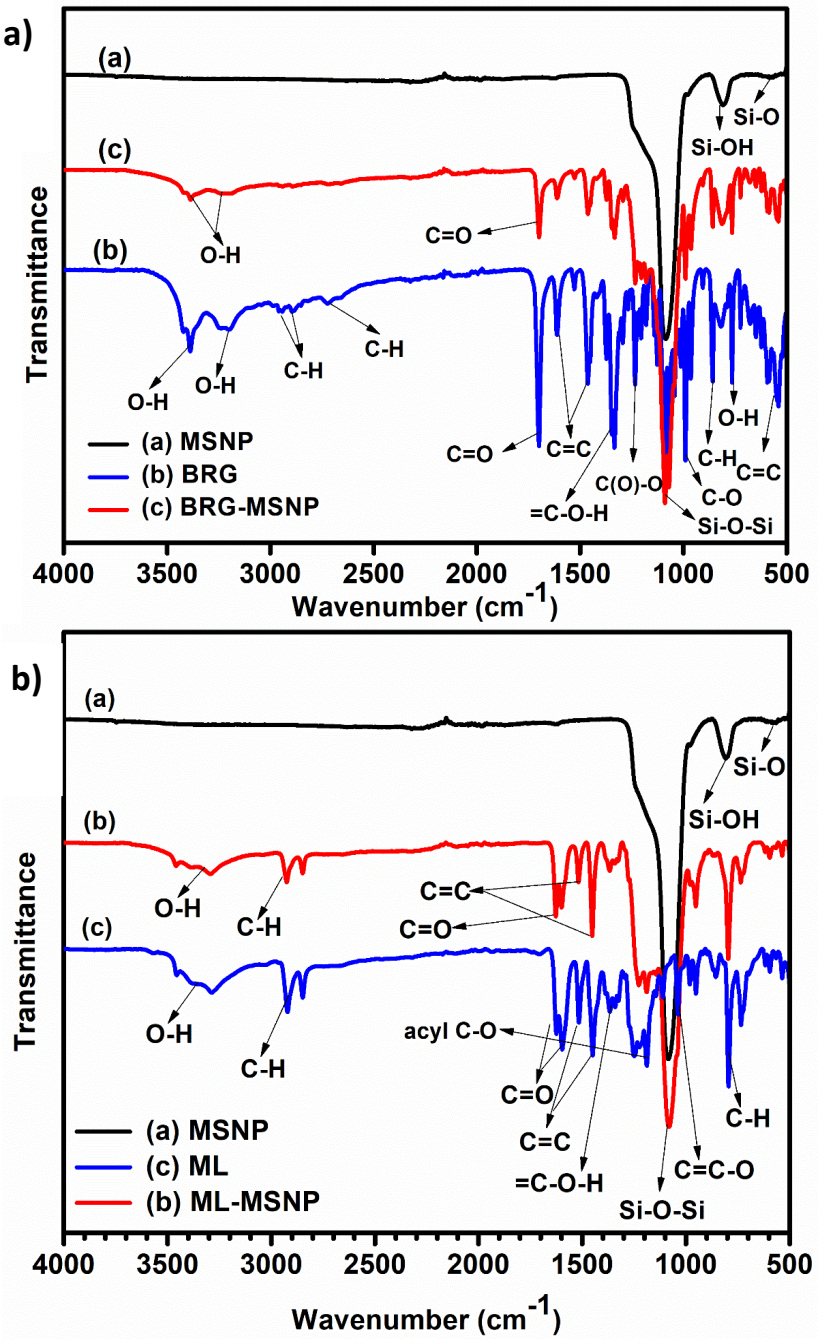

Figure 3.4. a) FTIR analysis of mesoporous silica nanoparticle (MSNP), bergenin (BRG), and prepared bionanocomposite (BRG-MSNP) **b)** FTIR analysis of mesoporous silica nanoparticle (MSNP), malabaricone C (ML), and prepared bio nanocomposite (ML-MSNP).

The Fourier transform infrared analysis of mesoporous silica nanoparticle (MSNP), bergenin (BRG), malabaricone C, prepared bio-nano composites BRG-MSNP and ML-MSNP are given in **Figure 3.4a** and **Figure 3.4b.**

All possible interactions between the inhibitor and the nanocontainers can be understood from this spectrum. The broadband present at 3387 cm^{-1} and 3195 cm^{-1} is assigned to usual –OH stretching vibrations which are characteristics of alcoholic and phenolic compounds. Bergenin contains different kinds of hydroxyl groups viz. phenolic, primary, and secondary alcohol groups. Aliphatic and aromatic C-H stretching vibrations are observed at 2955, 2888, and 2722 cm^{-1}, etc. The peak at 1697 cm^{-1} represents the C=O group of lactone ring of bergenin. In the fingerprint region, C-OH out of plane bending, C-O stretching, C=C-H bend, etc. was found. The shoulder peak between 1100 and 1300 cm^{-1} represents Si-CH_2, the peak at 980 cm^{-1} stands for silanol group (Si-OH), and 462 cm^{-1} represents Si-O rocking. All the characteristics peaks of both MSNP and BRG are present in BRG-MSNP nanocomposite, ensuring the loading of green inhibitor into the container material. Similarly, in the case of malabaricone C, all the fundamental and fingerprint frequencies for ML and MSNP are present in ML-MSNP. In both bio-nano composites, there is no significant change in the position of any of the frequencies corresponding to vibration or bending. This information clearly indicates there is no chemical reaction happening by the loading; only a physisorption method is used to load the compound in the container.

3.4.2.2. Morphology and size analysis- Scanning Electron Microscopy

Surface morphology and elemental analysis of the prepared particles were carried out after the synthesis. The surface of the nano containers seems to be roughened surface with spherical morphology, and it is maintained even after the loading of the compound, indicating surface structural stability. Subsequently, the EDS analysis (**Figure 3.5)** confirmed the presence of C, O, and Si in the composites, and the corresponding weight percentage of each element are tabulated. The higher amount of C and O in the elemental compositions of bionanocomposite justifies and ensures the complete coverage of the green inhibitor on the MSNP and confirmed the successful formation of the BRG-MSNP and ML-MSNP hybrid.

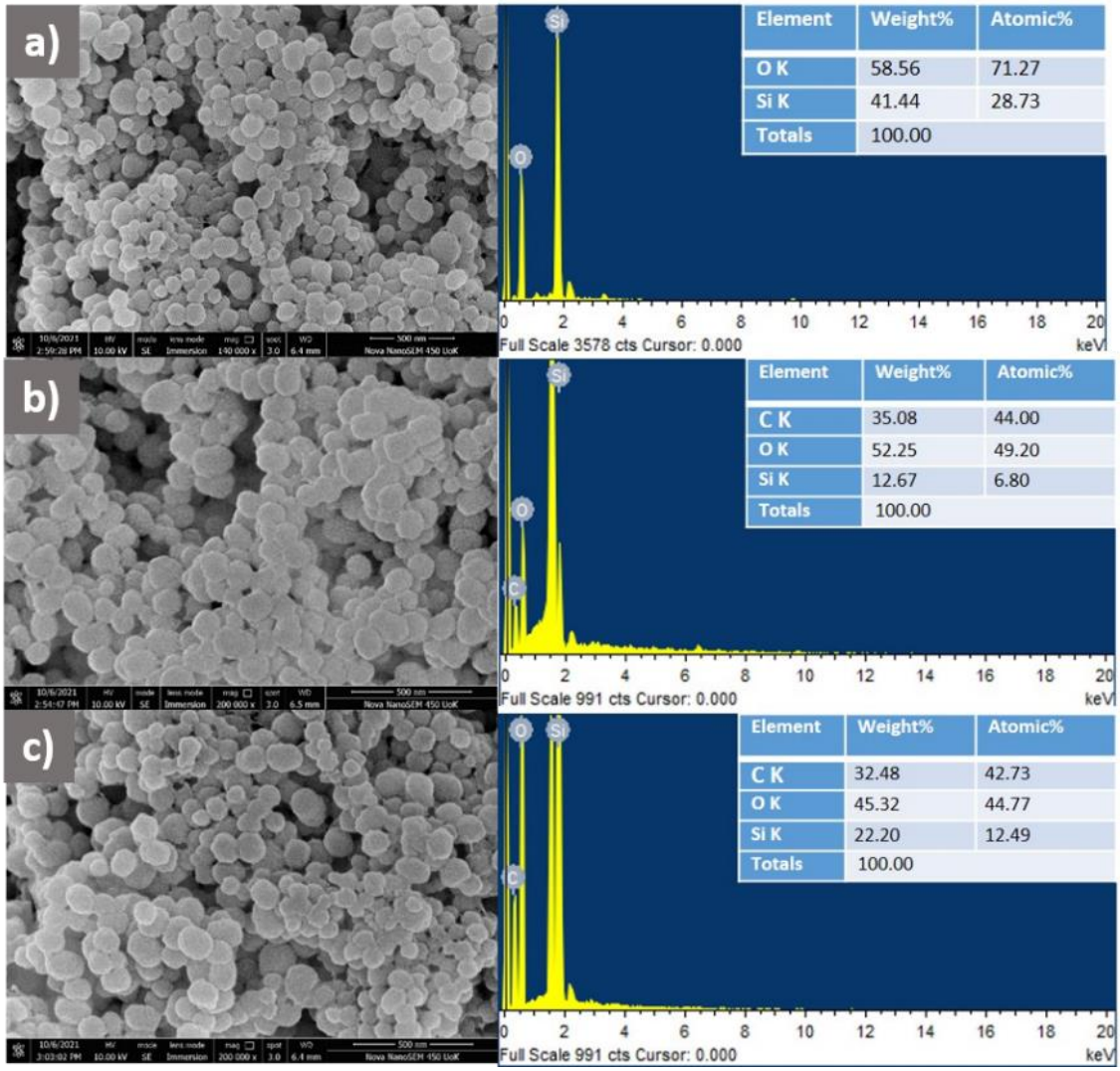

Figure 3.5. SEM images and EDS spectra of **a)** MSNP, **b)** BRG-MSNP and **c)** ML-MSNP

3.4.2.3. Morphology and size analysis- Transmission Electron Microscopy (TEM)

The TEM micrographs in **Figure 3.6** show the Mesoporous silica nanoparticles and loaded particles BRG-MSNP and ML-MSNP. The particles are spherical in morphology and are polydisperse. The mesoporous nature of the containers is evident in the TEM images, and it allows the adsorption of the inhibitors inside the containers. After the loading, the pores are seen to be covered, and the surface seems to be more or less smooth than the empty container surface. The surface of BRG-MSNP seems to be smoother, and it is visibly bulkier than the MSNP and ML-MSNP, which indicate much better loading for bergenin. It is also evident from the loading percentage calculated by thermogravimetric analysis. The difference in loading percentage can be attributed to the difference in structure. Bergenin is more planar, and in the case of malabaricone C, due to the longer alkyl chain, it can assume different geometries, which may decrease the loading percentage.

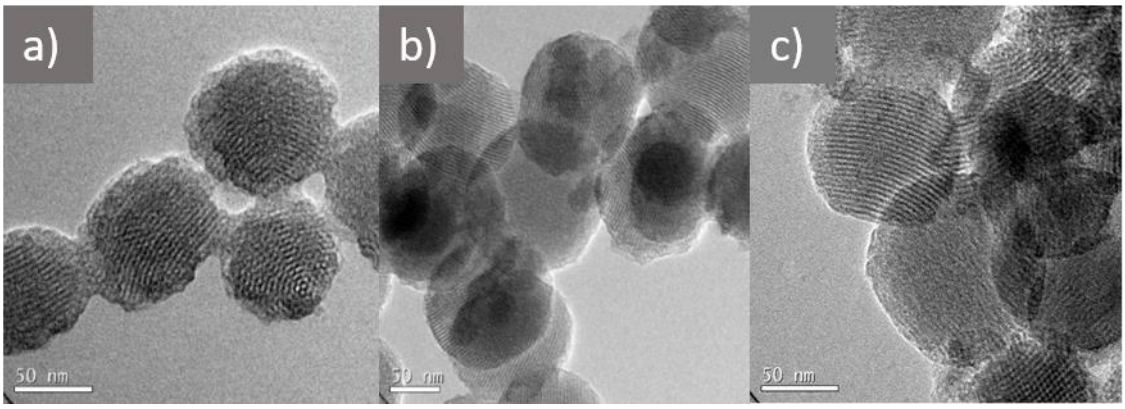

Figure 3.6. TEM micrographs and of **a)** MSNP, **b)** BRG-MSNP and **c)** ML-MSNP

3.4.2.4. Thermogravimetric analysis

From the data obtained by the thermal analysis (**Figure 3.7**) of the container, individual phytochemicals, the prepared bio-nano composites and the epoxy coating, the stability of each sample and the percentage of loading of green inhibitor in each composite sample was calculated.

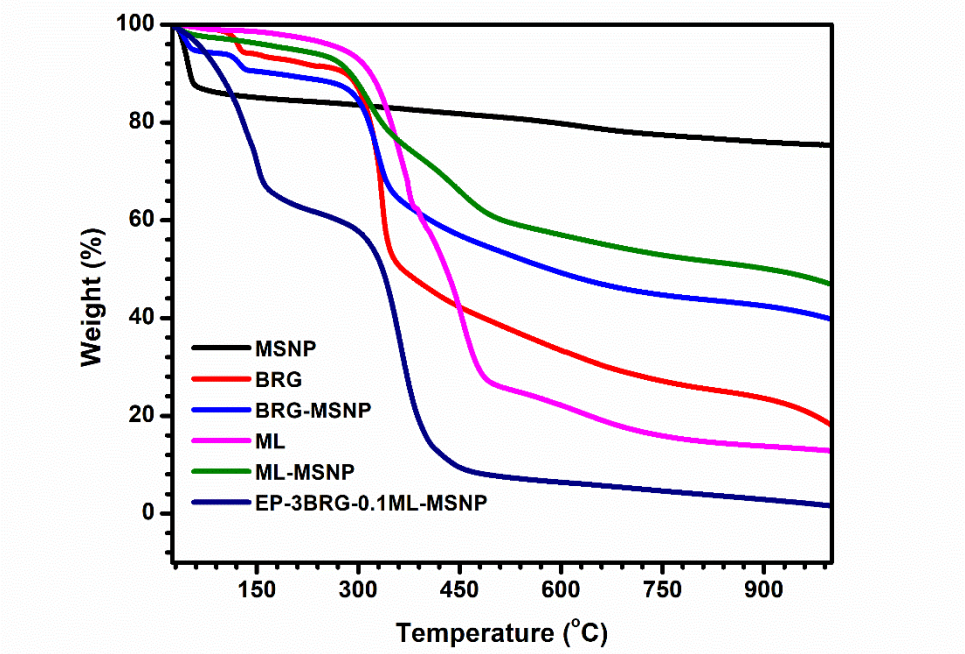

Figure 3.7. Thermal stability analysis of **a)** Mesoporous silica nanoparticles **b)** bergenin **c)** BRG-MSNP **d)** malabaricone C **e)** ML-MSNP **f)** Cured epoxy composite coating with BRG-MSNP and ML-MSNP nanoparticles.

The composites and coating are stable up to 300°C. Tiny weight loss observed in the initial time in the case of mesoporous silica containers, compounds and composites are

due to the evaporation of physically and chemically absorbed water. The higher weight reduction experienced in the case of coatings is due to the evaporation of water and organic solvent like butanol used during the dip coating procedure. Both the composites have similar degradation pattern and the presence of the organic components reduced the weight of final residue of the nanocomposite compared to empty containers.

3.4.2.5. Nitrogen adsorption/desorption analysis

BET and BJH methods were used for the characterisation of the nanocomposites and nanoparticle. **Figure 3.8** shows N_2 adsorption-desorption isotherm for MSNP, BRG-MSNP, and ML-MSNP to analyse the structure. The hysteresis loop of ML-MSNP and BRG-MSNP showed lower adsorption of N_2 compared to MSNP as the inhibitor molecules occupy the pores. The structural parameters like specific surface areas by BET model and pore diameter and pore volume calculated by the BJH model, are given in **Table 3.1**. Successful incorporation of the green inhibitor inside the mesoporous silica is indicated by the reducing trend in the parameters.

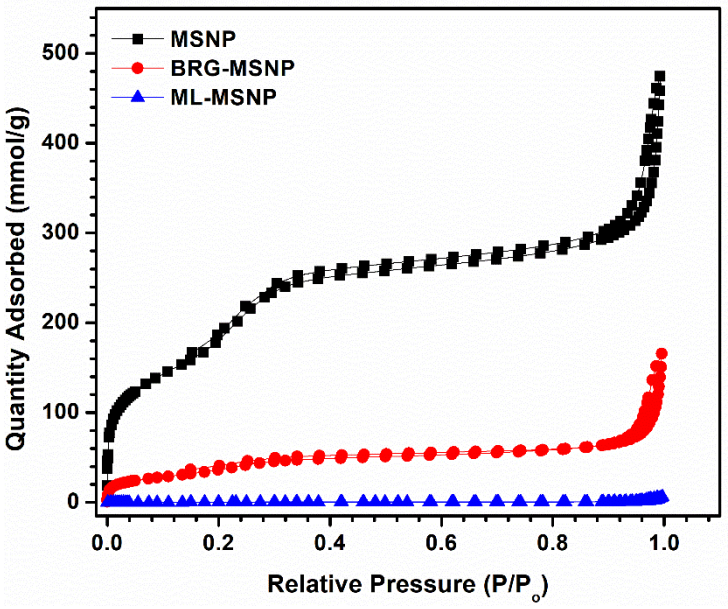

Figure 3.8. Nitrogen adsorption/desorption isotherm for MSNP, BRG-MSNP, and ML-MSNP

Table 3.1. Surface area and pore size analysis of the prepared nanoparticles and the bio-nano composites BRG-MSNP and ML-MSNP

Samples	BET Surface Area (m^2/g)	Total Pore Volume (cm^3/g)	Pore diameter by BJH (nm)
MSNP	729.70	0.68	3.75
BRG-MSNP	144.04	0.23	70.24
ML-MSNP	19.17	0.15	30.63

3.4.3. Corrosion inhibition potential evaluation in saline media of varying pH

3.4.3.1. Corrosion inhibition efficiency of the whole extract

The corrosion inhibition potential of VIL extract was more clearly evident in the potentiodynamic studies shown in **Figure 3.9**. Even with a small concentration of extract in the electrolytic solution, a good inhibition property was observed. The potential of the extract in corrosion inhibition is reflected in corrosion current density (i_{corr}) and corrosion potential (E_{corr}) values (**Table: 3.2**). The measured impedance data for various concentrations of *Vateria indica* leaf extract were plotted and analysed as the Nyquist plot (**Figure 3.9)** reveals the inhibition efficiency of 0, 100, 300, and 500 ppm VIL extract for mild steel samples in terms of resistance in saline media. The impedance measurements exhibited increased resistance values due to the corrosion inhibition property of the phytochemicals present in the plant extract.

Table 3.2. Potentiodynamic polarisation and electrochemical impedance analysis of the VIL extract and calculation of inhibition efficiency

S/N No.	Conc. of the extract (ppm)	Potentiodynamic polarisation			EIS	
		E_{corr} (V)	i_{corr} (μAcm^{-2})	η (%)	R_{ct} ($\Omega\ cm^2$)	IE_{EIS} %
1.	0	-0.666	30.53	_	851.9	_
2.	100	-0.774	17.52	42.61	1128	24.53
3.	300	-0.728	5.39	82.43	1377	38.11
4.	500	-0.700	1.98	93.52	2418	65.02

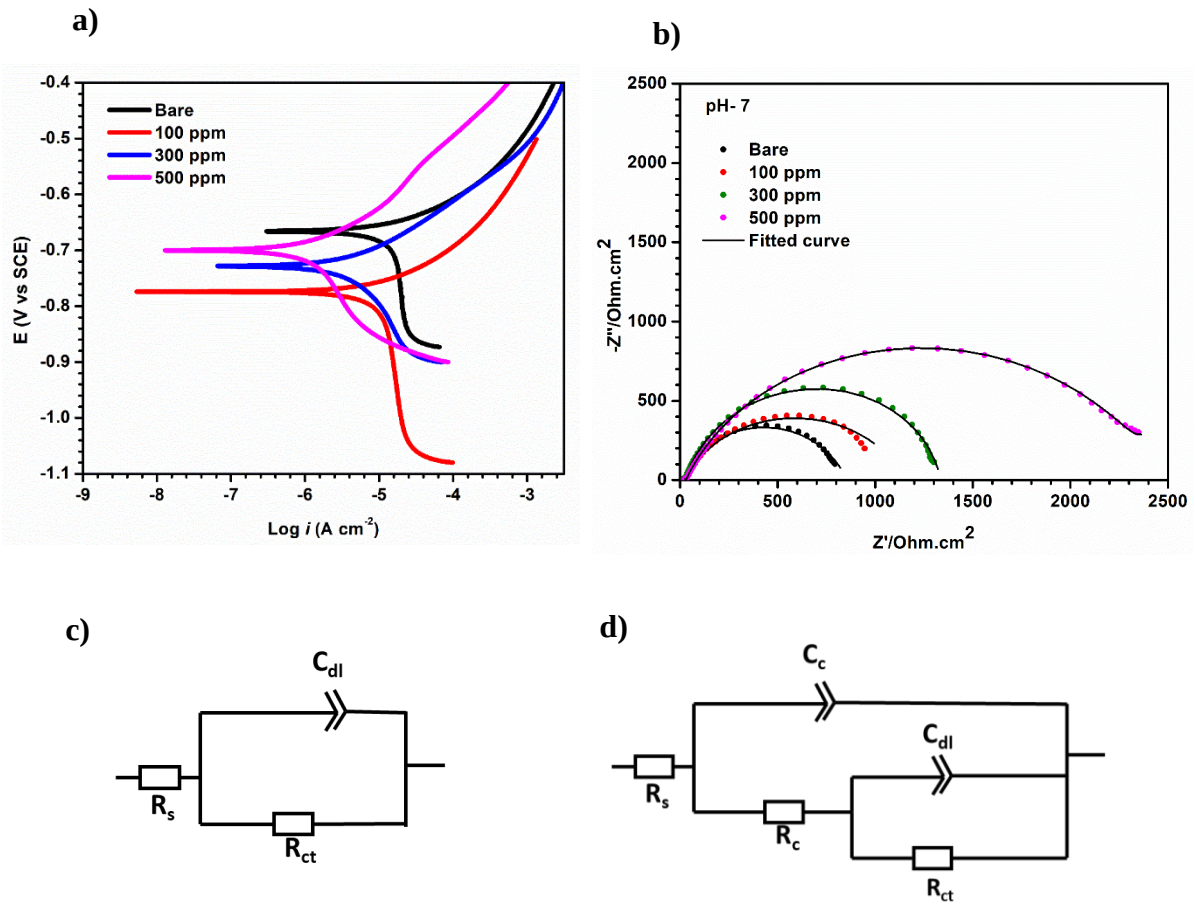

Figure 3.9. Potentiodynamic polarisation analysis and impedance measurements of MS samples in the presence VIL extract in 3.5 wt.% NaCl solution. **a)** Tafel plots **b)** Nyquist plots for extract level studies **c)** EEC for bare MS samples without VIL extract **d)** EEC for MS samples in the presence of VIL extract.

On adding a minute amount of the extract 100 ppm exhibited 42.61% of inhibition efficiency but showed a negative effect on E_{corr} values. However, concentration of 300 ppm brought a significant corrosion inhibition on mild steel, viz., the i_{corr} value is decreased to 5.386 µA/cm^2 from 30.53 µA/cm^2 with an inhibition efficiency of 82.43%. Nevertheless, the E_{corr} value shifted to a more negative potential than bare mild steel. To evaluate the influence of concentration on inhibition potential, the study is repeated with a concentration of 500 ppm and resulted in an efficiency of 93.52%. The fitted equivalent electrochemical circuit (EEC) can be represented as in **Figure 3.9**. The bare mild steel can be fitted using the EEC $R_s(C_{dl}R_{ct})$ and in the presence of extracts the bio-film coated samples can be fitted using the circuits $R_s(C_cR_c(C_{dl}R_{ct}))$. Where R_s is the solution resistance, C_{dl} and R_{ct} are double layer capacitance and the charge transfer resistance respectively. The plant extract forms a coating on the surface of the mild steel by adsorption of the phytochemicals present in it.

C_c is the capacitance offered by the coating and the resistance derived from this capacitance is denoted as R_c. The increase in the concentration of the extract increases the surface coverage and thus the resistance values. As the R_c value increases, resistance towards the interaction with the electrolyte or other corrosive ions increases and better the resistance of the coating [16].

3.4.3.2. Immersion test analysis and surface topology for mild steel and Al-6061 alloy

The inhibition efficiency (IE%) and surface coverage (θ) are calculated **with equation (3.1)** and **(3.2)**. The corrosion inhibition potential of bergenin nanocomposite determined by the immersion test of MS and Al-6061 alloys in saline medium for 30 days are given in **Table 3.3.**

Table 3.3. Immersion test result for MS and Al-6061 alloy samples- effect of bergenin nanocomposites

Sample	**pH 4**		**pH 7**		**pH 10**	
	IE (%)	θ	IE (%)	θ	IE (%)	θ
Bare MS in saline medium with green inhibitor composite (0.5 g/L)	83.01	0.83	89.22	0.89	80.92	0.81
Bare Al-6061 in saline medium with green inhibitor composite (0.5 g/L)	82.72	0.83	88.56	0.89	80.10	0.80

The topologic changes of mild steel surfaces are investigated with and without a green inhibitor using the scanning electron microscope. The metal surfaces were severely affected by the chloride solution. But the samples immersed in the presence of inhibitor molecule showed a much lesser effect of corrosion, and the groves and the irregular voids were of very low intensity (**Figure 3.10**). Elemental analysis of the surface shows a lower percentage of oxide formation in the presence of the green inhibitor nanocomposite, which indicates inhibition of the formation of corrosion products.

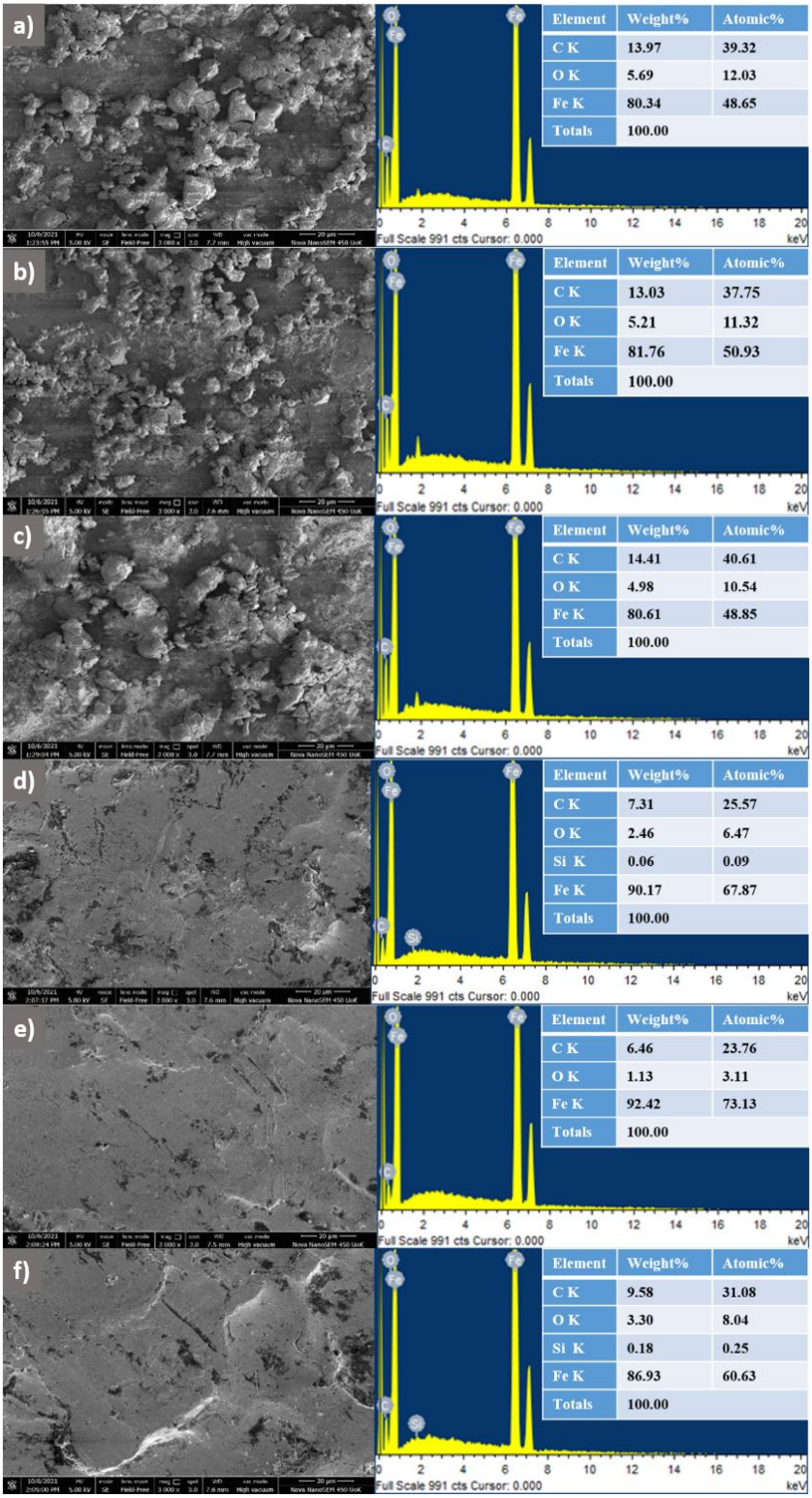

Figure 3.10. SEM images and elemental analysis of MS coupons immersed in 3.5 wt.% NaCl solution without of inhibitor **a-c)** and in the presence of inhibitor BRG-MSNP (0.5 g/L) after 30 days **d-f)**. **a)** at pH 4 **b)** at pH 7 **c)** at pH 10 **d)** at pH 4 **e)** at pH 7 **f)** at pH 10.

3.4.3.3. Epoxy-bio-nanocomposite coatings' efficiency analysis for mild steel samples

The Tafel plots of potentiodynamic polarisation analysis at pH 7 is given in **Figure 3.11**. This shows that the addition of bergenin nanocomposite to epoxy medium can effectively prevent the corrosion of mild steel samples in 3.5 wt.% NaCl solution. The potentiodynamic polarisation parameters for bare and coated mild steel samples at neutral medium are obtained from the Tafel polarization curves and are tabulated in **Table 3.4**. These data clearly indicate that the current density is decreased by the addition of inhibitor into the coating matrix. As the concentration increases, the inhibition efficiency of the polymer matrix also increases, but beyond a particular concentration, the corrosion current starts to increase, and the potential of coating tends to decrease slightly. As the concentration of the bergenin increases, the curves are shifted to more positive potentials with respect to the bare mild steel; it indicates the anodic protection by the formation of a film on the surface. The E_{corr} values of the bare mild steel shifted from -0.666 V to -0.256 V the case of coating with 3 wt.% of bio-nanocomposite. The i_{corr} values decreased to 0.054 μ Acm^{-2} from 30.53 μ Acm^{-2} in the case of comparison with bare mild steel with an inhibition efficiency of 99.82%. Adding a small amount of malabaricone C composite to the best concentration of bergenin, the i_{corr} value showed the best performance, and the corrosion potential is slightly moved to the negative potential, but the inhibition efficiency was still 99.83%. This suggests that when the second composite is added, the entire matrix exhibits mixed inhibitor behaviour to some extent in addition to the anodic inhibition protection by bergenin. A passivation is observed in all the coatings containing bio nanocomposites. This passivation region ensures the stability of the coating over a wide potential range.

Nyquist plot of MS samples in 3.5 wt.% NaCl solution at neutral pH is presented in **Figure 3.11**. The difference in the Nyquist plots at low and high frequencies was used to obtain the charge transfer resistance (R_{ct}) values. All coatings have an increasing trend in R_{ct} values and semi-circular loop radius compared to bare MS, indicating that they have excellent electrical resistance to corrosive elements and good barrier properties. The efficiency of the inhibitor in corrosion inhibition can be calculated by the impedance measurements from the R_{ct} values using the equation,

$$IE_{EIS}\ \% = \left[\frac{Rct - R*ct}{Rct}\right] \times 100$$

Where,

R^*_{ct} = the charge-transfer resistances for the bare mild steel sample.

R_{ct} = the charge-transfer resistances for coated mild steel samples.

The Nyquist plot for bare and mild steel samples were fitted using Zsimpwin software. The electrochemical equivalent circuit for mild steel samples in saline media can be represented as $R_s(C_{dl}R_{ct})$ and for all other coatings the EEC is $R_s(C_cR_c(C_{dl}\ R_{ct}))$ with increasing resistance values. R_s is the solution resistance and pure capacitance term was replaced by constant phase angle element $C_{PE.}$ The capacitance and resistance due to the epoxy coatings is represented by C_c, R_c which occurs at high-frequency region. In general, Rc is related to resistance towards the penetration of electrolytes, i.e., larger Rc represents better corrosion resistance of coating [16,17]. The capacitance offered by the electrical double layer between the metal surface and the electrolyte is represented as double-layer capacitance C_{dl}, and the resulting resistance derived from the capacitance is R_{ct} respectively the medium-low frequency elements. The capacitive elements C_{dl} and C_c followed the reverse order of resistance elements. Higher value of C_c indicates a higher electrolyte uptake of the coating. So, the lower values of capacitive elements indicate good corrosion protection of epoxy bio-nanocomposite coatings[18]. The fitted equivalent circuit diagram for the coating's studies of mild steel in saline medium can be represented as in **Figure 3.11**, which explains the mechanism of corrosion inhibition of the modified epoxy coatings.

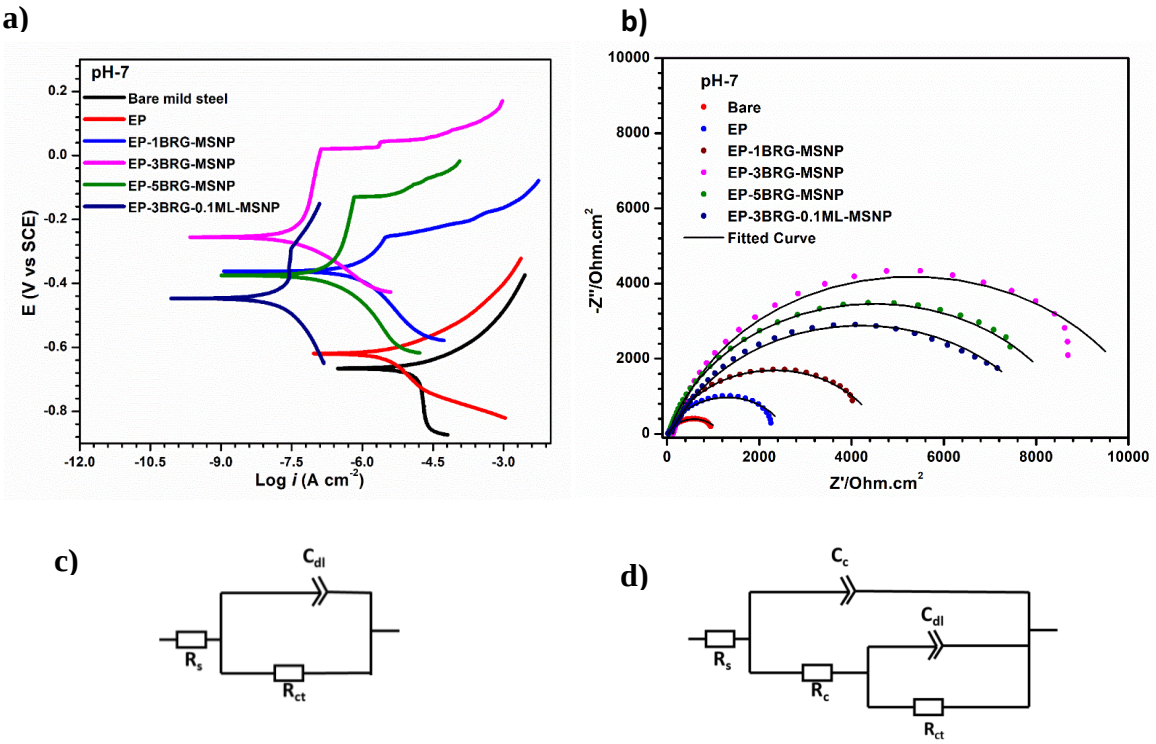

Figure 3.11. Potentiodynamic polarisation and impedance measurements for MS and epoxy coated MS samples with different concentrations of green inhibitor composites at

pH-7. **a)** Tafel plots **b)** Nyquist plots **c)** EEC for bare MS and **d)** EEC for coated samples in saline medium.

Table 3.4. Inhibition efficiency calculation from potentiodynamic polarisation and electrochemical impedance analysis of the coated samples

S/N	Substrate	Potentiodynamic polarisation			EIS	
		E_{corr} (V)	i_{corr} (μ Acm^{-2})	η (%)	R_{ct} (Ω cm^2)	IE_{EIS} (%)
1.	Bare mild steel	-0.666	30.53		1128	
2.	EP	-0.619	4.818	84.20	2574	56.17
3.	EP-1BRG-MSNP	-0.362	0.836	97.26	4614	75.60
4.	EP-3BRG-MSNP	-0.256	0.054	99.82	10030	88.80
5.	EP-5BRG-MSNP	-0.375	0.299	99.02	8939	87.40
6.	EP-3BRG-0.1ML-MSNP	-0.447	0.051	99.83	9443	88.05

The corrosion inhibition efficiency is also examined in acidic and alkaline pH. The coating was effective at pH 4 and pH 10. However, the best performance was in a neutral medium. The EIS measurements of mild steel samples in acidic and alkaline pH spectra were fitted using ZSimpWin 3.21 software showed excellent resistance values. The R_{ct} and the IE% were determined. The measured impedance and fitted curves and potentiodynamic polarisation study are shown in **Figure 3.12.**

Table 3.5. Electrochemical impedance parameters and polarization evaluation of mild steel samples in various pH

Sample	pH 4					pH 10				
	Potentiodynamic polarisation parameters			EIS		Potentiodynamic polarisation parameters			EIS	
	E_{corr} (V)	i_{corr} (μ Acm^{-2})	η (%)	R_{ct}	IE_{EIS} (%)	E_{corr} (V)	i_{corr} (μ Acm^{-2})	η (%)	R_{ct} (Ω cm^2)	IE_{EIS} (%)
Bare	-0.592	24.51	_	1461	_	-0.641	29.77	_	1509	_
EP	-0.658	5.97	75.6	4099	64.36	-0.613	5.10	82.9	2927	48.5
EP-3BRG-MSNP	-0.677	0.88	96.4	6525	77.61	-0.605	2.77	90.7	11310	86.7

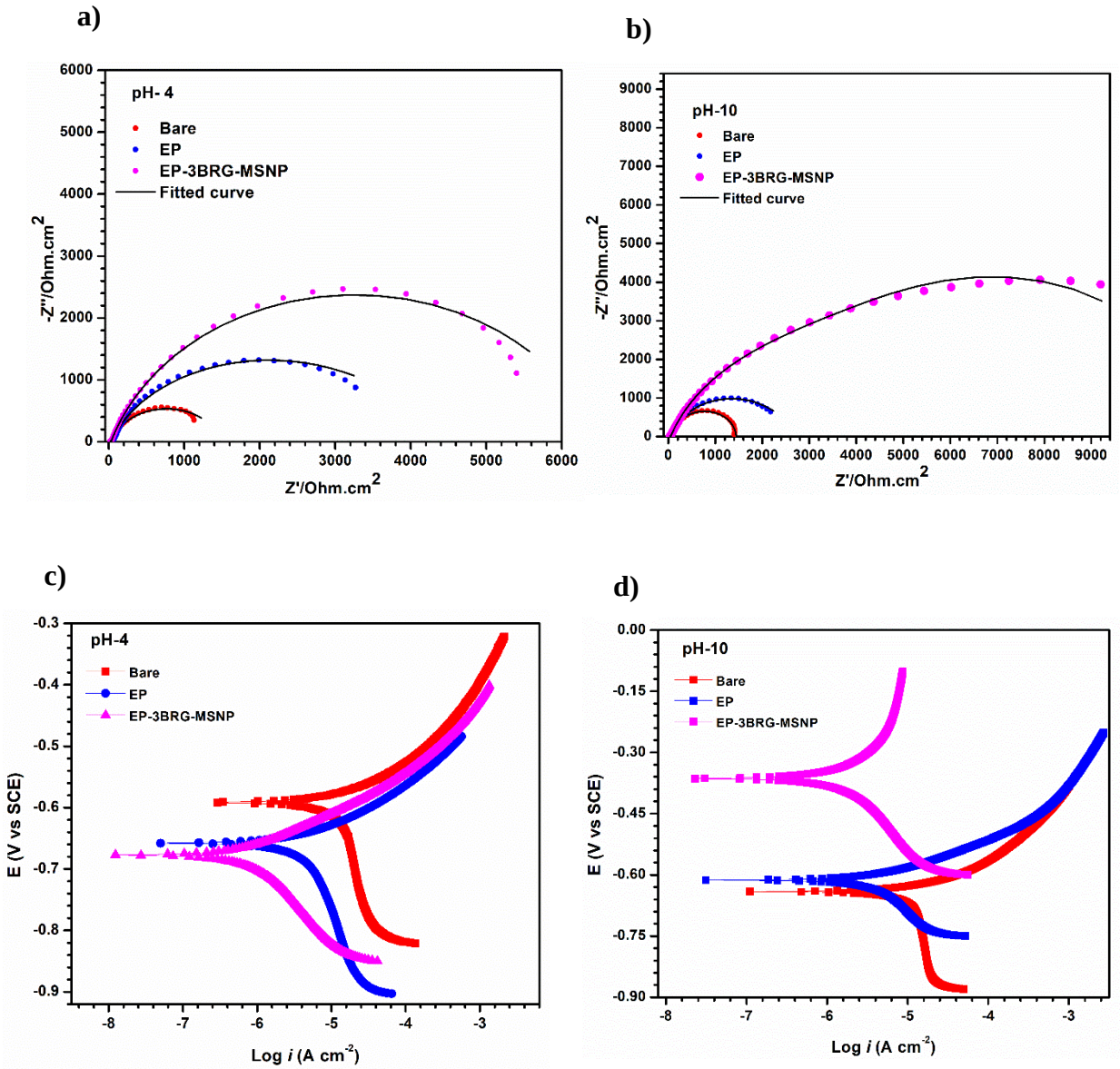

Figure 3.12. Nyquest plots of mild steel samples **a)** at pH-4 and **b)** at pH-10. Tafel plots of mild steel samples at **c)** pH-4 and **d)** pH-10 saline solution at 298 K.

3.4.3.4. *Protective Epoxy-bio-nanocomposite coatings' inhibition efficiency analysis for Al-6061 alloy*

The corrosion inhibition potential of the prepared bionanocomposite is also tested for Al-6061 alloy. The optimized concentration of 3% BRG-MSNP and pH 7 is used for coating studies in aluminium samples. The sample is coated by dip coating method, and the inhibition efficiency is determined by comparing the performance with bare Al-6061 samples and epoxy coated samples. Tafel plot for potentiodynamic polarisation analysis of Al-6061 samples is depicted in **Figure 3.13**. There is a significant surge in the corrosion

potential (E_{corr}) and a considerable reduction in the corrosion current (i_{corr}) value. The electrochemical parameters obtained, E_{corr}, i_{corr}, and inhibition efficiency η, are given in **Table 3.5**. In addition to the passivation caused by the oxide layer formation in the bare Al-6061 there is a huge passivation area in the epoxy coating and the bergenin composite coating. In the case of coating with bergenin a second passivation region is also observed. This passivation increases the corrosion protection ability of the coating to a great extent.

Nyquist plot of Al-6061 samples in 3.5 wt.% NaCl solution at neutral pH is shown in **Figure 3.13**. The equivalent electrochemical circuit is fitted using ZsimpWin software. The R_{ct} values were determined and compared. The increase in the R_{ct} value indicates the development of the protective insulating layer on the metal. The EEC diagram is shown in **Figure 3.13c** and **Figure 3.13d.** The equivalent electrochemical circuit for bare Al-6061alloy samples in saline media can be represented as $R_s(C_{dl}R_{ct}(C_{oxi}R_{oxi}))$ and for all other coatings the EEC is $R_s(C_cR_c(C_{dl}R_{ct})(C_{oxi}R_{oxi}))$ with increasing resistance values. R_s is the solution resistance and pure capacitance term was replaced by constant phase angle element $C_{PE.}$ In the case of bare alloy, the capacitance offered by the electrical double layer between the metal surface and the electrolyte is represented as double-layer capacitance C_{dl}, and the resulting resistance derived from the capacitance is R_{ct} respectively in the high frequency region. While corrosion reaction of Al-6061 alloy in the corrosion medium and the resistance ($R_{oxi)}$ offered by the corrosion product aluminium oxide layer is the second resistance appearing at low frequency region [19]. In the case of epoxy coated samples the high-frequency elements C_c and R_c are equal to the capacitance and resistance offered by the coatings; the medium-low frequency elements C_{dl}, R_{ct} are double-layer capacitance and charge-transfer resistance, respectively. R_c and R_{ct} are related to inhibition of the penetration of electrolytes and corrosive ions and electron transfer, respectively. C_c and C_{dl} are related to the absorption of electrolyte and double-layer capacitance phenomenon. Higher resistance values and lower C_c and C_{dl} values confirms a better corrosion protection by the modified epoxy coatings [20]. During the immersion time some of the corrosive ions may reach the metal surface and formation of corrosion products occurs [21].

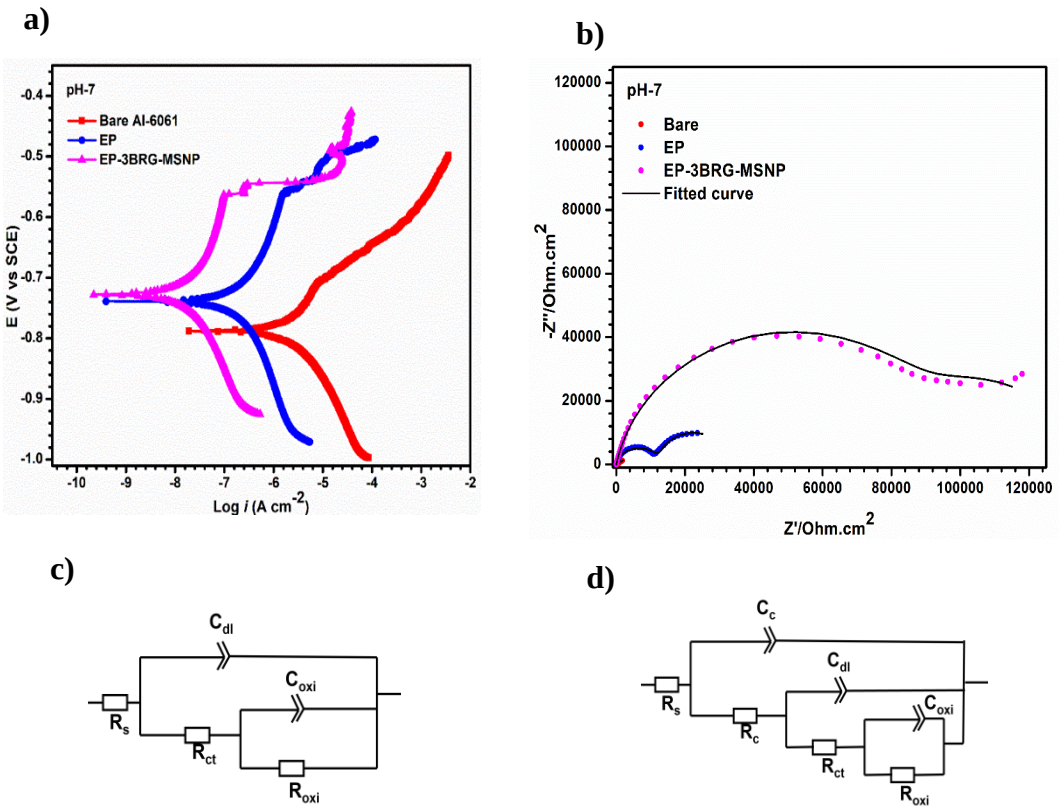

Figure 3.13. Potentiodynamic polarisation and impedance measurements for bare and modified epoxy coated Al-6061 samples at pH 7. **a)** Tafel plot **b)** Nyquist plot **c)** EEC for bare Al-6061 and **d)** EEC for coated Al-6061 samples in saline medium.

Table 3.6. Electrochemical parameters and inhibition efficiency obtained from potentiodynamic polarization measurements and impedance study of Al-6061 samples in near-neutral medium.

S/N	Substrate	**Potentiodynamic polarisation**			**EIS**	
		E_{corr} (V)	i_{corr} (μ Acm^{-2})	η (%)	R_{ct} (Ω cm^2)	η (%)
1.	Bare Al-6061	-0.788	1.941		3634	
2.	EP	-0.739	0.294	84.85	$3.321x10^4$	89.05
3.	EP-3BRG-MSNP	-0.728	0.029	98.51	$4.28x10^5$	99.15

3.4.4. Corrosion inhibition mechanism between green inhibitor molecule and the metal surface

The successful inhibition action of green inhibitors is due to the formation of a protective film over the surface of MS and Aluminium alloy. Many mechanisms are happening on the metal surface depending on the interaction between the phytochemical and the metal surface. This may be physisorption, chemisorption, or retro donation [22,23]. Different functional groups like hydroxyl, carbonyl, amino, carboxylic acid, etc., present in the phytochemicals participate in this adsorption procedures [24]. The binding force between the surface metal atoms and the inhibitor layer is the interaction of lone pair of electrons from the oxygen atom and the pi-electron cloud of the two inhibitors with the Al^{3+} and Fe^{3+} ions. In the case of bergenin-composite coating there are three possible interactions; 1) The un-hybridized p-orbital on the delocalized aromatic systems interact with the metal d-orbitals. 2) The un-hybridized p-orbital on the double bonds present in the molecule interact with the metal d-orbitals. 3) The sp^3 hybridized orbital on the heteroatom oxygen containing lone pair of electrons on the molecule interact with metal d-orbitals. The metal ion and the inhibitor interact like a Lewis acid-base pair *via* a coordination bond [25]. This interaction prevents corrosion in two ways. 1) It can prevent the leaching out of the metal ions, 2) The coating prevents the interaction of metal ions with water molecules and other hazardous ions like chloride and sulfate ions and preventing corrosion product formation. The interactions can be depicted as in **Figure 3.14.**

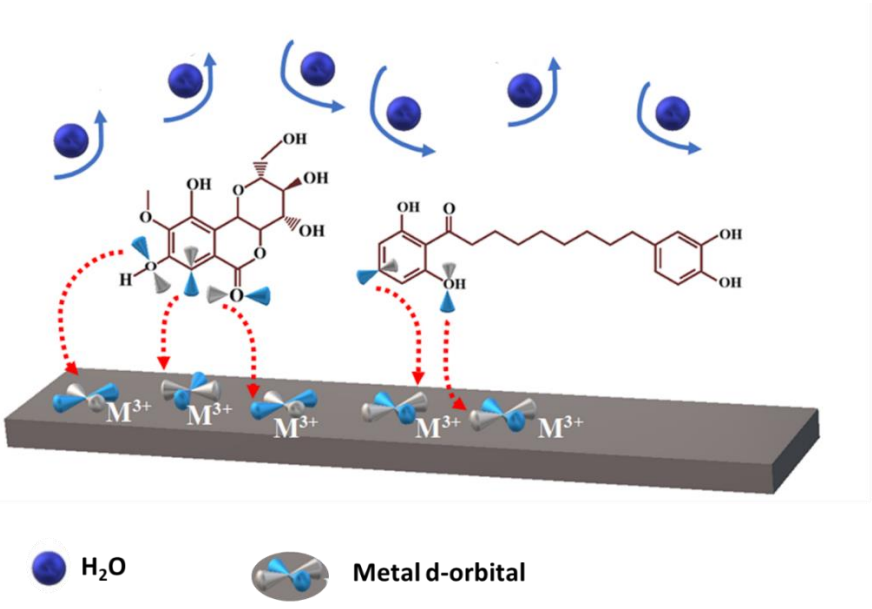

Figure 3.14. Schematic representation for the corrosion inhibition mechanism and replacement of water molecules with green inhibitor protective layer.

3.4.5. Antibacterial action of epoxy-based coatings

Antimicrobial agent coated aluminium discs qualified the antimicrobial activity test using modified AATCC-147 protocol against both the gram negative *P. aeruginosa* as well as gram positive *S. aureus* with respect to uncoated discs. But the coating is highly active against gram negative organism instead of gram positive one. Qualitative analysis of antimicrobial action by zone inhibition method is shown in **Figure 3.15.**

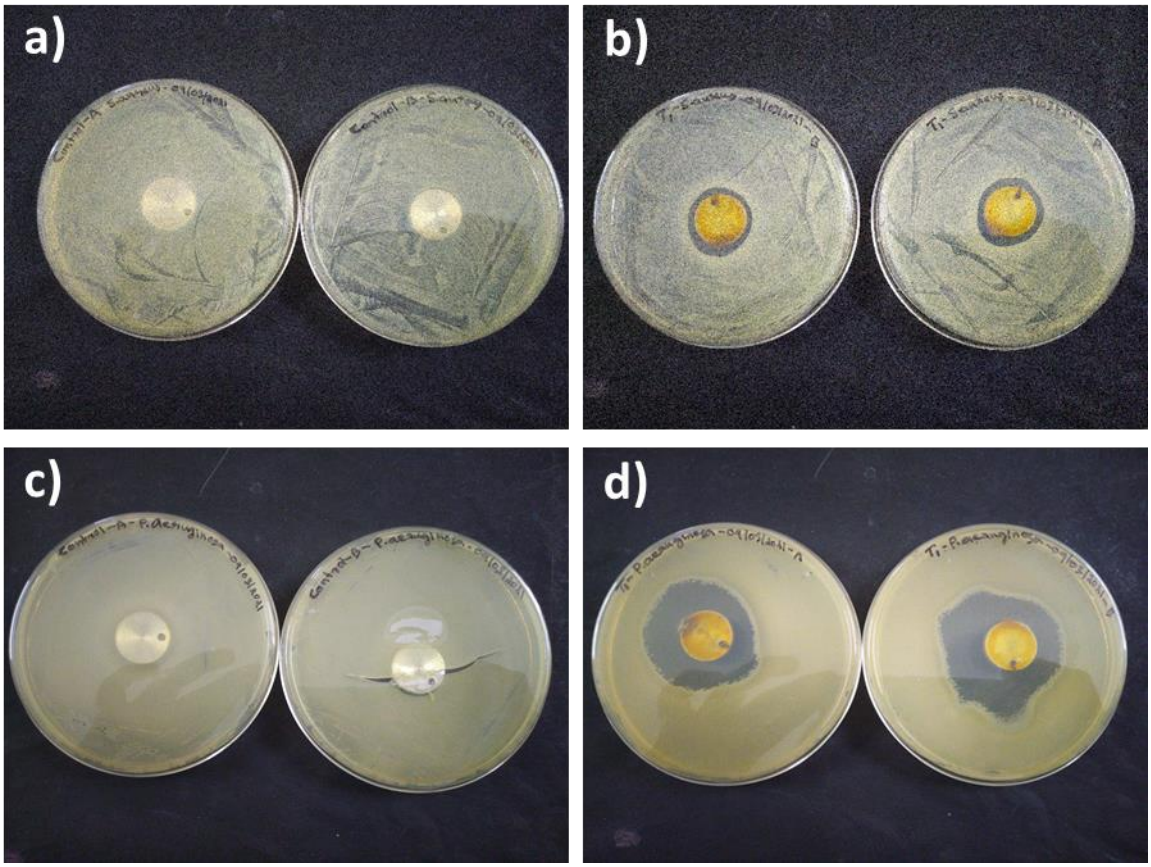

Figure 3.15. Qualitative test results against *S. aureus* and *P. aeruginosa*. **a)** control- *S. aureus* **b)** BRG-ML-MSNP coating- *S. aureus*, **c)** control- *P. aeruginosa* **d)** BRG-ML-MSNP coating- *P. aeruginosa* showing zone of inhibition.

This was further quantified using modified ASTM- AATCC-100 method. In quantitative analysis the control plates for *P. aeruginosa* counted an average 241±5 number of colonies in 10^1 dilutions, 50±2 and 3.5±0.5 in 10^2 and 10^3 dilutions respectively but the undiluted control plates counted numerous numbers of colonies. Similarly in the case of *S.aureus* the number of colonies found in the control plates as follows: 229±4 and 22.5±1.5 for 10^1, 10^2 dilutions respectively and no colonies was found in the 10^3 times diluted plating. Undiluted sample plates showed similar trend as in the case of *P. aeruginosa* which was numerous in number and the residual microbes on the metal surface also found

countless. Coming to the coated discs the colony count was zero even in the undiluted sample plating and plates kept for identifying residual microbes on the metal surface in both cases, which implies the 99% anti-microbial activity of the coatings. So, to conclude, even though the gram positive organism shows slight resistance to the coatings in qualitative analysis, prolonged exposure reduced the microbial load very effectively. The quantitative analysis (**Figure 3.16**) confirmed this trend. So, this plant derived coating on metal surfaces can be considered as one of the promising antimicrobial smart coatings.

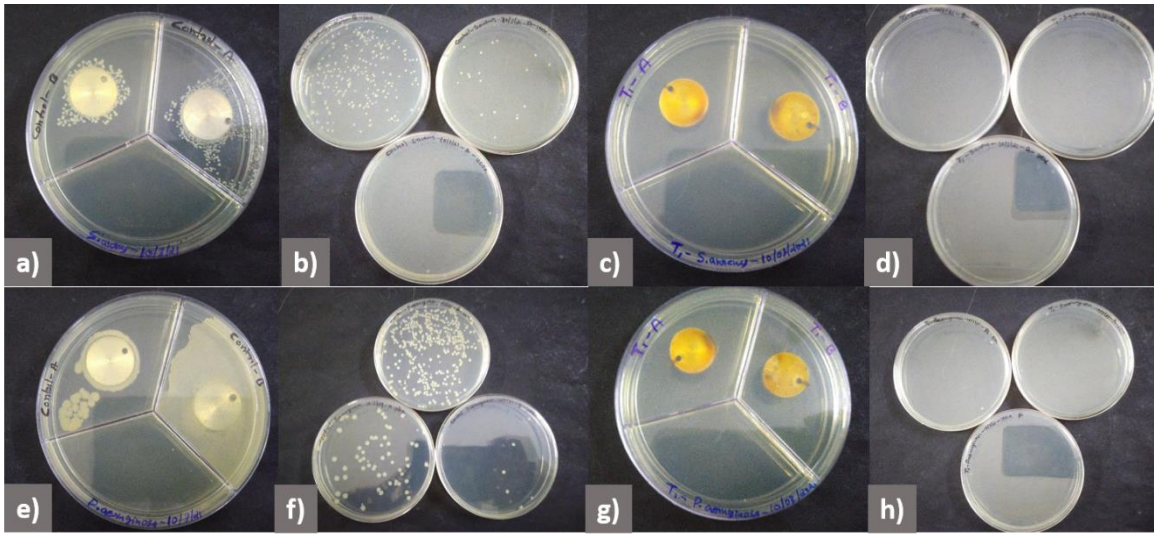

Figure 3.16. ***Quantitative test against S. aureus*** – **a)** Control plate with residual microbes, **b)** Control with 10x, 100x, 1000x dilutions, **c)** Test plate- no microbial colonies after 1hour incubation in saline means 99% killing, **d)** Test plate with 0x, 10x, 100x dilutions-no colonies present. ***Quantitative test against P. aeruginosa*****- e)** Control plate with residual microbes, **f)** Control with 10x, 100x, 1000x dilutions, **g)** Test plate- no microbial colonies after 1hour incubation in saline means 99% killing, **h)** Test plate with 0x, 10x, 100x dilutions-no colonies present.

3.5. Conclusions

The investigated epoxy matrix with a bio-nanocomposite of mesoporous silica nanoparticles with bergenin and malabaricone C as green corrosion inhibitors exhibited excellent corrosion protection for both Al-6061 alloy and mild steel in neutral, acidic, and basic environments. The best corrosion protection performance was provided in near-neutral media. The corrosion inhibition action increased with increasing concentration of bio-nanocomposites and slightly decreases after a certain limit. The best performance was displayed by epoxy coating containing 3 wt.% of bergenin bio-nanocomposite. The high availability of lone pair of electrons from the hetero atoms and the presence of pi electrons are responsible for this superior corrosion inhibition potential of bergenin. Smart anticorrosion coating with antimicrobial property is created by the addition of 0.1 wt.% of malabaricone C nanocomposites. Excellent antimicrobial property is achieved against gram-positive pathogen S. aureus and gram-negative pathogen *P. aeruginosa* both qualitatively and quantitatively. This smart coating can be effectively used for the simultaneous application of corrosion prevention and microbial proliferation and propagation control.

References

[1] A.S. Fouda, M.N. El-Haddad, Y.M. Abdallah, Septazole: Antibacterial Drug as a Green Corrosion Inhibitor for Copper in Hydrochloric Acid Solutions, International Journal of Innovative Research in Science, Engineering and Technology (An ISO. 2 (2013) 7073–7085. www.ijirset.com.

[2] S.B. Ulaeto, A. V. Nair, J.K. Pancrecious, A.S. Karun, G.M. Mathew, T.P.D. Rajan, B.C. Pai, Smart nanocontainer-based anticorrosive bio-coatings: Evaluation of quercetin for corrosion protection of aluminium alloys, Prog Org Coat. 136 (2019) 105276. https://doi.org/10.1016/j.porgcoat.2019.105276.

[3] C. Kamal, M.G. Sethuraman, Caulerpin- A bis-Indole Alkaloid as a Green Inhibitor for the Corrosion of Mild Steel in 1 M HCl Solution from the Marine Alga Caulerpa racemosa, Ind. Eng. Chem. Res. 51, 31, (2012) 10399–10407. https://doi.org/10.1021/ie3010379

[4] W. Emori, V.M. Bassey, H. Louis, P.C. Okonkwo, S. Zhao, K. Wei, P.C. Okafor, J. Wan, C.-R. Cheng, Anticorrosion and dispersive adsorption studies of natural andrographolide on carbon steel in acid-chloride environments, Bioelectrochemistry. 141 (2021) 107840. https://doi.org/10.1016/j.bioelechem.2021.107840.

[5] D. Patel, K. Patel, R. Kumar, M. Gadewar, V. Tahilyani, Pharmacological and analytical aspects of bergenin: a concise report, Asian Pac J Trop Dis. 2 (2012) 163–167. https://doi.org/10.1016/S2222-1808(12)60037-1.

[6] X. Gao, Y. Wang, J. Zhang, L. Lin, Q. Yao, G. Xiang, Bergenin suppresses the growth of colorectal cancer cells by inhibiting PI3K/AKT/mTOR signaling pathway, Tropical Journal of Pharmaceutical Research. 16 (2017) 2307–2313. https://doi.org/10.4314/tjpr.v16i10.1.

[7] N. Nazir, S. Koul, M.A. Qurishi, M.H. Najar, M.I. Zargar, Evaluation of antioxidant and antimicrobial activities of Bergenin and its derivatives obtained by chemoenzymatic synthesis, Eur J Med Chem. 46 (2011) 2415–2420. https://doi.org/10.1016/j.ejmech.2011.03.025.

[8] R. Srinivasan, M.J.N. Chandrasekar, M.J. Nanjan, B. Suresh, Antioxidant activity of Caesalpinia digyna root, J Ethnopharmacol. 113 (2007) 284–291. https://doi.org/10.1016/j.jep.2007.06.006.

[9] S. Sanjeev, M.K. Murthy, M.S. Devi, M. Khushboo, Z. Renthlei, K.S. Ibrahim, N.S. Kumar, V.K. Roy, G. Gurusubramanian, Isolation, characterization, and therapeutic activity of bergenin from marlberry (Ardisia colorata Roxb .) leaf on diabetic testicular

complications in Wistar albino rats, Environ Sci Pollut Res Int. 26(7), (201 doi: 10.1007/s11356-019-04139-9. 9), 7082-7101.

[10] J. Singh, A. Kumar, A. Sharma, Antianxiety activity guided isolation and characterization of bergenin from Caesalpinia digyna Rottler roots, J Ethnopharmacol. (2016) 0–1. https://doi.org/10.1016/j.jep.2016.11.016.

[11] T.D. Cuong, C.J. Lim, T. Thi, T. Trang, Y.H. Bae, N. Van Thu, Compounds from the Seeds of Myristica fragrans and Their Cytotoxic Activity, Natural product sciences 18 (2012) 97–101.

[12] G. Ji, S. Anjum, S. Sundaram, R. Prakash, Musa paradisica peel extract as green corrosion inhibitor for mild steel in HCl solution, Corros Sci. 90 (2015) 107–117. https://doi.org/10.1016/j.corsci.2014.10.002.

[13] M. Behpour, S.M. Ghoreishi, N. Soltani, M. Salavati-Niasari, M. Hamadanian, A. Gandomi, Electrochemical and theoretical investigation on the corrosion inhibition of mild steel by thiosalicylaldehyde derivatives in hydrochloric acid solution, Corros Sci. 50 (2008) 2172–2181. https://doi.org/10.1016/j.corsci.2008.06.020.

[14] R. Subramanian, P. Subbramaniyan, V. Raj, Isolation of bergenin from Peltophorum pterocarpum flowers and its bioactivity, Beni Suef Univ J Basic Appl Sci. 4 (2015) 256–261. https://doi.org/10.1016/j.bjbas.2015.06.002.

[15] J.P. Hou, H. Wu, Y. Wang, X.C. Weng, Isolation of some compounds from nutmeg and their antioxidant activities, Czech Journal of Food Sciences. 30 (2012) 164–170. https://doi.org/10.17221/509/2010-CJFS.

[16] M. Cai, X. Fan, H. Yan, Y. Li, S. Song, W. Li, H. Li, Z. Lu, M. Zhu, In situ assemble $Ti_3C_2T_x$ MXene@MgAl-LDH heterostructure towards anticorrosion and antiwear application, Chemical Engineering Journal. 419 (2021) 130050. https://doi.org/10.1016/j.cej.2021.130050.

[17] H. Yan, X. Fan, M. Cai, S. Song, M. Zhu, Amino-functionalized $Ti_3C_2T_x$ loading ZIF-8 nanocontainer@benzotriazole as multifunctional composite filler towards self-healing epoxy coating, J Colloid Interface Sci. 602 (2021) 131–145. https://doi.org/10.1016/j.jcis.2021.06.004.

[18] H. Yan, M. Cai, W. Li, X. Fan, M. Zhu, Amino-functionalized $Ti_3C_2T_x$ with anti-corrosive/wear function for waterborne epoxy coating, J Mater Sci Technol. 54 (2020) 144–159. https://doi.org/10.1016/j.jmst.2020.05.002.

[19] L. Wen, Y. Wang, Y. Zhou, J.-H. Ouyang, L. Guo, D. Jia, Corrosion evaluation of microarc oxidation coatings formed on 2024 aluminium alloy, Corros Sci. 52 (2010) 2687–2696. https://doi.org/10.1016/j.corsci.2010.04.022.

[20] H. Yan, M. Cai, J. Wang, L. Zhang, H. Li, W. Li, X. Fan, M. Zhu, Insight into anticorrosion/antiwear behavior of inorganic-organic multilayer protection system composed of nitriding layer and epoxy coating with $Ti_3C_2T_x$ MXene, Appl Surf Sci. 536 (2021) 147974. https://doi.org/10.1016/j.apsusc.2020.147974.

[21] D. Zeng, Z. Liu, L. Zou, H. Wu, Corrosion Resistance of Epoxy Coatings Modified by Bis-Silane Prepolymer on Aluminum Alloy, Coatings. 11 (2021) 842. https://doi.org/10.3390/coatings11070842.

[22] K. Dahmani, M. Galai, M. Ouakki, M. Cherkaoui, R. Touir, S. Erkan, S. Kaya, B. El Ibrahimi, Quantum chemical and molecular dynamic simulation studies for the identification of the extracted cinnamon essential oil constituent responsible for copper corrosion inhibition in acidified 3.0 wt% NaCl medium, Inorg Chem Commun. 124 (2021) 108409. https://doi.org/10.1016/j.inoche.2020.108409.

[23] X. Lai, J. Hu, T. Ruan, J. Zhou, J. Qu, Chitosan derivative corrosion inhibitor for aluminum alloy in sodium chloride solution: A green organic/inorganic hybrid, Carbohydr Polym. 265 (2021) 118074. https://doi.org/10.1016/j.carbpol.2021.118074.

[24] N. Bhardwaj, P. Sharma, V. Kumar, Phytochemicals as steel corrosion inhibitor: an insight into mechanism, Corrosion Reviews. 39 (2021) 27–41. https://doi.org/10.1515/corrrev-2020-0046.

[25] M.M. Fares, A.K. Maayta, M.M. Al-Qudah, Pectin as promising green corrosion inhibitor of aluminum in hydrochloric acid solution, Corros Sci. 60 (2012) 112–117. https://doi.org/10.1016/j.corsci.2012.04.002.

Chapter 4

Synergistic Smart Epoxy Coating from Three Plants of Meliaceae, Acanthaceae and Asteraceae Family

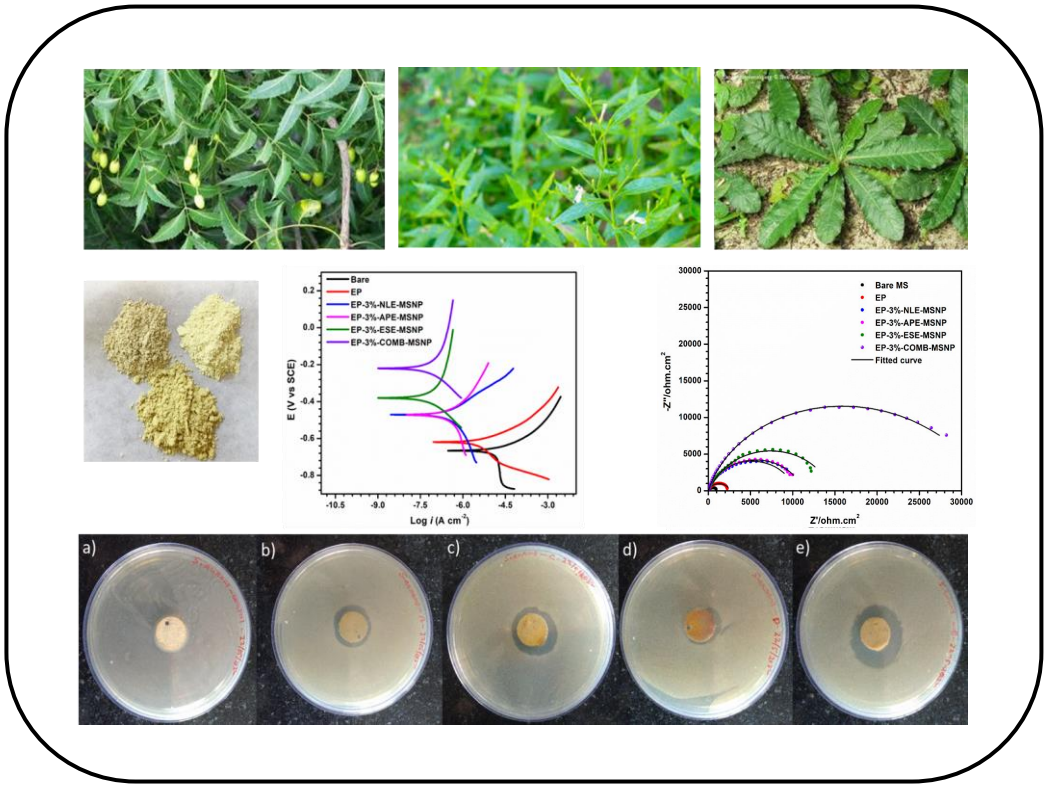

Abstract

The present invention is on the studies on formation of epoxy coating formulation based on the extracts from three different plants having potential antimicrobial characteristics loaded into silica nanocontainer showing enhanced anticorrosion and antimicrobial properties with the synergistic effect. The plant extracts used in the formulations are hydro-ethanolic extracts of *Azadirachta indica*, *Elephantopus scaber* and *Andrographis paniculata* three plants belonging to three different plant families. The extracts are loaded in the containers and dispersed in the epoxy medium with suitable solvents before application and curing. The coating with 3% extract combination showed 99.99% inhibition for both gram-positive and gram-negative bacteria. In addition, antiviral properties are also expected due to the presence of potent antiviral candidates like andrographolide in the plant extract. All three plants are known to possess excellent antibacterial, antifungal and antiviral properties. But the performances of the individual components were enhanced by the synergistic effect when three components are mixed. The coating exhibited excellent corrosion inhibition performance with an efficiency of 99.97%. Partial self-healing properties are also observed. The antimicrobial and anticorrosive properties observed in the coatings are greater than 99.95% resulting into potential multifunctional smart coating.

Keywords: Synergistic action, *Azadirachta indica*, *Elephantopus scaber*, *Andrographis paniculata,* Anticorrosion coating, Antimicrobial coating

4.1. Introduction

The possibility of proliferation and propagation of pathogens from the high touch surfaces has currently emerged as a looming threat in everyday public life in the case of infectious diseases. The scary numbers and emergence of new microbial variations in recent years demanded the development of new classes of effective smart coating formulations [1]. In this context, the exploration of new phytochemical agents from natural resources with the ability of anticorrosion and antimicrobial action has become more prominent. Owing to their enormous potential, fewer side effects, and cost-effectiveness green corrosion inhibitors with antimicrobial properties gathered much attention among researchers [2]. The use of a particular compound may lead to activity against a single or a group of organisms. But the incorporation of total plant extract from three different plants from different plant families will surely ensure a broad-spectrum antimicrobial action. A particular combination of some secondary metabolites was known to have synergistic activity enhanced to many folds [3]. There is still a possibility for an antagonist to act in some cases; so, a close evaluation is necessary.

Many secondary metabolites from the plants when combined give extraordinary results in many properties. The present invention relates the use of three herbs from three different families to get a smart coating with anticorrosion properties and broad-spectrum synergistic antimicrobial activity. The plants are *Azadirachta indica*, *Elephantopus scaber*, and *Andrographis paniculata* from the Meliaceae, Asteraceae, and Acanthaceae families (**Figure 4.1**). In addition, antiviral properties are also expected due to the presence of potent antiviral candidates like andrographolide in the plant extract [4,5]. All three plants are known to possess excellent antibacterial, antifungal and antiviral properties [6–8]. The extracts are loaded in the containers and dispersed in the epoxy medium with suitable solvents before application and curing.

Figure 4.1. The plants: *Azadirachta indica*, *Elephantopus scaber* and *Andrographis paniculata* from Meliaceae, Asteraceae, and Acanthaceae families

4.2. Materials and Methods

4.2.1. Materials

The solvent extraction method was used for the extraction of the active extract from the plant parts using the hydroethanolic system as the solvent. Tetraethyl orthosilicate, Butanol, NaOH, HCl, and DGEBA were obtained from Sigma Aldrich. Cetyltrimethylammonium bromide (CTAB) was purchased from SD Fine Chemicals. Ethanol and NaCl were procured from Merck Specialties Pvt. Ltd. All chemicals were used as-received without any refinement. The strain *S. aureus* and *E. coli* used were from the collection of MPTD of CSIR-NIIST, Thiruvananthapuram.

4.2.2. Methods

4.2.2.1. Extraction from three plant materials

Leaves of neem and all parts of *Elephantopus scaber* and *Andrographis paniculata* are collected from Thiruvananthapuram District of Kerala, washed, and dried at 40 °C in a hot air oven. A hydroethanolic solvent system (60:40) was used for the extraction. The extraction procedures followed the same procedures discussed in the previous chapters. After the complete extraction, the solvent is removed from the extract by using a rotary evaporator followed by freeze-drying. 1 kg of the plant parts gave around 100 g of extract.

4.2.2.2. Synthesis of the inhibitor-nanoparticle composite

The nanocontainer used for loading was prepared by the methods described in the Chapter 2. A solution of the extracts in ethanol was prepared at a concentration of 50 mg/mL, and the container was introduced to the mixture in a 1:2 ratios for loading. After continuous stirring for 24 h, the ethanol was removed with the help of a water bath at 80

°C. The extracts were loaded separately into the nanocontainers and the three powder composites obtained were vacuum dried and kept in a desiccator.

4.2.2.3. Substrate and coating preparation

In this study, the metal substrates used for the coating formation were MS and Al-6061 alloy samples. Samples of size 4 cm × 3 cm were used for the study, and only an area of 1 cm^2 was exposed to the saline solution in the cell. All the samples were polished with emery papers of varying grit sizes starting from 80 to 1000. Samples were degreased, washed with acetone and distilled water separately, and then oven-dried. The aluminium samples were further etched with low-concentration alkaline and acidic solutions for 60 seconds each before use.

The saline medium utilized throughout the investigation was 3.5 wt.% NaCl solution. From the previous chapters, we understood that the optimum concentration for this DGEBA-based epoxy is 3 wt.% of the nanocomposite. The composites were well dispersed in butanol with the help of an ultrasound sonicator before the addition. This inhibitor was then poured into the resin and mixed continuously to achieve a homogeneous mixture. After adding the hardener, the mixture is thoroughly mixed again and applied to the metal substrate without any delay. The resin and curing agent ratio were 2:1, and a dip-coating instrument was used to coat the samples at 500 mm/min speed. After room temperature curing for 24 hours, the samples were dried at 80 °C for 24 hours in an oven. The prepared samples were kept in a vacuum desiccator.

4.2.2.4. Electrochemical impedance and potentiodynamic polarization

A conventional three-electrode system with a platinum electrode as the counter electrode, a saturated calomel electrode (SCE) with fine Luggin capillary as the reference electrode and dip coated sample with the coating removed from one side as the working

electrode was used for EIS and Potentiodynamic polarization (PP) studies. The AC signal with a 5 mV amplitude perturbation at OCP in the frequency range 100 kHz–0.01 Hz was employed in the EIS analysis. The working electrode utilized in the investigation was exposed to a 1 cm^2 area. The anti-corrosion performance of all the extracts and the combination was analyzed by potentiodynamic and EIS methods. 3% coatings for the individual composites and the combination (1:1:1 ratio) were prepared (3% of bio-nanocomposite is the optimum concentration with best performance in the previous chapters for epoxy coatings). Polished MS and Al-6061 coupons were used to evaluate the performance. E_{corr} and i_{corr} were determined from the Tafel plot, and corrosion inhibition efficiency (η %) was obtained from the **equation (4.1)**,

$$\eta\ \% = \frac{icorr - icorr(coat)}{icorr} \qquad \textbf{…….. (4.1)}$$

Where i_{corr} and $i_{corr\ (coat)}$ are the current densities of with and without modified epoxy coatings.

To find the resistance values, the spectra were fitted using ZSimpWin software. R_{ct} and the inhibition efficiency of the coating in saline media, $I.E._{EIS}$ % were determined with the following **equation 4.2**.

$$I.E._{EIS}\ \% = \frac{Rct(coat) - Rct(MS)}{Rct(coat)} \text{ x } 100 \qquad \textbf{…….. (4.2)}$$

R_{ct} (coat) is the charge transfer resistance value of the coated samples and R_{ct} (MS) is the charge transfer resistance value of the bare mild steel samples. For the epoxy-coated working electrode, the time kept for stabilisation was 24 hours before starting the measurements.

4.2.2.5. Evaluation of antimicrobial action of the coating loaded with bio-nanocomposite

All the selected plants and their extracts are known for their very high antimicrobial activity. The activity of coatings containing 3% of individual samples and a combination of nanocomposites of a total of 3% were tested by coating on an aluminium disc of diameter 1.7 cm by dip-coating method and dried as same in the above-mentioned procedure. Later the antimicrobial action was determined qualitatively by the zone of inhibition method and quantitatively by AATCC-100 protocols.

a) Qualitative analysis of antimicrobial activity

The antimicrobial activity was screened qualitatively by modified AATCC-147 (ASTM) protocol. In which, actively growing 18 hours LB broth-grown microbial cultures of *E. coli* and *S. aureus*, cultures were used. 100 µl of 10 times normal saline diluted culture broth was used as inoculum for spread plating. The aluminium metal plate coated with anti-microbial agents was taken in 1.7 cm diameter discs and was used for testing. The uncoated discs were used as a control. For each organism, we kept duplicates to ensure accuracy and the plates were exposed to UV light for 20 minutes to avoid contamination with other organisms. The Luria Bertani (LB) agar plates were used for spread plating, after inoculation the metal plates were kept in the centre region of the petri-plate and incubated for 24 hours at 37 ºC to get the clear zone around the metal plates. Such samples were screened out to test quantitatively to know the percentage reduction of microbial growth.

b) Quantitative analysis of antimicrobial activity

The samples that passed qualitative screening were tested quantitatively using the ASTM- AATCC-100 protocol. In this test, the culture inoculum was prepared as mentioned in the qualitative test and the microbial load in the inoculum was adjusted to 10^8 on dilution

with normal saline. The culture inoculum was then added to sterile 9 mL of normal saline taken in 100 mL screw cap conical flasks and the UV sterilized coated metal discs and the control discs, followed by 1 hour, 180 rpm shaking incubation. Duplicate plates were prepared for each sample. After incubation, the inoculated saline with sample discs was serially diluted to 0x, 10x, 100x, 1000x and 10000x and done spread plating. The colonies formed after 24-hour incubation was counted and the percentage reduction was estimated to quantify the antimicrobial activity of test samples in comparison with control. The metal plates after incubation were also subjected to LB agar plating in order to find out the residual microbes absorbed on the metal surface.

4.2.2.6. Self-healing potential assessment of the coating

The coating formulation which showed the best performance in antimicrobial and anticorrosion studies is evaluated for its self-healing potential. The coating, which offered the best corrosion protection for mild steel, was also studied for an Al-6061 alloy. An artificial scratch of 0.1 mm thickness and 1 cm length was made by the sharp insertion of a razor blade, and the samples were immersed in saline media for a duration of 48 h. SEM images were taken at different time intervals to check the self-healing efficiency of the matrix.

4.3. Characterization Techniques

Functional groups present in the plant extracts, nanocontainers, and prepared bio-nano composites were analyzed by PerkinElmer FTIR, from PerkinElmer Singapore Pte Ltd. TEM images were captured using FEI Tecnai G2, T30 with EDAX working at 300 kV. Thermogravimetric analysis was performed using STA7300 Thermal Analysis System, Hitachi. SEM images were captured using FE- SEM, FEI NOVA NANOSEM 450 and the elemental analysis was carried out using Zeiss EVO 18 cryo-SEM Special Edition attached with EDS operating at 10–30 kV after sputtering with gold. DLS and zeta potential

measurements were done using Malvern Zetasizer Nano ZS90, Germany. N_2 adsorption-desorption procedure was carried out to confirm the mesoporous nature of the container, pore size, pore volume, and specific surface were analysed using Micromeritics, Tristar II, USA. BET and BJH methods were used to calculate the surface area, pore size, and pore volume. Electrochemical workstation of CH Instruments (CHI608E, CH Instruments Inc.) with a conventional three-electrode cell used for electrochemical impedance spectroscopy and potentiodynamic polarization studies. Dip coating was performed with Spectrodip Instruments dip coater (Chennai, India). EIS spectra obtained were fitted with ZSimpWin software. The coating thickness was measured using a Bruker DektakXT stylus optical profilometer.

4.4. Results and Discussions

4.4.1. Characterization of the nano-container, nanocomposite and inhibitor coatings

4.4.1.1. ATR-FTIR analysis

The mesoporous silica nanocontainer and the three bio-nanocomposites prepared (**Figure 4.2**) were evaluated using FTIR analysis. All the peaks present in the container and additional peaks representing organic functional groups were present in all the bio-nanocomposites ensuring the effective loading of the inhibitors into the nanocontainer and its surface (**Figure 4.3**). The peaks corresponding to the hydroxyl groups can be attributed to the presence of polyphenols, the other peaks ensured the presence of other functional groups bearing heteroatoms like alcohol, carbonyl groups etc. the presence of C=C ensured the presence of π electrons. These two are the essential characteristic of a good corrosion inhibitor.

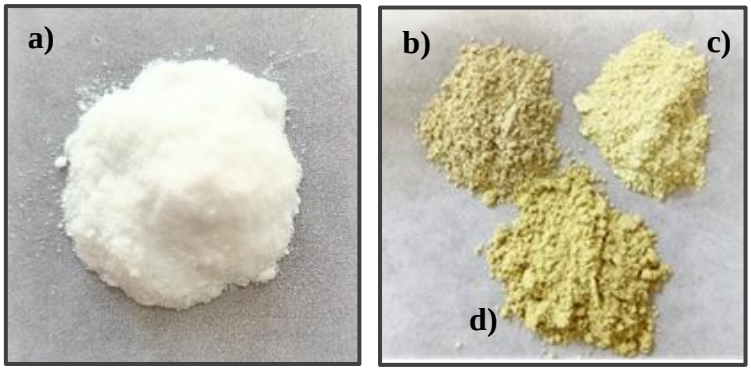

Figure 4.2. Images of **a)** mesoporous silica nanocontainer, the three bio-nanocomposites prepared from the three plants **b)** NLE-MSNP **c)** APE-MSNP and **d)** ESE-MSNP

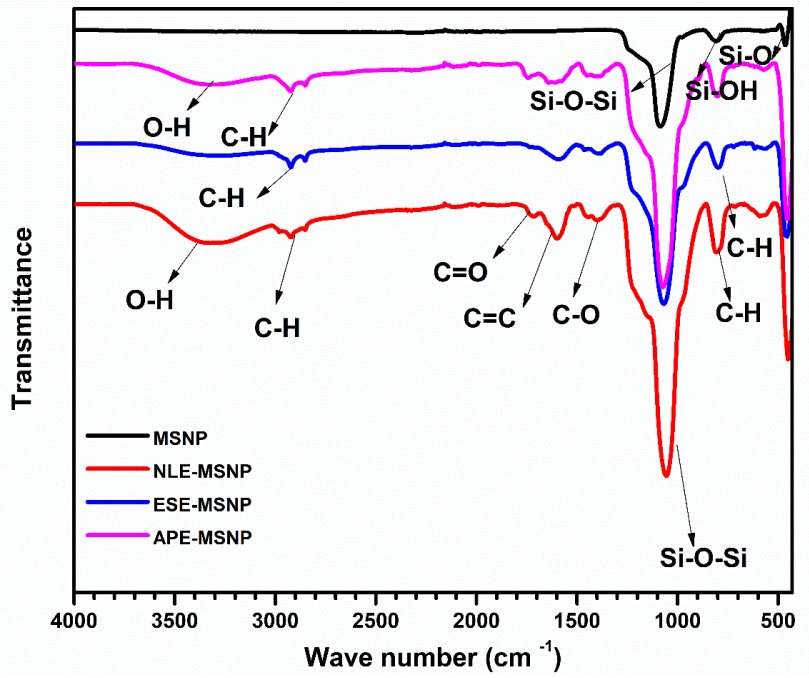

Figure 4.3. FTIR analysis of the nanocontainer and bio-nanocomposites

4.4.1.2. Morphology and size analysis- Scanning Electron Microscopy

Surface morphology and elemental analysis of the prepared particles were carried out after the synthesis. The surface of the nanocontainers seems to be roughened surface with spherical morphology, and it is maintained even after the loading of the compound, indicating surface structural stability (**Figure 4.4**).

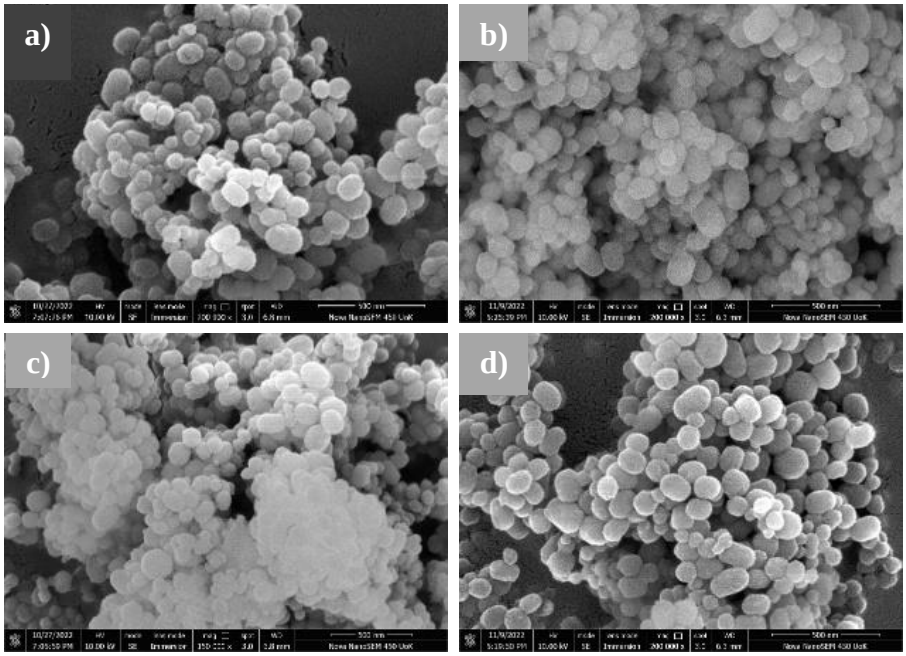

Figure 4.4. SEM micrographs of the synthesized nanoparticles **a)** MSNP, **b)** NLE-MSNP, **c)** APE-MSNP, and **d)** ESE-MSNP

4.4.1.3. Morphology and size analysis- Transmission Electron Microscopy (TEM)

The TEM micrographs in **Figure 4.5** show the Mesoporous silica nanoparticle (MSNP) and loaded particles NLE-MSNP, APE-MSNP and ESE-MSNP. The particles are spherical in morphology and are polydisperse. The mesoporous nature of the containers is evident in the TEM images, and it allows the adsorption of the inhibitors inside the containers. After the loading, the pores are seen to be covered, and the surface seems to be more or less smooth than the empty container surface.

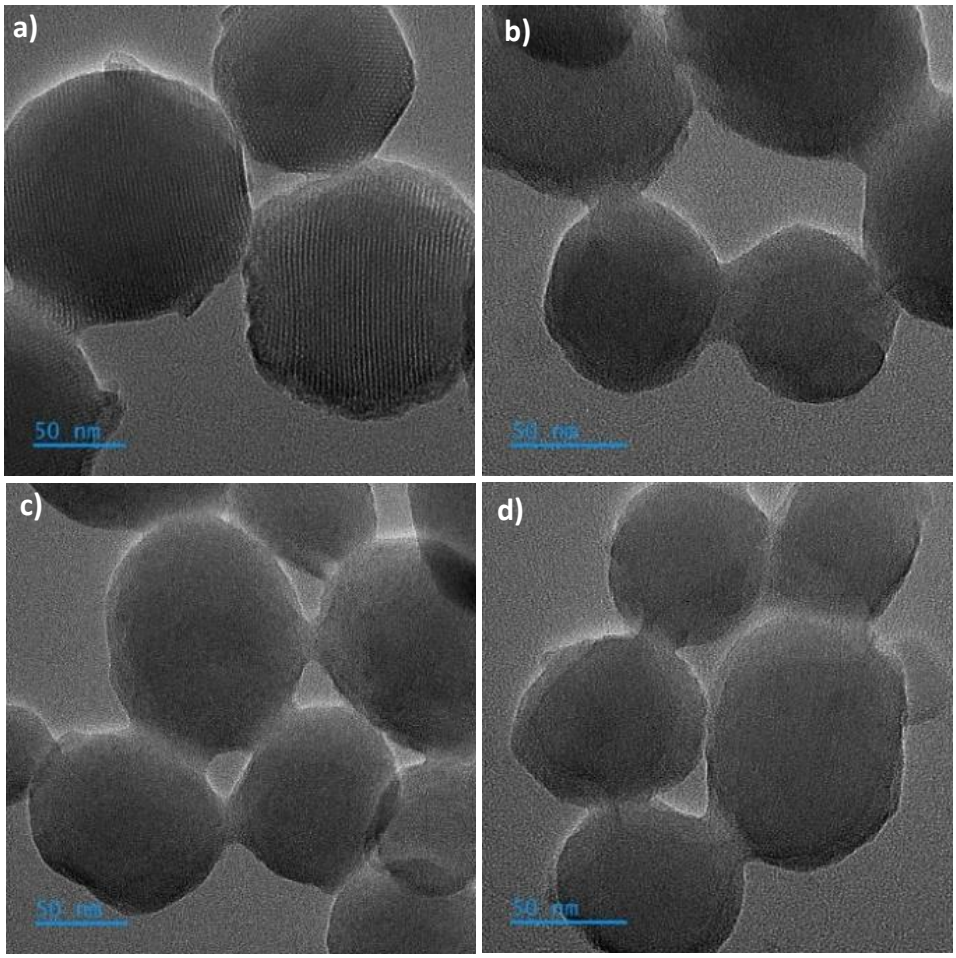

Figure 4.5. The TEM micrographs of the prepared nanoparticles. **a)** MSNP, **b)** NLE-MSNP, **c)** ESE-MSNP, and **d)** APE-MSNP

4.4.1.4. Thermogravimetric analysis

From the data obtained by the thermal analysis (**Figure 4.6**) of the container the prepared bio-nano composites and the epoxy coatings, the stability of each sample was examined. The tiny weight loss observed in the initial time in the case of mesoporous silica containers, compounds and composites is due to the evaporation of physically and chemically absorbed water. The higher weight reduction experienced in the case of coatings is due to the evaporation of water and organic solvent like butanol used during the dip coating procedure. All the composites have similar degradation patterns and the presence of the organic components reduced the weight of the final residue of the nanocomposite

compared to the nanocontainer. The coating was stable to rising temperatures up to around 290 °C.

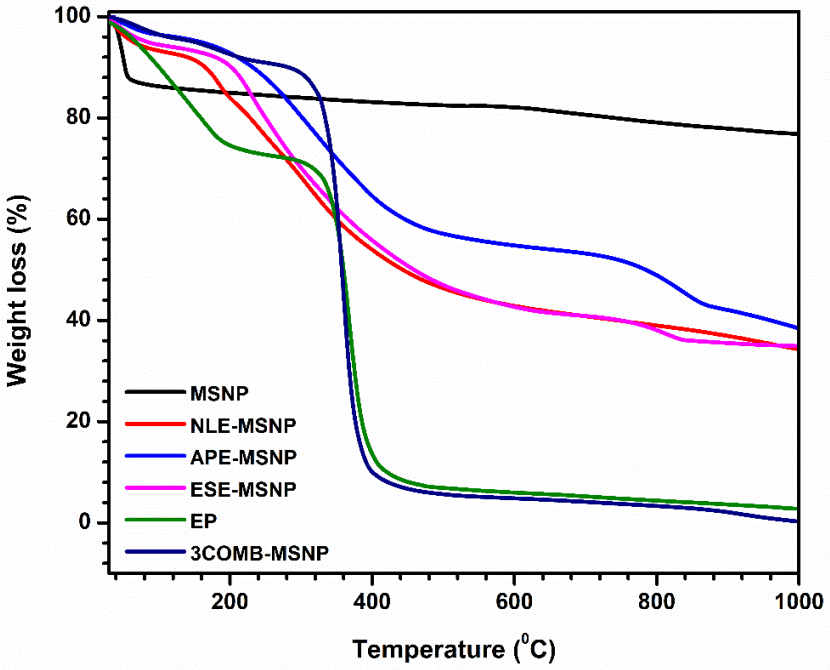

Figure 4.6. Thermal stability evaluation of nanocontainer, bio-nanocomposites and coatings

4.4.1.5. Nitrogen adsorption/desorption analysis

BET and BJH methods were used for the characterisation of the nanocomposites and nanoparticles. **Figure 4.7** shows N_2 adsorption-desorption isotherm for MSNP, NLE-MSNP, APE-MSNP, and ESE-MSNP to analyse the structure. The hysteresis loop of all the bio-nanocomposites showed lower adsorption of N_2 compared to MSNP as the inhibitor molecules occupy the pores. The structural parameters like specific surface areas by the BET model and pore diameter and pore volume calculated by the BJH model, are given in **Table 4.1.** Successful incorporation of the green inhibitor inside the mesoporous silica is indicated by the reducing trend in the parameters.

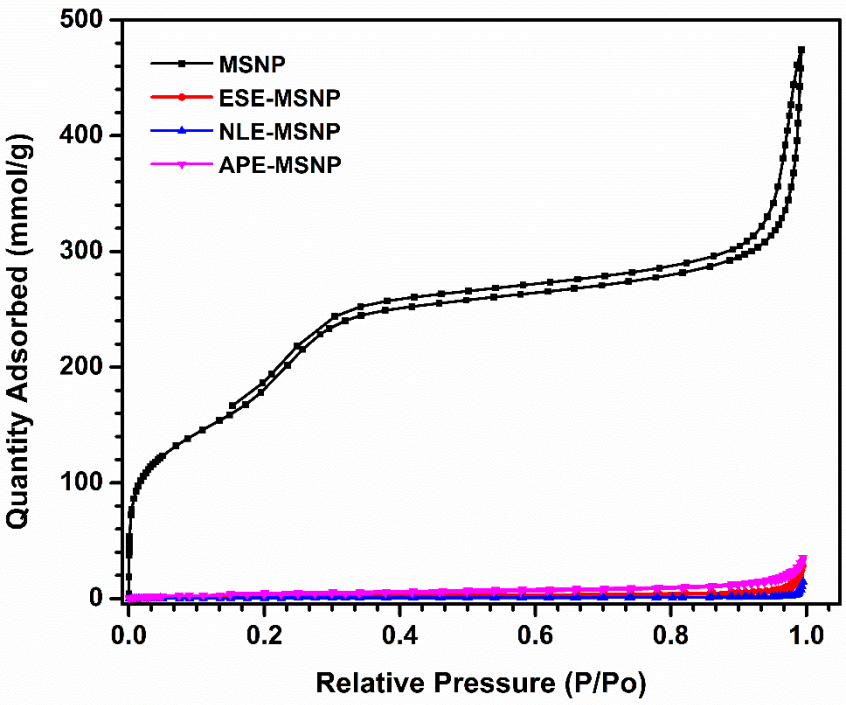

Figure 4.7. Nitrogen adsorption/desorption isotherm for MSNP, ESE-MSNP, NLE-MSNP and APE-MSNP

Table 4.1. Surface area and pore size analysis of the prepared nanoparticles and the bio-nano composites

Samples	BET Surface Area (m^2/g)	Total Pore Volume (cm^3/g)	Pore diameter by BJH (nm)
MSNP	729.70	0.68	3.75
ESE-MSNP	5.75	0.05	23.64
NLE-MSNP	1.68	0.02	45.76
APE-MSNP	13.52	0.05	16.13

4.4.2. Antimicrobial activity of the modified epoxy coatings

The detailed analysis of the quantitative results by the AATC-100 method confirmed the synergistic effect of the combination against both gram positive and gram negative species.

4.4.2.1. Qualitative analysis of the epoxy formulation

Initial screening of the three individual components and the combination of the three bio-nanocomposite by the zone of inhibition method showed all the coatings were effective against both gram positive and gram negative bacteria. But the larger zone of inhibition radius for the combination of composites suggested the possibility of a synergistic effect (**Figures 4.8 and 4.9**). All four samples under evaluation epoxy neem leaves composite coating (EP-NLE-MSNP), Epoxy- *Andrographis paniculata* composite coating (EP-APE-MSNP), and Epoxy- Elephantopus scaber composite coating (EP-ESE-MSNP) were found to be active against both gram positive and gram-negative pathogens. Antimicrobial agent-coated aluminium discs qualified for the antimicrobial activity test using modified AATCC-147 protocol against both the gram-negative *P. aeruginosa* as well as gram positive *S. aureus* with respect to uncoated discs. But the radius of the inhibition zone was found to be different for each sample. The coating which contains all three bio-nanocomposite exhibited greatest zone of inhibition around the sample for both microorganisms.

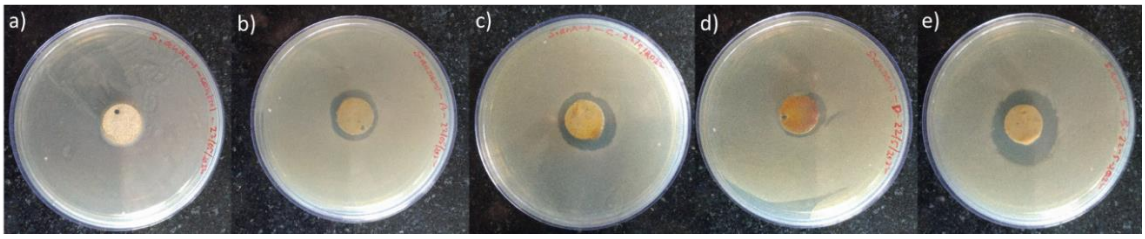

Figure 4.8. Qualitative analysis of antimicrobial action by zone inhibition against *S. aureus*: a) Control (d = 0 cm), b) EP-NLE-MSNP (d = 2.4 cm), c) EP-ESE-MSNP (d = 2.7 cm), d) EP-APE-MSNP (d = 1.9 cm), and e) Formulation containing 3-composites EP-COMB-MSNP (d = 3.6 cm). Where ‘d’ is diameter of the zone of inhibition.

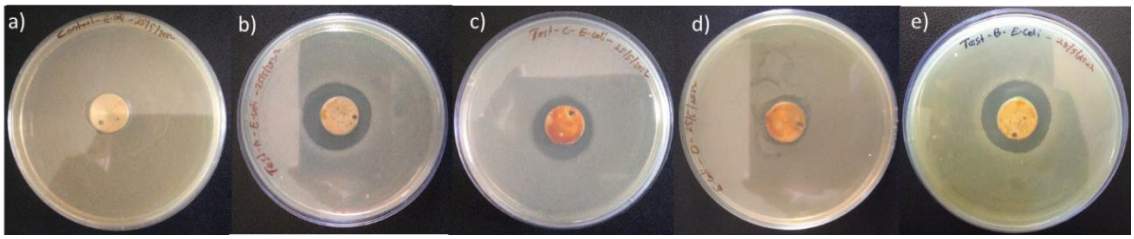

Figure 4.9. Qualitative analysis of antimicrobial action by zone inhibition against *E. coli*, a) Control (d = 0 cm), b) EP-NLE-MSNP (d = 2.8 cm), c) EP-ESE-MSNP (d = 2.6 cm), d) EP-APE-MSNP (d = 2.0 cm), and e) Formulation containing 3-composites EP-COMB-MSNP (d = 3.1 cm). Where ‘d’ is diameter of the zone of inhibition.

4.4.2.2. Quantitative analysis of the epoxy formulation

The inhibition efficiency percentage of each sample can be understood from the quantitative analysis. This was further quantified using a modified ASTM- AATCC-100 method. In quantitative analysis, the control plates for *E. coli* counted an average 239±5 number of colonies in 10^1 dilutions, and 51±2 and 2.5±0.5 in 10^2 and 10^3 dilutions respectively but the undiluted control plates counted numerous numbers of colonies. Similarly, in the case of *S. aureus* the number of colonies found in the control plates was as follows: 230±4 and 21.5±1.5 for 10^1, and 10^2 dilutions respectively and no colonies were found in the 10^3 times diluted plating. Undiluted sample plates showed a similar trend as in the case of *E. coli* which was numerous in number and the residual microbes on the metal surface were also found countless.

In the case of EP-NLE-MSNP, the *E. coli* colony count was 8± 0.5 in 10^1 dilutions, 10^2 showed 1 colony and no colony was observed in 10^3 times diluted plating. Similarly, in the case of *S. aureus* the number of colonies found in the plates was as follows: 11±0.5 and 1.8±0.2 for 10^1, and 10^2 dilutions respectively and no colonies were found in the 10^3 times diluted plating.

In the case of EP-APE-MSNP, *E. coli* colony count was 12±1in 10^1 dilutions, 10^2 showed 2.5±0.5 colonies and no colonies were observed in 10^3 times diluted plating. Similarly, in the case of *S. aureus* the number of colonies found in the plates was as follows: 12±0.5 and 2±0.4 for 10^1, and 10^2 dilutions respectively and no colonies were found in the 10^3 times diluted plating.

For EP-E-MSNP, the *E. coli* colony count was 4.8±0.5 in 10^1 dilutions, and no colonies were observed in 10^2 and 10^3 times diluted plating. Similarly, in the case of *S. aureus* the number of colonies found in the plates was as follows: 11.5±0.5 and 1.5±0.4 for 10^1, and 10^2 dilutions respectively and no colonies were found in the 10^3 times diluted plating.

The discs coated with the mixture of bio-nanocomposites (formulation), the colony count was zero even in the undiluted sample plating and plates kept for identifying residual microbes on the metal surface in both cases, which implies the 99.99% anti-microbial activity of the coatings.

So, to conclude, even though the gram-positive organism shows slight resistance to the coatings in qualitative analysis, prolonged exposure reduced the microbial load very

effectively for all the coatings. The quantitative analysis (**Figures 4.10 & 4.11**) confirmed this trend. The inhibition zone radius and the percentage of inhibition calculated from the quantitative analysis confirm the synergistic action of the three plant extracts. Hence, the coating developed from three plant extracts on metal surfaces can be considered as one of the promising anti-microbial smart coatings.

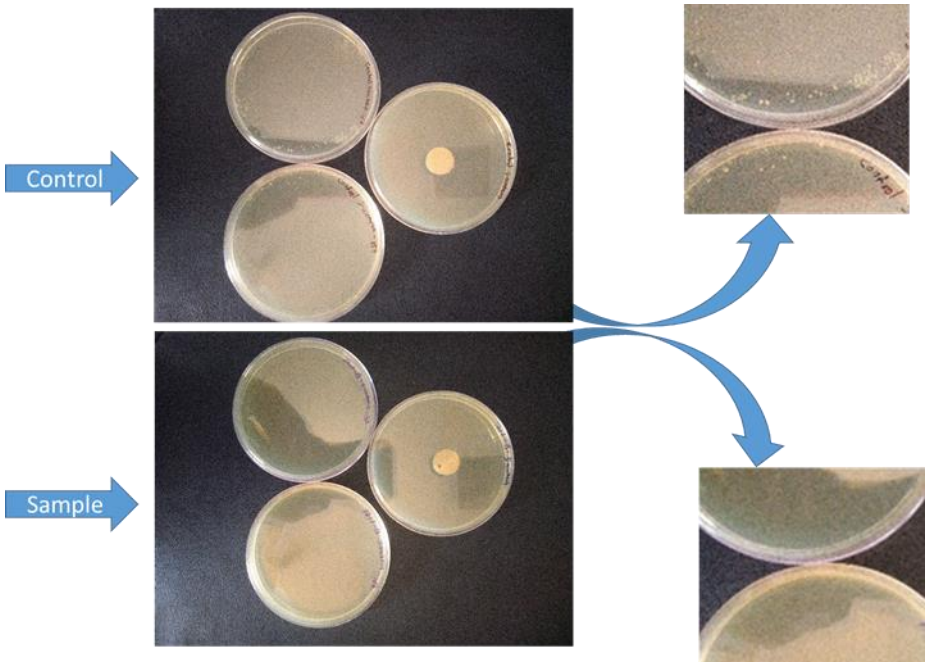

Figure 4.10. Quantitative analysis against *S. aureus* where control plates showed a large number of residual colonies and coated samples showing no residual colonies with 99.99% of inhibition efficiency.

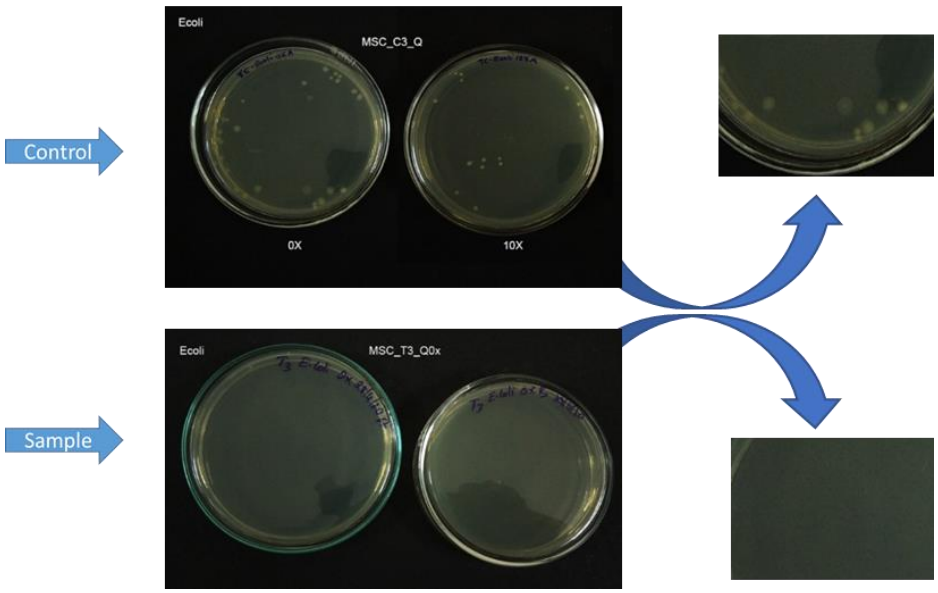

Figure 4.11. Quantitative analysis against *E. coli* where control plates showed a large number of residual colonies and coated samples showed no residual colonies with 99.99% of inhibition efficiency.

Table 4.2. Quantitative analysis of antimicrobial properties by AATCC-100 method

Sample	***E. coli* inhibition (%)**	***S. aureus* inhibition (%)**
EP-NLE-MSNP	96.5	< 95
EP-APE-MSNP	< 95	95
EP-ESE-MSNP	99	< 95
EP-COMB-MSNP	**99.99**	**99.99**

4.4.3. Anti-corrosion studies

4.4.3.1. Corrosion inhibition efficiency evaluation of the coating on mild steel

The anti-corrosion efficiency of the formulation of three bio-nanocomposites and the coatings containing single bio-nanocomposites were also evaluated. Electrochemical techniques like electrochemical impedance spectroscopy and potentiodynamic polarization studies were used for the evaluation of corrosion inhibition efficiency. All the coatings were found to be effective in corrosion inhibition of mild steel alloy in 3.5 wt.% NaCl solution. But the formulation containing the combination of three plant extracts showed the best performance with 99.97% corrosion inhibition in comparison with bare mild steel. All the coatings showed a positive shift in the corrosion potential and decreased corrosion current density in the potentiodynamic polarization experiments. In the electrochemical studies, the Nyquist plot (**Figure 4.12**) with a larger radius of resistance is observed for all the coatings.

The results obtained for bare mild steel, pure epoxy coating on mild steel, 3% NLE-MSNP coating, 3% APE-MSNP coating, 3% ESE-MSNP coating and the formulation 3%-COMB-MSNP on mild steel are given in **Table 4.3**. This shows an increasing trend in corrosion potential and a decreasing trend in corrosion current density. The Tafel plot (**Figure 4.12**) corresponding to the formulation containing the combination showed the greatest potential shift and least i_{corr} values, indicating a synergistic corrosion inhibition. The E_{corr} values of the bare mild steel shifted from -0.666 V to -0.467 V for EP-3%-NLE-MSNP coatings, -0.472 V for EP-3%-APE-MSNP coatings, and -0.380 V for EP-3%-ESE-MSNP. While in the case of coating containing a combination of all the composites (EP-

3%-COMB-MSNP), it tremendously shifted to a more positive side -0.171 V showing a synergistic effect. The i_{corr} values decreased from 30.53 μ Acm^{-2} to 0.1598 μ Acm^{-2} for EP-3%-NLE-MSNP, to 0.4853 μ Acm^{-2} for EP-3%-APE-MSNP, to 0.0895 μ Acm^{-2} for EP-3%-ESE-MSNP. For the coating containing a combination of all the nanocomposites (EP-3%-COMB-MSNP), the current density drastically decreased to 0.0065 μ Acm^{-2} with an inhibition efficiency of 99.97% compared with bare mild steel.

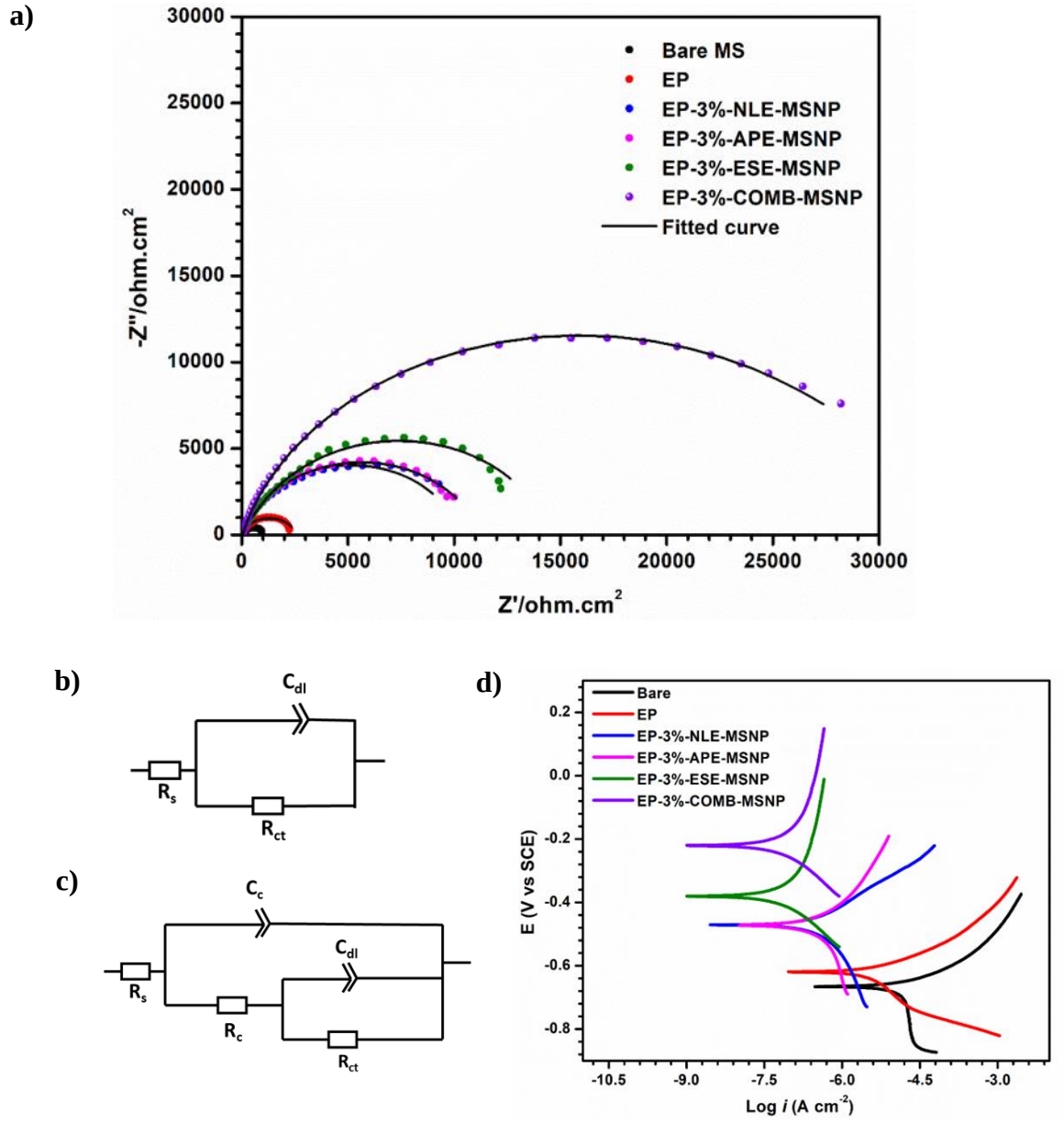

Figure 4.12. Electrochemical impedance spectroscopy and potentiodynamic polarisation studies of the coatings on mild steel. **a)** Nyquist plot, **b)** EEC for bare MS, **c)** EEC for coated samples, and **d)** Tafel plots for the samples

Table 4.3. Electrochemical parameters and corrosion inhibition efficiency obtained from EIS and PDP studies

S/N	Substrate	Potentiodynamic polarisation			EIS	
		E_{corr} (V)	i_{corr} (μ Acm^{-2})	η (%)	R_{ct} (Ω cm^2)	IE_{EIS} (%)
1	Bare M S	-0.666	30.53	-	1128	
2	Epoxy (EP)	-0.619	4.818	84.22	2574	56.17
3	EP-3%-NLE-MSNP	-0.467	0.1598	99.47	10280	89.02
4	EP-3%-APE-MSNP	-0.472	0.4853	98.41	11210	89.94
5	EP-3%-ESE-MSNP	-0.380	0.0895	99.70	14130	92.02
6	EP-3%-COMB-MSNP	-0.171	0.0065	99.97	31670	96.43

The Nyquist plot for bare and mild steel samples was fitted using Zsimpwin software. The electrochemical equivalent circuit for mild steel samples in saline media can be represented as $R_s(C_{dl}R_{ct})$ and for all other coatings the EEC is $R_s(C_cR_c(C_{dl}\ R_{ct}))$ with increasing resistance values. R_s is the solution resistance and pure capacitance term was replaced by constant phase angle element $C_{PE.}$ The capacitance and resistance due to the epoxy coatings are represented by C_c, R_c which occurs at high-frequency regions. In general, Rc is related to resistance towards the penetration of electrolytes, i.e., larger Rc represents better corrosion resistance of coating [9,10]. The capacitance offered by the electrical double layer between the metal surface and the electrolyte is represented as double-layer capacitance C_{dl}, and the resulting resistance derived from the capacitance is R_{ct} respectively the medium-low frequency elements. The capacitive elements C_{dl} and C_c followed the reverse order of resistance elements. A higher value of C_c indicates a higher electrolyte uptake of the coating. So, the lower values of capacitive elements indicate good corrosion protection of epoxy bio-nanocomposite coatings[11]. The fitted equivalent circuit diagram for the coating's studies of mild steel in the saline medium can be represented in

Figure 4.12, which explains the mechanism of corrosion inhibition of the modified epoxy coatings. The R_{ct} value increased from 1128 Ω cm^2 to 31670 Ω cm^2 in the case of modified epoxy coating containing all three nanocomposites with an inhibition efficiency of 96.43%.

4.4.3.2. Evaluation of corrosion inhibition efficiency of the coating on Al-6061

The corrosion inhibition potential of the prepared epoxy formulation is also tested for Al-6061 alloy. The optimized concentration of 3% COMB-MSNP is used for coating studies in aluminium samples. The sample is coated by a dip coating method, and the inhibition efficiency is determined by comparing the performance with bare Al-6061 samples and epoxy-coated samples. The Tafel plot for potentiodynamic polarisation analysis of Al-6061 samples is depicted in **Figure 4.13**. There is a significant surge in the corrosion potential (E_{corr}) and a considerable reduction in the corrosion current (i_{corr}) value. The electrochemical parameters obtained, E_{corr}, i_{corr}, and inhibition efficiency η, are given in **Table 4.4**. In addition to the passivation caused by the oxide layer formation in the bare Al-6061, there is a huge passivation area in the epoxy coating and the modified epoxy composite coating. This passivation increases the corrosion protection ability of the coating to a great extent.

Nyquist plot of Al-6061 samples in 3.5 wt.% NaCl solution at neutral pH is shown in **Figure 4.13**. The equivalent electrochemical circuit is fitted using ZsimpWin software. The R_{ct} values were determined and compared. The increase in the R_{ct} value indicates the development of the protective insulating layer on the metal. The EEC diagram is shown in **Figure 4.13c** and **Figure 4.13d.** The equivalent electrochemical circuit for bare Al-6061alloy samples in saline media can be represented as $R_s(C_{dl}R_{ct}(C_{oxi}R_{oxi}))$ and for all other coatings the EEC is $R_s(C_cR_c(C_{dl}R_{ct})(C_{oxi}\,R_{oxi}))$ with increasing resistance values. R_s is the solution resistance, and the constant phase angle element CPE replaced the pure capacitance term. In the case of bare alloy, the capacitance offered by the electrical double

layer between the metal surface and the electrolyte is represented as double-layer capacitance C_{dl}, and the resulting resistance derived from the capacitance is R_{ct} respectively in the high frequency region. While corrosion reaction of Al-6061 alloy in the corrosion medium and the resistance (R_{oxi}) offered by the corrosion product aluminium oxide layer is the second resistance appearing at low frequency region [12].

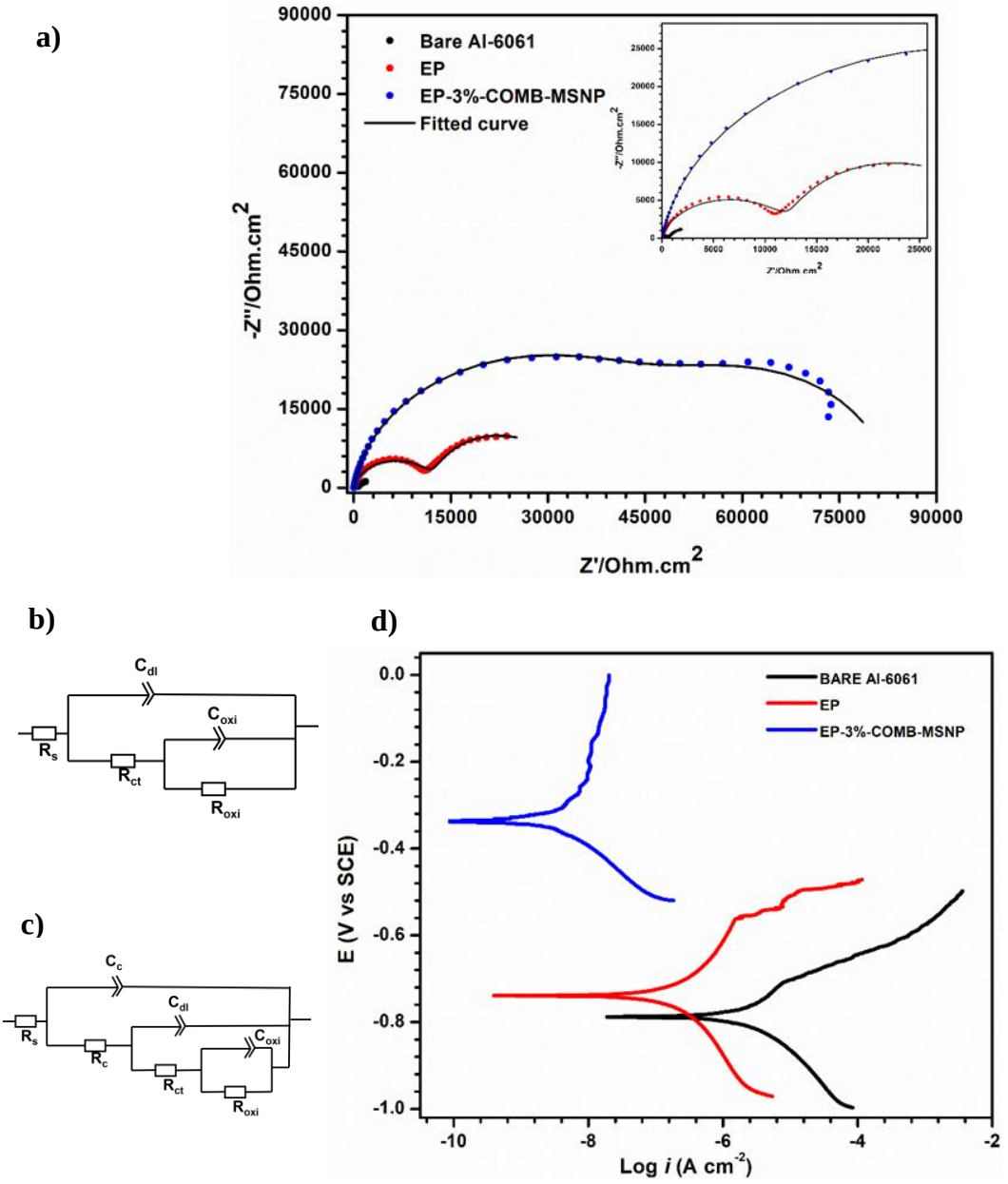

Figure 4.13. The corrosion inhibition evaluation of the synergistic formulation on Al-6061 alloys. **a)** Nyquist plot, **b)** EEC for bare Al-6061 sample, **c)** EEC for coated samples, and **d)** Tafel plot.

Table 4.4. Electrochemical parameters and corrosion inhibition efficiency of the modified synergistic epoxy coating on Al-6061 alloy

S/N	Substrate	Potentiodynamic polarisation			EIS	
		E_{corr} (V)	i_{corr} (μ Acm^{-2})	η (%)	R_{ct} (Ω cm^{2})	η (%)
1	Bare Al-6061	-0.788	1.941	-	3634	-
2	EP	-0.739	0.294	84.85	33210	89.05
3	EP-3 %-COMB-MSNP	-0.464	0.0064	99.67	82570	96.00

In the case of epoxy-coated samples, the high-frequency elements C_c and R_c are equal to the capacitance and resistance offered by the coatings; the medium-low frequency elements C_{dl}, and R_{ct} are double-layer capacitance and charge-transfer resistance, respectively. R_c and R_{ct} are related to the inhibition of the penetration of electrolytes and corrosive ions and electron transfer, respectively. C_c and C_{dl} are related to the absorption of electrolytes and the double-layer capacitance phenomenon. Higher resistance values and lower C_c and C_{dl} values confirm better corrosion protection by the modified epoxy coatings [13]. During the immersion time, some of the corrosive ions may reach the metal surface and the formation of corrosion products occurs [14].

The mechanism of corrosion inhibition is the coordination of the inhibitor molecule to the metal surface through lone pair donation, π electron donation and retro donation. In the case of extracts, a number of compounds will be present in each extract. In the synergistic formulation, it is the combined action of a larger number of molecules through different mechanisms. This may be physisorption, chemisorption, or retro donation [15,16]. Different functional groups like hydroxyl, carbonyl, amino, carboxylic acid, etc., present in the phytochemicals participate in this adsorption procedures [17]. The binding force

between the surface metal atoms and the inhibitor layer is the interaction of lone pair of electrons from the oxygen atom and the pi-electron cloud of the two inhibitors with the Al^{3+} and Fe^{3+} ions. In the case of composite coating there are three possible interactions; 1) The un-hybridized p-orbital on the delocalized aromatic systems interacts with the metal d-orbitals. 2) The un-hybridized p-orbital on the double bonds present in the molecule interacts with the metal d-orbitals. 3) The sp^3 hybridized orbital on the heteroatom oxygen containing lone pair of electrons on the molecule interacts with metal d-orbitals. The metal ion and the inhibitor interact like a Lewis acid-base pair *via* a coordination bond [18]. This interaction prevents corrosion in two ways. 1) It can prevent the leaching out of the metal ions, 2) The coating prevents the interaction of metal ions with water molecules and other hazardous ions like chloride and sulfate ions and prevents corrosion product formation.

4.4.4. Self-healing evaluation of the synergistic epoxy coating

An artificial scratch, 0.1 mm thick and 1 cm long, was made using a razor blade, and the samples were immersed in a saline media for different durations. The SEM images were taken and examined at 0 h, and 48 h. Only partial self-healing was observed (**Figure 4.14**) even after 48 h of immersion in the saline water containing 3.5 wt.% NaCl.

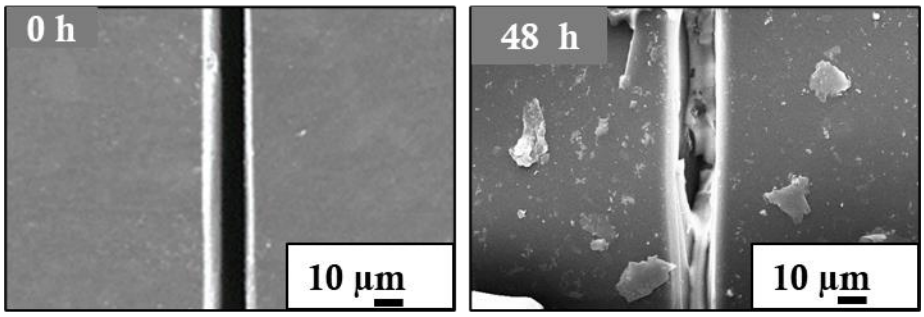

Figure 4.14. Self-healing evaluation of the modified epoxy coating with 3% bio-nanocomposite at **a)** 0 h and **b)** 48 h

4.4.5. Contact angle measurement and improvement of hydrophobicity of the modified epoxy coating

As observed in the first chapter, total extract-based coatings normally exhibit a lower contact angle and tend to be hygroscopic over time. The contact angle of the pure epoxy coating was 70.2°, after modification with the extract it was reduced to 60.75°. To increase the contact angle the allyl silane was added in 1-2% of the total weight of the epoxy and hardener. It was observed that for 1% coating, the value increased to 81.7° on further addition of 1% the value again increased to 95.5° (**Figure 4.15**). The surface is modified into a hydrophobic surface by the surface modifications using silane groups.

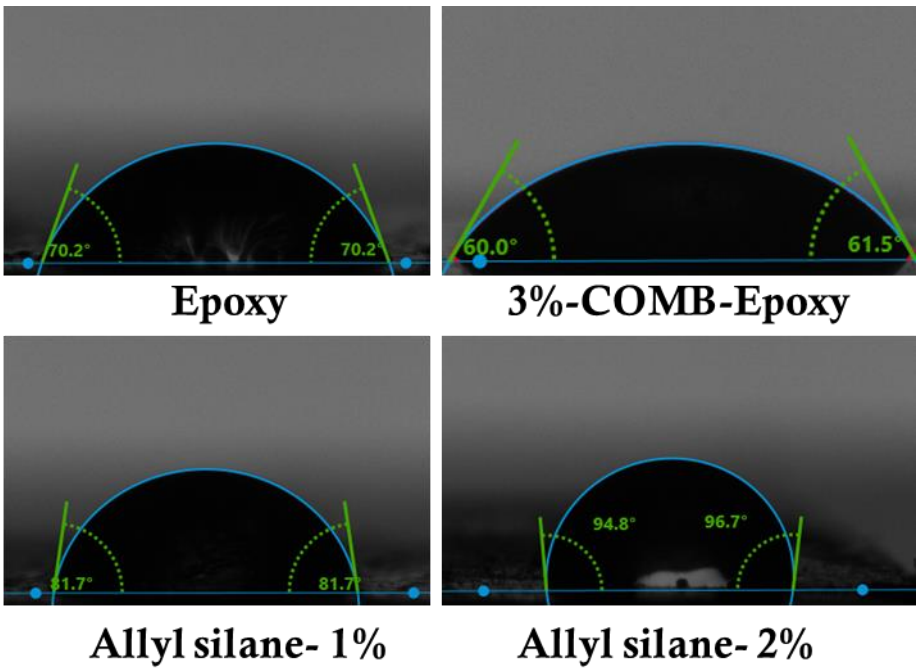

Figure 4. 15. The contact angle measurement and hydrophobic character of neat epoxy coating, extract-based epoxy coating, (extract + 1% allyl silane) coating and (extract + 2% allyl silane) coating

4.5. Mechanism of Synergistic Antibacterial and Anticorrosion Effects

Different bacterial targets have been exploited in the development of antimicrobial drugs like cell wall and protein synthesis, DNA and RNA synthesis, intermediary

metabolism, membrane function, ATP synthase *etc*. Each secondary metabolite's antibacterial action depends on any of these mechanisms. When they act simultaneously, it will result in more than one destruction mechanism. Sometimes, it is also possible for an antagonist to act, but in this study, it is the synergistic activity in the antimicrobial activity. The critical synergistic concentration is 1:1:1.

The corrosion inhibition potential of a molecule mainly depends on the hetero atom density, π-electron cloud, planarity, size, average surface area, electronegativity, Lewis acid-base nature etc. So, the combination of different molecules resulted in a synergistic effect in corrosion inhibition potential by simultaneous action of more than one corrosion inhibition mechanism.

4.6. Conclusion

Initial screening of the three individual components and the combination of the three bio-nanocomposite by the zone of inhibition method showed all the coatings were effective against both gram positive and gram negative bacteria. But the larger zone of inhibition radius for the combination of composites suggested the possibility of a synergistic effect happening. The detailed analysis of the quantitative results by the AATC-100 method confirmed the synergistic effect of the combination. The coating with 3% extract combination showed 99.99% inhibition for both gram-positive and gram-negative bacteria. Based on these promising results, anticorrosion property on the metal surface was further analysed to evaluate its synergistic effect. The anti-corrosion studies also shows 99.97% efficiency for the coating containing the combination of extracts. Only partial self-healing was observed even after 48 hours. The coating can be modified into a hydrophobic system by the incorporation of silane surface modification by allyl silane. The present study provides a highly active scaffold for the development of a cost-effective epoxy formulation with smart applications.

References

[1] S. Behzadinasab, A. Chin, M. Hosseini, L.L.M. Poon, W.A. Ducker, Biological and Medical Applications of Materials and Interfaces a Surface Coating that Rapidly Inactivates SARS-CoV-2 A Surface Coating that Rapidly Inactivates SARS-CoV-2, ACS Appl. Mater. Interfaces ,12, (2020), 34723–34727, doi.org/10.1021/acsami.0c11425.

[2] S.B. Ulaeto, A. V. Nair, J.K. Pancrecious, A.S. Karun, G.M. Mathew, T.P.D. Rajan, B.C. Pai, Smart nanocontainer-based anticorrosive bio-coatings: Evaluation of quercetin for corrosion protection of aluminium alloys, Prog Org Coat 136 (2019) 105276. https://doi.org/10.1016/j.porgcoat.2019.105276.

[3] G. Sharma, K. Raturi, S. Dang, S. Gupta, R. Gabrani, Combinatorial antimicrobial effect of curcumin with selected phytochemicals on *Staphylococcus epidermidis*, J Asian Nat Prod Res 16 (2014) 535–541. https://doi.org/10.1080/10286020.2014.911289.

[4] P. Panraksa, S. Ramphan, S. Khongwichit, D.R. Smith, Activity of andrographolide against dengue virus, Antiviral Res 139 (2017) 69–78. https://doi.org/10.1016/j.antiviral.2016.12.014.

[5] S. Gupta, K.P. Mishra, L. Ganju, Broad-spectrum antiviral properties of andrographolide, Arch Virol 162 (2017) 611–623. https://doi.org/10.1007/s00705-016-3166-3.

[6] R.N. Kharwar, V.C. Verma, A. Kumar, S.K. Gond, J.K. Harper, W.M. Hess, E. Lobkovosky, C. Ma, Y. Ren, G.A. Strobel, Javanicin, an Antibacterial Naphthaquinone from an Endophytic Fungus of Neem, Chloridium sp., Curr Microbiol 58 (2009) 233–238. https://doi.org/10.1007/s00284-008-9313-7.

[7] A. Jenny, S. Nath Paul, M. Dutta, M. Zia Uddin, Antibacterial activity of aerial part of extract of Elephantopus scaber Linn, https://www.researchgate.net/publication/287496710.

[8] P.K. Singha, S. Roy, S. Dey, Antimicrobial activity of Andrographis paniculata, Fitoterapia 74 (2003) 692–694. https://doi.org/10.1016/S0367-326X(03)00159-X.

[9] M. Cai, X. Fan, H. Yan, Y. Li, S. Song, W. Li, H. Li, Z. Lu, M. Zhu, In situ assemble $Ti_3C_2T_x$ MXene@MgAl-LDH heterostructure towards anticorrosion and antiwear application, Chemical Engineering Journal 419 (2021) 130050. https://doi.org/10.1016/j.cej.2021.130050.

[10] H. Yan, X. Fan, M. Cai, S. Song, M. Zhu, Amino-functionalized $Ti_3C_2T_x$ loading ZIF-8 nanocontainer@benzotriazole as multifunctional composite filler towards self-healing epoxy coating, J Colloid Interface Sci 602 (2021) 131–145. https://doi.org/10.1016/j.jcis.2021.06.004.

[11] H. Yan, M. Cai, W. Li, X. Fan, M. Zhu, Amino-functionalized $Ti_3C_2T_x$ with anti-corrosive/wear function for waterborne epoxy coating, J Mater Sci Technol 54 (2020) 144–159. https://doi.org/10.1016/j.jmst.2020.05.002.

[12] L. Wen, Y. Wang, Y. Zhou, J.-H. Ouyang, L. Guo, D. Jia, Corrosion evaluation of microarc oxidation coatings formed on 2024 aluminium alloy, Corros Sci 52 (2010) 2687–2696. https://doi.org/10.1016/j.corsci.2010.04.022.

[13] H. Yan, M. Cai, J. Wang, L. Zhang, H. Li, W. Li, X. Fan, M. Zhu, Insight into anticorrosion/antiwear behavior of inorganic-organic multilayer protection system composed of nitriding layer and epoxy coating with Ti3C2Tx MXene, Appl Surf Sci 536 (2021) 147974. https://doi.org/10.1016/j.apsusc.2020.147974.

[14] D. Zeng, Z. Liu, L. Zou, H. Wu, Corrosion Resistance of Epoxy Coatings Modified by Bis-Silane Prepolymer on Aluminum Alloy, Coatings 11 (2021) 842. https://doi.org/10.3390/coatings11070842.

[15] K. Dahmani, M. Galai, M. Ouakki, M. Cherkaoui, R. Touir, S. Erkan, S. Kaya, B. El Ibrahimi, Quantum chemical and molecular dynamic simulation studies for the identification of the extracted cinnamon essential oil constituent responsible for copper corrosion inhibition in acidified 3.0 wt% NaCl medium, Inorg Chem Commun 124 (2021) 108409. https://doi.org/10.1016/j.inoche.2020.108409.

[16] X. Lai, J. Hu, T. Ruan, J. Zhou, J. Qu, Chitosan derivative corrosion inhibitor for aluminum alloy in sodium chloride solution: A green organic/inorganic hybrid, Carbohydr Polym 265 (2021) 118074. https://doi.org/10.1016/j.carbpol.2021.118074.

[17] N. Bhardwaj, P. Sharma, V. Kumar, Phytochemicals as steel corrosion inhibitor: an insight into mechanism, Corrosion Reviews 39 (2021) 27–41. https://doi.org/10.1515/corrrev-2020-0046.

[18] M.M. Fares, A.K. Maayta, M.M. Al-Qudah, Pectin as promising green corrosion inhibitor of aluminum in hydrochloric acid solution, Corros Sci 60 (2012) 112–117. https://doi.org/10.1016/j.corsci.2012.04.002.

Chapter 5

Development of Oxyresveratrol Incorporated Bio-based Smart Nanocomposite Coating with Anti-corrosive, Self-healing, and Anti-microbial Properties

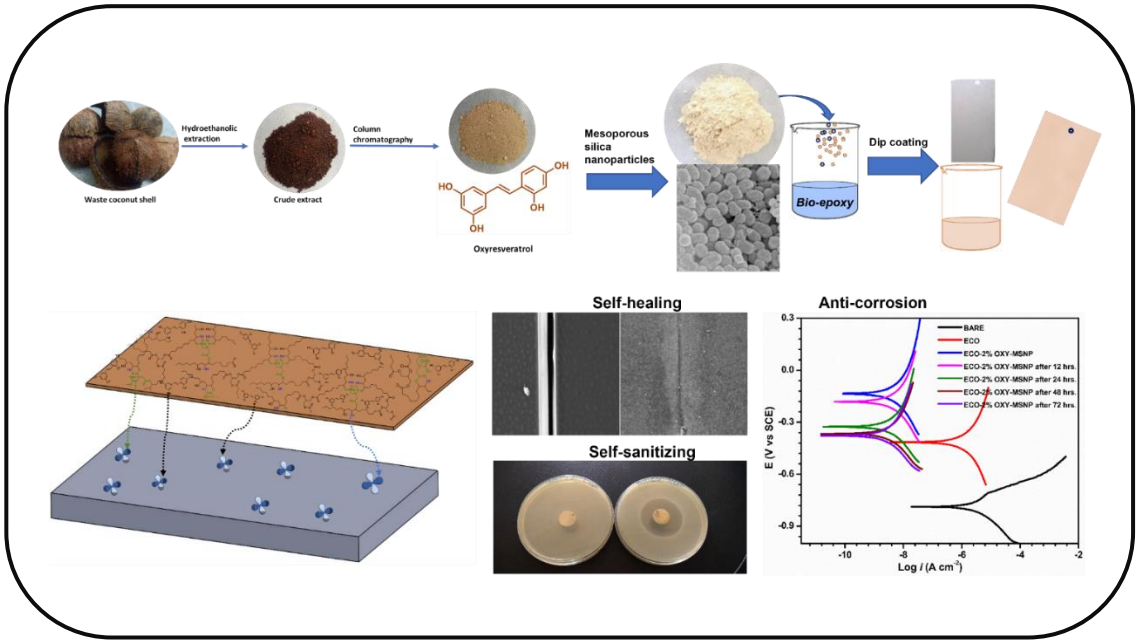

Abstract

Green and sustainable smart coatings with multiple functionalities that exhibit an excellent response to triggers are essential in order to reduce energy consumption, and usage of fossil resources, and to enhance economic impact. In current work, oxyresveratrol (OXY) is extracted from coconut shell waste and subsequently used as a green corrosion inhibitor, encapsulated in mesoporous silica (MSNP) nanocontainers. Castor oil is a non-edible vegetable oil; it is epoxidized and crosslinked with bio-sourced citric acid and reinforced with oxyresveratrol-silica nanoparticles. The bio-based composite coating showed excellent anti-corrosive properties with improved thermal stability. At 2 wt.% of OXY-MSNP content, the corrosion potential shifted to -0.028 V from -0.666 V, and the corrosion current reduced significantly from 30.53 μ Acm^{-2} to 0.0074 μ Acm^{-2} with an inhibition efficiency of 99.97%. The corrosive protection was found to be effective in 3.5 wt.% NaCl solutions of acidic, neutral, and basic media, thus demonstrating the suitability of the coating in all environments. The coating also showed complete self-healing potential within 48 h, as confirmed by SEM micrographs, Electrochemical Impedance Spectroscopy and Potentiodynamic Polarisation studies. The coating inhibited the growth of both gram-positive (*S. aureus*) and gram-negative (*E. coli*) bacteria revealing a strong antibacterial effect. This type of bio-based self-sanitizing composite coating paves the way for the development of multifunctional smart coatings with self-healing, antimicrobial and anticorrosion properties from waste material in a sustainable manner.

Keywords: Bio-nanocomposites; Coconut shell waste; Oxyresveratrol; Smart anticorrosive coating; Self-healing; Anti-microbial

5.1. Introduction

There are many challenges faced by the polymer and corrosion prevention industries, one of the major challenges in the coating and polymer industry is the development of eco-friendly, renewable, and sustainable coating materials. All the petroleum sources are rapidly depleting and this will culminate in resource scarcity in the near future. Moreover, the mining and purification of petroleum crude oil and the vast global usage of petroleum-based products will lead to severe environmental pollution, emission of greenhouse gases, and, thus, extreme climate change. This has led researchers to develop green and sustainable bio-based polymers and composites for various applications [1], as many of them display comparable properties with their petroleum-based counterparts.

Among the resins used for high-performance coating, Diglycidyl ether of bisphenol A (DGEBA) epoxy is the most common, accounting for about 75% of total epoxy consumption owing to its excellent properties. However, Bisphenol A, the major component of DGEBA-epoxy, is highly toxic, an endocrine disruptor, and also responsible for many serious health issues, and thus the food and drug control department of many countries debarred the use of bisphenol A [2]. Another component used for condensation in DGEBA synthesis is epichlorohydrin, a carcinogen, mutagen, and reprotoxic classified substance. Many natural phenols like vanillin, eugenol, lignin, and cardanol derivatives have been used in place of BPA in order to prepare bio-based epoxies [3]. Similarly, naturally resourced vegetable oils are widely used to prepare bio-epoxies with the desired properties for specific applications [4–7]. Linseed oil is one of the most explored vegetable oils with excellent properties. Castor oil is widely used in polymer industries for preparing various monomers and polymers owing to its non-edible nature, availability, and unique functionality with an inherent hydroxyl group and is unsaturated [8,9]. However, some modifications like corrosion inhibitors loaded nanocomposites [10,11] and nano-fillers with healing agents [12] are required to produce bio-epoxy composites for multifunctional coating applications.

Many organic and inorganic corrosion inhibitors like chromates, phosphates, and azoles, etc. are banned in many countries due to their negative impact on human health and the environment. Heavy metals are also excellent corrosion inhibitors but are also very lethal. Thus, the development of an environmentally friendly and side-effect-free bio-

sourced corrosion inhibitor is crucial to prepare coating material with improved anti-corrosive properties. The presence of heteroatoms, lone pairs of electrons and delocalised pi-electron clouds are responsible for the excellent corrosion inhibition property of many inhibitors [13–16]. Many plant extracts and individual phytochemicals from the leaves, roots, and fruits have recently been reported as green corrosion inhibitors [17]. The water extract of *Passiflora edulia* leaves is reported to be an excellent mixed-type corrosion inhibitor for Cu in the H_2SO_4 medium. The observations were also supported by theoretical calculations [18]. Quercetin a flavonoid present in onion, is reported to be active for aluminium alloy protection [19].

Stilbenoid oxyresveratrol is well known for its pharmaceutical applications, particularly dermatological treatments owing to its antimicrobial activity and skin-lightening efficiency [20,21]. Also, the conjugated pi-electron system geometry and the high density of oxygen heteroatoms with lone pairs suggest that the compound is a potential candidate for corrosion inhibition studies. There are many ways to derive this compound from plants, through chemical reactions and bio-transformations [22]. But the isolation from plants is the best choice because of the renewability, environmentally friendly, isolation following green chemistry principles, and cost-effectiveness of the process. Plants in the *Moraceae* family are good sources of oxyresveratrol, e.g., *Artocarpus altilis, Artocarpus lakoocha, Artocarpus hirsutus* [23] and mulberry.

Interestingly, many industrial waste biomasses like coconut shell waste can be used for the isolation of oxyresveratrol with reasonable yield. The number of coconut shells wasted each year at the place of origin, in households, in beaches, and in small- and large-scale industries is in the billions and results in a big environmental issue. Even after the extraction of oxyresveratrol, the residue can still be used for the preparation of many value-added products like charcoal, plywood, mosquito coils, and incense sticks [24] and previously reported products like briquettes, gardening materials, soles of shoes, ecological tiles, etc. [25].

In this study, a solution for major problems faced in the coating and corrosion prevention industry is achieved. All the toxic components like epoxy matrix, hardeners, and fillers are replaced with non-toxic, renewable, and environmentally friendly bio-based counterparts from sustainable sources. Fully bio-based multifunctional smart coating material composed of epoxidized castor oil cured with citric acid as a natural crosslinker,

and oxyresveratrol derived from coconut shell waste as green corrosion inhibitor loaded in a nanocontainer as the filler is evaluated. The coating exhibited excellent multifunctional properties, and the effect on corrosion protection, self-healing property, and antimicrobial action has been evaluated for both MS and Al-6061 alloys in various pH environments. The novelty of the present study is that the bio-epoxy-citric acid- oxyresveratrol system exhibited outstanding corrosion resistance with antimicrobial and self-healing effects, which has not been explored so far. Usually, achieving this multifunctionality is not commonly reported. The obtained i_{corr} (0.0074 μ Acm^{-2}) and E_{corr} (-0.028 V) achieved are outstanding compared to earlier reported corresponding values, along with excellent corrosion inhibition efficiency (99.97%) and complete self-healing (within 48 h) with the antimicrobial property.

5.2. Materials and Methods

5.2.1. Materials

The cold extraction method was used for the isolation of castor oil from the seeds of *Ricinus communis* using hexane as the solvent. Tetraethyl orthosilicate, THF, acetic acid, NaOH, HCl and citric acid were obtained from Sigma Aldrich. Oxyresveratrol was isolated from coconut shell waste and used as the corrosion inhibitor. Cetyltrimethylammonium bromide (CTAB) was purchased from SD Fine Chemicals. Ethanol and NaCl were procured from Merck Specialties Pvt. Ltd. All chemicals were used as-received without any refinement. The strain *S. aureus* and *E. coli* were procured from the collection of MPTD division NIIST, Thiruvananthapuram, Kerala.

5.2.2. Methods

5.2.2.1. Crude extract and oil separation and isolation of the inhibitor compound

Crushed coconut shell waste was used for the extraction of oxyresveratrol in slightly alkaline 4:6 hydroethanolic solvent, as the total phenolic content is reported to be present in higher amounts in alkaline extraction [26]. 1 kg of the crushed shell was soaked in 3 litres of the solvent in a round bottom flask with frequent agitation. The saturated solvent was removed periodically, and the extraction continued with fresh solvents yielded about 25 g of the extract. The lyophilized sample was packed into a silica gel column, and successive elution using hexane and ethyl acetate solvent system from lower to high polarity yielded

the desired compound at 60% hexane-ethyl acetate solvent mixture. A greyish-pink solid was obtained in the rotary evaporator, and the purity was initially checked with TLC analysis. The structure of the isolated compound is given in **Figure 5.1**. About 5 g of oxyresveratrol was isolated from 1 Kg of waste coconut shell. The residual mass can be used for the preparation of shell charcoal by burning in limited oxygen, and the solvents used can be recovered. This will result in the complete utilization of bio-mass without any waste product.

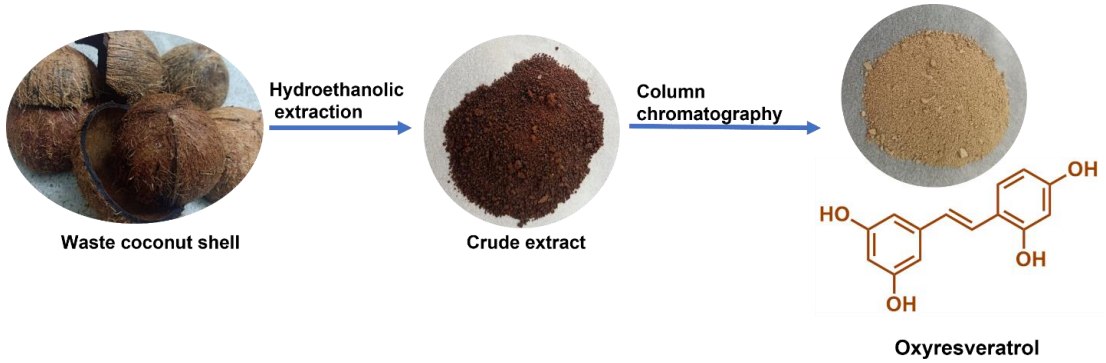

Figure 5.1. Isolation procedure and structure of oxyresveratrol from coconut shell waste

Dry seeds of *Ricinus communis* (castor oil seeds) were crushed, and a cold extraction method was adopted to isolate the oil. 1 kg of crushed seeds was stirred with 3 litres of hexane in a 5 L round bottom flask for two days. Then the mixture was filtered, and the hexane was re-collected by evaporating in a rotary evaporator at 40 °C at low pressure for reuse. The process was repeated twice, and about 500 mL of castor oil (CO) was collected.

5.2.2.2. Epoxidation of the isolated castor oil

The epoxidation of the oil was conducted in situ in the presence of glacial acetic acid and hydrogen peroxide as previously reported [27,28]. After the complete addition of the reagent, the reaction was kept in the same condition for 6 h. After completion of the reaction, the ion exchange resin was filtered. The organic layer was extracted, and the reaction mixture was quenched by washing with Na_2CO_3 and deionized water several times till pH 7. After separating the organic and aqueous phases, the organic layer was dried over $MgSO_4$. The solvents were removed by evaporating in a vacuum oven at 333 K.

5.2.2.3. Synthesis of the inhibitor-nanoparticle composite

The container for loading was prepared by the methods described in the previous works reported by the authors [19]. The CTAB in deionized water was used as a surfactant for the reaction, and NaOH solution was used for the reaction to occur in an alkali medium. 1 g of CTAB was dissolved in 480 mL of deionized water, and to this solution, 3.5 mL of 2 M NaOH solution was added. With a constant stirring rate of 750 rpm and temperature maintained at 353 K, 5 mL of the precursor compound TEOS was added to the solution in a dropwise manner at a constant rate of 1 mL/minute. The temperature, stirring rate, and the addition of the precursor compounds affect the prepared nanocontainers' size, pore size, and surface area. After 2 h, white fine powder was formed, which was subsequently centrifuged and washed with ethanol and deionized water twice to remove the template residues. Lyophilization followed by calcination at 600 °C yielded a free-flowing white powder of mesoporous silica nanoparticles.

A solution of oxyresveratrol (OXY) in ethanol was prepared at a concentration of 50 mg/mL, and the container was introduced to the mixture in a 1:2 ratio for loading. After continuous stirring for 24 h, the ethanol was removed with the help of a water bath at 353 K. The greyish-pink powder obtained was vacuum dried.

5.2.2.4. Substrate and coating preparation

In this study, the metal substrates used as the working electrodes were MS and Al-6061 alloy samples. Samples of measurement 4 cm × 3 cm were used for the study, and only an area of 1 cm^2 was visible to the saline solution in the cell. All the samples were polished with emery papers of varying grit size starting from 80 to 1000. Samples were degreased and washed with acetone and distilled water separately and then oven-dried. The aluminium samples were further etched with low-concentration alkaline and acidic solutions for 60 seconds each before use.

Nanocontainer loaded with green inhibitor oxyresveratrol was added to the epoxidized castor oil-citric acid system at varying concentrations e.g., 1%, 2%, and 3% of the total weight of composition. In the first step, 10 g of epoxidized castor oil (ECO) was weighed in a beaker. In another beaker, 10 mL of tetrahydrofuran (THF) and 1.5 g of citric acid (CA) as crosslinker were mixed till dissolution. The oxyresveratrol-mesoporous silica nanoparticle composite (OXY-MSNP) was dispersed in the THF solution, added to the ECO, and mixed thoroughly to obtain a uniform mixture. The whole mixture was stirred at

70 °C until evaporation of THF (1/4th of the added volume) occurred. Following this, the substrate was immediately coated with this ECO mixture by the dip-coating technique at a speed of 500 mm/min. After coating, the sample was left to cure at 80 °C for 4 h and, after that, at 120 °C for 6 h.

5.2.2.5. Weight loss and surface topology analysis after immersion in corrosive medium

The corrosion inhibition efficiency of the prepared bio-nanocomposite OXY-MSNP is examined by immersion test analysis prior to coating techniques and electrochemical analysis. A weight-loss test was conducted by hanging an M.S. sample of $1cm^2$ size in a beaker containing 300 mL of saline solution for 15 days. Another study was repeated in the presence of dispersed inhibitor composite in the saline medium of 0.5 G/L of inhibitor. Duplicates were also conducted for more accurate results. The difference in weight loss due to the immersion in the saline medium was measured after necessary surface cleaning and drying procedures. SEM micrographs were also taken to evaluate the surface topology and percentage elemental composition of the surface (indicates the corrosion product formation) for each sample. Inhibition efficiency and surface coverage [29] are evaluated using **equations (5.1)** and **(5.2)**,

$$IE(\%) = \frac{Wo - Wi}{Wo} \times 100 \qquad \text{..... (5.1)}$$

$$\theta = \frac{IE\ (\%)}{100} \qquad \text{..... (5.2)}$$

W_i and W_o represent the weight loss that happened to the samples in the medium containing inhibitor/no inhibitor.

5.2.2.6. Electrochemical impedance (EIS) and potentiodynamic polarisation (PP) studies

PP experiments and EIS analysis are the best methods to evaluate the corrosion inhibition efficiency of a substrate. The system under investigation was a conventional 3-electrode system consisting of a calomel electrode, platinum electrode, and the metal substrate as the working electrode. CHI608E workstation (CH Instruments Inc.) was used for the studies. A Spectrodip dip coater (Chennai) was used to prepare coated samples. An

AC signal with a perturbation of 5 mV at OCP in the range of 100 kHz–0.01 Hz was used for the impedance measurements. The obtained EIS plots were fitted using ZsimpWin software to find the electrochemical parameters. Up until the Chi-square value dropped to less than 9×10^{-4} or no further fitting improvement was seen, several circuits were investigated. All potentials were measured against SCE. Cathodic and anodic polarization curves were measured at a scan rate of 1 mV/s from −250 mV to +250 mV of the OCP values.

The corrosion prevention potential of the whole extract was analyzed prior to the separation of the major compound. The anti-corrosion performance of the extract of coconut shells was analyzed by potentiodynamic polarization and impedance spectroscopic methods. Solutions with varying concentrations of the extract, e.g., 0, 100, 300, and 500 ppm solutions in 3.5 wt.% NaCl solution was prepared, and polished mild steel coupons were used for the study. The corrosion inhibition efficiency (η%) can be obtained from the E_{corr}, i_{corr} values from the Tafel plot and is calculated by using the **equation (5.3)**,

$$\eta\% = \frac{icorr - icorr(CNSE)}{icorr} \qquad \textbf{……. (5.3)}$$

Where i_{corr} (CNSE) and i_{corr} are the corrosion current densities with and without the *Cocos nucifera* shell extract (CNSE).

The inhibition efficiency can also be calculated from the EIS measurements using **equation (5.4)**,

$$IE_{EIS}\ (\%) = [\frac{Rct - R*ct}{Rct}] \times 100 \qquad \textbf{……. (5.4)}$$

Where,

R^*_{ct} is the resistance offered by the bare sample

R_{ct} is the resistance offered by the coated sample

The modified ECO-coated samples were prepared, and the exact measurements were also performed to analyze the efficiency of the hybrid coating in the saline medium. Dip coating was done, and the polymer on the exposed side of the substrate was peeled off. The electrodes were kept in the system for about 30 minutes to attain a steady state before starting the experiments.

5.2.2.7. Assessment of self-healing potential

To evaluate the self-healing property, SEM micrographs, potentiodynamic polarisation, and electrochemical impedance measurements were used. The coating, which offered the best corrosion protection for mild steel, was also studied for an Al-6061 alloy. In addition, a coating with artificial scratch was also tested for its corrosion inhibition potential at definite time intervals such as, 0 h, 24 h, 48 h, and 72 h. By comparing the decrease in inhibition potential, an idea about the chance of self-healing is evaluated. SEM images were taken in order to confirm the self-healing efficiency of the matrix. The sample was prepared by coating the polymer matrix containing 2% of the composite on the surface of the polished metal. The coating was allowed to cure at 80 °C for 4 h and then at 120 °C for 6 h. The average coating thickness was 34 µm as measured by an optical profilometer. An artificial scratch of 0.1 mm thickness was made by the sharp insertion of a razor blade, and the samples were immersed in saline media for a different duration. The SEM images were taken and examined after 0, 12, 24, and 48 h.

5.2.2.8. Antimicrobial activity evaluation of the modified ECO coating

Oxyresveratrol and similar polyphenols are known for their antimicrobial property [30]. This self-sanitizing property against microbes is an added benefit for green corrosion-inhibiting coatings. A metal disc of 1.7 cm diameter was coated with the modified ECO formulation. The optimum concentration of oxyresveratrol calculated by the electrochemical method was used for coating, allowed to dry at 80 °C for 4 h and then at 120 °C for 6 h. Qualitative and quantitative analysis of the activity was analyzed with the zone of inhibition protocol and AATCC-100 protocols, respectively.

5.3. Characterisation Techniques

PerkinElmer FTIR (Model 2) was used for the functional group characterization of the compound, nanocontainer, and bio-composites. Purity of the compound and structural confirmation were performed with the help of ^{1}H, ^{13}C techniques using a Bruker Avance AMX 500 MHz NMR spectrometer; NMR solvent was acetone-d6 with 0.03% TMS used as internal standard. The degree of epoxidation (DOE) is calculated [31] by using **equation (5.5)**. The number of epoxide groups in the epoxidized sample and the number of double bonds present in the initial reactant can be replaced by the area integration of the

corresponding peaks in their respective NMR spectra. The glycerol protons can be taken as the internal standard.

$$DOE = \frac{Number\ of\ epoxide\ groups}{Number\ of\ starting\ double\ bonds} \times 100 \quad \text{..... (5.5)}$$

FE-SEM (FEI NOVA NANOSEM 450) and Zeiss EVO 18 cryo-SEM (EDS attached) were used for the morphology analysis and elemental composition determination of the nanocontainer, bio-nanocomposite, and the metal surfaces. A JEOL JEM F200 TEM was used for the structural morphology identification of the empty container and the loaded nanoparticles. STA7300 Thermal Analysis System, Hitachi, was used for the thermal stability analysis of the nanoparticles, isolated compound, and polymer composite. The TGA plot was measured in an inert atmosphere from 30 °C to 1000 °C in an argon atmosphere at a rate of 10 K/minute. A Tristar II, USA, system was used for the nitrogen adsorption-desorption analysis to determine the porous nature, specific surface area, and pore dimensions of the nanoparticles. Particles were degassed at 70 °C before the experiment, and the Brunauer-Emmett-Teller (BET) and Barrett-Joyner-Halenda (BJH) methods were employed to analyze the parameters.

5.4. Results and Discussion

5.4.1. Structural determination of epoxidized oil and isolated oxyresveratrol

^{1}H NMR is used to confirm the epoxidation of castor oil, and the spectra of CO and ECO are stacked together and shown in **Figure 5.2**. The epoxidation can be confirmed by the changes in the position and intensity of the peaks in both spectra. Peak intensity corresponding to the olefinic protons of CO at δ 5.39 and 5.56 ppm diminished significantly after epoxidation, and new peaks corresponding to protons attached to an oxirane group are observed between δ 2.95 and 3.15 ppm revealing the conversion of the double bonds into the epoxy ring. The olefinic protons were more deshielded than the protons attached to oxirane rings. The methine protons of the glycerol part in both CO and ECO remained unchanged in position and resonated between δ 5.30 to 5.26 ppm. No change in the position of methylene protons of the glycerol part was observed and resonated around δ 4.16 ppm and 4.31 ppm. The proton attached to the hydroxyl-bearing carbon in the CO shifted to a more deshielded region in the ECO spectra from δ 3.64 ppm to δ 3.88 ppm. Further, the degree of epoxidation is calculated by integrating the peak area corresponding to olefinic protons and protons attached to the oxirane ring and following the **equation (5.5)** found to be 76%.

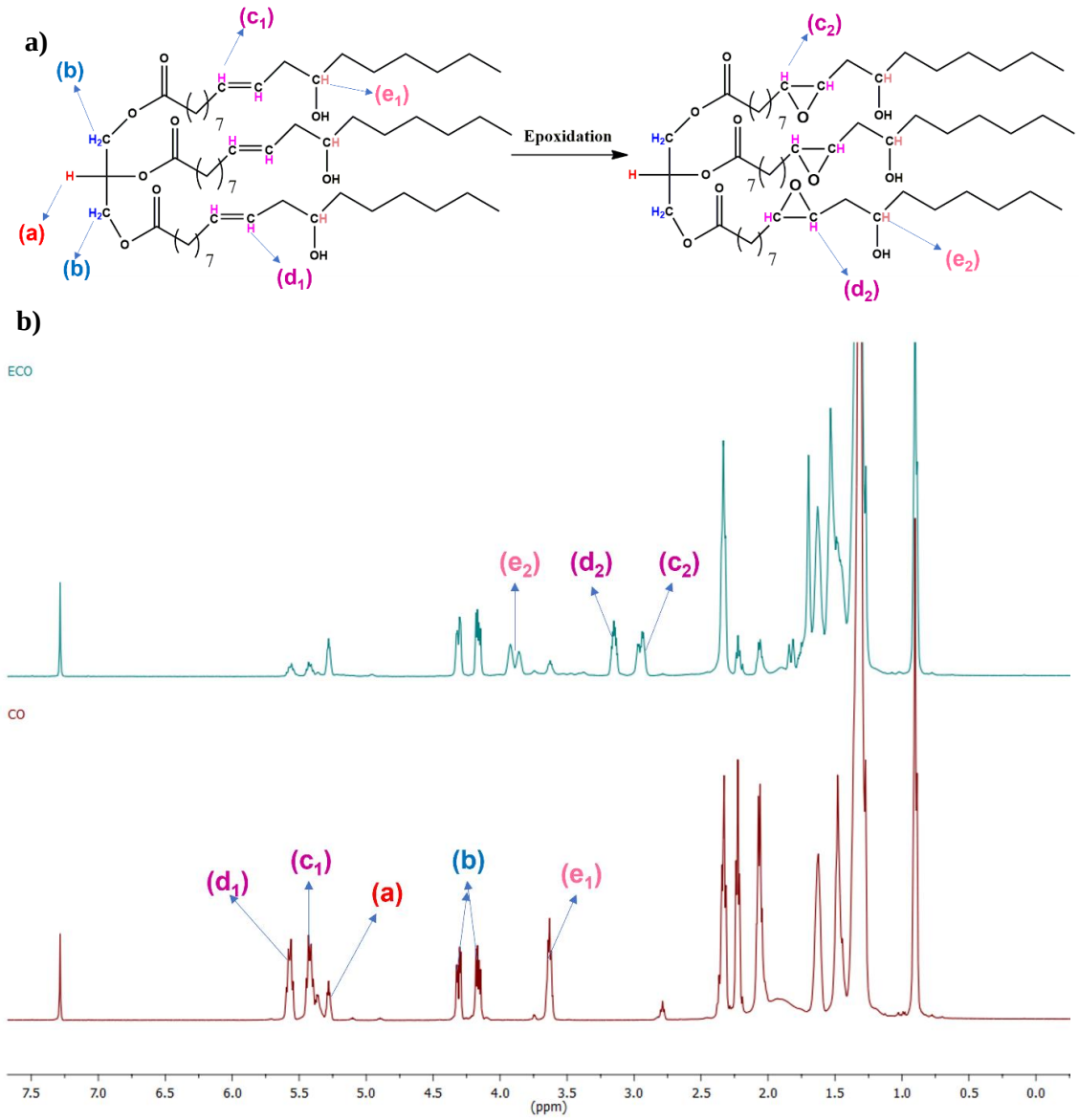

Figure 5.2. **a)** Epoxidation reaction **b)** the changes in the proton NMR of castor oil (CO) and epoxidized castor oil (ECO)

The proton NMR spectra of isolated oxyresveratrol (**Figure 5.3**) exhibited a signal for aromatic protons at δ 8.55 (s,1H), 8.28 (s, 2H), and 7.42(d,2H), etc., and olefinic protons as a doublet at 7.03 (d, 1H, J=16.5 Hz) and 6.90 (d, 1H, J=16.5 Hz) ppm, etc. Similarly, the ^{13}C NMR showed peaks at δ 158.7, 157.3, 139.98, 129.04, 128.2, and 125.9 ppm. High-resolution mass spectrometry showed a peak at m/z 245.0813, which is found to be the $(M+H)^+$ peak for oxyresveratrol. A similar observation with explanation has been reported earlier [32,33] confirming the isolation of oxyresveratrol.

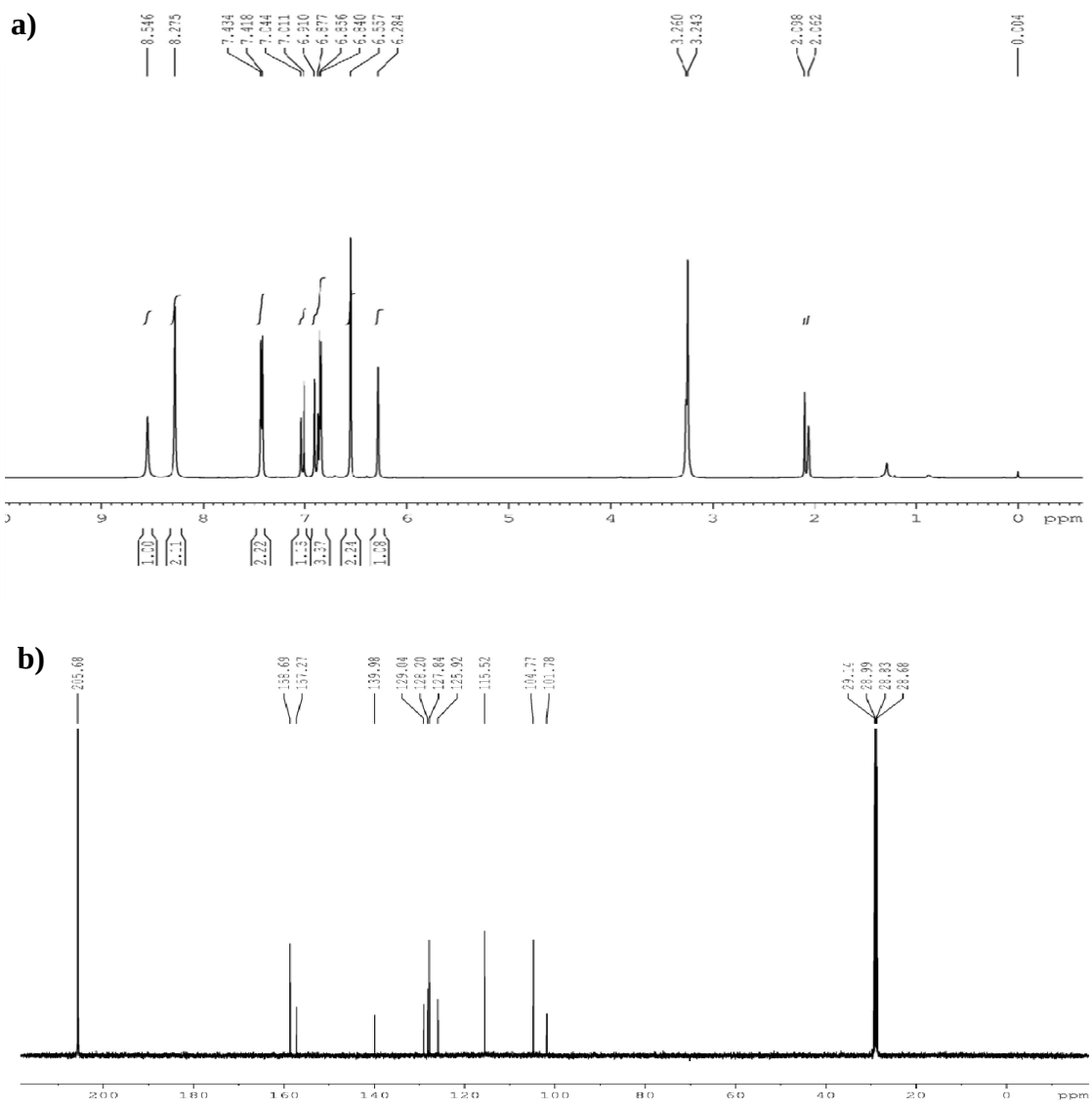

Figure 5.3. a) ^{1}H NMR spectrum of oxyresveratrol (500 MHz, acetone-*d*6) **b)** ^{13}C NMR spectrum of oxyresveratrol (125 MHz, acetone-*d*6)

5.4.2. Characterization of the container and prepared green inhibitor composite

5.4.2.1. *ATR-FTIR studies*

The FTIR analysis of silica nanoparticles (MSNP), oxyresveratrol (OXY), and bio-nanocomposite (OXY-MSNP) is given in **Figure 5.4.** The functional group confirmation and the effective loading can be done using FTIR techniques. The possible interactions and loading mechanism between the container and the inhibitor compound can be understood from the shift in the values of the absorption frequencies. The broad spectrum at 3188 cm^{-1}, corresponding to the stretching vibrations of O-H groups, represents the presence of phenolic/alcohol groups in the compounds, which is slightly shifted to 3199 cm^{-1} towards

the high-frequency region in the bio-nanocomposite. This indicates physical adsorption and no strong chemical bonds are formed during the bio-nanocomposite formation. In the case of inhibitor (OXY), low-intensity absorptions at 2765.8 cm^{-1} and 2687 cm^{-1} denote the existence of aromatic and aliphatic C-H stretching while C=C stretching frequencies are observed at 1611.8 cm^{-1} and 1590.2 cm^{-1}. It is noticeable that the corresponding bands of the inhibitor composite either became diminished or marginally shifted to higher values. This slight change indicates that only weak interaction occurs during the loading, and no other chemical bonds are formed or broken. The shoulder peak at 1101 cm^{-1} and 1298 cm^{-1} corresponds to residual Si-CH_2 bonds, while the peak at 981 cm^{-1} and at 461 cm^{-1} are attributed to silanol group (Si-OH), and Si-O rocking vibrations, respectively. The C-H stretching frequencies, C-C-H bending, etc., are also observed in the fingerprint region. The peaks below 1000 cm^{-1} represent C-H vibrations. The compound and the composites contain heteroatoms and pi-electron systems that can be donated to the metal d-orbital and help in the corrosion prevention mechanism. All the characteristic peaks of the nanocontainer and inhibitor compound are well observed in the case of the inhibitor composite, which confirmed the successful loading of the inhibitor into the nanocontainer. The occurrence of no bond formation enables the easy release of the inhibitor when required.

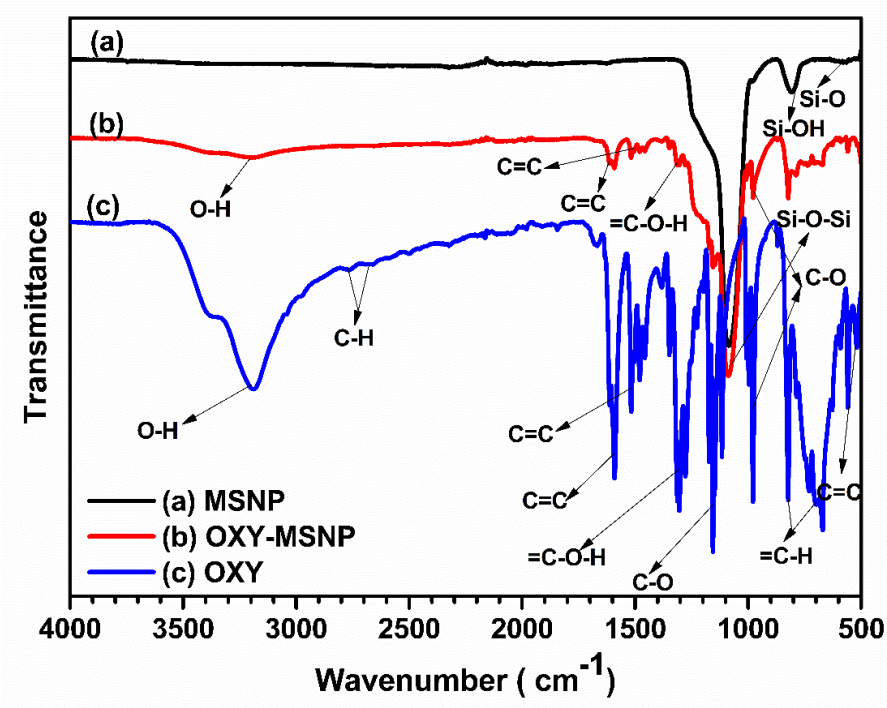

Figure 5.4. FTIR analysis of the container (MSNP), oxyresveratrol (OXY), and the bio-nanocomposite (OXY-MSNP)

5.4.2.2. *Morphology of the nanoparticles using SEM*

SEM images and EDAX spectra were used to understand the surface morphology, size and elemental analysis of the container nanoparticles and the loaded composites. As shown in **Figure 5.5,** the particles are found to retain their spherical morphology before and after the compound's loading, confirming their structural stability even after loading. The size was within 100-120 nm in both container and composite. The elemental analysis of the container showed the presence of only oxygen and silicon, indicating pure silica. However, after the loading, the percentage of both C and O was very high, revealing the presence of the organic component OXY. High carbon content in composites confirms the successful loading of the desired compound into the nanocontainer.

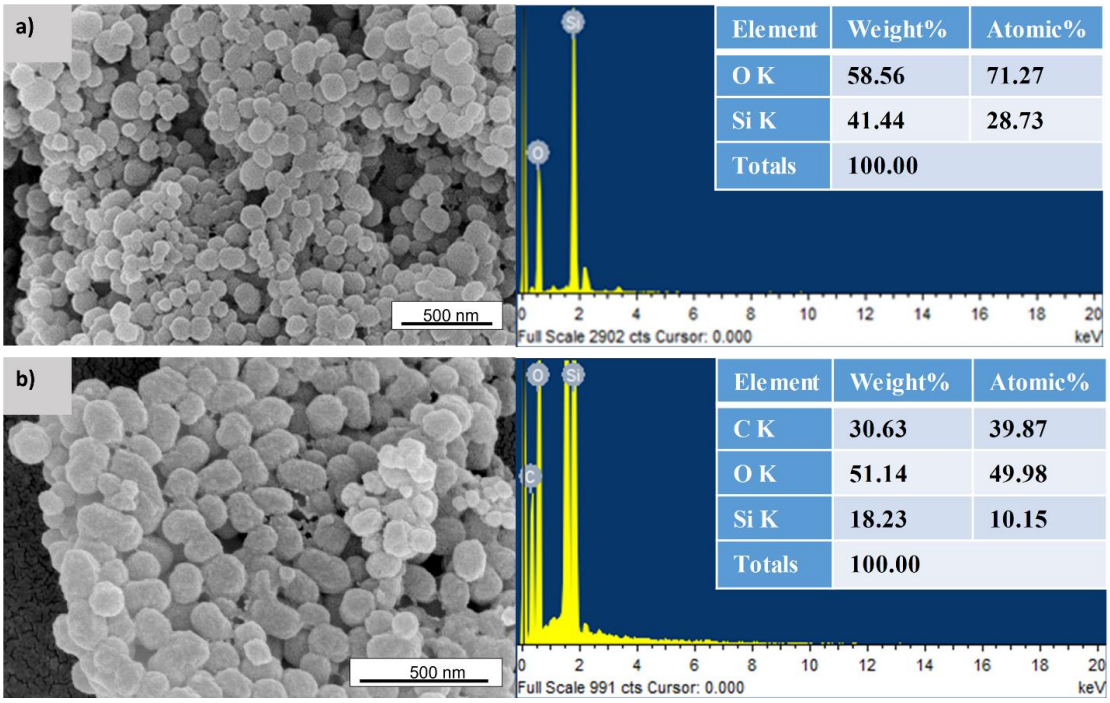

Figure 5.5. SEM micrographs and elemental composition of **a)** nanocontainer **b)** bio-nanocomposite OXY-MSNP

5.4.2.3. *Morphology of the nanoparticles using TEM*

TEM micrographs of the empty container MSNP and the prepared bio-nanocomposite OXY-MSNP are shown in **Figure 5.6** to confirm the loading. The nature of the prepared particles is identified as spherical, as observed in SEM, and the particles are primarily polydisperse. The mesoporous character of the particle is well visible in the TEM micrographs of the container with many channels and pores, which promotes the encapsulation of the compounds in the nanopores. After loading, the cavities seemed to be closed, and the surface of the container was found to be smoother than the empty container.

Further, the bulky nature of the composite particles also indicates the effective loading of oxyresveratrol [34]. The size of the empty container varied between 100-120 nm, while the loaded composite showed a slight increase in radius between 100-130 nm.

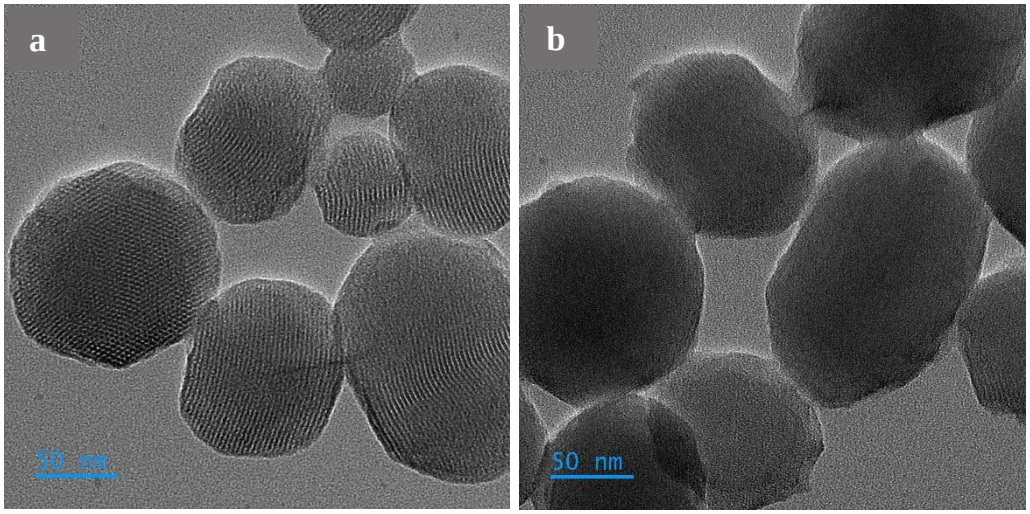

Figure 5.6. TEM images of **a)** MSNP and **b)** OXY-MSNP confirming the loading of the inhibitor

5.4.2.4. *Thermogravimetric analysis*

The TGA thermogram depicted in **Figure 5.7** shows the thermal stability of the nanocontainer, oxyresveratrol, bio-nanocomposite (OXY-MSNP), ECO, and modified ECO (coating with 2% of the bio-nanocomposite). The thermal stability of the OXY is slightly improved due to the incorporation in the nanocontainer. It is observed that crosslinked ECO starts degrading at 190 °C, beyond which the decomposition of ether and the ester linkages takes place in the range of 190-450 °C [27]. The addition of the hybrid filler increased the thermal stability of ECO coatings. T_{onset} and T_{10} of the composite coating are increased by 30 °C and 37 °C confirming its enhanced thermal stability compared to the neat ECO matrix.

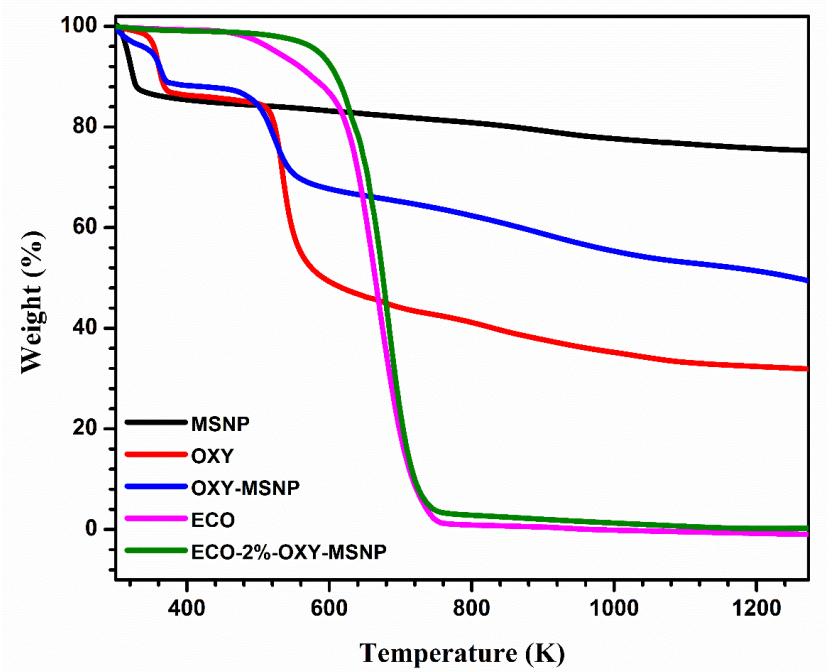

Figure 5.7. Temperature stability evaluation of **a)** containers **b)** oxyresveratrol **c)** OXY-MSNP **d)** ECO **e)** Modified ECO coating containing 2% OXY-MSNP.

5.4.2.5. *Surface area and porous nature evaluation of the particles*

N_2 adsorption-desorption isotherm for MSNP and OXY-MSNP is shown in **Figure 5.8**. The hysteresis loop of the prepared bio-nanocomposite showed lower adsorption of N_2 than that of the container, as the voids are filled with the loaded inhibitors. The structural parameters, like the surface areas, pore diameter, and volume, are presented in **Table 5.1**. The total surface area of the empty container reduced to 99.88 m^2/g from 729.68 m^2/g and the pore volume reduced to 0.20 cm^3/g from 0.68 cm^3/g suggesting the encapsulation of the inhibitor inside the container. These results correlate with the TEM micrographs showing closed micropores on the surface of the composite particles.

Table 5.1. Parameters obtained from the adsorption/desorption studies

Samples	Surface area (m^2/g)	Pore volume (cm^3/g)	Pore diameter (nm)
MSNP	**729.68**	**0.68**	**3.75**
OXY-MSNP	**99.88**	**0.20**	**8.16**

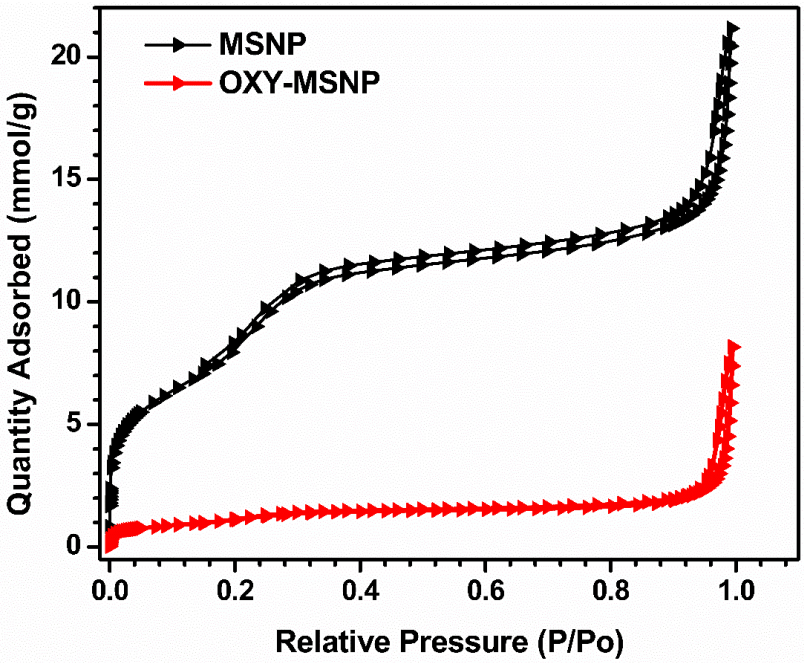

Figure 5.8. N_2 adsorption/desorption isotherm for the nanoparticles confirming the loading of the inhibitor

5.4.3. Evaluation of corrosion resistance potential of the extract and the composite

5.4.3.1. *Corrosion prevention potential of the extract*

In order to evaluate the corrosion inhibition potential of the total extract and its chances to give a potential corrosion inhibitor on further isolation, various concentrations of the *C. nucifera* shell ethanolic extract were dissolved in the saline medium containing 3.5 wt.% NaCl solution. The polished MS samples were taken as the working electrode, and the electrolyte solutions were saline solutions with extract concentrations of 0, 100, 200, and 500 ppm. The EIS and polarization studies showed the efficiency of the *C. nucifera* shell extract as a potential corrosion inhibitor, even at small concentrations. The EIS and polarisation plots are shown in **Figures 5.9 (a)** and, **(b),** and the parameters are depicted in **Table 5.2** by fitting the impedance circuits using Zsimpwin software. The bare mild steel was fitted with an equivalent electrochemical circuit (EEC), as shown in **Figure 5.9(c),** and all other circuits gave a more accurate fitting to **Figure 5.9(d).**

The bare MS can be fitted well with the EEC $R_s(C_{dl}R_{ct})$, and in the presence of extracts, curves can be fitted with the circuits $R_s(C_f\,R_f\,(C_{dl}R_{ct}))$. The circuit indicates the development of a strong film over the metal by the inhibitor compounds. The solution resistance, double-layer capacitance, and the resulting charge transfer resistance can be represented as R_s, C_{dl}, and R_{ct}, respectively. The capacitance and resistance offered by the

film formed were denoted as C_f and R_f [35]. Plant extract consists of several phytochemicals of varying structures and properties, which can undergo different adsorption mechanisms; they adsorb on the surface of the metal and form a protective coating on the surface. As the amount of the extract increases, thus, the effectiveness of the corrosion resistance also increases, which can be attributed to the increase in the area covered and thickness of the layer formed. With the concentration of the extract, the radium of the semi-circular loop also increased; this indicates the replacement of water molecules from the metal/solution interface by the inhibitor molecules. Which in turn reduces the charge transfer process and thus metal ion corrosion [16,36].

A similar fact of concentration-dependent anti-corrosive behaviour of the extract is also observed in the Tafel plot. As the augment of extract, the corrosion current density tends to decrease. The initial addition of the 100 ppm extract showed a slightly negative shift in the E_{corr} values, showing a reduction in cathodic reactions. But the i_{corr} values supported the corrosion inhibition nature of the extract with 91.4% corrosion inhibition efficiency compared to bare mild steel. At 300 ppm concentration, E_{corr} shifted to more positive values showing a great reduction in reaction at the anodic reaction sites. Nevertheless, η still exhibited above 90% inhibition, confirming a reasonable corrosion inhibition. It is important to note that at a higher concentration of 500 ppm, the E_{corr} value is significantly improved to -0.471 V and the i_{corr} value to 0.38 μ Acm^{-2} with a 98.7% inhibition (**Table 5.2**). The E_{corr} values changed to the more positive potential range by a value greater than 85 mV, so the extract acts as an anodic-type corrosion inhibitor. In the anodic branch, despite the large positive shift in the corrosion potential, the slope of the polarisation curves augments suddenly. This is due to the desorption of the adsorbed molecule after a certain potential. But the higher adsorption process rate and lower desorption process rate protect the metal from corrosion [18,37].

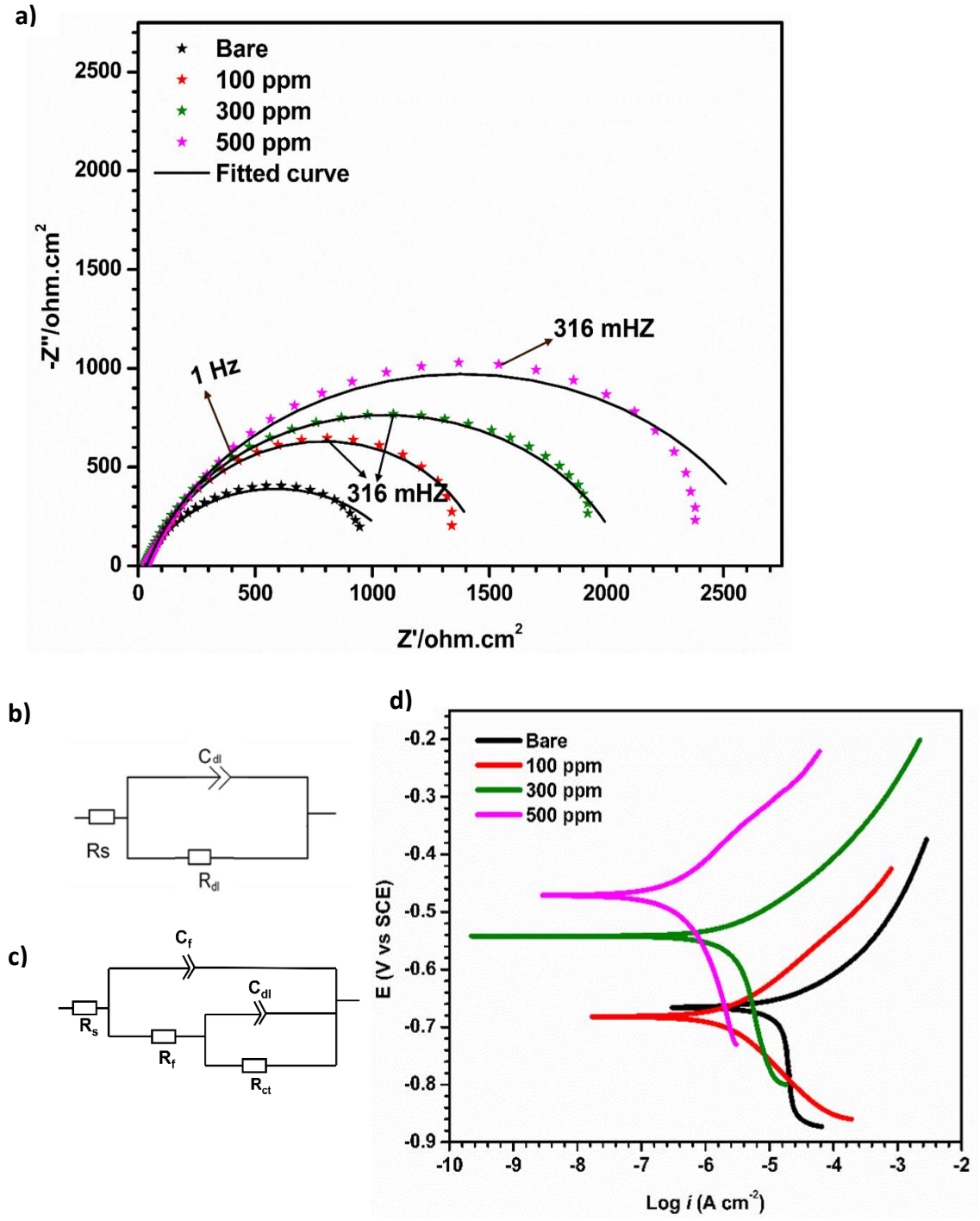

Figure 5.9. Electrochemical study results showing **a)** Nyquist plot, **b)** EEC for bare MS, **c)** EEC for different concentrations of extracts in the corrosive medium, and **d)** Tafel plot

The presence of higher amounts of polyphenols in the coconut shell is the reason for this enhanced response [38]. The coordination of the polyphenols via the lone pair of electrons in the heteroatom with the metal atom resulted in the formation of the protective

coating. A tight chemisorption is formed by the coordination of the lone pair of electrons to the metal d-orbitals, and physisorption occurred due to the electrostatic attraction of charges on the compound and the surface charge [16,36]. Fe-inhibitor complex formation increases with increasing concentration of the extract, which is clearly evident in the polarisation plots. Based on these findings, one of the marker compounds from the total extract, oxyresveratrol, is isolated and loaded into the containers for further studies to confirm its corrosion inhibition potential.

Table 5.2. Electrochemical parameters for the study of the corrosion prevention potential of the extract dispersed in the corrosive medium.

S/N No.	**Concentration**	**Potentiodynamic polarisation**			**EIS**	
		E_{corr}	i_{corr}	Inhibition efficiency	R_f	IE $_{EIS}$
	(ppm)	*(V)*	(μ Acm^{-2})	(%)	(Ω cm^2)	(%)
1.	0	-0.666	30.53	_	1120	_
2.	100	-0.682	2.60	91.4	1692	33.8
3.	300	-0.542	3.0	90.2	2084	46.3
4.	500	-0.471	0.38	98.7	2731	59

5.4.3.2. *Weight loss and surface topology studies for the samples in the presence of oxyresveratrol bio-nanocomposite*

For further confirmation of the potential of the isolated compound oxyresveratrol, its composite was used in a weight loss test for corrosion inhibition of the MS and Al-6061 alloy. The inhibition efficiency (IE%) and surface coverage (θ) for the bio-nanocomposite OXY-MSNP are determined from an immersion study of 15 days in the saline medium in the presence and absence of the composite. (**Table 5.3).** The surface topographic changes in the case of mild steel with and without the presence of the inhibitor composite were evaluated with the help of SEM micrographs (**Figure 5.10).**

SEM analysis revealed the topological changes that occurred to mild steel surfaces during immersion in the saline medium at different pH. In all the pH systems studied, the bare MS sample immersed in the saline medium was severely affected by the chloride ions, a large amount of corrosion products, and very deep groves and voids observed on the surface, particularly in the acidic and alkaline conditions. While in the case of MS samples in the presence of OXY-MSNP, significantly less amount of corrosion products and a

smoother surface are observed in the SEM micrographs in all the experimental conditions (**Figure 5.10**).

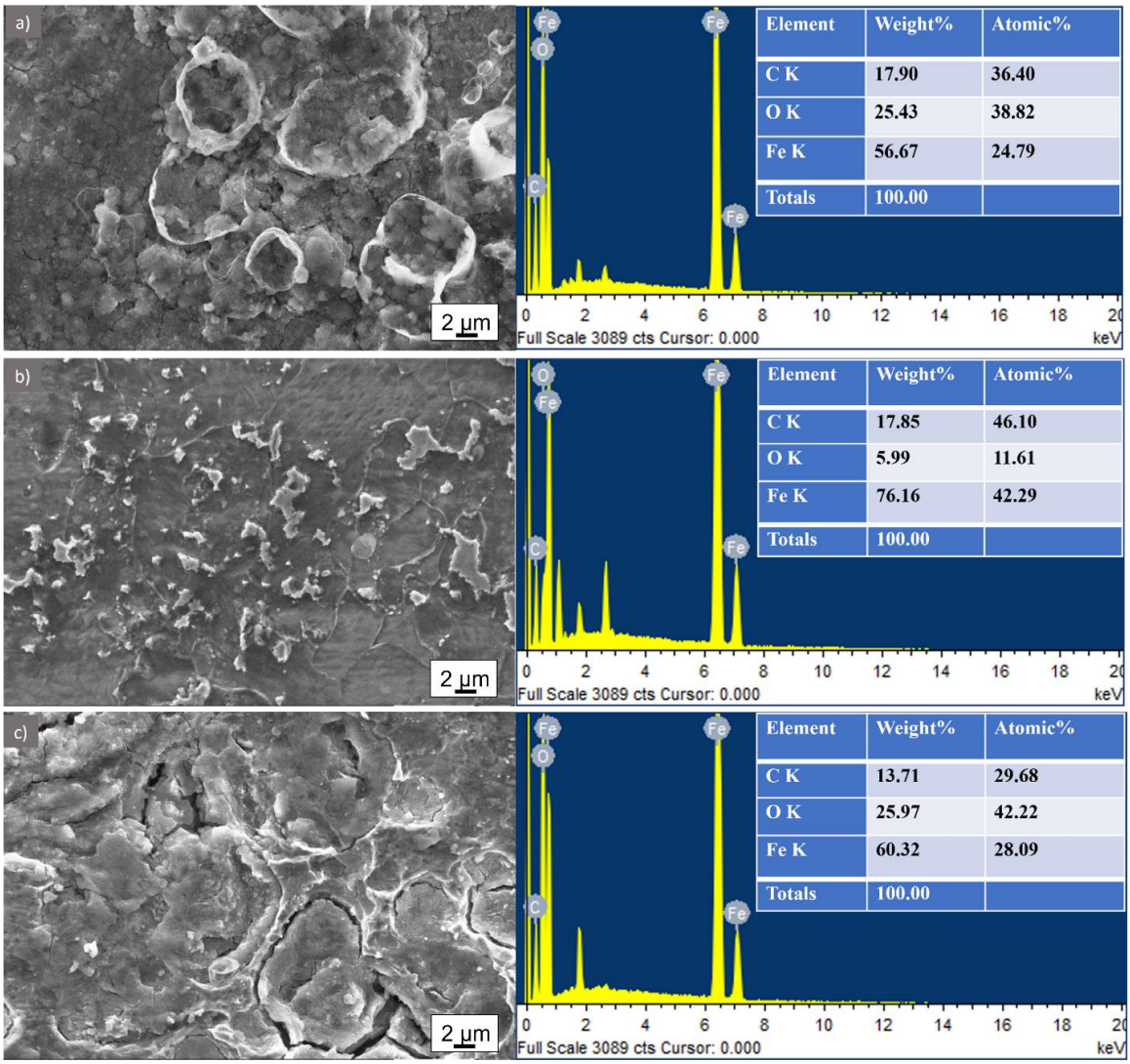

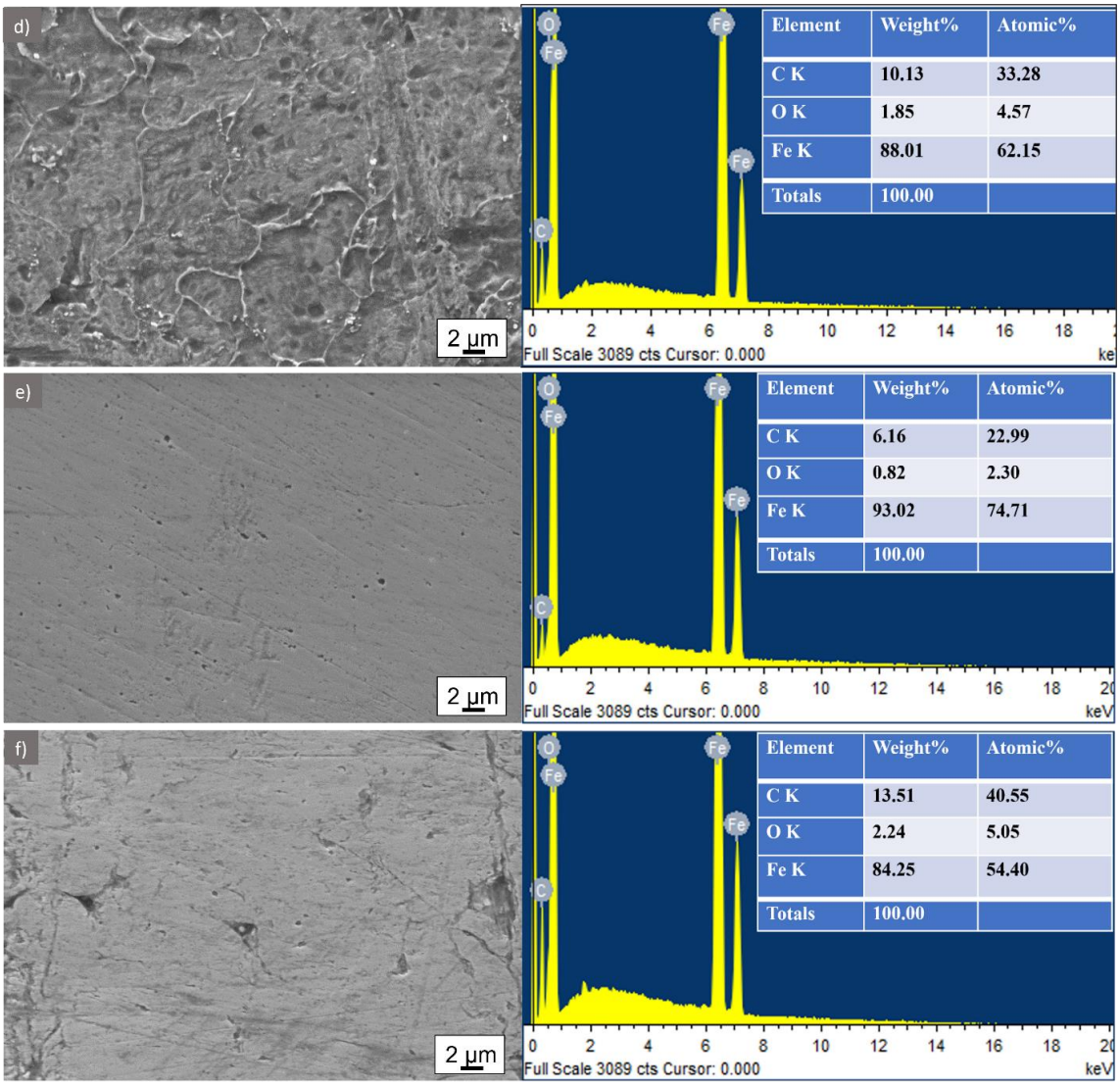

Figure 5.10. Surface topological comparison of samples of mild steel from the immersion test. **a), b),** and **c)** MS samples immersed in saline solution without the composite at various pH 4, 7, and 10, respectively, **d), e)** and **f)** samples immersed in the presence of the composite at various pH 4,7, and 10, respectively.

In agreement with the surface morphology evaluation of samples, the elemental analysis of the surface clearly states that in the presence of OXY-MSNP, corrosion product formation is very low. The bare samples gave an oxygen content of 25.43%, 5.99%, and 25.97% at pH 4, 7, and 10, respectively. But in the presence of OXY-MSNP, it reduced to 1.85%, 0.82%, and 2.24% suggesting inhibition of corrosion product formation.

Table 5.3. Immersion test outputs showing the effect of oxyresveratrol composite in corrosion inhibition of MS and Al-6061

Substrate	pH 4		pH 7		pH 10	
	IE (%)	θ	IE (%)	θ	IE (%)	θ
MS in the presence of bio-nanocomposite (0.5 g/L)	85.31	0.85	90.42	0.90	86.46	0.86
Al-6061 in the presence of bio-nanocomposite (0.5 g/L)	84.01	0.84	91.23	0.91	87.03	0.87

5.4.3.3. *Corrosion inhibition efficiency of the modified bio-epoxy coating on mild steel*

EIS and PP analysis was used to evaluate the corrosion inhibition efficiency of the oxyresveratrol nanocomposite for mild steel at various concentrations of the composite in the ECO matrix. In all the cases of mild steel samples, the stabilized OCP values were slightly more anodic than the E_{corr} values obtained in polarisation studies. The inhibition efficiency of the composite was evident in the Tafel plot and the Nyquist plot compared to bare MS. In the Tafel plots, there is a significant positive shift in the E_{corr} and a vast decrease in the i_{corr} in all the compositions. This improved trend is noticed due to the formation of a protective layer and anodic protection. Among all the compositions, the coating with 2 wt.% of the bio-nanocomposite exhibited maximum inhibition efficiency. The corrosion potential of the bare mild steel -0.666 V increased to -0.028 V, and the i_{corr} decreased from 30.53 to 0.0074 μAcm^{-2}. The cathodic branch and anodic branch appear parallel in each increasing concentration of inhibitor. This indicates that the rate of both anodic and cathodic reactions is reduced by the modified epoxy coating. But the E_{corr} values were moved to the positive potential range by a value >> 85 mV, so the modified epoxy coating acts more as an anodic type inhibitor coating. The potentiodynamic polarization parameter obtained from the Tafel plot and the calculated inhibition efficiency percentage is listed in **Table 5.4**.

Beyond this concentration, the corrosion current density is slightly changed, and the corrosion potential changes to a more negative value. This may be due to the agglomeration of the nanoparticles in the ECO matrix and change in surface morphology, which results in the nanoporous nature of the coating, allowing the electrolyte penetration

into the system. However, the 3% coating also exhibited excellent corrosion inhibition efficiency (99.85%) compared to bare mild steel in terms of i_{corr} values.

The electrochemical impedance of mild steel conducted in a near-neutral medium and the resultant Nyquist plot, the fitted circuits, etc., are shown in **Figure 5.11,** and the EIS parameters are presented in **Table 5.4**. Compared to the bare mild steel sample, all the coatings showed higher resistance values and a large radius of the semi-circular loop. As the concentration of the inhibitor increased, the radius and, thus, the R_{ct} values of the semi-circular loop also increased. The incorporation of 2% OXY-MSNP in coating yield the maximum R_{ct} value of 1789000 Ω cm^2 in agreement with the results from the potentiodynamic polarization studies. Beyond that, the radius of the semicircle tends to decrease, and the R_{ct} value decreases, but it still shows adequate protection for the metal surface, as explained in the earlier section. This shows the excellent corrosion inhibition potential and barrier properties of the modified ECO coating than many other bio-epoxy systems [39,40] . From the resistance values extracted from the graph, the percentage of inhibition potential can be calculated using equation (5).

The EEC of the bare mild steel can be represented as $R_s(C_{dl}R_{ct})$, and for all other coatings, the EEC is $R_s(C_cR_c(C_{dl}\,R_{ct}))$. Where R_s is the solution resistance, the constant phase element (CPE) was used to replace the pure capacitance behaviour. C_{dl} is the double-layer capacitance offered by the electrical double layer, and R_{ct} is the charge transfer resistance, medium-low frequency elements. The huge resistance offered by the modified ECO coating is represented as R_c and the capacitance as C_c, which are observed at the high-frequency side of the curve [35,41]. The parameters resistance and capacitance always followed a reverse order. The larger the resistance value and smaller the capacitance value, the better the coatings' corrosion protection efficiency. A higher value of C denotes a higher absorption of the electrolyte by the polymer matrix [42].

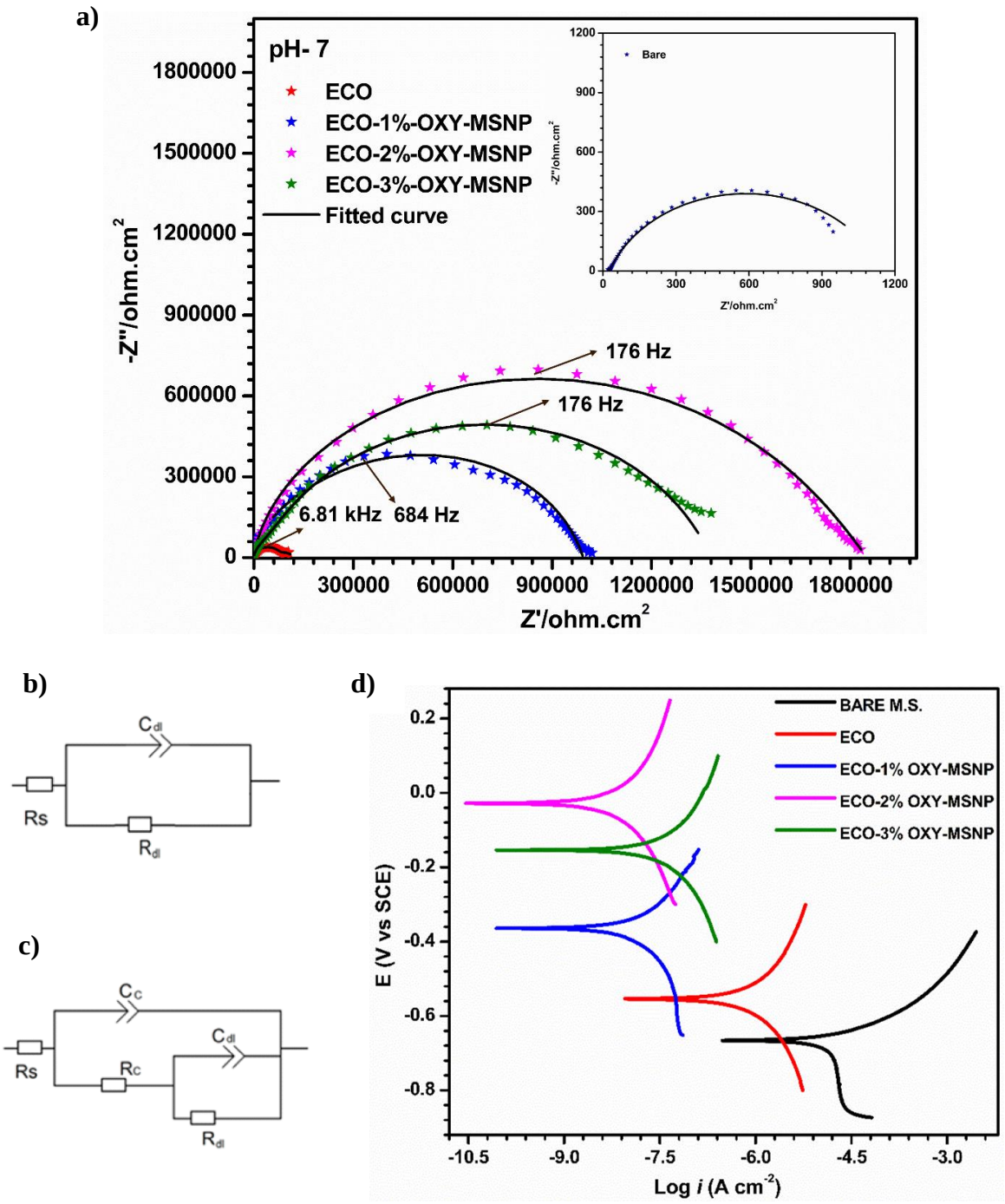

Figure 5.11. Result of electrochemical studies of the intact coating, **a)** Nyquist plots, **b)** EEC for MS, **c)** EEC for coated substrates, and **d)** Tafel plot in the saline medium.

Table 5.4. Parameters from the Nyquist and Tafel plots and the calculated efficiency of the intact coatings

S/N	Sample	Potentiodynamic polarisation			EIS	
		E_{corr} (V)	i_{corr} (μ Acm^{-2})	η (%)	R_{ct} (Ω cm^2)	IE $_{EIS}$ (%)
1.	Bare mild steel	-0.666	30.53		1128	
2.	ECO	-0.554	0.9770	96.80	76680	98.50
3.	ECO-1%OXY-MSNP	-0.364	0.0182	99.94	994000	99.88
4.	ECO-2%OXY-MSNP	-0.028	0.0074	99.97	1789000	99.94
5.	ECO-3%OXY-MSNP	-0.154	0.0434	99.85	1380000	99.92

5.4.3.4. *Inhibitor release profile and pH-dependent corrosion inhibition efficiency*

To evaluate the stability and corrosion inhibition potential of the coatings in the different media, the potentiodynamic polarisation and EIS experiments were repeated at pH 4 and pH 10. In both alkaline and acidic conditions, both the ECO coating with and without OXY-MSNP exhibited excellent corrosion resistance. In the Tafel plots, it is evident that the corrosion potential of all the coatings increased, and the corrosion current density decreased to a vast extent compared to bare mild steel samples with an efficiency of 95.92% and 94% in pH 4 and pH 10, respectively. It is evident that the coating provided adequate protection in all the pH ranges, and the best performance was observed in solutions around pH 7. The Tafel plots are shown in **Figure 5.12**, and the parameters are tabulated in **Table 5.5.**

The release profile of the inhibitor from the container at different pH solutions was studied to explain the different efficiencies. There is enhanced corrosion prevention in the acidic and alkaline pH when compared to the efficiency of the pure epoxy in the acidic and alkaline medium. There is a marked difference in the efficiency of the pure epoxy in three different mediums, but comparable results were observed in the modified epoxy coatings. The higher release of the inhibitor compounds at the acidic and alkaline solutions is responsible for this improvement in performance. 5 mg each of nanocomposites were added to 50 ml of saline solutions of pH 4, pH 7 and pH 10. After 10 minutes the absorbance was measured for each solution and is given in **Figure 5.12c.** The pH-triggered release of the

silica nanoparticles is responsible for higher release in acidic pH, while the anion formation and the resultant increased solubility are responsible for the higher release at the basic pH. The deprotonation of the hydroxyl groups of the oxyresveratrol will result in a benzoquinone-like structure temporarily, which is responsible for the shift in the UV position and slight colour change of the solution.

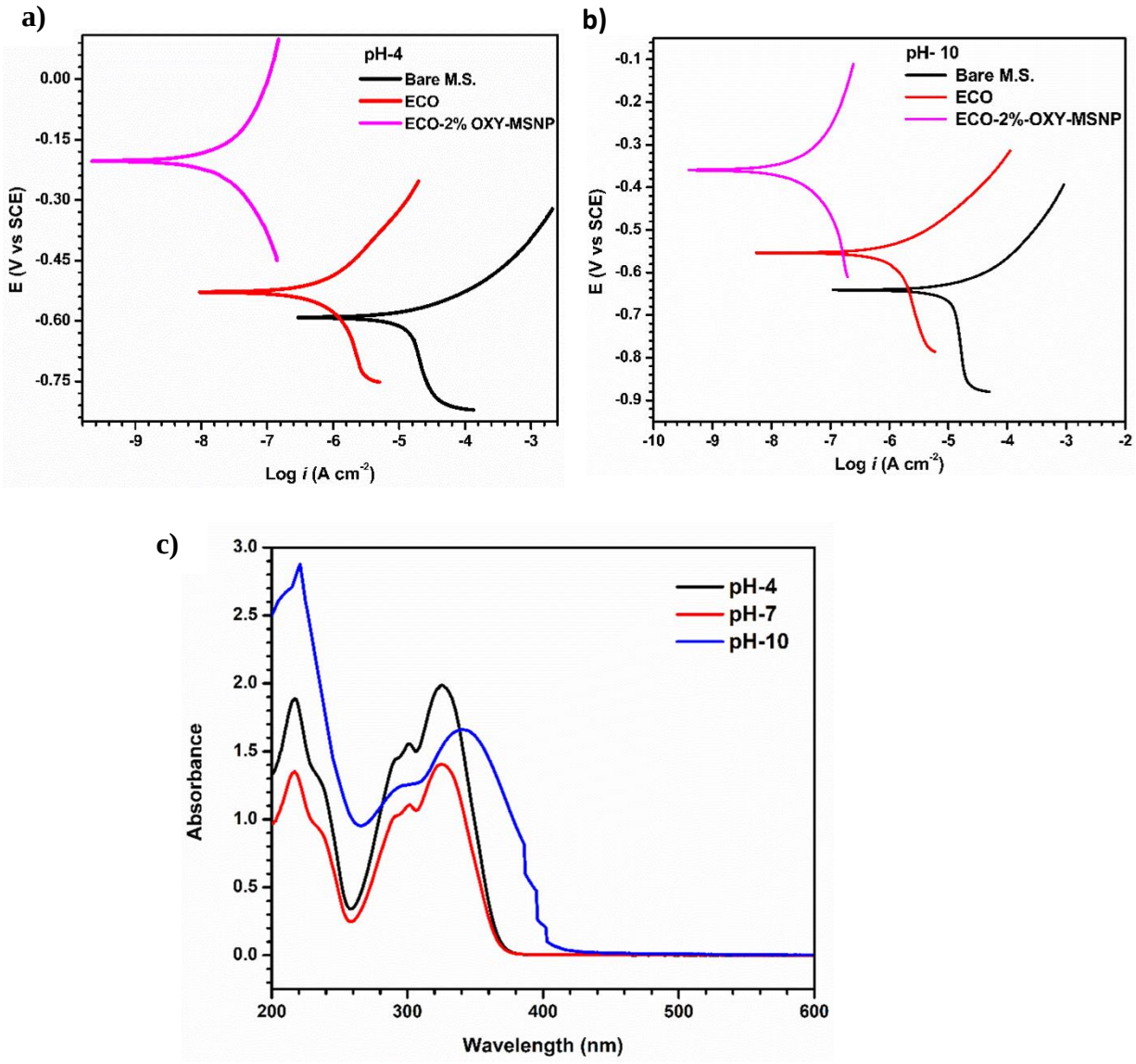

Figure 5.12. Potentiodynamic polarisation studies of the intact coating containing 2% inhibitor, **a)** Tafel plot at pH-4 **b)** Tafel plot at pH-10, and **c)** release profile of the inhibitor from the container at different pH

Table 5.5. Parameters and inhibition efficiency of the intact coating for mild steel samples at pH 4 and pH 10

S/N	Substrate	Potentiodynamic polarisation pH 4			Potentiodynamic polarisation pH 10		
		E_{corr} (V)	i_{corr} (μ Acm^{-2})	η (%)	E_{corr} (V)	i_{corr} (μ Acm^{-2})	η (%)
1.	Bare mild steel	-0.592	24.51	_	-0.641	29.77	_
2.	ECO	-0.529	1.0070	95.92	-0.554	1.7920	94.0
3.	ECO-2%-OXY-MSNP	-0.203	0.0239	99.92	-0.359	0.0437	99.86

Compared to previous reports of the DGEBA based epoxy and green corrosion inhibitor-based system, the ECO-green corrosion inhibitor system exhibited improved performance in terms of E_{corr}, i_{corr}, and corrosion inhibition efficiency. An excellent self-healing effect was also observed for this more flexible bio-based epoxy system. Many epoxidized castor oil-based protective coatings were reported to contain various organic, inorganic, and bio-based fillers. The ECO-oxyresveratrol matrix showed improved performance over many other castor oil-based systems in R_{ct} improvement, i_{corr} reduction, and corrosion efficiency improvement [43,44]. The most evident improvement was in the anodic shift of the E_{corr} values. The incorporation of the inorganic fillers improved the thermal stability to a degree.

As the best corrosion protection was noticed in the composition with 2% bio-nanocomposite, the same concentration was used for further study with the Al-6061 substrate.

5.4.3.5. *Corrosion prevention potential and self-healing efficiency analysis of the coating on Al-6061 alloy*

As observed in the case of MS, the coating containing 2% composite exhibited a substantial potential difference towards the positive potential (from -0.788 V to -0.136 V) and a significant decrease in the corrosion current value (from 1.941 μ Acm^{-2} to 0.0040 μ Acm^{-2}) for Al-6061 samples. Unlike mild steel samples, in the case of Al alloy samples, a very slight anodic shift was observed in E_{corr} compared to OCP as a layer of $Al(OH)_3$

formed on the surface of the samples [45]. Both the changes indicate the outstanding corrosion inhibition property of the bio-nanocomposite coating on aluminium alloy with 99.79% inhibition efficiency in terms of i_{corr} value. The Nyquist plot also showed an enormous increase in the R_{ct} values and showed a 99.95% inhibition for the coating compared to the bare Al-6061 alloy.

To evaluate the possibility of self-healing, an artificial scratch 10 mm in length and 0.1 mm thick, was made on the surface of the coating containing 2% of the inhibitor composite. All the experiments to evaluate the corrosion inhibition efficiency were repeated on the same sample with a scratch at time intervals of 0 h, 24 h, 48 h, and 72 h, whilst immersed in the same corrosive medium in the electrochemical cell. The observed results suggested the possibility of an intrinsic self-healing efficiency. Comparing the Tafel plots at various time intervals showed a shift in the corrosion potential towards more negative values, however, the coating still exhibited excellent corrosion protection compared to bare and pure ECO-coated samples. Although the corrosion current values tend to decrease with time for the scratched coating, the i_{corr} value is 0.0043 μ Acm^{-2}. After 24 h, the value changed to 0.0035 μ Acm^{-2} which further reduced to 0.0030 μ Acm^{-2} after 72 h immersion, with an inhibition efficiency of 99.84% (**Table 5.6**), suggesting active self-healing in the saline medium.

On fitting the Nyquist plots for all the coatings, the $R_s((C_{dl}R_{ct})\ (C_{oxi}\ R_{oxi}))$ circuit fitted for the bare Al-6061 Nyquist plot, which shows the formation of the corrosion product, aluminium oxide, on the surface and the small resistance offered by the corrosion products. The ECO coating gave an EEC of $R_s(C_cR_c(C_{dl}R_{ct})(C_{oxi}\ R_{oxi}))$, the 2% coating fitted well for $R_s(C_c(R_c(C_{dl}(R_{ct}W))))$ and all other coatings with the scratch, fitted for the circuit $R_s(C_c(R_c(C_{dl}R_{ct})(C_{oxi}(R_{oxi}W))))$. In all the circuits, R_s represents the solution resistance, and C_c and R_c represent the constant phase element (CPE) and resistance offered by the polymer coating. The elements C_{dl} and R_{ct} represent the double-layer capacitance and thus the emerging charge transfer resistance (**Figure 5.13**). Depending on the varying inhibition efficiency and the immersion time exposed to the saline water, the corrosion products will be formed in varying amounts, particularly in the low-performance ECO coating and in the scratched coatings. The elements C_{oxi} and R_{oxi} represent the CPE and resistance offered by the corrosion products [46,47]. The additional element represented by the W is the Warburg impedance [46], which indicates the diffusion of the formed oxides in the medium. Higher R_c and lower C_c and C_{dl} values by the ECO coating containing the green corrosion inhibitor suggest good corrosion protection (Yan et al., 2021a). The elements C_{oxi}, R_{oxi}, and W (in

the case of ECO coatings and coatings with scratch immersed for a long time in saline water) suggest the formation of a small amount of corrosion products, the resistance offered by the oxide and its diffusion through the pores. Because, as the scratched coating is being immersed in the saline medium, some corrosive ions may enter the matrix before the self-healing takes place. This will result in trapped and stable corrosion products in the matrix, which will later act as a layer of protection for the aluminium surface. The Nyquist plot can be divided into two parts, the capacitive arc at the higher frequency represents the polymer part, and the second part from the end of the arc, a straight line at a lower frequency, representing stable corrosion products in small amounts [48].

The possibility of self-healing potential is more evident in the polarisation studies than in the EIS analysis. Even though the E_{corr} changes, the i_{corr} values remain almost constant. The EIS measurement will give an average response to the total exposed surface. Since there is a defect in the coating, the values of corrosion parameters will be obviously different from that of the intact coating, which is clearly depicted in both EIS and polarisation studies. Also, if there is no self-healing occurring, the surface will be severely affected and damaged after each EIS and destructive polarisation test. But this was not observed in the tests and in the parameters, which revealed the self-healing during the immersion. Compared to the 0 h reading (6296900 Ω cm^2), there was an increase in the R_{ct} value of the scratched coating after 12 h (7631800 Ω cm^2), this is due to the possible self-healing. The further decrease in resistance values observed is due to the absorption of electrolytes in the polymer matrix during long immersion, and continuous polarisation tests carried out on the same sample. Polarisation techniques are destructive methods that reduce the efficiency of the coating to an extent. This gives an initial idea of possible self-healing and the confirmation of the self-healing obtained from the SEM micrographs.

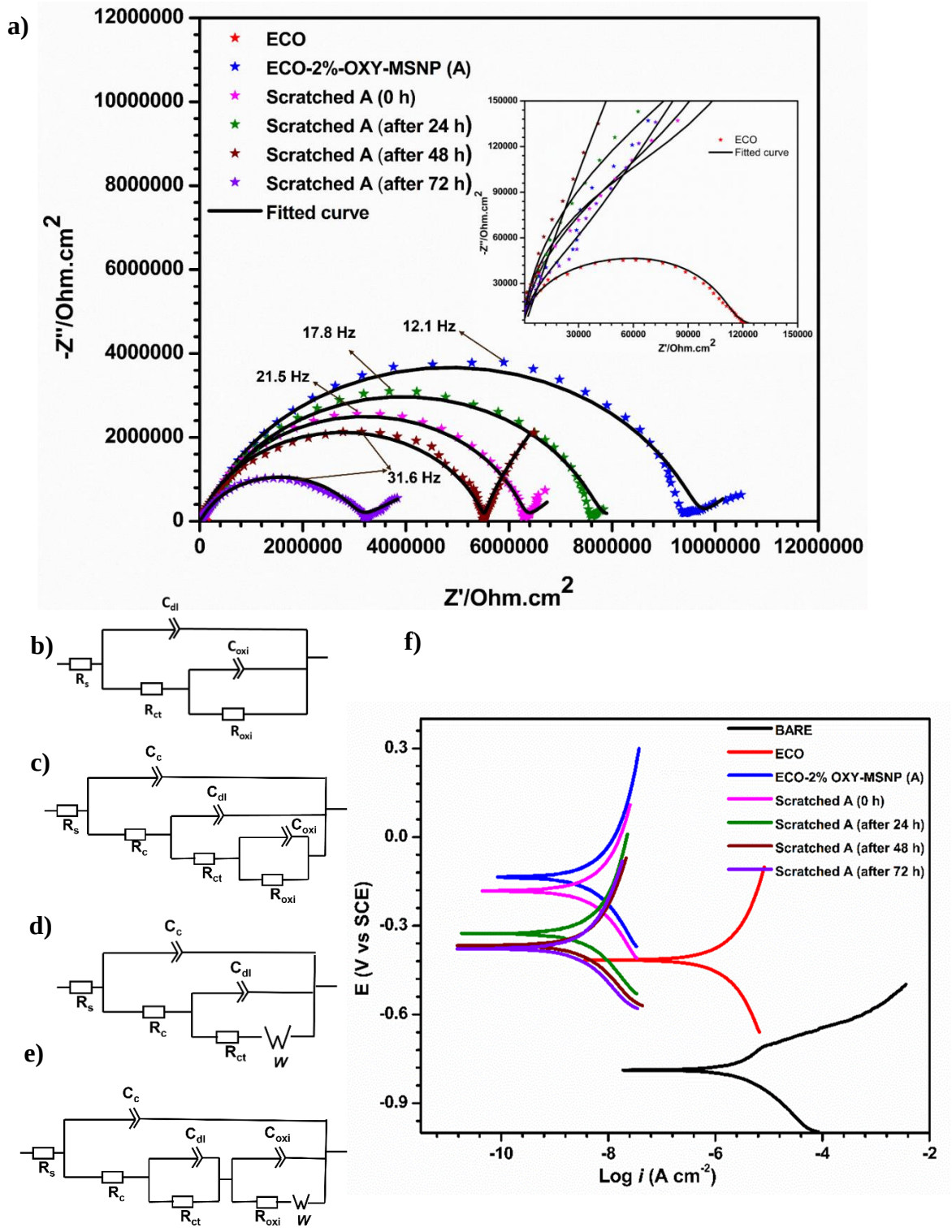

Figure 5.13. **a)** electrochemical impedance measurement for bare Al-6061 alloy, intact coatings and scratched coatings **b)** EEC for bare alloy**, c)** EEC for ECO coated sample**, d)** EEC for 2% coating (intact), **e)** EEC for 2% coatings (scratched) at different time intervals **f)** Tafel plots

Table 5.6. Electrochemical parameters and corrosion inhibition efficiency obtained for the modified ECO coatings (intact and scratched) on aluminium alloy in 3.5 wt.% NaCl solution

S/N	Substrate	Potentiodynamic polarisation			EIS	
		E_{corr} (V)	i_{corr} (μ Acm^{-2})	η (%)	R_{ct} (Ω cm^2)	η (%)
1.	Bare Al-6061	-0.788	1.941	-	4536	-
2.	ECO	-0.416	1.100	43.33	860900	99.47
3.	ECO-2%OXY-MSNP (A)	-0.136	0.0040	99.79	9644400	99.95
4.	(A) with a scratch (0 h)	-0.182	0.0043	99.79	6296900	99.92
5.	(A) with a scratch (24 h)	-0.326	0.0035	99.82	7631800	99.94
6.	(A) with a scratch (48 h)	-0.367	0.0035	99.82	5813000	99.92
7.	(A) with a scratch (72 h)	-0.378	0.0030	99.84	3746400	99.88

5.4.4. Corrosion inhibition mechanism

The polymer matrix keeps the corrosive ions away from the metal surface by passive protection, thus protecting the metal from deterioration. In active protection, different mechanisms act together; the self-healing action cures the damage and prevents the ions and water from entering the polymer matrix and reaching the metal surface. Not only the protection of metal, but also the maintenance of structural integrity and material property is also ensured by the self-healing action. Also the heteroatoms in the bio-nanocomposites donate their lone pair of electrons to the d-orbitals of the metal atom [49]. In oxyresveratrol, both heteroatom and pi-electron densities are very high. The loosely bound pi electrons flow to the metal d-orbitals [48]. Both these actions prevent the oxidation of the metal and prevent the formation of corrosion products. Retro donation from the metal atoms to the vacant molecular orbitals of the inhibitor makes the adhesion to the surface stronger [50]. The additional hydroxyl groups in the castor oil and the newly formed hydroxyl groups by the ring opening of the epoxy group in the ECO-CA copolyester will contribute to the self-healing mechanism and Lewis's acid-base interaction [51]. These

above factors resulted in the excellent corrosion inhibition exhibited by the epoxidized castor oil-oxyresveratrol bio-nanocomposite matrix. The possible inhibition mechanisms are demonstrated in **Figure 5.14.**

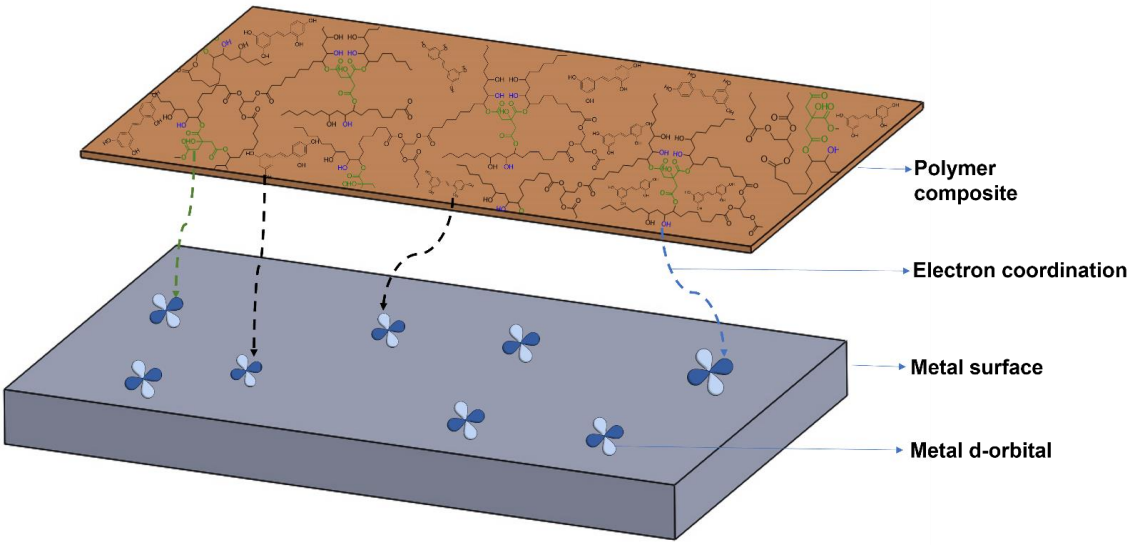

Figure 5.14. Corrosion inhibition mechanism of the modified epoxidized castor oil-based coating containing oxyresveratrol nanocomposites.

5.4.5. Evaluation and mechanism of the self-healing of ECO- nanocomposite coating

An artificial scratch, 0.1 mm thick and 1 cm long, was made using a razor blade, and the samples were immersed in a saline media for different durations. The SEM images were taken and examined after 12 h, 24 h, and 48 h. The curing was almost complete after 48 h of immersion in the saline water containing 3.5 wt.% NaCl. Surface coverage by forming corrosion products from the scratch is not observed in the SEM images (**Figure 5.15**). **Figure 5.15a** shows the artificial scratch made by the blade at 0 h without immersion, with the scratch clearly visible. After immersion in the saline medium for 12 h, it shows the formation/release of some products from the scratch. At 24 h, there were no extra particles, the scratch was almost healed, and the healing was complete by 48 h (**Figure 5.15d).** The vegetable oil-based epoxy matrix has an inherent self-healing property [52–54]. **Figure 5.15e** is the magnified image in the beginning of the healing, showing both polymer phase ripples, inhibitor release and hybrid formation.

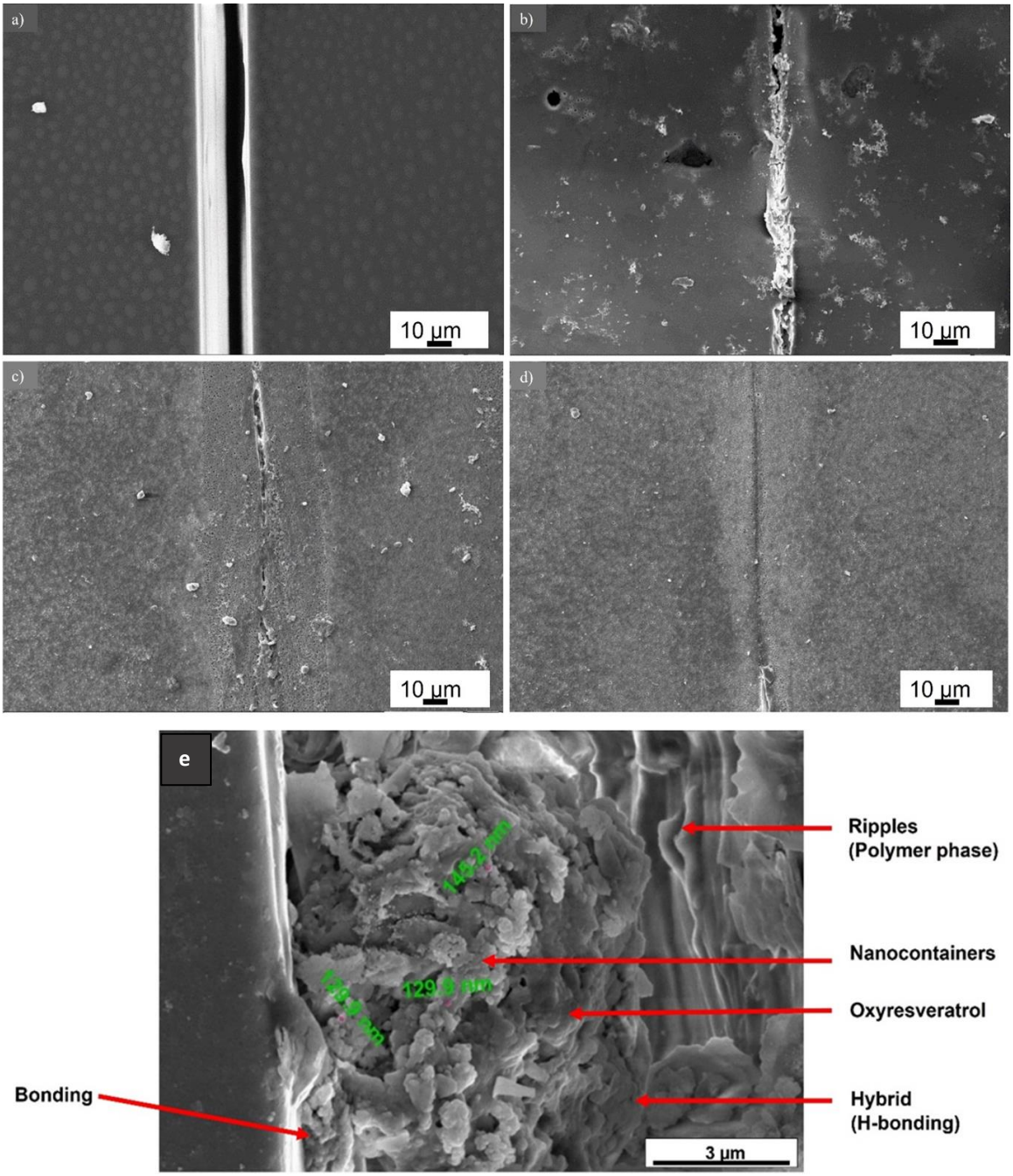

Figure 5.15. SEM micrographs of the scratched and healed surfaces in NaCl Solution after **a)** 0 h, **b)** 12 h, **c)** 24 h, **d)** 48 h, **e)** initial stage of self-healing showing different mechanisms of healing.

Generally, mobility and unreacted epoxies are claimed as the reason for healing properties. As compared to epoxy matrix, bio-based epoxy systems are more flexible and allow movements and bond formations. To date, there are many postulated theories to explain the healing mechanisms of epoxy polymers, like micro-Brownian motion,

mechanical interlocking, and an entropic mechanism [55]. In the bio-based castor oil-oxyresveratrol matrix, we propose a combination of prevailing mechanisms:

1) formation of reversible hydrogen bonding (hydroxy groups from the castor oil chain and the phenolic hydroxyl groups of oxyresveratrol). The presence of inherent hydroxyl groups, as well as the hydroxyl groups formed during the ring-opening reaction, shows the possibilities of intermolecular and intra-molecular hydrogen bonding [56].

2) dispersal of the inhibitor compound from the broken nanocomposite followed by its reaction with the metal and polymer functional groups resulting in the filling of the created defects [57].

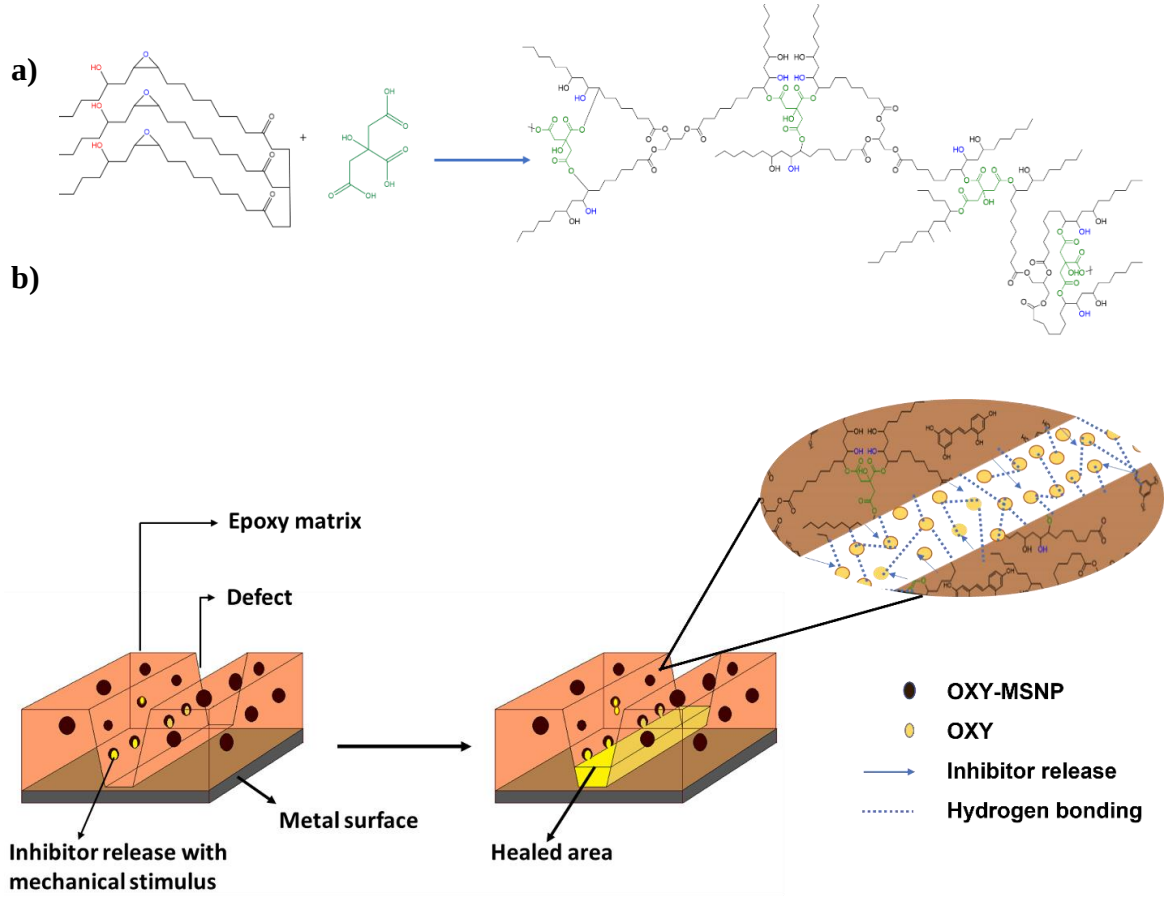

Figure 5.16. a) Formation of additional hydroxyl groups by the polyester formation reaction which helps the self-healing action **b)** Mechanism of self-healing by the inhibitor releasing action and enhanced hydrogen bonding of the modified ECO coating

The FE-SEM micrographs at higher magnifications show the small spherical structures of the nanocontainers, similar to that observed by TEM. Around the nanocontainers (spherical beads), a mass of amorphous particles was also seen, which is supposed to be the inhibitor oxyresveratrol. Ripples noticed in the composite correspond to

the toughened polymer phase, which is bonded to the oxyresveratrol through hydrogen bonding (**Figure 5.15e)**. A schematic of the proposed mechanism is shown in **Figure 5.16.**

5.4.6. Self-sanitizing efficiency of the coating

The zone of inhibition method was used for the qualitative evaluation of the antibacterial nature of the coatings on the metal surface. An aluminium disc of radius 1.7 cm was coated and used in this method. The coated samples were compared with a bare aluminium disc, and the changes in microbial growth were observed. In the case of the coated sample, the zone of inhibition was observed for both the gram-positive and gram-negative species **(Figure 5.17**). *E. coli* was the gram-negative bacteria used in the test, and the experiment showed a zone of inhibition of 3.5 cm diameter. *S. aureus* was the gram-positive bacteria used for the analysis, and the test exhibited a 4.25 cm diameter for the zone of inhibition on average. The coating containing empty mesoporous silica container was not active against the organisms, so the activity was solely due to the inhibitor.

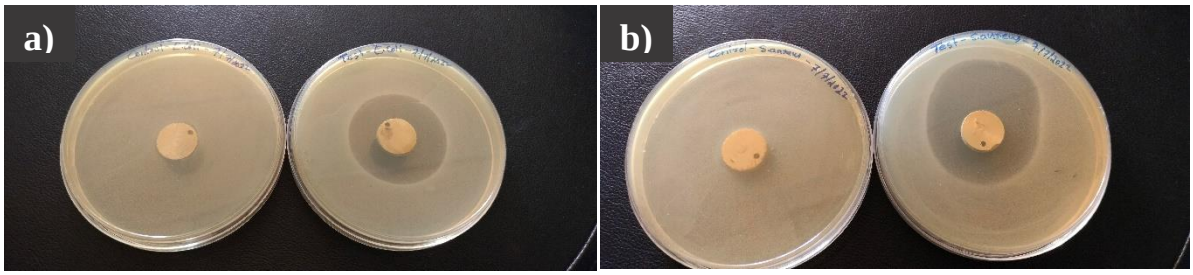

Figure 5.17. Qualitative evaluation of the antibacterial nature of the ECO coating modified with bio-nanocomposite, **a)** test results against *E. coli*- control versus test sample **b)** test results against *S. aureus*- control versus test sample.

ASTM- AATCC-100 protocols were used to quantitatively confirm the above results. 392.5 colonies were observed on average in the control plates for the *E. coli* in the 10^7 times dilutions in the quantitative test, while in the case of the undiluted samples, an infinite number of colonies were observed. In the quantitative test for the uncoated control plates for *S. aureus*, the 10^6 times diluted solution gave a number count of 251.5 colonies on average. The trend observed for the undiluted samples is found to be the same as that for *E. coli* with an infinite number of colonies. In both cases, the colonies on the metal surface are also found to be numerous and fast-growing. The ECO composite coated discs containing 2% bio nanocomposite shows the colony count for *E. coli* as 18 in the 10^7 times diluted sample showing an inhibition efficiency of 95.4% in a one-hour exposure. In the

case of S. aureus, there were 51.5 residual colonies in 10^6 dilutions, corresponding to an inhibition efficiency of 80% in one hour of exposure. **Figure 5.18** shows residual colonies for the control and test samples against the organisms at higher dilutions. Hence, this polymer composite matrix from the bio-based source is an excellent solution for the prevention of the proliferation and propagation of microbes from high-touch surfaces.

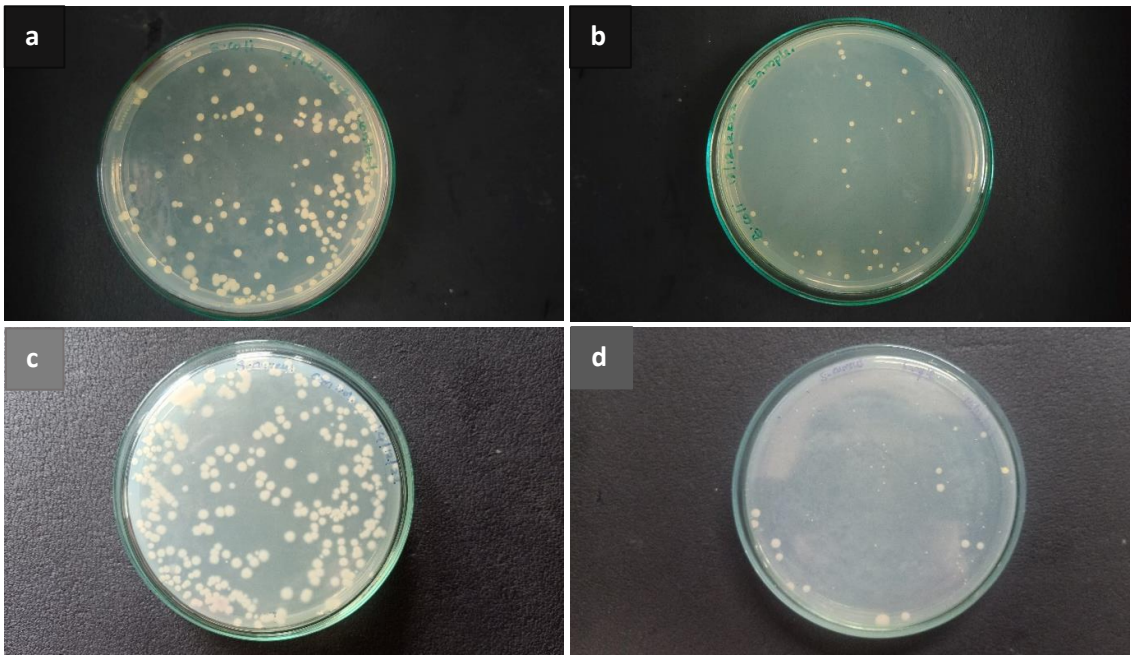

Figure 5.18. Quantitative analysis test results showing the residual microbial colonies for **a)** *E. coli* control sample, **b)** *E. coli* test sample, **c)** *S. aureus control sample, and* **d)** *S. aureus* test samples.

The major antimicrobial mechanisms of phytochemicals are membrane rupture, interruption of protein synthesis, cell wall synthesis, ribonucleic acid synthesis, deoxyribonucleic acid (DNA) synthesis, inhibition of membrane function, and ATP synthase, etc. Much literature suggests that the major mechanism of the antimicrobial action of oxyresveratrol is membrane rupture. Cytoplasmic membrane disruption and disbursal of cell contents were evident from TEM images [58]. The antimicrobial action and mechanism of the modified epoxy coating based on this property are shown in **Figure 5.19**.

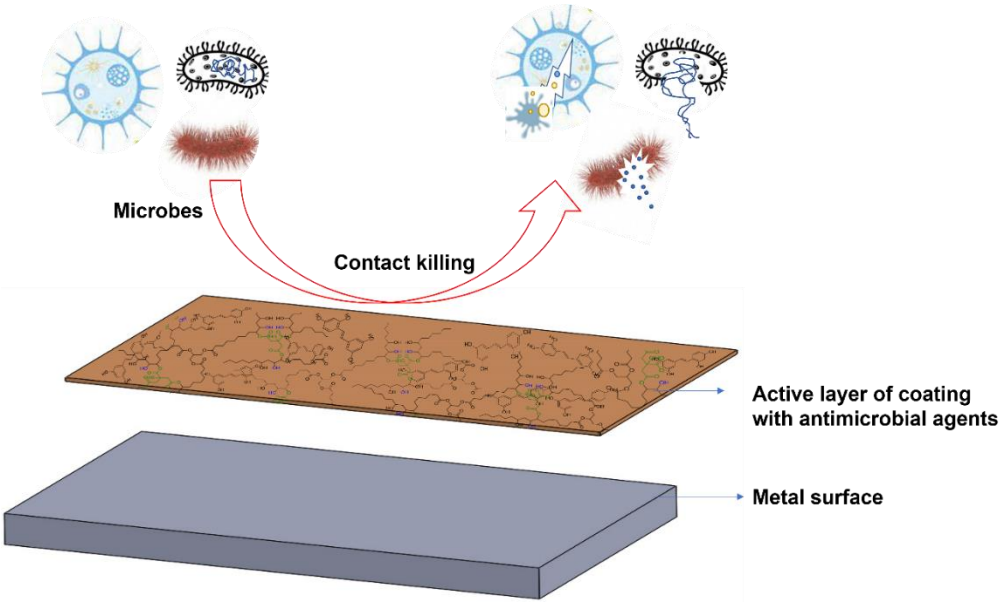

Figure 5.19. Contact killing mechanism of the modified epoxy coating by membrane disruption and cytoplasm release.

5.5. Conclusions

Multifunctional bio-epoxy coating is prepared from epoxidized castor oil crosslinked with citric acid and reinforced with coconut shell waste-derived oxyresveratrol-mesoporous silica nanoparticle composite fillers. The coating containing 2% of the green inhibitor exhibited the best performance, with 99.95% and 99.97% for aluminium-6061 and mild steel samples, respectively. In both cases, the corrosion potential showed a significant positive shift (for mild steel, the potential changed from -0.666 V to -0.028 V, and for aluminium -0.788 V to -0.136 V). Whilst the corrosion current density significantly decreased (from 30.53 μ Acm^{-2} to 0.0074 μ Acm^{-2} and from 1.941 μ Acm^{-2} to 0.0040 μ Acm^{-2}, for mild steel and Al-6061 alloy respectively in pH 7 medium) compared to bare alloy samples, even in all media with different pH. The self-healing response of the coating showed complete healing of the artificial scratch within 48 h, as corroborated by SEM micrographs, impedance measurements, and potentiodynamic polarization studies with an inhibition efficiency of 99.92%. The coating displayed antibacterial features by inhibiting the growth of both gram-positive and gram-negative bacteria and showed its self-sanitizing nature by preventing the proliferation of pathogens and their propagation from high-touch surfaces. The developed bio-composites possess smart and multifunctional properties. They increase the efficiency of the system and enhance the aesthetics of the surfaces by antibacterial and self-healing potential.

References

[1] X.Q. Liu, W. Huang, Y.H. Jiang, J. Zhu, C.Z. Zhang, Preparation of a bio-based epoxy with comparable properties to those of petroleum-based counterparts, Express Polym Lett. 6 (2012) 293–298. https://doi.org/10.3144/expresspolymlett.2012.32.

[2] A. Cna'ani, E. Dener, E. Ben-Zeev, J. Günther, T.G. Köllner, V. Tzin, M. Seifan, Phylogeny and abiotic conditions shape the diel floral emission patterns of desert Brassicaceae species, Plant Cell Environ. 50 (2021) pce.14045. https://doi.org/10.1111/pce.14045.

[3] I. Faye, M. Decostanzi, Y. Ecochard, S. Caillol, Eugenol bio-based epoxy thermosets: from cloves to applied materials, Green Chem. 19 (2017) 5236–5242. https://doi.org/10.1039/C7GC02322G.

[4] R. Li, A. Bahadori, J. Xin, K. Zhang, B. Muhunthan, J. Zhang, Characteristics of bioepoxy based on waste cooking oil and lignin and its effects on asphalt binder, Constr Build Mater. 251 (2020) 118926. https://doi.org/10.1016/j.conbuildmat.2020.118926.

[5] S.K. Sahoo, V. Khandelwal, G. Manik, Synthesis and characterization of low viscous and highly acrylated epoxidized methyl ester based green adhesives derived from linseed oil, Int J Adhes Adhes. 89 (2019) 174–177. https://doi.org/10.1016/j.ijadhadh.2019.01.007.

[6] M. Alam, D. Akram, E. Sharmin, F. Zafar, S. Ahmad, Vegetable oil based eco-friendly coating materials: A review article, Arabian Journal of Chemistry. 7 (2014) 469–479. https://doi.org/10.1016/j.arabjc.2013.12.023.

[7] V. Khandelwal, S.K. Sahoo, A. Kumar, S.K. Sethi, G. Manik, Bio-sourced electrically conductive epoxidized linseed oil based composites filled with polyaniline and carbon nanotubes, Compos B Eng. 172 (2019) 76–82. https://doi.org/10.1016/j.compositesb.2019.05.050.

[8] S. Allauddin, R. Narayan, K.V.S.N. Raju, Synthesis and Properties of Alkoxysilane Castor Oil and Their Polyurethane/Urea–Silica Hybrid Coating Films, ACS Sustain Chem Eng. 1 (2013) 910–918. https://doi.org/10.1021/sc3001756.

[9] L. Zhang, M. Zhang, L. Hu, Y. Zhou, Synthesis of rigid polyurethane foams with castor oil-based flame retardant polyols, Ind Crops Prod. 52 (2014) 380–388. https://doi.org/10.1016/j.indcrop.2013.10.043.

[10] A. Keyvani, M. Yeganeh, H. Rezaeyan, Application of mesoporous silica nanocontainers as an intelligent host of molybdate corrosion inhibitor embedded in the epoxy coated steel, Progress in Natural Science: Materials International. 27 (2017) 261–267. https://doi.org/10.1016/j.pnsc.2017.02.005.

[11] J. Tedim, S.K. Poznyak, A. Kuznetsova, D. Raps, T. Hack, M.L. Zheludkevich, M.G.S. Ferreira, Enhancement of Active Corrosion Protection via Combination of Inhibitor-Loaded Nanocontainers, ACS Appl Mater Interfaces. 2 (2010) 1528–1535. https://doi.org/10.1021/am100174t.

[12] D. Grigoriev, E. Shchukina, D.G. Shchukin, Nanocontainers for Self-Healing Coatings, Adv Mater Interfaces. 4 (2017) 1600318. https://doi.org/10.1002/admi.201600318.

[13] L. Guo, J. Tan, S. Kaya, S. Leng, Q. Li, F. Zhang, Multidimensional insights into the corrosion inhibition of 3,3-dithiodipropionic acid on Q235 steel in H_2SO_4 medium: A

combined experimental and in silico investigation, J Colloid Interface Sci. 570 (2020) 116–124. https://doi.org/10.1016/j.jcis.2020.03.001.

[14] L. Guo, R. Zhang, B. Tan, W. Li, H. Liu, S. Wu, Locust Bean Gum as a green and novel corrosion inhibitor for Q235 steel in 0.5 M H_2SO_4 medium, J Mol Liq. 310 (2020) 113239. https://doi.org/10.1016/j.molliq.2020.113239.

[15] B. Tan, S. Zhang, X. Cao, A. Fu, L. Guo, R. Marzouki, W. Li, Insight into the anti-corrosion performance of two food flavors as eco-friendly and ultra-high performance inhibitors for copper in sulfuric acid medium, J Colloid Interface Sci. 609 (2022) 838–851. https://doi.org/10.1016/j.jcis.2021.11.085.

[16] B. Tan, B. Xiang, S. Zhang, Y. Qiang, L. Xu, S. Chen, J. He, Papaya leaves extract as a novel eco-friendly corrosion inhibitor for Cu in H2SO4 medium, J Colloid Interface Sci. 582 (2021) 918–931. https://doi.org/10.1016/j.jcis.2020.08.093.

[17] S.Z. Salleh, A.H. Yusoff, S.K. Zakaria, M.A.A. Taib, A. Abu Seman, M.N. Masri, M. Mohamad, S. Mamat, S. Ahmad Sobri, A. Ali, P. Ter Teo, Plant extracts as green corrosion inhibitor for ferrous metal alloys: A review, J Clean Prod. 304 (2021) 127030. https://doi.org/10.1016/j.jclepro.2021.127030.

[18] B. Tan, W. Lan, S. Zhang, H. Deng, Y. Qiang, A. Fu, Y. Ran, J. Xiong, R. Marzouki, W. Li, Passiflora edulia Sims leaves Extract as renewable and degradable inhibitor for copper in sulfuric acid solution, Colloids Surf A Physicochem Eng Asp. 645 (2022) 128892. https://doi.org/10.1016/j.colsurfa.2022.128892.

[19] S.B. Ulaeto, A. V. Nair, J.K. Pancrecious, A.S. Karun, G.M. Mathew, T.P.D. Rajan, B.C. Pai, Smart nanocontainer-based anticorrosive bio-coatings: Evaluation of quercetin for corrosion protection of aluminium alloys, Prog Org Coat. 136 (2019) 105276. https://doi.org/10.1016/j.porgcoat.2019.105276.

[20] S. Hu, Z. Zheng, X. Zhang, F. Chen, M. Wang, Oxyresveratrol and trans-dihydromorin from the twigs of Cudrania tricuspidata as hypopigmenting agents against melanogenesis, J Funct Foods. 13 (2015) 375–383. https://doi.org/https://doi.org/10.1016/j.jff.2015.01.010.

[21] D.-K. Joung, S.-H. Mun, S.-H. Choi, O.-H. Kang, S.-B. Kim, Y.-S. Lee, T. Zhou, R. Kong, J.-G. Choi, D.-W. Shin, Y.-C. Kim, D.-S. Lee, D.-Y. Kwon, Antibacterial activity of oxyresveratrol against methicillin-resistant Staphylococcus aureus and its mechanism, Exp Ther Med. 12 (2016) 1579–1584. https://doi.org/10.3892/etm.2016.3486.

[22] K. Likhitwitayawuid, Oxyresveratrol: Sources, Productions, Biological Activities, Pharmacokinetics, and Delivery Systems, Molecules. 26 (2021) 4212. https://doi.org/10.3390/molecules26144212.

[23] M.T. Meenu, G. Kaul, M. Shukla, K.V. Radhakrishnan, S. Chopra, Cudraflavone C from *Artocarpus hirsutus* as a Promising Inhibitor of Pathogenic, Multidrug-Resistant *S. aureus* , Persisters, and Biofilms: A New Insight into a Rational Explanation of Traditional Wisdom, J Nat Prod. 84 (2021) 2700–2708. https://doi.org/10.1021/acs.jnatprod.1c00578.

[24] D.S. KUMAR, C. BOSE, S.K. SHAJI, N. PANDURANGAN, G.B. KUMAR, A. BANERJI, B.G. NAIR, Coconut shell derived bioactive compound Oxyresveratrol mediates regulation of Matrix metalloproteinase 9, International Journal of Pharma and Bio Science. 8 (2017). https://doi.org/10.22376/ijpbs.2017.8.1p202-210.

[25] L.A. Nunes, M.L.S. Silva, J.Z. Gerber, R. de A. Kalid, Waste green coconut shells: Diagnosis of the disposal and applications for use in other products, J Clean Prod. 255 (2020) 120169. https://doi.org/10.1016/j.jclepro.2020.120169.

[26] oxyresveratrol alkali extraction, (n.d.).

[27] S.K. Sahoo, V. Khandelwal, G. Manik, Development of completely bio-based epoxy networks derived from epoxidized linseed and castor oil cured with citric acid, Polym Adv Technol. 29 (2018) 2080–2090. https://doi.org/10.1002/pat.4316.

[28] S.K. Sahoo, V. Khandelwal, G. Manik, Development of toughened bio-based epoxy with epoxidized linseed oil as reactive diluent and cured with bio-renewable crosslinker, Polym Adv Technol. 29 (2018) 565–574. https://doi.org/10.1002/pat.4166.

[29] G. Ji, S. Anjum, S. Sundaram, R. Prakash, Musa paradisica peel extract as green corrosion inhibitor for mild steel in HCl solution, Corros Sci. 90 (2015) 107–117. https://doi.org/10.1016/j.corsci.2014.10.002.

[30] J.-H. Lee, Y.-G. Kim, C.J. Raorane, S.Y. Ryu, J.-J. Shim, J. Lee, The anti-biofilm and anti-virulence activities of *trans*- resveratrol and oxyresveratrol against uropathogenic *Escherichia coli*, Biofouling. 35 (2019) 758–767. https://doi.org/10.1080/08927014.2019.1657418.

[31] V. Khandelwal, S.K. Sahoo, A. Kumar, G. Manik, Electrically conductive green composites based on epoxidized linseed oil and polyaniline: An insight into electrical, thermal and mechanical properties, Compos B Eng. 136 (2018) 149–157. https://doi.org/10.1016/j.compositesb.2017.10.030.

[32] M. Mei, J.-Q. Ruan, W.-J. Wu, R.-N. Zhou, J.P.-C. Lei, H.-Y. Zhao, R. Yan, Y.-T. Wang, In Vitro Pharmacokinetic Characterization of Mulberroside A, the Main Polyhydroxylated Stilbene in Mulberry (*Morus alba* L.), and Its Bacterial Metabolite Oxyresveratrol in Traditional Oral Use, J Agric Food Chem. 60 (2012) 2299–2308. https://doi.org/10.1021/jf204495t.

[33] M. Nayak, M. Majeed, A. Nagarajan, L.A. Mundkur, Evaluation of in vitro antioxidant potential, anti-Inflammatory activity and melanogenesis inhibition of Artocarpus hirsutus Lam. extracts LactoSporin View project Immune modulation and Atherosclerosis in ApoB48/Ldlr mice: Correlation of immune response and gene expression with disease progression View project Evaluation of in vitro antioxidant potential, anti-inflammatory activity and melanogenesis inhibition of Artocarpus hirsutus Lam. extracts, Article in International Journal of Scientific & Technology Research. 6 (2017) 1. www.ijstr.org.

[34] B. Qian, M. Michailidis, M. Bilton, T. Hobson, Z. Zheng, D. Shchukin, Tannic complexes coated nanocontainers for controlled release of corrosion inhibitors in self-healing coatings, Electrochim Acta. 297 (2019) 1035–1041. https://doi.org/10.1016/j.electacta.2018.12.062.

[35] M. Cai, X. Fan, H. Yan, Y. Li, S. Song, W. Li, H. Li, Z. Lu, M. Zhu, In situ assemble $Ti_3C_2T_x$ MXene@MgAl-LDH heterostructure towards anticorrosion and antiwear application, Chemical Engineering Journal. 419 (2021) 130050. https://doi.org/10.1016/j.cej.2021.130050.

[36] B. Tan, J. He, S. Zhang, C. Xu, S. Chen, H. Liu, W. Li, Insight into anti-corrosion nature of Betel leaves water extracts as the novel and eco-friendly inhibitors, J Colloid Interface Sci. 585 (2021) 287–301. https://doi.org/10.1016/j.jcis.2020.11.059.

[37] Y. Guo, J. Wang, D. Zhang, T. Qi, G.L. Li, pH-responsive self-healing anticorrosion coatings based on benzotriazole-containing zeolitic imidazole framework, Colloids Surf A Physicochem Eng Asp. 561 (2019) 1–8. https://doi.org/10.1016/j.colsurfa.2018.10.044.

[38] N. Li, H. Jiang, J. Yang, C. Wang, L. Wu, Y. Hao, Y. Liu, Characterization of phenolic compounds and anti-acetylcholinase activity of coconut shells, Food Biosci. 42 (2021) 101204. https://doi.org/10.1016/j.fbio.2021.101204.

[39] M.B. Hegde, K.N.S. Mohana, K. Rajitha, A.M. Madhusudhana, Reduced graphene oxide-epoxidized linseed oil nanocomposite: A highly efficient bio-based anti-corrosion coating material for mild steel, Prog Org Coat. 159 (2021) 106399. https://doi.org/10.1016/j.porgcoat.2021.106399.

[40] R.S. Komartin, B. Balanuca, M.I. Necolau, A. Cojocaru, R. Stan, Composite Materials from Renewable Resources as Sustainable Corrosion Protection Coatings, Polymers (Basel). 13 (2021) 3792. https://doi.org/10.3390/polym13213792.

[41] H. Yan, X. Fan, M. Cai, S. Song, M. Zhu, Amino-functionalized $Ti_3C_2T_x$ loading ZIF-8 nanocontainer@benzotriazole as multifunctional composite filler towards self-healing epoxy coating, J Colloid Interface Sci. 602 (2021) 131–145. https://doi.org/10.1016/j.jcis.2021.06.004.

[42] H. Yan, M. Cai, W. Li, X. Fan, M. Zhu, Amino-functionalized $Ti_3C_2T_x$ with anti-corrosive/wear function for waterborne epoxy coating, J Mater Sci Technol. 54 (2020) 144–159. https://doi.org/10.1016/j.jmst.2020.05.002.

[43] S.I. Bhat, S. Ahmad, Castor oil-TiO_2 hyperbranched poly (ester amide) nanocomposite: a sustainable, green precursor-based anticorrosive nanocomposite coatings, Prog Org Coat. 123 (2018) 326–336. https://doi.org/10.1016/j.porgcoat.2018.06.010.

[44] M.B. Hegde, K.N.S. Mohana, K. Rajitha, A.M. Madhusudhana, Reduced graphene oxide-epoxidized linseed oil nanocomposite: A highly efficient bio-based anti-corrosion coating material for mild steel, Prog Org Coat. 159 (2021) 106399. https://doi.org/10.1016/j.porgcoat.2021.106399.

[45] K. Mansouri, K. Ibrik, N. Bensalah, A. Abdel-Wahab, Anodic Dissolution of Pure Aluminum during Electrocoagulation Process: Influence of Supporting Electrolyte, Initial pH, and Current Density, Ind Eng Chem Res. 50 (2011) 13362–13372. https://doi.org/10.1021/ie201206d.

[46] X. Li, H. Castaneda, Application of Electrochemical Techniques on Study of Effect of Nano-ZnO in Conductive Polyaniline Containing Zinc-Rich Primer, Int J Spectrosc. 2018 (2018) 1–15. https://doi.org/10.1155/2018/7160381.

[47] L. Wen, Y. Wang, Y. Zhou, J.-H. Ouyang, L. Guo, D. Jia, Corrosion evaluation of microarc oxidation coatings formed on 2024 aluminium alloy, Corros Sci. 52 (2010) 2687–2696. https://doi.org/10.1016/j.corsci.2010.04.022.

[48] B. John, P.R. Rajimol, T.P.D. Rajan, S.K. Sahoo, Design and fabrication of nano textured superhydrophobic and anti-corrosive silane-grafted ZnO/bio-based polyurethane bilayer coating, Surf Coat Technol. 451 (2022) 129036. https://doi.org/10.1016/j.surfcoat.2022.129036.

[49] N. Bhardwaj, P. Sharma, V. Kumar, Phytochemicals as steel corrosion inhibitor: an insight into mechanism, Corrosion Reviews. 39 (2021) 27–41. https://doi.org/10.1515/corrrev-2020-0046.

[50] X. Lai, J. Hu, T. Ruan, J. Zhou, J. Qu, Chitosan derivative corrosion inhibitor for aluminum alloy in sodium chloride solution: A green organic/inorganic hybrid, Carbohydr Polym. 265 (2021) 118074. https://doi.org/10.1016/j.carbpol.2021.118074.

[51] M.M. Fares, A.K. Maayta, M.M. Al-Qudah, Pectin as promising green corrosion inhibitor of aluminum in hydrochloric acid solution, Corros Sci. 60 (2012) 112–117. https://doi.org/10.1016/j.corsci.2012.04.002.

[52] S. Ataei, S.N. Khorasani, R.E. Neisiany, Biofriendly vegetable oil healing agents used for developing self-healing coatings: A review, Prog Org Coat. 129 (2019) 77–95. https://doi.org/10.1016/j.porgcoat.2019.01.012.

[53] A.B. Chaudhari, P.D. Tatiya, R.K. Hedaoo, R.D. Kulkarni, V. V. Gite, Polyurethane Prepared from Neem Oil Polyesteramides for Self-Healing Anticorrosive Coatings, Ind Eng Chem Res. 52 (2013) 10189–10197. https://doi.org/10.1021/ie401237s.

[54] X. Wei, J. Ge, F. Gao, F. Chen, W. Zhang, J. Zhong, C. Lin, L. Shen, Bio-based self-healing coating material derived from renewable castor oil and multifunctional alamine, Eur Polym J. 160 (2021) 110804. https://doi.org/10.1016/j.eurpolymj.2021.110804.

[55] M. Peñas-Caballero, M. Hernández Santana, R. Verdejo, M.A. Lopez-Manchado, Measuring self-healing in epoxy matrices: The need for standard conditions, React Funct Polym. 161 (2021) 104847. https://doi.org/10.1016/j.reactfunctpolym.2021.104847.

[56] S.J. García, H.R. Fischer, S. van der Zwaag, A critical appraisal of the potential of self healing polymeric coatings, Prog Org Coat. 72 (2011) 211–221. https://doi.org/10.1016/j.porgcoat.2011.06.016.

[57] E. V. Skorb, D. Fix, D. V. Andreeva, H. Möhwald, D.G. Shchukin, Surface-Modified Mesoporous SiO_2 Containers for Corrosion Protection, Adv Funct Mater. 19 (2009) 2373–2379. https://doi.org/10.1002/adfm.200801804.

[58] D.-K. Joung, S.-H. Mun, S.-H. Choi, O.-H. Kang, S.-B. Kim, Y.-S. Lee, T. Zhou, R. Kong, J.-G. Choi, D.-W. Shin, Y.-C. Kim, D.-S. Lee, D.-Y. Kwon, Antibacterial activity of oxyresveratrol against methicillin-resistant Staphylococcus aureus and its mechanism, Exp Ther Med. 12 (2016) 1579–1584. https://doi.org/10.3892/etm.2016.3486.

ABSTRACT

Name of the student: **Rajimol P. R.** Registration No.: **10CC18A39009**

Faculty of Study: **Chemical Sciences** Year of Submission: **2023**

AcSIR academic centre/CSIR Lab: **CSIR-National Institute for Interdisciplinary Science and Technology, Thiruvananthapuram, Kerala**

Name of the Supervisor(s): **Dr. T. P. D. Rajan** **Dr. K. V. Radhakrishnan**

Title of the thesis: **Multifunctional Smart Coatings Derived from Biomass Extracts for Mild Steel and Aluminium Alloys**

The replacement of petroleum-based epoxy with bio-based epoxy and synthetic organic and inorganic inhibitors with plant extracts and phytochemicals will lead to the developments of an environmentally friendly and side-effect-free bio-sourced corrosion inhibitor coatings. Also, smart coatings with anti-corrosion, self-healing, hydrophobic and antimicrobial properties can achieve reduced maintenance costs, increased life, fewer accidents, and preventing the propagation and proliferation of pathogens etc. For this, a plant extract or compound with excellent corrosion inhibition property along with antimicrobial property should be identified. Also, a method to load the inhibitor with increased shelf-life, controlled release property and trigger response should be ensured. Encapsulation in mesoporous silica (MSNP) nanocontainers is used for this purpose. **Chapter 1** gives a brief introduction to natural product-based multifunctional corrosion inhibitors for smart coatings. The multifunctionality of plant-based anticorrosive smart coatings find potential applications in various fields as described in the chapter. It also explains the idea of different smart coatings and gives a detailed literature survey of various bio-based smart coatings. **Chapter 2** is on the development of a multifunctional smart epoxy coating from the extract of marigold flower waste and its marker compound quercetagetin. The coating exhibited anticorrosive, antimicrobial and self-healing properties, and complete self-healing was observed within 48 hours. **Chapter 3** describes the smart multifunctional epoxy coating prepared by incorporating bio-nanocomposites of two isolated phytochemicals, bergenin and malabaricone C, which showed excellent corrosion inhibition properties and self-sanitizing effect. **Chapter 4** deals with the development of a synergistic epoxy formulation by the incorporation of hydro-ethanolic extracts of *Azadirachta indica*, *Elephantopus scaber* and *Andrographis paniculata*. The combination of three plant extracts resulted in an increased corrosion inhibition potential and antimicrobial efficiency due to the synergistic combination of the compounds. **Chapter 5** illustrates the use of oxyresveratrol extracted from coconut shell waste as a green corrosion inhibitor. Castor oil is a non-edible vegetable oil, it is epoxidized and crosslinked with bio-sourced citric acid and reinforced with oxyresveratrol-silica nanoparticles. The bio-based composite coating showed excellent anti-corrosive properties with improved thermal stability, self-sanitizing, self-healing properties. **Chapter 6** summarises various studies carried out on the development of multifunctional smart coatings from different plant phytochemicals as corrosion inhibitor and antimicrobial agent.

Details of the Publications Emanating from the Thesis Work

Published

1. **P.R. Rajimol**, Ulaeto S. B., A. Raj, P. Anoop, Rajan T.P.D., S.K. Sahoo, Radhakrishnan K.V., & Sukumaran Rajeev, "Development of oxyresveratrol incorporated bio-based smart nanocomposite coating with anti-corrosive, self-healing, and anti-microbial properties". ***Green chemistry***, **2023**, **25**, 7189-7215, DOI: 10.1039/D3GC00773A
2. **P. R. Rajimol**, Ulaeto, S. B., Puthiyamadam, A., Neethu, S., Rajan, T. P. D., Radhakrishnan, K. V., & Sukumaran, R. K. "Smart anticorrosive and antimicrobial multifunctional epoxy coating using bergenin and malabaricone C bio-nanocomposite dispersoids on mild steel and aluminium-6061 alloy". ***Progress in Organic Coatings***, 169 (2022):106924, doi.org/10.1016/j.porgcoat.2022.106924
3. **P. R. Rajimol**, Ulaeto, S. B., Rajan, T. P. D., Radhakrishnan, K. V. "Natural Product-Based Multifunctional Corrosion Inhibitors for Smart Coatings". Corrosion Mitigation: Biomass and Other Natural Products. Walter de Gruyter GmbH & Co KG, 2022.

Manuscript submitted

4. **P. R. Rajimol**, Sarah Bill Ulaeto, Samuel A. S., Radhakrishnan K. V, T. P. D. Rajan, "Eco-friendly anticorrosive-self-healing smart coating using Quercetagetin derived from marigold floral waste: a solution for mild steel and aluminium corrosion in the marine environment". (Manuscript Submitted)

Papers from Other Related Works

1. **P. R. Rajimol**, Akhil B.S., Radhakrishnan K. V, "Exploring the Phytochemical Profile and Biological Activities of Clerodendrum infortunatum". ACS Omega,2023, https://doi.org/10.1021/acsomega.2c08080
2. John B, **Rajimol P R**, Rajan TPD, Sahoo SK. Design and fabrication of nano textured superhydrophobic and anti-corrosive silane-grafted ZnO/bio-based polyurethane bilayer coating. Surface and Coatings Technology. 2022 Dec 15; 451:129036.
3. Ulaeto SB, Mathew GM, Pancrecious JK, **Rajimol P R**, Karun AS, Rajan TP. Azadirachta indica (Neem) self-healing efficacy assessment in epoxy primer coatings:

A bio-responsive strategy for counteracting corrosion. Colloids and Surfaces A: Physicochemical and Engineering Aspects. 2023 Feb 5; 658:130684.

4. Arsha AG, Manoj V, Akhil MG, Anbukkarasi R, **Rajimol P R**, Rajan TP. Squeeze infiltration processing and characterization of silicon reinforced composites. Materials Today Communications. 2022 Aug 1; 32:103870.
5. Arsha AG, Akhil MG, Manoj V, **Rajimol P R**, Anbukkarasi R, Rajan TP, Dhanalakshmi S. Functionally Graded Al-SiC Composites by Squeeze Infiltration Technique. International Journal of Metalcasting. 2023 Feb 11:1-1.
6. **P. R. Rajimol**, Ulaeto S. B., Ben John, Rajan T. P. D., "Metal-Organic Frameworks (MOFs) based functionalized thin film coating for corrosion protection". Walter de Gruyter GmbH & Co KG, 2023.
7. Sarah Bill Ulaeto, **Rajimol P. R**., Inime Ime Udoh, Gincy Marina Mathew, TPD Rajan. "Polymer-Based Coating for Steel Protection, Highlighting Metal-Organic Framework as Functional Actives: A Review". Corros. Mater. Degrad. 2023, 4 (2), 284-316
8. Sarah Bill Ulaeto, **Rajimol P. R**., Inime Ime Udoh, Gincy Marina Mathew, TPD Rajan. "Organic Corrosion Inhibitors for the Protection of Steel Substrate" (Review: Corrosion and Materials Degradation, MDPI- under revision)

PATENT- Related to the thesis

1. A bio-based epoxy formulation for coating on metallic surfaces having excellent corrosion inhibition potential and 99.99% bactericidal efficiency**.,** Rajimol Puthenpurackal Ravi, Thazhavilai Ponnu Devaraj Rajan, Radhakrishnan Kokkuvayil Vasu, Anoop Puthiyamadam, Rajeev Kumar Sukumaran (Patent Application: 0207NF2022)

Posters Presented and Attended in Conferences

1. Phytochemical investigation of bio-actives from the roots of *Clerodendrum infortunatum* Linn. **Rajimol P. R.** and Radhakrishnan K. V. 8th Annual meeting of Biomedical Sciences & Conference on Deliberation on Translation of Basic Scientific Insights into Affordable Healthcare Products. February 25-27, 2019 (Best paper award).

2. Dihydro-*β*-agarofuran sesquiterpenoids from the seed of *Celastrus paniculatus* Wild. and their glucosidase inhibitory Activity. **Rajimol P. R.,** Sasikumar P., Sharathna P. and K. V. Radhakrishnan. Current Trends in Herbal Drugs and Pharma Industry, 29,30 March 2019.

3. Phytochemical investigation of rhizomes of *Zingiber nimmonii* and *Zingiber zerumbet.* **Rajimol P. R,** Ajish K. R, Greeshma Gopalan, M. Sabu and K. V. Radhakrishnan*. International Seminar on Phytochemistry, 26,27 March 2018.

4. Biomass Derived Corrosion Inhibitors and Coatings for Mild Steel and Aluminium Alloys – Role of Bergenin. **Rajimol P.R**., Sarah Bill Ulaeto, T.P.D. Rajan, K.V. Radhakrishnan. NCMST, 2021, IIST Trivandrum

5. Development of Oxyresveratrol Incorporated Bio-based Smart Nanocomposite Coating with Anti-corrosive, Self-healing, and Anti-microbial Properties. **Rajimol P. R.**, Sarah Bill Ulaeto, Anoop Puthiyamadam, Sushanta Kumar Sahoo, T. P. D. Rajan*, K. V. Radhakrishnan, and Rajeev K. Sukumaran. AMMT, 2023, CSIR-NIIST Trivandrum.